December 2020

An Integrative Approach Concerning Radiological Protection of the Environment: Plant Influence on Biogeochemistry and Transport, Plant Uptake, and Non-Human Biota Dosimetry for Select Radionuclides

Dawn Angel Montgomery
Clemson University, dawn.angel.montgomery@gmail.com

AN INTEGRATIVE APPROACH CONCERNING RADIOLOGICAL PROTECTION OF THE ENVIRONMENT: PLANT INFLUENCE ON BIOGEOCHEMISTRY AND TRANSPORT, PLANT UPTAKE, AND NON-HUMAN BIOTA DOSIMETRY FOR SELECT RADIONUCLIDES

A Dissertation
Presented to
the Graduate School of
Clemson University

In Partial Fulfillment
of the Requirements for the Degree
Doctor of Philosophy
Environmental Engineering and Earth Sciences

---

by
Dawn Angel Montgomery
December 2020

Accepted by:
Dr. Nicole Martinez, Committee Chair
Dr. Brian Powell
Dr. Daniel Kaplan
Dr. Nishanth Tharayil

ABSTRACT

The fields of radioecology and environmental radiation protection encompass a multitude of interdisciplinary specialties relating to the use, transport, and effects associated with radioactive substances in the environment, which often must inform each other in an integrated and iterative manner. As these fields have begun to consider a more holistic approach to environmental radiation protection, there is not only a need to evaluate fate and transport of radionuclides in the environment, but also a need to consider the dose and impacts to non-human biota residing in contaminated (or potentially contaminated) areas. Thus, the overall objective of this work was to demonstrate an explicit, integrated, and holistic approach to environmental radiation protection in a soil-plant-hydrologic system. This was accomplished through a series of radionuclide transport studies and non-human biota dosimetric model development. The focused objective of the transport studies was to examine and quantify the influence of an indigenous grass species, *Andropogon virginicus* (broomsedge), on the mobility of a broad suite of radionuclides (technetium, cesium, neptunium, and uranium) in the vadose zone of Savannah River Site (SRS) soil. Specific experiments sought to elucidate and quantify key influential factors associated with individual system components; batch experiments probed impacts of root exudates on sorption, and hydroponic plant experiments investigated tissue uptake and translocation potential, accounting for the influence of plant growth stage. These experiments were then combined into an integrated system utilizing laboratory-scale vegetated and unvegetated soil columns allowing radionuclide uptake, transport, and soil profile distributions to be evaluated in a controlled, but more environmentally realistic system. Concurrently, the

main objective of the dosimetric modeling portion of this work was to develop and compare several increasingly realistic, organism-specific computational dosimetric models for *A. virginicus* and to apply plant uptake data (from hydroponic uptake experiments) to determine organism dose rates as an example of application. In addition to the individual studies informing each other, this work also has the potential to influence and inform future work on this system or in the wider radioecology community. For example, both the transport studies and the dosimetric models may be useful for tiered environmental risk assessment evaluations and the most anatomically realistic, higher fidelity dosimetric models have the potential to be utilized in organism-specific dose-effect studies.

DEDICATION

To Haiden and Rowan.

ACKNOWLEDGMENTS

I am extremely grateful and proud to have been able to work under the guidance of both of my advisors, Dr. Nicole Martinez and Dr. Brian Powell. Thank you both for your patience, support, advice, and allowing me to direct my research toward my specific interests. I would especially like to thank Dr. Martinez for her friendship, willingness to listen (to me complain), for her thorough reviews, and for enriching my tenure as a graduate student with several unique travel and training opportunities abroad that I never expected to have. Those trips were invaluable in terms of what I was able to learn as well as the connections I was able to form with other scientists in the radioecology field. In addition to Drs. Martinez and Powell, I would also like to acknowledge and thank my other committee members, Drs. Dan Kaplan and Nishanth Tharayil, for their thoughtful exams, reviews, advice, and interesting field work opportunities that have allowed me to grow as a researcher. Additionally, many parts of this work could not have been done without collaboration with Nimisha Edayilam, thank you for supplying the plants used in this work and for showing me how to properly care for them. Finally, this work may not have (ever) been completed if it weren't for some very hardworking undergraduates - Thank you, Andrew Sheriff, Hayden Paige, Marc Mason, and Jenn Paloni, I would probably be here another two years without your help.

I would also like to thank all of the members of the Martinez and Powell research groups past and present. In particular, I am tremendously grateful to Drs. Hilary Emerson, Miller Wylie, and Shanna Estes for providing training and help in the lab anytime I asked, especially with the ICP-MS and SEM. Additionally, I don't think anyone can get through

graduate school (or life really) without people around to vent to sometimes. Thank you, Lisa, Megan, Stephanie, Rachel, Mara, Kathryn, Becca, and Kayla, for being willing to listen.

Finally, without financial support I probably would not have returned to graduate school at all. Therefore, I would also like to acknowledge the various funding entities associated with this work, including the United States Department of Energy Office of Science, Office of Basic Energy Sciences and Office of Biological and Environmental Research and the Nuclear Regulatory Commission, as well as the financial support I have received through the Montgomery and the Post 9/11 GI Bills.

TABLE OF CONTENTS

Table of Contents (Continued)

Page

LIST OF TABLES

Table Page

List of Tables (Continued)

Table Page

List of Tables (Continued)

Table Page

LIST OF FIGURES

Figure Page

List of Figures (Continued)

Figure Page

List of Figures (Continued)

Figure Page

List of Figures (Continued)

Figure Page

List of Figures (Continued)

Figure Page

CHAPTER ONE

INTRODUCTION AND DISSERTATION OVERVIEW

1.1. Introduction

The intention of contemporary environmental radiation protection is to protect the environment in the explicit sense, with consideration given to various worldviews (e.g., anthropocentric, ecocentric, biocentric, etc.), as opposed to assuming that adequate protection of man results in sufficient environmental protection (ICRP, 2017, 2009a, 2008, 2007, 2003). Thus, as is similar to human radiation protection and risk assessment, a more holistic approach to environmental radiation protection has been advocated for with implementation being actively addressed by the International Commission on Radiological Protection's (ICRP) Task Group 105 (ICRP, 2014, 2003; Pentreath, 2002). With these considerations, there is not only a need to evaluate fate and transport of radionuclides in the environment, but also a need to consider the dose received by non-human biota residing in impacted areas, in part through development of biologically relevant dosimetric models; thereby, allowing accurate dose-effect relationships and appropriate protection standards to be defined and implemented (ICRP, 2017; Martinez et al., 2016; Pentreath, 2009). Given this contemporary mindset concerning environmental radiation protection, the goal of this dissertation as a whole was to set the groundwork for and demonstrate the development of a more explicit, integrated, and holistic approach to environmental radiation protection for a soil-plant-hydrologic system through both radionuclide transport studies and non-human biota dosimetric model development. Of specific interest in this work was the indigenous grass species *Andropogon virginicus* (broomsedge), a biogeochemically broad suite of

environmentally relevant radionuclides (technetium, cesium, neptunium, and uranium), and a Savannah River Site (SRS; Aiken, SC) soil.

Technetium-99 (^{99}Tc), cesium (^{137}Cs and ^{135}Cs), neptunium-237 (^{237}Np) and uranium (^{238}U, ^{235}U, and ^{234}U) are long-lived risk drivers associated with both civilian and military nuclear applications. These radionuclides have been, or have the potential to be, released to the environment from various sources, such as legacy nuclear waste, proposed spent nuclear fuel repositories, and from potential fuel reprocessing or recycling streams (Bradbury and Baeyens, 2000; Carlton et al., 1993; Choppin, 2007; Maher et al., 2012; NCRP, 2006; Schulte and Scoppa, 1987). The Department of Energy's (DOE) SRS is one of several active legacy DOE locations in the United States for which this type of radioactive environmental contamination is present (Burger, 2000; Carlton, 1997; Carlton et al., 1993, 1992; Evans et al., 1992; Icenhower et al., 2010; Maher et al., 2012; NCRP, 2006; Savannah River Nuclear Solutions, 2016; Schulte and Scoppa, 1987). In addition, the selected radionuclides are expected to be mobile to varying extents depending on the prevailing environmental conditions, among other factors, and therefore pose potential hazards to human and environmental health. Furthermore, this suite of radionuclides encompasses a wide range of biogeochemical behavior characterized by different sorption mechanisms, redox activity, solubility, overall mobility, and bioavailability allowing for a unique and self-consistent opportunity to intercompare the radionuclide specific biogeochemical effects throughout the specific studies encompassed by this work.

The presence and growth of plants at contaminated (or potentially contaminated) sites can lead to a variety of consequences, such as food-chain transport associated with

plant uptake and foraging activities, and increased contaminant mobility due to plant induced biogeochemical interactions that may alter the solubility and/or speciation of the contaminants (Dakora and Phillips, 2002; Huang et al., 1998; Jones and Darrah, 1994; Napier et al., 2007; Robertson et al., 2003; Wang et al., 2015). Thus, it is not entirely surprising that several long term SRS lysimeter experiments evaluating contaminant transport in the vadose zone have demonstrated upward migration that was hypothesized to be related to plant presence and uptake (Demirkanli et al., 2009, 2007; Kaplan et al., 2014, 2010). Considering the impactful role plants play in these transport phenomena, efforts to understand plant-mediated mobility of radioactive contaminants is an important consideration in management and stewardship strategies at legacy contamination sites, nuclear waste repositories, and nuclear material processing facilities. Since the grass species *A. virginicus* is a widespread native grass in the southern part of North America, including at SRS, and it is tolerant to a variety of stressors, such as nutrient poor soil, it was selected as the model plant species of interest for this work (Campbell, 1983; Ezaki et al., 2008). Additionally, wild type grass is the small terrestrial reference plant recommended in ICRP Publication 108, so utilizing a grass species as a model plant for this study allows for valuable comparison to ICRP parameters and values (ICRP, 2017, 2008).

1.2. Dissertation Overview

In order to achieve the overall goal of this dissertation, i.e., demonstrate an explicit, integrated, and holistic approach to environmental radiation protection, both environmental transport studies and non-human biota dosimetric model development were employed. The

central goal of the transport studies was to elucidate and quantify the factors associated with plant presence (*A. virginicus* specifically) that may play a role in the alteration of the speciation, mobility, and migration patterns of the radionuclides in the vadose zone of SRS soil. In order to evaluate this complex system in a systematic way and to quantify parameters of significance that were suspected to factor into the plant-mediated mobility of the radionuclides in the soil-plant-hydrologic system, the transport studies were broken into three phases. Interactions between individual system components were evaluated in the first two experimental phases (i.e., soil-pore water sub-system and plant-hydrologic sub-system), then, all three components were combined into an integrated system in the third experimental phase (i.e., soil-plant-hydrologic system). Concurrent with the transport studies, and to achieve the goal of demonstrating the integrative concept of holistic environmental radiation protection, several increasingly realistic plant-specific computational dosimetric models for *A. virginicus* were developed, compared (to one another and to ICRP values), and integrated with data from hydroponic plant uptake studies to determine organism dose rates as an example of application. A graphical representation of the evolution of the work developed in this dissertation is depicted in **Figure 1.1**.

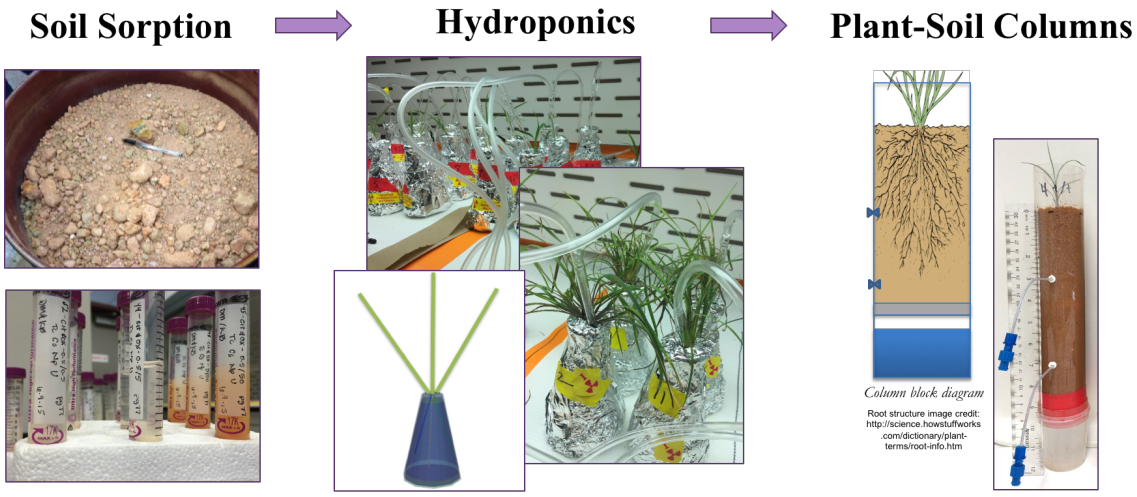

Figure 1.1: Graphical representation of the progression of the work in this dissertation.

The first set of experiments (Chapter 2) investigated the soil-pore water component. The objective of these experiments was to quantify distribution coefficients (K_d) of the radionuclides to SRS soil under baseline and organic acid amended conditions to evaluate the potential for plant exudates to modify the biogeochemical behavior of the radionuclides in the soil-pore water system. Batch sorption experiments were utilized with amended systems containing citrate and/or oxalate as plant exudate surrogates in varying ligand:radionuclide concentration combinations. For the highest ligand concentrations, increased sorption was noted for ^{237}Np and ^{99}Tc while ^{238}U sorption decreased and desorption of native ^{238}U was observed. Cesium sorption was not notably affected by the amendments to the system. This indicates that ligand presence, if available in sufficient quantities, may also affect the biogeochemistry of ^{99}Tc, ^{237}Np, and ^{238}U in an *in-situ* soil-

plant-hydrologic system and thus, may warrant consideration in robust environmental transport or risk assessment models.

The second set of experiments (Chapter 3) focused on plant uptake of the radionuclides in the plant-hydrologic system, i.e., hydroponic (HP) plant uptake. The objective of the HP studies was to quantify the potential for *A. virginicus* to take up and translocate the radionuclides in a controlled and ideal setting as well as to investigate differences associated with plant life stage. Seedling and established plant specimens were grown in a continually aerated, radionuclide spiked Hoagland nutrient solution under a 12-hour light cycle and were harvested at 24 hours, 3 days and 5 days. Digested plant tissues (roots and shoots) and HP solution were evaluated for radionuclide content to determine concentration ratios (CR, $\mu g_{radionuclide}$ kg^{-1} dry plant mass per $\mu g_{radionuclide}$ $L^{-1}$of HP solution) for comparisons between harvest day, plant part, and plant age. Translocation from roots to shoot tissues was greatest for radionuclides with nutrient analogs (i.e., ^{99}Tc and ^{133}Cs) while the actinides, ^{237}Np and ^{238}U, predominantly partitioned to root tissues. Additionally, seedling CRs were, in most cases, significantly greater than CRs for established plants. This was proposed to be, in part, due to greater relative transpiration rates, nutrient uptake, and biomass production for seedlings compared to established plants. Thus, in addition to geochemical and plant uptake considerations, plant life stage may influence radionuclide transport in the natural environment and related system-specific or dynamic environmental transport models.

The third set of experiments (Chapter 4) examined the combined soil-plant-hydrologic system. Minimal data exists examining combined soil-plant-water systems and

impacts of coupled physical, chemical, and biological reactions on radionuclide mobility and migration in the subsurface on a detailed (e.g. not bulk soil) level, particularly regarding upward migration of radionuclides (Ashworth et al., 2003; Ashworth and Shaw, 2006, 2005; Demirkanli et al., 2009, 2007; Kaplan et al., 2014, 2010; Wheater et al., 2007). Thus, the overall objective of this study was to evaluate to what extent the presence of *A. virginicus* affected the mobility and distribution of the radionuclides in laboratory-scale vegetated and unvegetated soil columns. Plant presence in soil columns resulted in significantly reduced radionuclide release from the columns for all radionuclides and significant alteration of radionuclide distributions within the soil profiles for ^{99}Tc and ^{237}Np, including notable upward migration for ^{237}Np. These effects were mainly due to plant transpiration induced hydrologic changes and radionuclide specific contributions from plant uptake. Soil profiles of ^{133}Cs and ^{238}U were not notably altered by plant presence due to their native abundance in SRS soil and their relatively high sorption affinities. However, analysis and comparison of soil, plant, and aqueous phase system components between treatment groups indicated that plant presence resulted in mobilization of native ^{238}U from the soil compartment and subsequent affiliation with plant tissues; thus, processes similar to the ligand facilitated desorption of native ^{238}U noted in the batch sorption experiments of Chapter 2 likely occurred in the rhizosphere soils of the column experiments and contributed to this effect. Overall, the results of these column experiments provided promising links to the experiments investigating individual system components (i.e., batch sorption and hydroponic uptake studies) as well an extensive data set that could

be utilized to develop, parameterize, and validate potential future radionuclide transport modeling efforts for this or similar systems.

In addition to the investigations into plant-mediated radionuclide transport, plant-specific computational dosimetric modeling was employed to extend the breadth of the experimental studies towards a more holistic consideration of environmental radiation protection, similar to the approach implemented for human radiation protection. Thus, the objective of Chapter 5 was to develop and compare several increasingly realistic organism-specific computational dosimetric models and to apply hydroponic plant uptake data (from Chapter 3) to determine organism dose rates as an example of application. Three different phantoms representing the organism and its immediate surroundings were created in this work: (1) a stylized phantom in which simple geometric shapes (e.g., ellipsoids, cylinders, etc.) represented plant (organs) and its surroundings, (2) a voxel phantom which utilized CT imagery of a plant specimen, and (3) a hybrid phantom based on the refinement of the voxel phantom. Monte Carlo dosimetric modeling was conducted with each phantom to determine dose coefficients (DC) associated with internal and external exposure of the plant. Comparison of modeled DCs to each other and to ICRP DCs for wild grass were generally consistent for internal DCs, but there were some deviations in external DCs due mainly to differences in phantom geometry. Whole-organism total dose rates determined from modeled DCs and ICRP DCs were comparable, but some differences in the relative contribution of external and internal sources of dose were noted, which is likely to have implications in dose-effect studies. The development of the models within this work have contributed significantly to the radioecology and environmental radiation protection

communities directly as they represent the first published voxel and hybrid models for any plant species. Additionally, as the models developed within this work were in relatively good agreement, it was recommended that a fit-for-purpose approach should be applied when considering use implementation of more complex dosimetric models in general, taking into account the level of detail and realism required for specific studies or evaluations.

1.3. Scientific Merit

The factors examined in this work (e.g., plant exudate activity and resulting radionuclide interactions and mobility effects, plant uptake, plant life stage, plant hydrologic requirements, etc.) can all have a significant impact on the overall transport through the vadose zone and subsequent transport into the biosphere through plant uptake. Depending on the radionuclide and prevailing system conditions some radionuclides will be affected more than others; for example, ^{99}Tc and ^{237}Np transport is greatly affected by the presence and growth of plants due to their inherent high mobility in oxic environments and subsequent movement with water in the system, including uptake into the plant itself. Thus, adequately investigating and quantifying these types of factors affecting radionuclide transport is paramount in developing appropriate, robust environmental transport and risk assessment models. Additionally, impacts to and dose received by non-human biota have gained more interest within contemporary radioecology and environmental radiation protection communities as they consider a more explicit and holistic approach to non-human biota radiation protection appropriate (Garnier-Laplace et al., 2015; Hinton et al., 2013; Mothersill et al., 2018; Sheppard, 2003; Thorne, 2018). This is, in part, achieved

through development of biologically relevant dosimetric models so that accurate dose-effect relationships can be evaluated allowing appropriate protection standards to be defined and implemented. Hence, the incorporation of organism-specific dosimetric modeling in this work is an example of how experimental biogeochemical transport experiments can be applied to inform computational dosimetry in radioecology and environmental radiation protection efforts. Overall, this dissertation demonstrates the multidisciplinary and interconnected nature of the radioecology and environmental radiation protection disciplines and how investigating these types of systems in an integrated manner, with individual components informing the more complex systems, can result in a broader and more nuanced understanding of the system overall.

CHAPTER TWO

THE INFLUENCE OF CITRATE AND OXALATE ON $^{99}Tc^{VII}$, Cs, Np^{V}, AND U^{VI} ON SORPTION TO A SAVANNAH RIVER SITE SOIL

[As published in the Journal of Environmental Radioactivity 172, 130-142 with minor revisions]

Abstract

Batch sorption experiments were conducted with 0.5 to 50 ppb ^{99}Tc, ^{133}Cs, ^{237}Np, and U in the presence and absence of citrate and/or oxalate in a 25 g/L Savannah River Site (SRS) soil suspension. Citrate and oxalate were the ligands of choice due to their relevancy to plant exudates, the nuclides were selected for their wide range of biogeochemical behavior, and the soil from SRS was selected as a model Department of Energy (DOE) site soil. Batch samples were continually mixed on a rotary shaker and maintained at a pH of approximately 5. Analysis via ICP-MS indicated that sorption of ^{237}Np increased with ligand concentration compared to baseline studies, as did sorption of ^{99}Tc although to a lesser extent. The increased sorption of ^{237}Np is proposed to be due to a combination of factors that are dependent on the ligand(s) present in the specific system including, ligand dissolution of the soil by citrate and formation of tertiary soil-oxalate-Np complexes. The increased ^{99}Tc sorption is attributed to the dissolution of the soil by the ligands, leading to an increase in the number of available sorption sites for ^{99}Tc. Uranium sorption decreased and dissolution of native uranium was also observed with increasing ligand concentration, thought to be a result of the formation of strong U-ligand complexes remaining in the aqueous phase. The majority of these effects were observed at the highest ligand

concentrations of 50 mg_C/L. No notable changes were observed for the ^{133}Cs system, which is ascribed to the minimal interaction of Cs^+ with these organic ligands.

2.1. Introduction

2.1.1. Background and motivation

Technetium-99 (^{99}Tc), cesium (^{137}Cs and ^{135}Cs), neptunium-237 (^{237}Np) and uranium (^{238}U, ^{235}U, and ^{234}U) are all present to varying extents in legacy nuclear waste, proposed spent nuclear fuel repositories and in potential fuel reprocessing and recycling streams (Bradbury and Baeyens, 2000; Carlton et al., 1993; Choppin, 2007; Maher et al., 2012; NCRP, 2006; Schulte and Scoppa, 1987). The quantitative distribution of the isotopes is system dependent. For example, all of the listed isotopes are present in legacy waste. Comparatively, whereas ^{99}Tc and ^{137}Cs are of major concern in advanced waste forms resulting from nuclear fuel recycling scenarios, the concentrations of actinides in such waste will be minimal. The selected radionuclides are long-lived risk drivers in the Department of Energy (DOE) complexes and are expected to be mobile and potentially hazardous to human and environmental health. Furthermore, this suite of radionuclides encompasses a broad range of biogeochemical behavior characterized by different sorption mechanisms, redox activity, solubility, overall mobility and bioavailability, and can thus be used to inform the behavior of similar radionuclides. Of the many DOE complexes, the Savannah River Site (SRS; Aiken, South Carolina) is the location of interest as this study is part of a larger DOE EPSCoR (Experimental Program to Stimulate Competitive Research) initiative in South Carolina. Increased site specific knowledge on the biogeochemical behavior and transport mechanisms of radionuclides (or other

contaminants of concern) allows for more appropriate and quantifiable risk assessment development which is pertinent in the management of such contamination in the environment (NCRP, 2006). While this work's intention is not to develop such a risk assessment model, it does provide important insights into mechanisms and factors that affect the environmental mobility of the aforementioned nuclides that may be of importance in the future improvement of appropriate risk management practices.

The overall objective of this work is to gain a conceptual understanding of Tc, Cs, Np, and U sorption to SRS soil in the presence and absence of naturally occurring organic ligands via batch sorption experiments in order to elucidate the potential for plant exudates to modify the biogeochemical behavior of these nuclides. The specific objectives of this study include:

(1) Provide baseline distribution coefficients to give an indication of the expected mobility and solid to aqueous partitioning of each radionuclide.

(2) Quantify the changes in the biogeochemical behavior of the aforementioned radionuclides in the presence of varying concentrations of naturally occurring plant relevant organic ligands.

(3) Identify what factors induce a significant impact on mobility in comparison to the baseline results and what mechanisms may be responsible for the changes.

2.1.1.1. Technetium

Technetium-99 is of particular environmental concern in spent fuel reprocessing and storage due to its relatively high fission yield (~6%), long half-life (2.11×10^5 years) and high mobility in oxic environmental conditions as the pertechnetate ion (TcO_4^-)

(Icenhower et al., 2010). Transport of technetium in the environment is governed by complex, coupled biogeochemical processes including redox reactions, complexation with organic exudates, uptake in plants, and sorption to mineral surfaces (Icenhower et al., 2010; Schulte and Scoppa, 1987). Technetium is predominantly found in the environment as pertechnetate, which is very weakly complexing and thus highly mobile with very low, sometimes even negative, distribution coefficient (K_d) values reported in literature (Icenhower et al., 2010; Kaplan et al., 2008). The minimal sorption is explained by the predominance of negative surface charge on sediments, which repel the anionic pertechnetate (Icenhower et al., 2010). However, there is potential for ligand (e.g., plant exudate) facilitated decrease in mobility if (1) Tc^{VII} is reduced to Tc^{IV}, (2) if complexation reactions occur with the ligands, or (3) if ligand facilitated disturbances of soil particles exposes more viable sorption sites on the mineral surfaces (Icenhower et al., 2010; Liu et al., 2012). Oxic conditions are expected to be maintained throughout this work, so ^{99}Tc is expected to persist in the system as the weakly interacting pertechnetate ion. Alterations to the soil will become an increasingly important factor affecting the sorption behavior of ^{99}Tc.

2.1.1.2. Cesium

Cesium-137 exists as a monovalent cation (Cs^+) in natural waters and is a contaminant of concern and risk driver at former nuclear materials processing facilities, such as SRS, due to its relatively long half-life (~30 years) and its relative abundance in legacy radiological waste (Zaunbrecher et al., 2015). With a much longer half-life, ^{135}Cs ($t_{1/2}$ = 2.3 million years) is a potential risk driver for longer-term disposition of spent

nuclear fuel or waste forms from reprocessing. A wide range of factors can influence the type and extent of Cs sorption and mobility in a system, including soil mineralogy, clay content, cation exchange capacity, concentration of Cs, presence of competing cations, moisture content, pH, ionic strength, etc. (Bostick et al., 2002; Goto et al., 2014; NCRP, 2006; Zaunbrecher et al., 2015b). The initial aqueous concentration of Cs in the system impacts the distribution coefficient by dictating the exchange site it will sorb to and how reversible that sorption process is with respect to competing ions (Bostick et al., 2002; Bradbury & Baeyens, 2000). Strong absorption to many types of clay is characteristic of Cs (Goto et al., 2008). Hydroxy-interlayered vermiculite (HIV) and kaolinite are the dominant clays in SRS soil, and the former has been attributed as the major sorption site for Cs in SRS soil (Goto et al., 2014; Zaunbrecher et al., 2015b). In particular, Cs exhibits a strong selectivity for the fairly limited HIV interlayer wedge sites (Goto et al., 2014; Zaunbrecher et al., 2015b). Cesium is held strongly in these HIV sites which govern the cation-exchange capacity of the SRS and can become strongly fixed to these sites over time (Goto et al., 2014; Zaunbrecher et al., 2015b). Goto et al. (2008) reported concentration dependent K_d values for various SRS soils ranging from 4.7 – 1460 L/kg for slightly acidic samples (pH of 4.12 to 4.92 closest to the conditions of this study), the majority of the K_d values were around or below 100 L/kg, apart from the very low cesium concentration samples. Due to the moderately strong sorption to the HIV grains present in SRS soils, Cs is expected to exhibit limited mobility in the subsurface, although its presence in pore water yields the potential for biological uptake (Bostick et al., 2002; NCRP, 2006; Zaunbrecher et al., 2015b).

2.1.1.3. Neptunium

The long half-life (2.14 x 10^6 years) and high mobility in oxic conditions as the pentavalent neptunyl ion ($Np^VO_2^+$) make ^{237}Np an environmental concern. Even with the relatively low yield (0.03%) of ^{237}Np in spent fuels initially, the long half-life of ^{237}Np results in its dominance after 100,000 years (Kaszuba and Runde, 1999). The presence of Np as $Np^VO_2^+$ under environmental conditions indicates that Np, similar to Tc, will be weakly complexing, and resistant to hydrolysis due to its relatively low effective charge compared to actinides of other (III, IV and VI) oxidation states (Choppin, 2007). Studies on similar SRS soils have resulted in distribution coefficient (K_d) values of 4.26-9.05 L/kg (Miller, 2010). Law et al. reported microbial mediated reduction of Np^V to Np^{IV} results in increased complexation and sorption to minerals, with reported slow ability to reoxidize and remobilize after reduction (2010). Generally sorption of Np(V) to mineral surfaces will increase with increasing pH; however, several studies have found that complexation of Np(V) with carbonate and natural organic matter can decrease sorption at high pH values (Arai et al., 2007; Girvin et al., 1991; Kohler et al., 1999; Li & Tao, 2003; Schmeide & Bernhard, 2010). Under the oxic conditions of this study, neptunium is expected to persist in the pentavalent state. Geochemical speciation modeling discussed below shows that neptunium will persist as the free NpO_2^+ ion as well as Np(V)-citrate and Np(V)-oxalate complexes. Thus, the influence of changes in neptunium chemical speciation on sorption to SRS soil will be examined in this work.

2.1.1.4. Uranium

The ubiquitous presence and high relative quantity of uranium in legacy nuclear waste, spent nuclear fuel, uranium or nuclear material processing facilities, and proposed nuclear fuel repositories dictates that it is a major nuclide of concern in the environment (Choppin, 2007; Dong and Wan, 2014; Maher et al., 2012). Uranium is found in the hexavalent state in aqueous oxic environmental conditions as the uranyl ion ($U^{VI}O_2^{2+}$) with high solubility and mobility (Morss et al., 2010). Its presence in the hexavalent state dictates that it undergoes hydrolysis above pH of about 3 and exhibits a relatively high complexation affinity with many ligands (compared to Np^{V} and Tc^{VII}) including carbonate, citrate, and oxalate (Clark et al., 1995; Morss et al., 2010). Additionally, U^{VI} also readily sorbs to mineral surfaces resulting in comparatively high K_d values, substantially greater than those for the other nuclides in this study. Uranium is also present in the tetravalent oxidation state under reducing conditions corresponding with a low solubility, producing precipitates such as uraninite (UO_2) (Maher et al., 2012). Formation of U(VI) complexes with carbonate, citrate, and oxalate change the formal charge of the uranyl ion and minimize sorption to mineral surfaces at circumneutral pH values as neutral or negatively charged U:ligand complexes partition to the aqueous phase (Alliot et al., 2005; Kohler et al., 2004; Lenhart & Honeyman, 1999; Murphy et al., 1999). Under the conditions of this work, the hexavalent UO_2^{2+} ion is expected to persist and U(VI)-citrate and U(VI)-oxalate complexes will form based on the U:ligand molar ratios as discussed below.

2.1.1.5. Ligands/exudates

Several transition metals such as iron (Fe), zinc (Zn), manganese (Mn) and copper (Cu), are essential for the normal physiology of plants, as they serve as cofactors for many key enzymes involved both in carbon and nitrogen metabolism and are vital for the normal functioning of mitochondria and plastids (Romheld and Marschner, 1991). However, the bioavailability of these transition metals in most soils is typically orders of magnitude lower than plant needs (Schmidt, 1999). For example, iron, though the fourth most abundant element in the Earth's crust, is the third most limiting nutrient for plant growth, due to its limited solubility (Lindsay and Schwab, 1982; Schmidt, 1999). Hence, plants rely on elaborate strategies, with multiple layers of redundancy, for the uptake of metal nutrients from soils (Curie and Briat, 2003). During most forms of nutrient stress, roots actively or passively release significant amounts of cellular metabolites into the rhizosphere (Bais et al., 2003). These rhizodeposites are comprised of complex mixtures of carbohydrates, amino acids, organic acids, phenolic compounds, fatty acids, sterols, vitamins, enzymes, purines/nucleosides as well as inorganic ions, gaseous molecules and root border cells all of which influence the acquisition of mineral nutrients (Dakora and Phillips, 2002). Sugars, amino acids, and organic acids are thought to be the major components of root exudates (Farrar et al., 2003). Organic acids directly facilitate the dissolution of metal nutrients from the insoluble mineral phase (Jones and Darrah, 1994), while amino acids and sugars indirectly affect plant nutrition by increasing microbial metabolism in the rhizosphere (Farrar et al., 2003). In soil, the reaction of organic acids with different metals depends on many factors including solid phase sorption/desorption, diffusion rates, hydrolysation, and

microbial degradation. Citric and oxalic acids, the intermediaries of the energy generating tricarboxylic acid cycle, are the major components of most root exudates, especially in plants that experience micronutrient stress. For example, enhanced secretion of citrate has been reported for various plants encountering Fe deficiency, consequently forming Fe complexes that are readily absorbed by roots (Jones et al., 1996). Apart from increasing the bioavailability of metals, these organic acids could also decrease the metal toxicity through complexation reactions (Osawa and Kojima, 2006). Organic compounds in root exudates such as organic acids, alcohols, phenols and proteins may also function as carbon and nitrogen sources for microorganisms capable of degrading organic contaminants (Salt et al., 1998). Hence, root exudates play a fundamental role in the mobility and availability of metal ions through diverse mechanisms.

2.1.2. Working Hypothesis

Ligands interact with soil surfaces and/or aqueous metal ions via various mechanisms potentially leading to alteration of the normally observed metal ion sorption in the absence of ligands (Parks, 1990; Schindler, 1990; Stumm, 1992). The general interactions of the ligand coupled with the particular geochemical behavior unique to each radionuclide ion will dictate the overall effect on sorption in the presence of the ligand amendment. Among the factors that dictate an ion's interaction probability, the effective charge of the ion is fundamental to the prediction of ion interaction. For example, the hexavalent UO_2^{2+}, with the highest effective charge in this suite of ions, is expected sorb strongly to surfaces and have comparatively high complexation affinity. Whereas, TcO_4^- is expected to behave in a contrasting manner resulting in minimal sorption and low

complexation affinity. Cs^+ and NpO_2^+ are expected to behave in less extreme manners, with Cs^+ exhibiting a higher sorption affinity as compared to NpO_2^+.

Three notable processes are hypothesized to be the main means of interaction between the ligands (citrate and/or oxalate) and the other components in the system, i.e. the radionuclide ($^{99}TcO_4^-$, $^{133}Cs^+$, $^{237}NpO_2^+$ and UO_2^{2+}) and/or Savannah River Site soil, leading to changes in observed metal sorption:

(1) Ligand-metal radionuclide aqueous complexation, L-M complexes (Stumm & Morgan, 1996). Formation of L-M complexes will effectively decrease the sorption of the radionuclide to the soil surface as the L-M complex remains in the aqueous phase. This will be most probable for metal ions with an inherently strong sorption affinity; in this case UO_2^{2+} is expected to be affected by this type of ligand interaction if the ligand-uranyl complex outcompetes the sorption of UO_2^{2+} to the soil surfaces.

(2) Formation of type B ternary complexes between the soil surface, polydentate ligand and metal radionuclide, S-L-M complexes (Schindler, 1990; Stumm, 1992). Type B ternary complexes will result in increased sorption of the radionuclide to the soil surface for those radionuclides that would otherwise weakly sorb in absence of complexing ligands. The likely candidate for effects due to this type of interaction is NpO_2^+ as it is a weakly sorbing ion in general, mainly staying in the aqueous phase in the absence of chelating ligands and weakly complexes with the ligands when present.

(3) Ligand promoted dissolution of mineral surfaces of the soil, similar to that described by Stumm (1992). This dissolution or mineral surface disturbance will lead to an increase in sorption due to a greater available surface area as the particle size of the solids decrease (Parks, 1990). An increased reactive surface area could also be the result of disaggregation of smaller particles and the dispersion of surface coatings of larger mineral grains. The increased sorption resulting from this mechanism is an indirect effect of the ligand interacting with the soil surfaces and particles as compared to a direct effect on the metal radionuclide ion as described in hypothesis (1) and (2). This type of ligand interaction will most likely induce a sorption increase for ions that are normally weakly sorbing or complexing such as, TcO_4^- and NpO_2^+ as more sorption sites become available.

2.2. Materials and Methods

2.2.1. Batch sorption methods

The soil samples used in this study were taken from SRS's West Borrow Pit; the properties are summarized in **Table 2.1**. The surface area was determined using $N_2(g)$ adsorption on a Micrometrics ASAP 2020. Potentiometric titrations of the SRS soil were performed in 50 g/L soil suspensions in 0.01 M, 0.05 M, and 0.1 M NaCl using a Metrohm 836 Titrando. Cation exchange capacity (CEC) and acidity were determined by Mehlich extraction by Clemson University's Agriculture Service Laboratory. Extractable Fe and Al was determined by citrate-bicarbonate-dithionite (CBD) extraction (Loeppert and Inskeep, 1996) and organic matter content was determined by loss on ignition (Nelson and

Sommers, 1996). The particle size was determined using a standard hydrometer method (Gee and Bauder, 1996).

Table 2.1: Chemical and physical characteristics of the SRS soil

Property	Measurement
Surface Area	14.1 m^2/g
pH (50/50 soil/water)	4.76
Point of zero charge	4.9
Sand/Silt/Clay (%)	66/14/20
Organic matter	0.90%
CEC	3.3 meq/100g
Acidity	2.4 meq/100g
CBD extractable Fe	6.01 ± 0.68 mg/g
CBD extractable Al	1.98 ± 0.20 mg/g

The soil properties listed in **Table 2.1** indicate this is a sandy clay loam. The relatively low organic matter content necessitated addition of organic ligands to simulate plant exudates. The CEC is relatively low but contains sufficient capacity to facilitate sorption of trace level radioisotopes such as ^{137}Cs. The moderate surface area and extractable Fe and Al content indicate there are reactive surfaces capable of binding relatively strongly sorbing ions such as NpO_2^+ and UO_2^{+2}. The low pH indicates a net negative surface charge will develop at circumneutral pH values that will enhance sorption of cations via increased electrostatic attraction. Each of these processes and properties along with the influences on radionuclide sorption will be discussed below.

A stock solution containing 100 ppb each of ^{133}Cs (a stable analog for ^{137}Cs and ^{135}Cs; High-Purity Standards, Charleston, SC), ^{237}Np (Eckert & Ziegler Isotope Products, Valencia, CA), ^{99}Tc (Eckert & Ziegler Isotope Products, Valencia, CA) and U (High-Purity Standards, Charleston, SC) was prepared in a background electrolyte solution of 0.01 M

sodium chloride (NaCl). The radionuclide stock solution was then adjusted to a pH value of 5 by adding small volumes of 0.1 M HCl or 0.1M NaOH. Three ligand stock solutions were prepared containing citrate, oxalate, and a mixture of citrate and oxalate at concentrations of 100 mg_C/L each for all solutions. The citrate stock solutions were prepared using sodium citrate dihydrate ($Na_3C_6H_5O_7 \cdot 2H_2O$; Fisher Scientific) and the oxalate stock solutions were prepared using oxalic acid dihydrate ($C_2H_2O_4 \cdot 2H_2O$; J. T. Baker). All three stock ligand solutions were prepared in a background electrolyte solution of 0.01 M NaCl and pH adjusted to 5 using the same method described previously. The background electrolyte solution of 0.01 M NaCl used in the preparation of the radionuclide and ligand stock solutions was selected in order to closely mimic natural conditions at SRS.

In order to examine the influence of organic ligands on radionuclide sorption to SRS soil an experimental matrix was developed to vary ligand (0.5, 5, and 50 mg_C/L) and radionuclide concentration (0.5, 5, and 50 ppb (or µg/L)) such that a matrix of nine samples were prepared from each ligand stock solution (citrate, oxalate and citrate/oxalate mixture) for a total of 27 ligand batch samples. This experimental matrix ensured each combination of radionuclide and ligand concentrations would be achieved in order to fully understand how each variable would influence the final result. A smaller subset of the experimental matrix of five samples for each ligand group were prepared as control samples without soil to determine if sorption to the walls of the centrifuge tubes had an influence for any of the radionuclides. The baseline batch set, without ligands, was prepared in triplicate to ensure a proper reference for comparison for a total of nine baseline batch samples.

Batch experiments were performed in 15 mL polypropylene centrifuge tubes with 0.25 g of SRS soil to 10 mL of aqueous solution to produce 25 g/L soil suspension. The aqueous phase consisted of a mixture of 0.01 M NaCl background solution, radionuclide stock solution, and ligand stock solution for the ligand batch sets or 0.01 M NaCl background solution and radionuclide stock solution for the baseline batch sets. Stock solution additions were carefully pipetted to achieve the desired concentrations defined in the experimental matrix; all additions were monitored gravimetrically.

After initial sample preparation, all samples were pH adjusted as needed to a pH of 5 and placed on an end-over-end rotating mixer. Sampling events at one, three and ten days of mixing were completed by removing a 1.3 mL homogeneous aliquot from each batch tube and centrifuging the aliquot for 20 minutes at 8000 rpm. After centrifugation, 1 mL of the centrifuged supernatant was diluted with 9 mL of 2% nitric acid (HNO_3) in preparation for analysis by inductively coupled plasma mass spectrometry (ICP-MS). After each sampling event and every day between the sampling events, the pH of each sample was measured and re-adjusted if necessary to a pH of 5 in order to maintain a constant pH throughout the experiment. Data for the ten day sampling event was used in calculations and reported herein, one and three day sampling data was monitored to verify the samples had reached equilibrium by the day ten sampling event.

Analysis, via ICP-MS, of samples collected and prepared at each sampling event was performed to determine the aqueous concentration of all four radionuclides in each sample. With knowledge of the initial aqueous concentration and the newly measured aqueous concentration, the concentration of nuclide sorbed to the soil could be determined

using the following equations. Equations are written for Np as an example but specific calculations were performed for each nuclide. The sediment concentration of Np ($\mu g_{Np}/kg_{sediment}$) was calculated using the following equation:

$$[\mathrm{Np}]_{sed} = \frac{\left([\mathrm{Np}]_{aqu,o} - [\mathrm{Np}]_{aqu}\right)V_L}{m_{sed}} \quad \textbf{(2.1)}$$

Where: $[\mathrm{Np}]_{aqu,o}$: Initial aqueous Np concentration (ppb, µg/L)

$[\mathrm{Np}]_{aqu}$: Equilibrated (ICP-MS measured) aqueous Np concentration (ppb, µg/L)

$[\mathrm{Np}]_{sed}$: Equilibrated sediment Np concentration (ppb, µg/kg)

V_L: Sample liquid volume, mL

m_{sed}: Sample sediment mass, g

The sediment water partitioning constant, K_d (mL/g), was calculated via the following equation:

$$K_d = \frac{[\mathrm{Np}]_{sed}}{[\mathrm{Np}]_{aqu}} \quad \textbf{(2.2)}$$

The percent of Np sorbed was calculated via the following equation:

$$f_s = 1 - \frac{[\mathrm{Np}]_{aqu}}{[\mathrm{Np}]_{aqu,o}} \quad \textbf{(2.3)}$$

The K_d equation (**Equation 2.2**) is numerically equivalent to the traditional K_d equation proposed in ASTM D4646 which has been used in previous sorption tests (ASTM, 2003; Kaplan, 2009). The changes observed in the K_d for each radionuclide were correlated with the influence the organic ligands, citrate and oxalate, had on the sorption of ^{133}Cs, ^{237}Np, ^{99}Tc and U to SRS soils.

2.2.2. Sequential Extraction Methodology

Sequential extraction was used to compare the leaching behavior of native Cs, Th, and U in the soil. It is important to note that no additional Cs, Th, or U was added to these soils. Therefore, these sequential extraction data give information on the long-term sequestration of Cs, Th, and U in soils. These data provide a comparison of the long-term equilibrium state of Cs and U relative to the short-term batch sorption experiments of this work. Two extraction procedures, mBCR and Tessier, were used for comparison (Rauret et al., 1999; Tessier et al., 1979). The mBCR procedure is a modified method of the Standards, Methods, and Testing Program (formerly Bureau Commune de Reference, BCR) of the European Commission. The fractions for the mBCR procedure are exchangeable, reducible, and oxidizable respectively, in order of decreasing mobility. The fractions for the Tessier procedure are exchangeable, bound to carbonates, bound to iron and manganese oxides, bound to organic matter and residual fractions respectively, in order of decreasing mobility. Each of the extraction steps are described below. Samples were rinsed with distilled deionized water between each extraction step. In all cases, a one gram aliquot of soil was carried through the extraction procedure and samples were prepared in triplicate. The reported uncertainties below are the standard deviation of triplicate measurements.

2.2.2.1. Tessier Method

1. The exchangeable fraction used 8 mL of 1.0 M magnesium chloride to extract the most mobile metal ions from the soil. These metals are sorbed to the surfaces of the soil, and are most readily bioavailable to the environment.

2. The bound to carbonates fraction used 8 mL of 1.0 M sodium acetate at pH 5. The metals in this fraction are susceptible to a change in pH (acidic solution). The metals in this phase are less mobile and are less readily available than the metals in the exchangeable fraction.
3. The bound to iron and manganese oxides fraction used 20 mL of 0.04 M hydroxylamine in 25% v/v acetic acid with a pH of 2. The metals in this fraction are susceptible to reducing conditions and are less mobile than the metals in the bound to carbonates fraction.
4. The bound to organic matter fraction used 3 mL of 0.02 hydrogen peroxide to decompose organic matter and 5 ml of 3.2 M ammonium acetate to induce oxidizing conditions necessary for metal extraction. These metals are released from decomposed organic matter and are less mobile than the metals in the bound to iron and manganese fraction.
5. The residuals fraction used 4 mL of perchloric acid and 20 mL of hydrofluoric acid to destroy crystal lattices and fully digest the soil sample. The metals in this fraction are assumed to be immobile and are not bio-available.

2.2.2.2. mBCR Method

1. The exchangeable fraction used 40 mL of 0.11 M acetic acid to extract the most mobile metal ions from the soil.
2. The reducible fraction used 40 mL of 0.5 M hydroxylamine hydrochloride at pH of 1.5. The metals in this fraction are susceptible to a change in pH (acidic solution)

and reducing conditions. The metals in this phase are less mobile and are less readily available than the metals in the exchangeable fraction.

3. The oxidizable fraction used hydrogen peroxide to decompose organic matter and 50ml of 1 M ammonium acetate to induce oxidizing conditions necessary for metal extraction. These metals are released from decomposed organic matter and are less mobile than the metals in the reducible fraction.

2.3. Results and Discussion

2.3.1. Geochemical Speciation Modeling

As one of the critical elements of this study is to quantify the influence of citrate and oxalate on radionuclide sorption to SRS soil, simulations of each radionuclide-ligand system were performed to determine the aqueous species of each radionuclide present in each case. Simulations were performed using Geochemist workbench v8 using the LLNL thermochemical database (Delany and Lundeeen, 1990). The exact concentrations of radionuclides and ligands used in the experimental portion of this work were used in the simulations. Even the highest concentrations of citrate and oxalate used in this work were not sufficient to form complexes with cesium and will not form complexes with technetium. Thus, Cs^{+} and TcO_4^{-} are expected to persist. However, there were significant changes in uranyl and neptunyl speciation with changing ligand concentrations. Formation of $NpO_2(C_2O_4)^{-}$ and $NpO_2(C_2O_4)_2^{-3}$ complexes increased as the oxalate concentration increased (**Figure 2.1a**) and this was coincident with the decrease in the concentration of free NpO_2^{+}. The 1:2 complex $NpO_2(C_2O_4)_2^{-3}$ formation is limited until the concentration of oxalate is at the highest level. Formation of $NpO_2(citrate)^{-2}$ complexes were limited in the

mixed Np-citrate-oxalate simulations and were limited to less than 5% in the binary Np-citrate simulations. Thus, in the combined oxalate-citrate-neptunyl system, the Np-oxalate complexes and the free NpO_2^+ ion persisted. Similar behavior was observed for the uranyl system though there was a greater extent of $UO_2(citrate)^-$ and $UO_2(C_2O_4)_2^{-2}$ formation as compared with similar neptunyl complexes (**Figure 2.1b**). Formation of these metal-ligand complexes is hypothesized to influence the extent of Np(V) and U(VI) sorption as discussed in the hypotheses above. Such speciation analysis is used in the results and discussion section below to infer the influence of changes in speciation on radionuclide sorption.

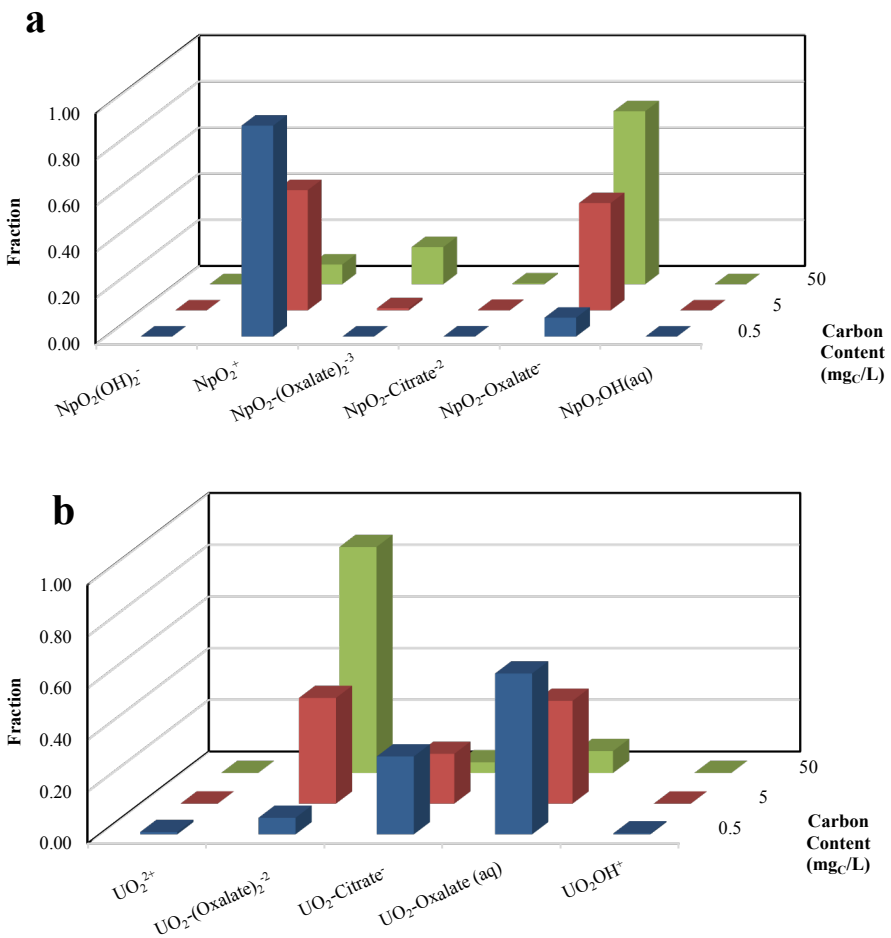

Figure 2.1: Geochemical speciation simulations of Np(V) (a) and U(VI) (b) in the presence of both oxalate and citrate simultaneously at pH 4.8 in 10 mM NaCl. Citrate and oxalate concentrations are listed in the legend. Simulation performed using Geochemist Workbench v8 and the thermo.com.V8.R6+ database (Delany and Lundeeen, 1990).

2.3.2. Sequential Extraction Data

The sequential extraction data from the mBCR and Tessier procedures are shown in **Figure 2.2**.

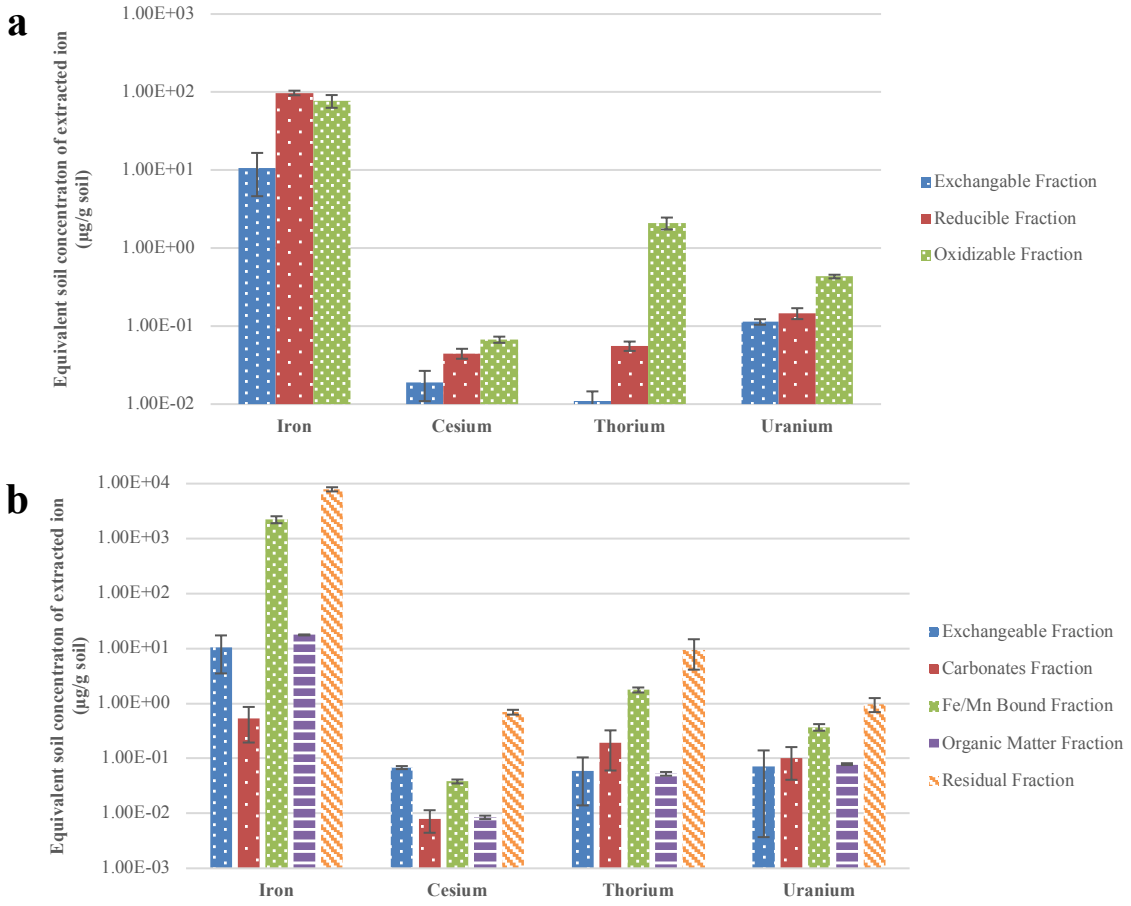

Figure 2.2: Selected results from mBCR (a) and Tessier (b) sequential extraction studies.

These data indicate a complimentary nature of the sequential extraction techniques. The most notable difference is greatly increased extraction of all ions using the Tessier method compared with mBCR. Cs partitioning is primarily in the exchangeable and residual fractions of the Tessier method. Both uranium and thorium are most strongly found in the "residual" fraction though low concentrations are leached into all phases. The

observation of the majority of native Cs, Th, and U in the "residual" fraction of the Tessier method indicates the potential for an aging process through which these elements become more strongly bound to the soil matrix with time. This is particularly notable for Cs, which is expected to bind to mineral surfaces via ion exchange and would be expected in the "exchangeable" fraction. As discussed below, Cs exhibits relatively weak sorption and the K_d values decrease with increasing total Cs concentration. Furthermore, previous studies have demonstrated that Cs primarily sorbs via ion exchange and thus is expected to be found within the exchangeable fraction (Goto et al., 2014; Zaunbrecher et al., 2015b). The second largest pool of Cs is found in the exchangeable fraction and the largest pool is in the residual fraction. This change from the labile exchangeable fraction to the relatively recalcitrant residual fraction is hypothesized to be due to Cs migration into clay layers as previously observed for mica (Brouwer et al., 1983; Comans and Hockley, 1992; Sawhney, 1972; Zachara et al., 2002; Zaunbrecher et al., 2015a). This soil is dominated by kaolinite clays with <5% smectite/illite clay phases. Migration of Cs into clay interlayers has been demonstrated for 2:1 clays phases and, though there is a relatively low concentration of these phases in this SRS soil, even a small fraction would be sufficient for sorption of the relatively low Cs concentration used in these experiments (Goto et al., 2014; Zaunbrecher et al., 2015b).

Iron occurred at the highest concentrations of all analytes measured and was present in all leached fractions. Previous studies have shown strong sorption of uranium to iron oxide phases (Bargar et al., 2000; Dong and Wan, 2014; Giammar and Hering, 2001; Lenhart and Honeyman, 1999; Payne et al., 1998; Waite et al., 1994). Therefore, it is

expected these phases will be the dominant sorption sites for uranium. This is consistent with the sequential extraction data where the largest pools of iron and uranium are found in the Fe/Mn oxide extraction and residual fraction of the Tessier method. A similar correlation was not observed for the mBCR extraction. The largest pool of iron was found in the reducible and oxidizable fractions. This is likely due to reduction of Fe(III) to more soluble Fe(II) by hydroxylamine hydrochloride in the reducible fraction and complexation of iron with acetate (which is present at a higher concentration in the oxidizable fraction relative to the exchangeable fraction). Additionally, uranium is expected to become more strongly sorbed upon reduction thus, the largest pool of uranium is found in the oxidizable fraction. The observation of correlated partitioning of iron and uranium in the sequential extraction data indicates that the sorption behavior discussed below can be described as a competition between uranium complexation with oxalate and citrate and uranium sorption to iron oxide mineral phases.

2.3.3. Baseline K_d values

The average distribution coefficients for the baseline experiments (no ligand present) were found to be within ranges previously reported for similar soils (**Table 2.2**).

Table 2.2: Average baseline distribution coefficients

Nuclide	Average K_d(mL/g)	SD	Minimum	Maximum	Range from previous studies
^{99}Tc	-0.2	0.9	-3.0	1.1	-2.9 – 11.2 [a]
^{133}Cs	108	72	4	245	4.7 – 1460[b]
^{237}Np	5.5	1.8	2.3	7.7	4.26 – 9.05 [c]
^{238}U (low)	813	33	785	849	1.2 – 34,000 [d]
^{238}U (high)	3476	176	3324	3744	

[a](Kaplan et al., 2008) [b](Goto et al., 2008) [c](Miller, 2010) [d](Serkiz and Johnson, 1994) .

Two values are shown for uranium because non-linear sorption was observed, with higher K_d values associated with samples having initial concentrations of 5 ppb and 50 ppb. The general sorption trend follows what is expected based on the effective charge of the ion, ion size, complexation affinity and the predominance of negatively charged surface sites for the sediment with $UO_2^{2+} >> Cs^+ > NpO_2^+ > TcO_4^-$.

2.3.4. Ligand effects on soil

Increasing the ligand concentration resulted in greater dispersion of the soil suspension in which the clay portion of the soil stayed suspended for longer. This is proposed to be due to disaggregation of the particles and development of a net repulsive surface charge. Although limited, particle size analysis on select samples suggests that only the 50mg_C/L citrate or citrate/oxalate samples were correlated with smaller particle sizes (<1000nm) in comparison to 0.5 mg_C/L. SEM investigation into the effects of ligand concentration on the soil show that the clay fraction appears to be removed from the silicate sand grains when exposed to higher ligand concentrations (**Figure 2.3**). This dissolution of the clay portion of the sediment has the potential to impact the sorption and mobility of the radionuclides in question by either exposing more available surface sites for sorption or allowing for leaching of native uranium from the soil.

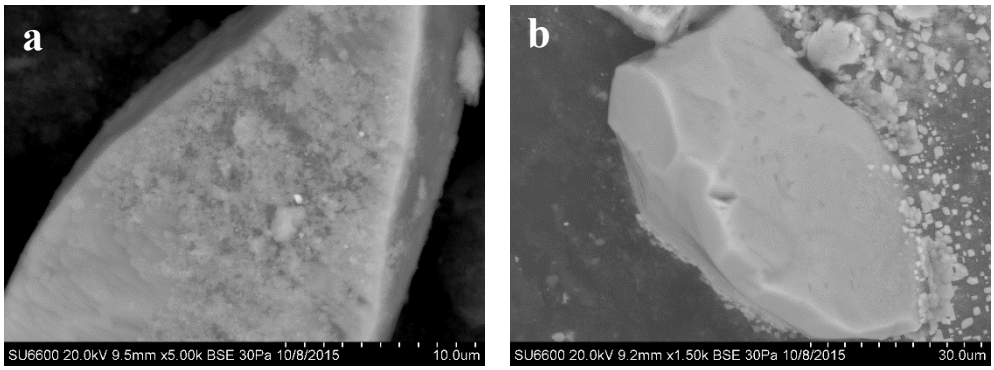

Figure 2.3: SEM images of a silicate sand grain from a 0.01 M NaCl, 25 g/L SRS soil solution with (a) 0.5 mg_C/L each of citrate and oxalate and (b) 50 mg_C/L each of citrate and oxalate. The grain with the higher ligand concentration (b) is stripped of the clay coating seen on the silicate grain in presence of low ligand concentration (a).

2.3.5. Technetium

The distribution coefficients for ^{99}Tc and SRS soil with varying concentrations of citrate and oxalate are shown in **Figure 2.4**. The presence of 50 mg_C/L generally resulted in slightly increased sorption of technetium to SRS soil. The maximum baseline ^{99}Tc K_d value from these studies was 1.1 mL/g (**Table 2.2**). In comparison, the citrate/oxalate mixture (**Figure 2.4c**) produced the greatest increase in K_d values (maximum K_d of 4.3 mL/g). Citrate and oxalate alone (**Figure 2.4a** and **Figure 2.4b** respectively) also resulted in higher sorption for the highest ligand concentrations, to a lesser degree than the combination of ligands, with maximum K_d values of 2.6 and 2.8 mL/g, respectively. Lower concentrations of citrate and/or oxalate did not result in any substantial departures from baseline values with the exception of one anomolous low value for citrate at 5 mg_C/L and 5 ppb ^{99}Tc (**Figure 2.4a**).

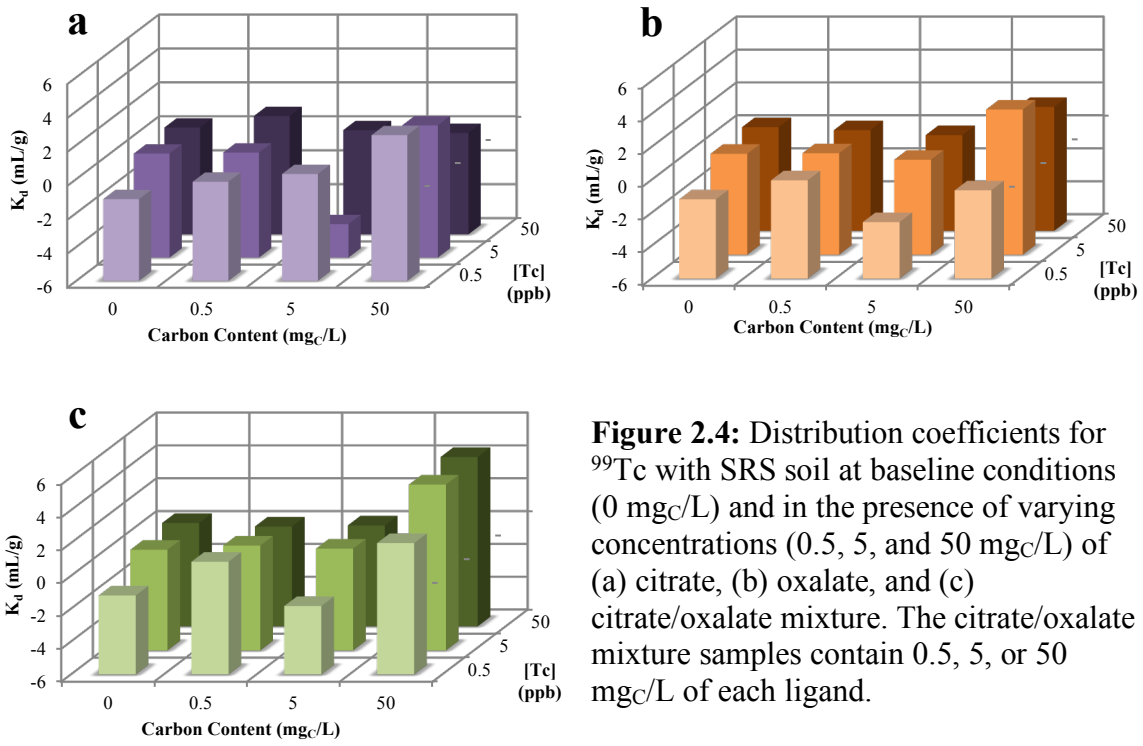

Figure 2.4: Distribution coefficients for ^{99}Tc with SRS soil at baseline conditions (0 mg_C/L) and in the presence of varying concentrations (0.5, 5, and 50 mg_C/L) of (a) citrate, (b) oxalate, and (c) citrate/oxalate mixture. The citrate/oxalate mixture samples contain 0.5, 5, or 50 mg_C/L of each ligand.

The primary mechanism resulting in the increased sorption observed for ^{99}Tc with increasing ligand concentration is proposed to be an indirect effect due to the soil disturbances caused by the ligands. Based on the point of zero charge of 4.9, the SRS soil is expected to have mostly neutral or negative surface sites at pH of 5. Therefore, the anionic pertechnetate sorbs very weakly to it. The slight increase in sorption at higher ligand concentrations can be attributed to the increase in exposed mineral surface area and sorption sites due to the ligand facilitated disaggregation of the soil particles. Visual observations and dynamic light scattering measuremtnes have indicated that the soil particles become more dispersed with increasing ligand concentration. The resulting decrease in particle size aggregates is proposed to yield a greater amount of reactive surface

area which causes ain increase in Tc sorption. This phenomena is consistent with working hypothesis (3).

Working hypothesis (1) and (2) are not supported for ^{99}Tc. Since technetium is present as the very weakly interacting pertechnetate, it is not expected to form L-M complexes with the citrate or oxalate, both of which are anionic at the pH used for this study. This expectation coupled with the experimental observation that sorption of ^{99}Tc increases with an increase in ligand concentration, versus decreasing, leads to the dismissal of working hypothesis (1). Additionally, the inability of ^{99}Tc to complex with citrate or oxalate alone also indicates that a tertiary complex is not expected to form, refuting working hypothesis (2) for ^{99}Tc.

2.3.6. Cesium

Distribution coefficients calculated for ^{133}Cs in the presence of citrate, oxalate, and a mixture of both citrate and oxalate can be seen in **Figure 2.5**, along with baseline distribution coefficients. All three ligand-radionuclide systems exhibit the same behavior and show no influence of ligand concentration on the distribution coefficients. These results are consistent with the preliminary simulations performed in Geochemists Workbench, which showed no Cs-ligand complexes forming at even the highest ligand concentrations. Differences in the distribution coefficients seen in **Figure 2.5** can be attributed to an initial ^{133}Cs concentration dependence which is consistent with the ion exchange model of Cs sorption (Bostick et al., 2002; Bradbury and Baeyens, 2000; Zaunbrecher et al., 2015b). These results show no influence of the presence of ligands or

the concentration of ligands on the distribution coefficient of ^{133}Cs in SRS soils as compared to baseline values presented in **Table 2.2**.

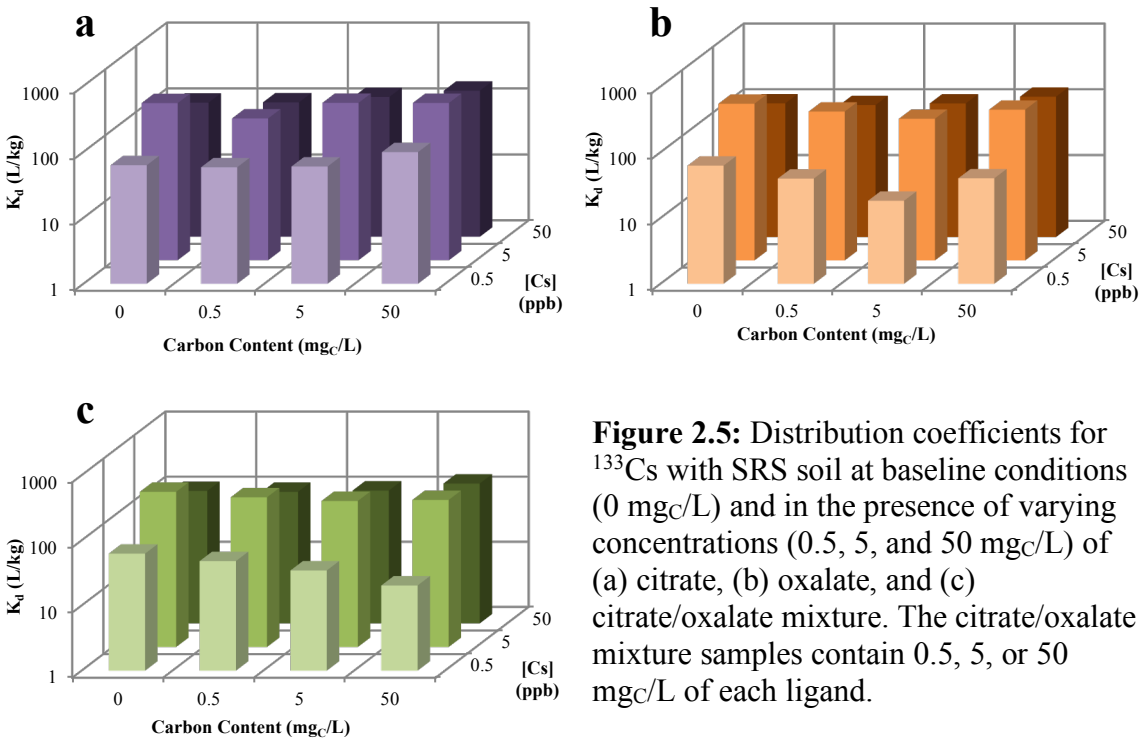

Figure 2.5: Distribution coefficients for ^{133}Cs with SRS soil at baseline conditions (0 mg_C/L) and in the presence of varying concentrations (0.5, 5, and 50 mg_C/L) of (a) citrate, (b) oxalate, and (c) citrate/oxalate mixture. The citrate/oxalate mixture samples contain 0.5, 5, or 50 mg_C/L of each ligand.

2.3.7. Neptunium

Citrate alone induced the greatest effect on sorption of ^{237}Np at high citrate concentrations with a maximum K_d value of 476 mL/g for the 50 mg_C/L, 0.5 ppb ^{237}Np sample compared to baseline values between 4.4 and 6.7 mL/g; less drastic effects were observed for higher ^{237}Np concentrations (**Figure 2.6a**). The use of oxalate alone had a much less extreme effect compared to the use of citrate. In the oxalate only system the K_d approximately doubled between the baseline and 50 mg_C/L values for all ^{237}Np concentrations with a maximum value of 13 mL/g (**Figure 2.6b**). The citrate/oxalate

mixture produced similar results to the citrate experiment, but to a lesser extent, with a maximum K_d of 168 mL/g (**Figure 2.6c**).

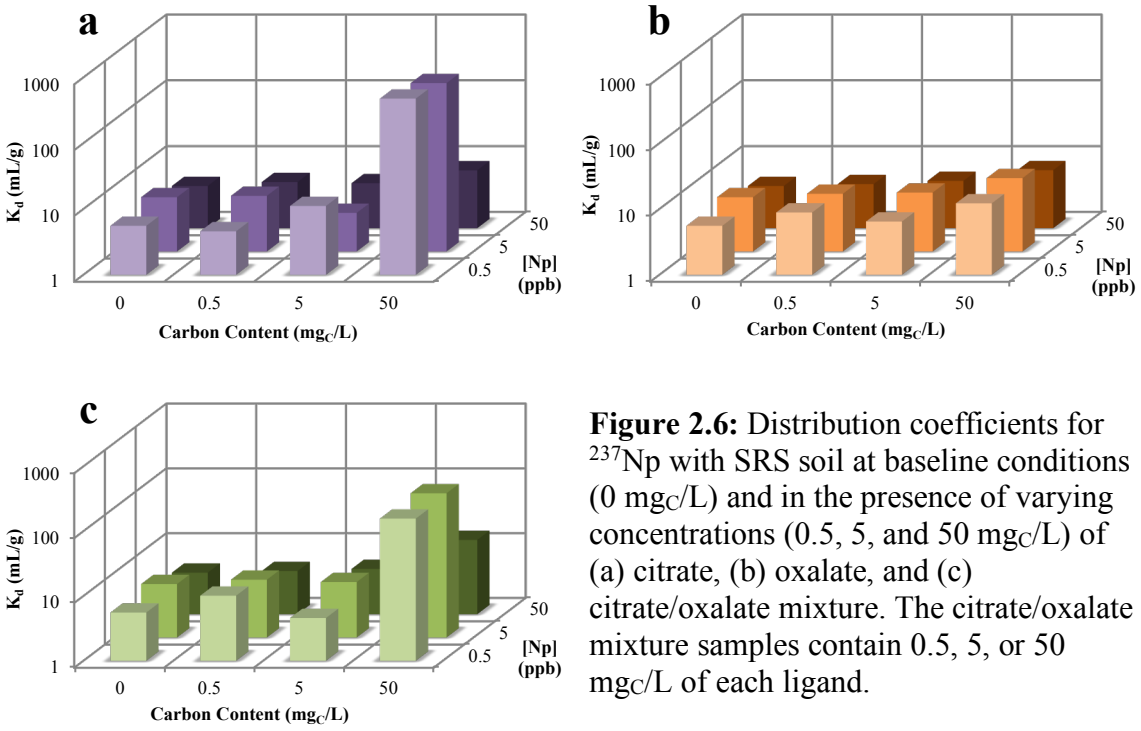

Figure 2.6: Distribution coefficients for ^{237}Np with SRS soil at baseline conditions (0 mg_C/L) and in the presence of varying concentrations (0.5, 5, and 50 mg_C/L) of (a) citrate, (b) oxalate, and (c) citrate/oxalate mixture. The citrate/oxalate mixture samples contain 0.5, 5, or 50 mg_C/L of each ligand.

Geochemist Workbench models presented in section *2.3.1* show that $^{237}Np^{V}O_2^+$ complexes very weakly with citrate but it has a greater affinity for complexation with oxalate. The complexation of ^{237}Np increases with increasing oxalate concentration ranging from 8% to 91% of the total aqueous ^{237}Np being complexed with oxalate at 0.5 mg_C/L to 50 mg_C/L respectively. This differing complexation affinity between ligands for ^{237}Np along with the experimental results (**Figure 2.6**) suggest support of several of the presented working hypothesis.

2.3.7.1. Neptunium and Citrate

The weak complexation affinity of ^{237}Np with citrate indicates that there will be minimal or no effect on sorption of ^{237}Np due to Np-citrate complexes. Furthermore, tertiary complexes are thus not expected to form. This is sufficient evidence to reject working hypothesis (1) and (2). In absence of tertiary complexes, the drastic increase in sorption at high citrate concentrations is most likely due to ligand induced disturbances of the sediment, which expose a greater number of surface sites for which ^{237}Np strongly binds; support of working hypothesis (3). The less drastic increase in K_d associated with the 50 mg_C/L, 50 ppb ^{237}Np sample indicates that a limited number of excess sorption sites were exposed as a result of the ligand promoted dissolution of the sediment.

2.3.7.2. Neptunium and Oxalate

The strong complexation affinity between ^{237}Np and oxalate accompanied with the (approximately two-fold) increase in experimental K_d values indicate that working hypothesis (2) is supported for the oxalate system. At low oxalate concentrations, as the oxalate complexes with the ^{237}Np, the majority of the Np-oxalate complex remains in the aqueous phase, as indicated by the lack of K_d increase at low and medium oxalate concentrations. Since the sorption affinity to the soil for ^{237}Np is already low and a further decrease in sorption was not observed, the Np-oxalate complex is not considered more favorable than the ^{237}Np sorption reaction for the fraction that has already sorbed. Thus, working hypothesis (1) is not supported. However, as the oxalate concentration is increased further, to 50 mg_C/L, a larger fraction of the ^{237}Np exists as Np-oxalate complex as shown in the Geochemist Workbench models of section *2.3.1* (see **Figure 2.1a**). Hence, it

becomes favorable under these conditions for a ternary, S-oxalate-Np, complex to form and noticeably increase the sorption of ^{237}Np. Thus, evidence for support of working hypothesis (2). Oxalate is not expected to have as drastic an effect on the soil surfaces as citrate, thus working hypothesis (3) is not considered to be a majority factor leading to the increased sorption observed in the oxalate system.

2.3.7.3. Neptunium, Citrate and Oxalate

The presence of both citrate and oxalate produced intriguing results that support multiple working hypothesis. Based on the citrate/oxalate results, comparison to the single ligand systems, Geochemist Workbench models supporting Np-oxalate complexation (and thus, S-oxalate-Np formation) as well as the citrate promoted dissolution of the soil, it appears that all working hypothesis are supported for this system. Comparing the citrate/oxalate system to the citrate system, the maximum K_d values decrease by about a third, supporting working hypothesis (1). This is thought to be due to the Np-oxalate complex forming, limiting sorption of ^{237}Np to the soil to some degree over the citrate system. As the citrate is still present and there is still a drastic increase in sorption in comparison to baseline results it is concluded that citrate induced disturbances of the soil still occurs thus, working hypothesis (3) is supported. In essence, the increase in sorption sites created by citrate dissolution of the soil increases sorption, as was done in the citrate system but, the presence of oxalate and the favorability of the Np-oxalate complex over the Np-S sorption reaction hinders this increase. It is also likely that some fraction of the Np-oxalate form Np-oxalate-S ternary complexes as proposed in the oxalate system, support of working hypothesis (2), but this is less obvious and judging by the only two fold K_d

increase in the oxalate system it is a minor effect in comparison to the citrate dissolution of the soil.

2.3.8. Uranium

Geochemist Workbench models presented in section *2.3.1* show that greater than 99% of the aqueous uranium is complexed with either citrate or oxalate when the ligands are present, i.e. there is almost no free uranium in solution when these ligands are available. Thus, the ligands strongly bind uranium and as the ratio of ligand to uranium increases, a coincident decrease in sorption of uranium would be expected. For example, citrate and other ligands have been shown to cause desorption and solubilization and thus, mobilize uranium (Kantar and Honeyman, 2006; Lozano et al., 2011; Read et al., 1998). Overall, from the baseline conditions to the systems with 50 mg_C/L, this decrease in uranium sorption is experimentally confirmed and is most apparent in the 50 mg_C/L samples at the highest ligand to uranium ratios (i.e. the 0.5 ppb and 5 ppb samples with 50 mg_C/L) (**Figure 2.7**). The K_d values of the 50 ppb uranium with 50 mg_C/L of citrate or oxalate are also lower than the baseline, but to a lesser degree, specifically by 917 mL/g and 543 mL/g respectively (**Figure 2.7a** and **Figure 2.7b**). There is a more drastic decrease in K_d for the citrate/oxalate combination to ~3 mL/g for the 50 ppb uranium sample, the lowest positive K_d attained (**Figure 2.7c**). The three order of magnitude decreases in K_d value observed at 50 mg_C/L of the combined citrate and oxalate with 50 ppb uranium may be due to the alteration of the soil by citrate with further complexation by oxalate. The K_d values for samples containing 0.5 and 5 ppb uranium are negative for all 50 mg_C/L samples (**Figure 2.7**), indicating that not only are the ligands preventing adsorption but they are also

leaching native uranium from the soil. The distribution of uranium in this soil is unknown but is expected to be heterogeneous. Thus, the observed scatter in the data could be due to variations in the availability of native uranium in the soil. There are several outliers of this general decreasing trend within the data set for which no explanation has been determined as of yet; specifically, the slight increase in K_d values over baseline for several of the 0.5 and 5 mg_C/L samples (**Figure 2.7**). In general, the minimized sorption at high ligand concentrations indicates that the citrate and/or oxalate L-M complexes are more favorable for uranium than is sorption to the soil. Thus, eliciting a decrease in sorption as the L-M complexes are formed and stay in solution, supporting working hypothesis (1).

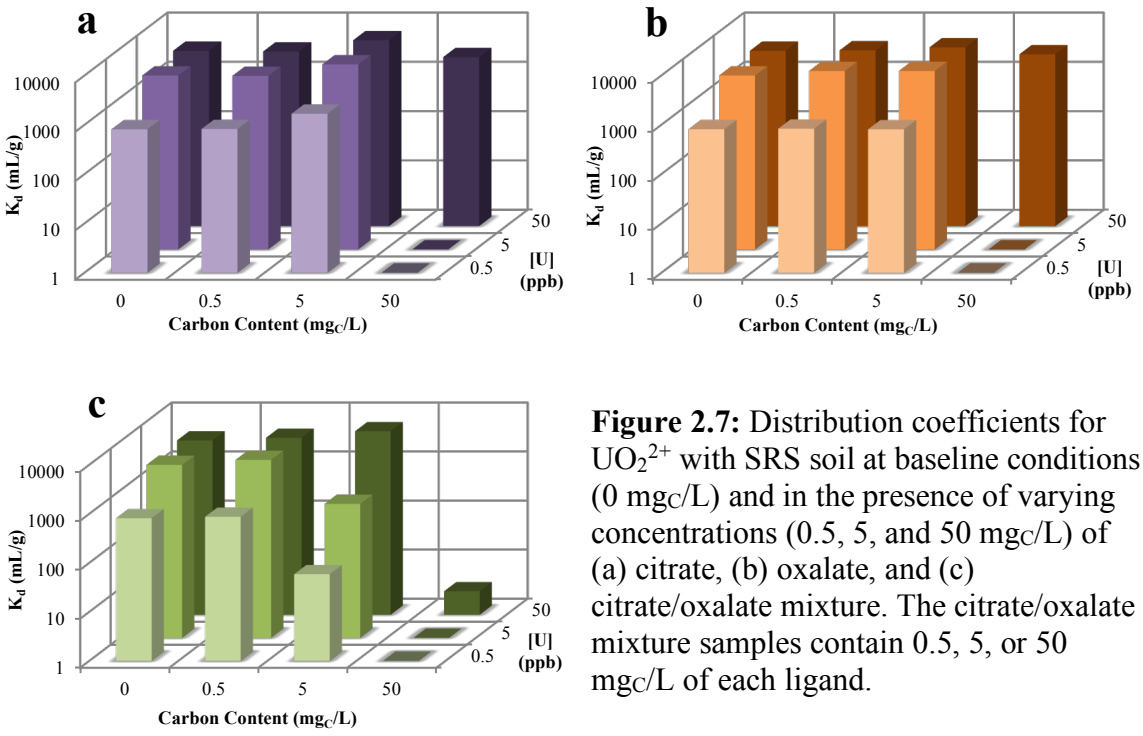

Figure 2.7: Distribution coefficients for UO_2^{2+} with SRS soil at baseline conditions (0 mg_C/L) and in the presence of varying concentrations (0.5, 5, and 50 mg_C/L) of (a) citrate, (b) oxalate, and (c) citrate/oxalate mixture. The citrate/oxalate mixture samples contain 0.5, 5, or 50 mg_C/L of each ligand.

Working hypothesis (2) and (3) do not appear to be supported in the uranium system. The rejection of these working hypotheses is based on the noted decrease in K_d

values with increasing ligand concentration. With regards to working hypothesis (2), this decrease indicates that the ligands are not forming ternary complexes with uranium and the soil surfaces. If such a complex were forming, an increase in K_d values would be observed with increasing ligand concentration. Furthermore, the rejection of working hypothesis (3) is corroborated since there was not an increase in K_d values for the highest citrate and/or oxalate concentrations as was observed for ^{99}Tc and ^{237}Np. Thus, it is evident that the L-U complexes appear to remain in the aqueous phase even if the surface coatings of the soil are disturbed as discussed above.

2.4. Conclusion

Amendment of batch sorption studies on SRS soil with citrate and/or oxalate increased the sorption of ^{99}Tc and ^{237}Np over baseline results for the highest ligand concentrations, had little to no effect on ^{133}Cs sorption, and decreased sorption of U (even causing dissolution of native uranium). The primary mechanism for the increased sorption of ^{99}Tc is hypothesized to be due to ligand facilitated dissolution of the clay fraction of the soil. This also is thought to play a role in the increased sorption of ^{237}Np combined with formation of Np-oxalate and thus, S-oxalate-Np complexes. The decreased sorption and dissolution of U is attributed to the favorability of ligand-U aqueous complexes over sorption to the soil. The alteration of the mobility and sorption behavior of ^{99}Tc, ^{237}Np and U in the organic ligand amended systems of this work indicates that if these ligands are present in the contaminated subsurface, the *in-situ* biogeochemistry of these nuclides has the potential to be altered.

The variability in the exhibited sorption behavior as a result of citrate and oxalate amendments is a result of the wide range of biogeochemistry of this suite of nuclides owing to the inherent properties, interaction mechanisms, and behavior of each particular type of ion. While these results were not entirely unexpected, they do provide valuable insight into the systems particular to SRS. Thus, these studies are seen as stepping-stones and the results herein will be used to guide future work in elucidating the potential impacts that plant exudates may have on the biogeochemical behavior of this suite of nuclides.

Additionally, the numerical K_d values and trends determined in these studies as well as the general effects of the ligands (particularly citrate) on the soil can be used to directly inform increasingly complicated miscible displacement studies and modeling efforts for the larger overarching research initiative at hand. As shown in **Table 2.2**, the K_d values measured in this work in the absence of organic ligands are comparable to several previous studies on soils with similar properties to the sandy clay loam used in this work. The variation in K_d values in the presence of citrate and oxalate indicates a potential change in the mobility of the ion based on the change in chemical speciation or a change in the ligand-mineral or ligand-ion interactions. Moreover, previous studies have examined sorption of the individual ions of interest in this paper to soils. However, using one soil in this work to examine multiple radionuclides will allow for a self-consistent comparison of the data for which can aid in the testing and validation of thermodynamic sorption databases. This will be the subject of future work regarding these soil-radionuclide systems.

Acknowledgements

This material is based upon work supported by the U.S. Department of Energy Office of Science, Office of Basic Energy Sciences and Office of Biological and Environmental Research under Award Number DE-SC-00012530. Partial faculty support (NEM) was provided by the U.S. Nuclear Regulatory Commission Nuclear Education Grant #NRC-HQ-13-G-38-002. The authors would like to acknowledge Hilary P. Emerson and E. Miller Wylie for their training, assistance, and contributions to this project.

CHAPTER THREE

THE UPTAKE AND TRANSLOCATION OF ^{99}Tc, ^{133}Cs, ^{237}Np, AND ^{238}U INTO *ANDROPOGON VIRGINICUS* WITH CONSIDERATION OF PLANT LIFE STAGE

[As published in the Health Physics Journal 115(5), 550-560 with minor revisions]

Abstract

Hydroponic uptake studies were conducted to evaluate the uptake and translocation of ^{99}Tc, ^{133}Cs (stable analog for ^{137}Cs), ^{237}Np and ^{238}U into established and seedling *Andropogon virginicus* specimens under controlled laboratory conditions. Plant specimens were grown in radionuclide spiked Hoagland nutrient solution for 24 hours, 3 days, and 5 days. Translocation to shoots was greatest for ^{99}Tc and ^{133}Cs, likely due to their analogous nature to plant nutrients, while ^{238}U (and ^{237}Np to a lesser extent) predominantly partitioned to root tissue with less extensive translocation to the shoots**.** Plant age contributed significantly to differences in concentration ratios (CR) for all nuclides in shoot tissues ($p \leq 0.024$), with higher CRs for seedling specimens. Additionally, duration of exposure was associated with significant differences in CRs of ^{133}Cs and ^{99}Tc for seedlings ($p = 0.007$ and $p = 0.030$, respectively) while plant part (root or shoot) was associated with significant differences in CRs of established plants ($p < 0.001$ for both nuclides). Statistically significant increases in radionuclide uptake in seeding specimens relative to established plants under controlled conditions suggests that in addition to geochemical factors, plant life stage of wild grasses may also be an important factor influencing radionuclide transport in the natural environment.

3.1. Introduction

3.1.1. Motivation and objectives

Plant-mediated mobility of radioactive contaminants is an important factor that should be considered in management and stewardship strategies at legacy contamination sites, nuclear waste repositories, and nuclear material processing facilities. The presence and growth of plants at these sites can lead to a multitude of effects ranging from food-chain transport, due to plant uptake and foraging activities, to increased contaminant mobility within the vadose zone as a result of plant induced biogeochemical interactions that may alter the solubility and/or speciation of the contaminants (Dakora and Phillips, 2002; Huang et al., 1998; Jones and Darrah, 1994; Napier et al., 2007; Robertson et al., 2003; Wang et al., 2015). The US Department of Energy's (DOE) Savannah River Site (SRS, Aiken, South Carolina) is one of several active legacy DOE locations in the United States for which this type of radioactive environmental contamination is present (Burger, 2000; Carlton, 1997; Carlton et al., 1993, 1992; Evans et al., 1992; Icenhower et al., 2010; Maher et al., 2012; NCRP, 2006; Savannah River Nuclear Solutions, 2016; Schulte and Scoppa, 1987). Additionally, previous field lysimeter experiments at SRS evaluating contamination transport in the vadose zone have demonstrated anomalous upward migration for Cs, Sr, and Pu which has not been fully explained, but was presumed that plant uptake was a substantial contributing factor (Demirkanli et al., 2009, 2007; Jantzen et al., 2008; Kaplan et al., 2014, 2010).

Uptake into various species of plants from both hydroponic and soil systems has been studied by many to determine associated uptake parameters, often concentration ratios (CR), and factors affecting uptake for a variety of nuclides (Ashworth and Shaw, 2005; Broadley and Willey, 1997; Cataldo et al., 1988; Choi et al., 1998; Duquène et al., 2006; Ebbs et al., 1998; Garten, Jr et al., 1986; Greger, 2004; Hattink et al., 2000; Sheppard and Evenden, 1987; Soudek et al., 2011; Tagami and Uchida, 2005; Viehweger and Geipel, 2010; Wildung et al., 1977). Additionally, many of these datasets have been compiled into databases which document CRs (ranges and means) of many nuclides for broad classes of plants (e.g. herbs, grasses, trees, etc.) (IAEA, 2014; ICRP, 2009a). These compiled databases mainly document soil:plant CR values, which are highly variable due to the complexity of the soil-plant system, type of soil, specific plant species, environmental conditions, etc.

The objective of this work is to evaluate the propensity for uptake and translocation of ^{99}Tc, ^{237}Np, ^{238}U, and ^{133}Cs (stable analogue for ^{137}Cs) into the grass species *Andropogon virginicus* (broomsedge) from hydroponic (HP) nutrient solution under controlled and ideal laboratory growth conditions in order to develop species specific CRs necessary to model more complex and environmentally relevant scenarios. The controlled conditions minimize extraneous nutrient and environmental stressors and allows for elucidation of potential factors affecting uptake that are not confounded by external stressors or competition with radionuclide interactions with soil, among other factors. This work is part of a larger, ongoing effort to understand, define, and model the major biogeochemical interactions that control radionuclide mobility (Dogan et al., 2017; Falta and Wang, 2017; Montgomery et

al., 2017; Powell et al., 2015). The controlled evaluation of plant uptake provides valuable insight into factors potentially contributing to previously observed upward migration in SRS lysimeters for which *A. virginicus* began to grow naturally and, when coupled with previous work, informs larger scale, increasingly complex experimental systems that more closely mimic natural conditions.

Four major factors are hypothesized to contribute to differences in plant tissue CRs for this work. First, the specific metal ion and its associated biogeochemical behavior, i.e. overall uptake and CRs are expected to be different for the different metal ions based on their speciation, analogous nature to plant nutrients, presence as a free ion, etc. Second, different plant tissues (roots or shoots) are expected to exhibit variable uptake and thus different CRs due to various plant nutrient uptake, translocation, and protective strategies or mechanisms, although this is also dependent upon the metal ion (Greger, 2004; Robertson et al., 2003). Third, duration of exposure (time grown) in the contaminated media is expected to have an effect on CRs due to potential continual intake of the radionuclides into the plant unless an equilibrium condition is reached quickly within the study timeframe (Choi et al., 1998; Shinonaga et al., 1999). Fourth, plant life stage is considered as it has been shown to contribute to differences in metal accumulation as a result of factors such as differences in rate of vegetative growth, rate of nutrient uptake and dilution effects for increased biomass (Ambe et al., 1999; Bell et al., 1988; Dinelli and Lombini, 1996; Ekvall and Greger, 2003; Garland et al., 1981; Salt et al., 2004, 1997). Comparisons between established and seedling *A. virginicus* specimens will allow evaluation of the extent of influence life stage has on the system for this particular species.

3.1.2. Plant uptake considerations

The bioavailability of metal ions is strongly dependent on the physical environmental conditions and the biogeochemistry of the particular ion under those conditions (Robertson et al., 2003). Many physical, chemical, and biological factors influence the uptake and transport of metals in plants, including metal concentration, chemical competition, pH, water content, organic matter content, electrochemical potential, redox potential, plant transpiration rate, etc. Additionally, different types of plants have specific strategies for acquiring nutrients or dealing with stress (Brown et al., 1991; Reichman, 2002). Ions that are not required for plant growth but that are chemically similar to essential nutrients may be taken up, translocated, and potentially metabolized in plant tissues to a greater extent than other analytes through associated nutrient acquisition mechanisms and transport pathways (Dakora and Phillips, 2002; Robertson et al., 2003). Of the radionuclides in this study, Cs^+ is chemically analogous to the essential nutrient K^+ and TcO_4^- has been proposed to be associated with plant uptake mechanisms typical of molybdate, selenate, sulfate, nitrate, chloride and phosphate (Bennett and Willey, 2003; Cataldo et al., 1983; Robertson et al., 2003). In addition to being able to actively forage for essential nutrients, plants also have developed various protective mechanisms that limit metal uptake (e.g. binding metals to cell walls, sequestration of metals in vacuoles, etc.) and detoxify high levels of metals taken into plant tissues through chelation (Briat and Lebrun, 1999; Clemens, 2001; DalCorso, 2012; Nascimento and Xing, 2006; Rascio and Navari-Izzo, 2011; Robertson et al., 2003; Zenk, 1996). These protective mechanisms will

also play a role in the uptake, translocation, and distribution of some non-essential metal ions if the plant recognizes and responds to their presence.

Considerable knowledge on plant uptake comes from the study of iron-deficiency induced plant foraging strategies, which include either creating a reducing environment around the roots (Strategy I) or releasing chelators (Strategy II). As a graminaceous monocot, *A. virginicus* employs Strategy II and excretes chelates into the rhizosphere to solubilize inorganic Fe^{III} and form complexes that can be recognized and taken up. This strategy, more efficient than Strategy I, can mobilize other metals as well, and in a nutrient poor soil such as SRS soil, may be a dominant factor in metal uptake. The presence of free metal ions and/or complexes produced by microbial activity and the decomposition of organic matter may have greater influence on metal uptake than plant exudates in nutrient rich soils (Brown et al., 1991; Curie and Briat, 2003; Reichman, 2002), and future experiments give consideration to these latter variables. The utilization of laboratory hydroponic experiments herein allows for evaluation of the extent to which *A. virginicus* may take up these specific radionuclides under controlled, ideal conditions, thus providing valuable information on the potential plant-specific contribution to radionuclide mobility.

3.2. Materials and methods

3.2.1. Radionuclide and plant species selection

The suite of radionuclides in this study were selected since they encompass a wide range of complex and coupled biogeochemical behavior and are all long-lived risk drivers in the US DOE complex as they are expected to be mobile, thus presenting potential hazards to human and environmental health (Bradbury and Baeyens, 2000; Burger, 2000;

Carlton et al., 1993; Choppin, 2007; Icenhower et al., 2010; Maher et al., 2012; NCRP, 2006; Schulte and Scoppa, 1987). The *A. virginicus* complex is a closely interrelated group of nine species of C4 perennial grasses (Poaceae) that range over the southern part of North America, with the Coastal Plain of the United States home to large, diverse populations (Campbell, 1983; Ezaki et al., 2008). Because it is a widespread indigenous grass species in the Southeastern United States and as it has been shown to be tolerant to a variety of stressors such as nutrient poor soil present at SRS, *A. virginicus* was chosen as a model plant for this study (Ezaki et al., 2008).

3.2.2. Hydroponic plant uptake studies

Andropogon virginicus was grown hydroponically to enable uptake experiments to be conducted under controlled laboratory conditions. Wild type *A. virginicus* seeds, collected from Clemson, SC, were initially germinated for approximately two weeks in a commercial germination mixture. Following germination, seedlings were transplanted into 250 mL Erlenmeyer flasks containing continually aerated Hoagland nutrient solution for hydroponic growth and acclimation at the Clemson University Greenhouse Complex (Hoagland and Arnon, 1950). The greenhouse was maintained at 30/20°C with a 14-hour photoperiod and the Hoagland nutrient solution was exchanged at weekly intervals until transfer to the laboratory setting. Laboratory hydroponic studies consisted of growing seedling (4-6 weeks old) or established (several months old) *A. virginicus* specimens in aluminum foil covered 250 mL Erlenmeyer flasks containing Hoagland nutrient solution under a 12-hour light cycle with continual aeration, **Figure 3.1**.

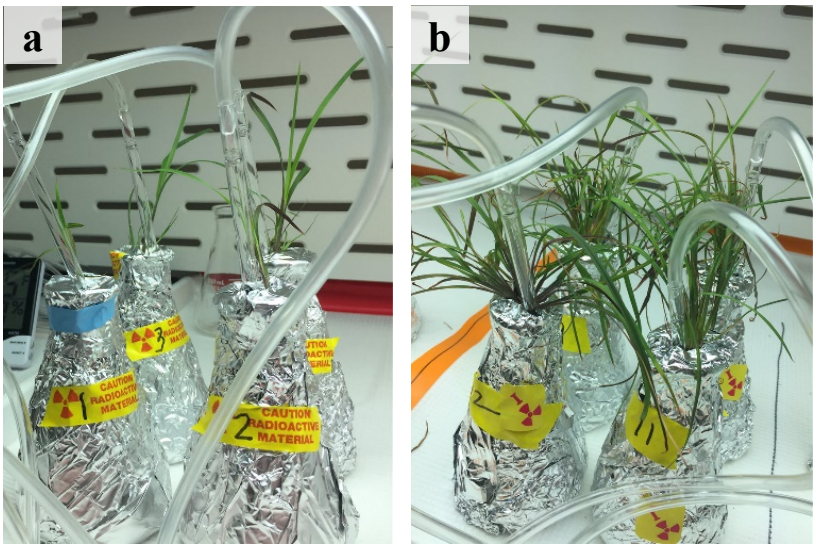

Figure 3.1: Laboratory hydroponic experimental set up of seedling (a) and established (b) specimens in covered flasks.

After an initial laboratory acclimation period of approximately one week the nutrient solution was exchanged for fresh nutrient solution spiked with ~75 µg L^{-1} (~48 Bq mL^{-1}) ^{99}Tc (Eckert & Ziegler Isotope Products, Valencia, CA) and ~10 µg L^{-1} ^{237}Np (~0.25 Bq mL^{-1}; Eckert & Ziegler Isotope Products, Valencia, CA), ^{133}Cs (stable analog for ^{137}Cs and ^{135}Cs; High-Purity Standards, Charleston, SC) and ^{238}U (~$1.2x10^{-4}$ Bq mL^{-1}; High-Purity Standards, Charleston, SC); light and aeration conditions remained unchanged. Plants were harvested in quadruplicate after 24 hours, 3 days, and 5 days of exposure. One control group of four specimens, grown in unspiked Hoagland nutrient solution, was also harvested at 5 days after the nutrient solution exchange. The maximum harvest time of 5 days was implemented so that the spiked nutrient solution would not have to be replaced during the active uptake portion of the experiment. Additionally, one plant from each harvest group was selected for autoradiography to obtain a visual representation of the uptake and translocation of ^{99}Tc with harvest time.

At the time of harvest, the plants were carefully rinsed with distilled deionized water (DDI) and gently covered with paper towels for several minutes to remove excess surface moisture. The roots were then carefully separated from the shoots, each portion was placed into individual 100 mL covered beakers, and the fresh mass of each specimen tissue (root or shoot) was recorded. The covered specimens were oven dried at 50°C to a constant weight to obtain dry plant tissue mass. The oven dried plant tissues were acid digested on a hotplate using HNO_3 and H_2O_2 following EPA Method 3050B, Section 7.2 (EPA, 1996). Four method blanks (empty beakers) were subjected to the same drying conditions, chemical additions and heating conditions to monitor for potential contamination. The resulting digestate and DDI digestion beaker rinse were filtered through 0.2 μm polypropylene syringe filters and the filter was rinsed with approximately 5 mL of 2% HNO_3. The filtered digestate samples as well as hydroponic solution samples were diluted and/or neutralized as appropriate for analysis of ^{133}Cs, ^{237}Np and ^{238}U via inductively coupled mass spectrometry (ICP-MS, Thermo Scientific XSeries 2; ^{133}Cs limit of detection (LOD) of $1.8x10^{-2}$ μg L^{-1}, ^{237}Np LOD of $9.0x10^{-6}$ μg L^{-1}, ^{238}U LOD of $5.3x10^{-4}$ μg L^{-1}) and ^{99}Tc via liquid scintillation counting (LSC, PerkinElmer Tri-Carb 4910TR; minimum detectable concentration (MDC) of $2.8x10^{-2}$ Bq mL^{-1}). The LOD from ICP-MS analysis is dependent on various factors and may change between separate runs on the instrument; the LODs reported above are the maximum values associated with the radionuclides from all runs. Similarly, the MDC on the LSC is dependent upon count time and the sample matrix, among other factors, and thus the above MDC for ^{99}Tc LSC analysis is the maximum MDC determined between multiple sample group runs. Analysis allowed

determination of hydroponic solution concentrations and plant tissue concentrations of each radionuclide in order to compare plant uptake of each of the radionuclides for the three exposure times and plant life stages. Additionally, the ^{99}Tc concentration was sufficiently high to allow for the use of autoradiography to monitor the distribution of ^{99}Tc in the plants following uptake. The concentrations of ^{237}Np and ^{238}U were sufficiently low such that their levels of radioactivity and associated contributions to the LSC and autoradiography signals were minimal in comparison to ^{99}Tc. Thus, ^{237}Np, ^{238}U, and ^{133}Cs were all monitored in mass units and ^{99}Tc was monitored in activity units (see **Equation 3.1** discussed below). All can be adjusted to molar units as preferred.

Concentration ratio (CR) is a ratio used to normalize plant concentration to media concentration so that multiple data points and specimens can be effectively compared (Beresford et al., 2008; Brown et al., 2008; IAEA, 2014; ICRP, 2009a). The CR was calculated from the aqueous HP solution concentrations and plant tissue concentrations by:

$$CR_{\text{plant part:HP solution}} = \frac{C_{\text{plant part}}}{C_{\text{HP solution}}} \qquad (\mathbf{3.1})$$

where, $CR_{\text{plant part:HP solution}}$ is the concentration ratio of the plant activity (or mass) concentration to the HP solution activity (or mass) concentration (kg L^{-1}), $C_{\text{plant part}}$ is the concentration of radionuclide in the plant, the activity (or mass) of radionuclide per kg of dry plant material (Bq kg^{-1} or µg kg^{-1}), and $C_{\text{HP solution}}$ is the concentration of radionuclide in the HP solution, the activity or (mass) of radionuclide per L of HP solution (Bq L^{-1} or µg L^{-1}). Here CR is calculated with respect to dry plant tissue, as it was measured, because water content varies from plant to plant. Some CR values in the literature utilize fresh plant

mass, and the ratio of dry mass to fresh mass is used to compare the results of this work to values in the literature.

3.2.3. Statistical analysis

Various analysis of variance (ANOVA) statistical tests were conducted for each radionuclide to determine the significance of the effects of treatment length (harvest day: 1, 3, 5), plant part (root or shoot), and plant age (established or seedling) on CR. Dixon's test (extreme value test) was conducted to determine if anomalous or suspect data points were outliers and thus, if exclusion was appropriate (Dixon, 1953). Two-sample, one-tailed T-tests were conducted to compare overall mean CRs for seedling and established plants by plant part and radionuclide. Linear regression analysis was conducted to determine if CR changed in time for each plant part and radionuclide to gain insight into the rate of uptake. That is, regression was used to determine if the intercept and/or slope of the CR vs harvest day regression line was different than zero. In all cases, significance was taken as $p < 0.05$. All statistical analyses were conducted with Minitab (Minitab18, State College, PA).

3.3. Results and discussion

3.3.1. ANOVA results

A three-way ANOVA was run for each radionuclide on a total of 48 samples (24 roots and 24 shoots) to examine the effect of harvest day, plant part, and plant age on the CR. As an exception, due to observation of several suspect CRs, five outliers in ^{133}Cs data were identified (three root and two shoot CRs for established plants) by performing Dixon's test; due to the extreme nature of these outliers, exclusion of these data was

deemed appropriate. Uranium had the only significant three-way interaction, $F(2, 36) = 4.58$, $p = 0.017$. Cesium had a significant two-way interaction between harvest day and plant age ($F(2, 31) = 4.90$, $p = 0.014$), while Np had a significant two-way interaction between plant part and plant age ($F(1, 36) = 8.15$, $p = 0.007$). These significant interaction terms imply that changes in the CR due to harvest day and/or plant are dependent on plant age. Two-way ANOVA analyses were thus run separately for each plant age grouping (seedling or established), 24 samples per group (12 roots and 12 shoots), to better examine the effects of harvest day and plant part on the concentration ratio. Results from these two-way ANOVAs are shown in **Table 3.1**, with significant p-values underlined and bolded.

Table 3.1: Results of two-way ANOVA analysis (p-values) for CR comparing factors for specimens grouped by plant age.

	^{99}Tc	^{133}Cs	^{237}Np	^{238}U
Seedlings				
Plant part	0.763	0.355	**<0.001**	**<0.001**
Harvest day	**0.030**	**0.007**	**0.020**	0.480
Interaction	0.255	0.596	0.281	0.477
Established plants				
Plant part	**<0.001**	**<0.001**	**<0.001**	**<0.001**
Harvest day	0.071	0.738	**<0.001**	**0.006**
Interaction	0.684	0.518	**0.002**	**0.006**

A significant p-value indicates rejection of the null hypothesis of equal means (or no interaction term) and an acceptance that there is a statistically significant difference between the particular means (or interaction between the factors considered). Although there was a significant interaction term for both ^{238}U and ^{237}Np, examination of the main effects of plant part and harvest day separately indicated that each was indeed a significant

contributor to differences in CR; the only non-significant term was harvest day when considering ^{237}Np roots only ($p = 0.051$).

Two-way ANOVAs were also run by plant part (root or shoot, 24 samples each), considering seedlings and established plants together to determine if CRs of each plant part was significantly affected by the age of the plant. Plant age was associated with significantly different CRs for all nuclides in shoot tissues (all p-values less than 0.024), but only for ^{99}Tc and ^{237}Np in root tissues ($F(1,18) = 11.96$, $p = 0.003$ and $F(1,18) = 35.51$, $p < 0.001$, respectively).

3.3.2. Autoradiography: visual representation of plant uptake and distribution of ^{99}Tc

Under the oxic, neutral pH conditions of these experiments, ^{99}Tc predominantly presents as the highly soluble heptavalent pertechnetate ion (TcO_4^-). The low sorption and complexation affinity of TcO_4^- leads to high bioavailability and potentially high plant uptake (Icenhower et al., 2010; Robertson et al., 2003). Qualitative evidence of this behavior was demonstrated using autoradiography; there is an increase in intensity of the autoradiography signal between plants exposed for 3 or 5 days compared to 1 day for both established and seedling specimens (**Figure 3.2**).

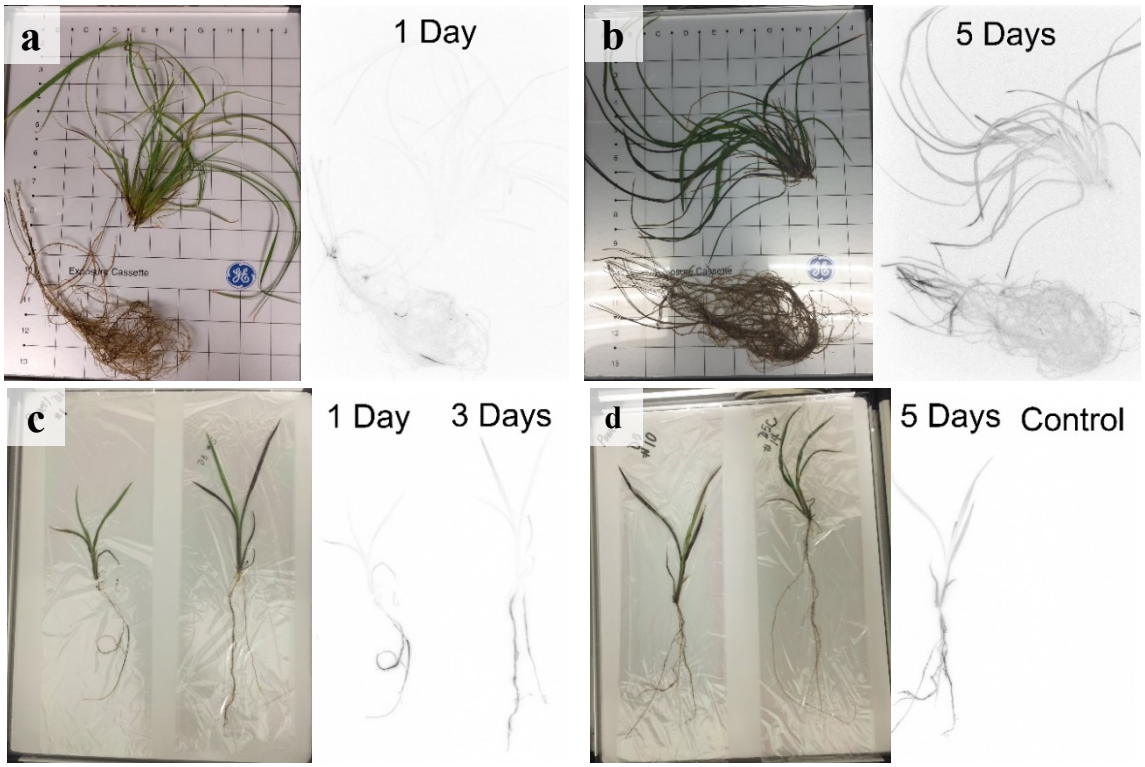

Figure 3.2: Autoradiography of established plants (top row: (a) harvest day 1; (b) harvest day 5) and seedlings (bottom row: (c) harvest days 1 and 3; (d) harvest day 5 and control). The qualitative increase in color intensity indicates a positive correlation of the uptake/translocation of ^{99}Tc into the plant tissues with treatment time (harvest day). Note that the intensity of the autoradiography images for the established plants cannot be directly compared with the seedling specimen images due to use of different autoradiography plates.

The regression coefficients of the independent variable harvest day (i.e. the slope) for established and seedling shoot specimens were significantly different than zero and positive (β_1 = 0.978, p = 0.002 and β_1 = 4.47, p = 0.026 respectively), quantitatively confirming that ^{99}Tc shoot CR increases with treatment duration as seen in **Figure 3.2**. Additionally, the regression line intercepts for ^{99}Tc root CR were significantly different than zero (β_0 = 7.13, p = 0.029 and β_0 = 12.06, p = 0.012 respectively for established plants and seedlings), indicating that roots take up ^{99}Tc almost immediately. This was also the

case for the roots of all other radionuclides, except for ^{237}Np in established roots ($\beta_0 = 3.92$, p=0.060).

3.3.3. Concentration ratios: quantitative analysis of plant uptake

Concentration ratios for each nuclide with respect to plant part (roots and shoots) and harvest day are shown in **Figure 3.3**. The CRs for the seedling specimens were generally greater than CRs for established plants. One-tailed T-tests were used to test the null hypothesis that the difference in means by plant age is zero, with the alternative hypothesis that the difference in means is greater than zero, where the seedling CR is larger than established plant CR. With the exception of the roots of ^{133}Cs and ^{238}U ($p = 0.100$ for both), seedling plant CRs were significantly greater than established CRs (all p-values $\leq$ 0.017).

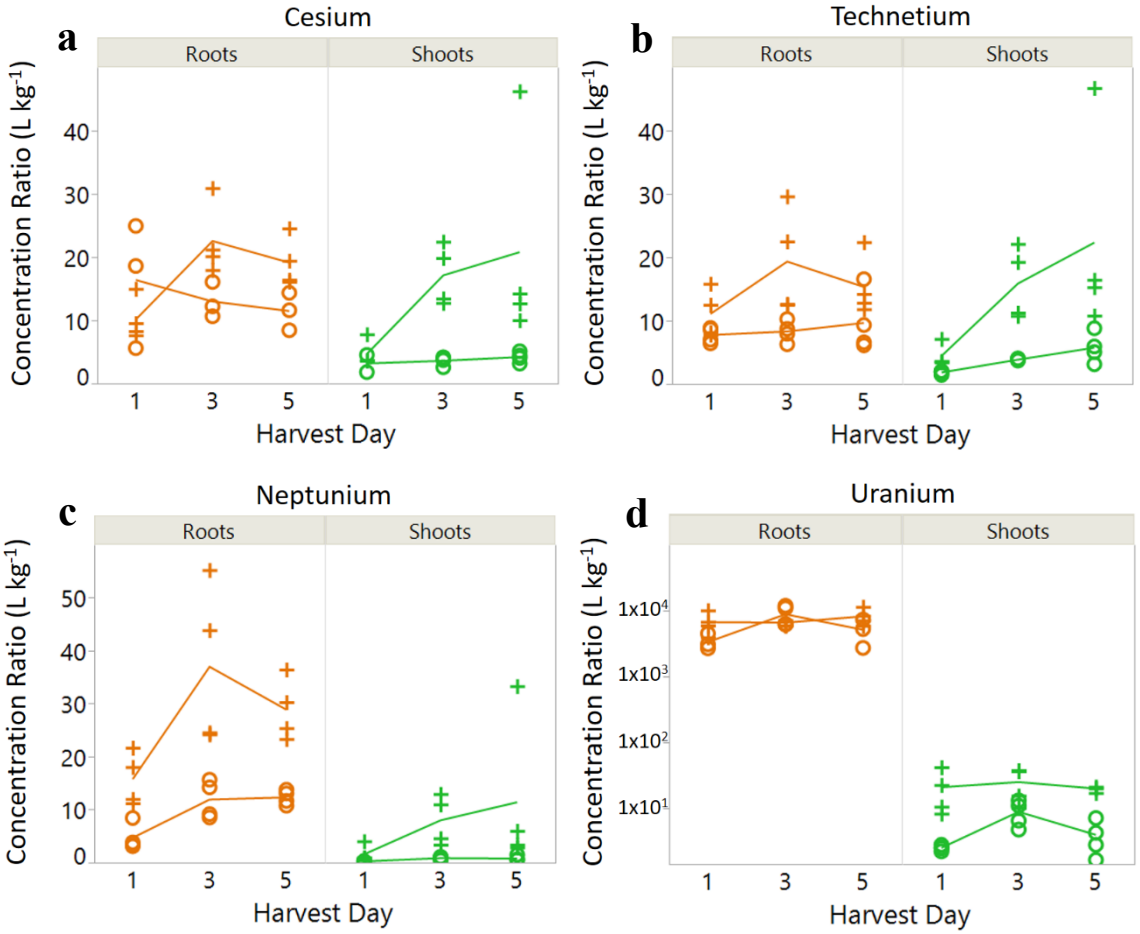

Figure 3.3: Concentration ratios (µg kg^{-1} dry weight per µg L^{-1} of solution) by harvest day, plant tissue, and plant age. Points represent individual CRs of the specimen tissues ('+' for seedlings and 'o' for established plants) and the lines signify the average CR and trend between the harvest days.

While the exact mechanisms responsible are not specifically investigated here, higher CRs of seedlings are likely in part due to greater relative nutrient uptake, transpiration rates, and biomass production compared to established plants (Ekvall and Greger, 2003). Thus, plant age seems to be an important factor that may warrant consideration. Further laboratory uptake studies as well as investigation of uptake in field scenarios, where remediation or site risk assessments are of interest, may be beneficial.

The uptake of ^{99}Tc and ^{133}Cs were similar in magnitude and trend, except for established plant roots (**Figure 3.3a** and **Figure 3.3b**). Harvest day was a significant factor for both ^{99}Tc and ^{133}Cs in seedling specimens, and plant part was significant for established specimens (**Table 3.1**). Regression analysis showed that seedling shoot CR increased significantly with time ($\beta_1 = 4.03$, $p = 0.046$ for ^{133}Cs; ^{99}Tc results above), and that root CRs remained essentially constant. Interestingly, CR differences between tissues were not significant for seedling specimens (**Table 3.1**; **Figure 3.3a** and **Figure 3.3b**). Continually increasing seedling shoot CRs with time as well as higher shoot translocation is likely related to greater relative growth, nutrient uptake, and transpiration rates for seedling specimens, among other biological and chemical factors. Although regression analysis indicated that, overall, the slopes of root CR vs harvest day were not significantly different from zero (except ^{237}Np in established roots, $\beta_1 = 1.909$, $p = 0.005$), most mean root CRs increased from day 1 to day 3, and decreased from day 3 to day 5. This may be indicative of a stress response by the plants correlating with observation of visual plant stress response signs, such as purpling of treatment plant shoots noted at later harvest times.

The similarity in uptake along with the particularly high translocation to the shoots for both ^{99}Tc and ^{133}Cs can, at least partly, be attributed to their analogous nature to essential plant nutrients, associated uptake pathways, and metabolic incorporation mechanisms (Cataldo et al., 1983; Robertson et al., 2003). As discussed above, the low sorption and complexation of TcO_4^- leads to the expectation of high bioavailability and consequent plant uptake (Icenhower et al., 2010; Robertson et al., 2003), as seen in **Figure 3.2** and **Figure 3.3**. Cesium is present as the monovalent Cs^+ ion and exhibits intermediate

mobility in subsurface soils due to its strong selective sorption to many clay minerals, but is expected to persist as the free ion in pore and surface waters making it available for plant uptake under these conditions (Bostick et al., 2002; Montgomery et al., 2017; NCRP, 2006; Zaunbrecher et al., 2015b). Thus, cesium and technetium both represent weakly complexing ions and provide a comparison of anion and cation uptake. While the CR of technetium is generally higher than cesium in soil-plant systems (IAEA, 2014; ICRP, 2009a), the similarity in their magnitude for the hydroponic-plant system presented herein may be attributed to a combination of the lack of available material (soil) for the ^{133}Cs to sorb to leading to increased ^{133}Cs uptake and the availability of sufficient essential plant nutrients provided by the Hoagland nutrient solution, which have been shown to decrease the uptake of technetium due to competition effects (Bennett and Willey, 2003; Cataldo et al., 1983).

The uptake and translocation to the shoots was the lowest for ^{237}Np even though the uptake into the roots was similar to or higher than that of ^{133}Cs and ^{99}Tc, depending upon plant age (**Figure 3.3c**). Additionally, some similar trends discussed for ^{99}Tc and ^{133}Cs are noted for ^{237}Np: seedling CRs are greater than those for established specimens and root CRs decrease or begin to level off by the final harvest day (**Figure 3.3c**). All of these effects are likely associated with the differences in nutrient uptake and transpiration rates of seedlings compared to established plants and potential stress responses as discussed above. However, in contrast to ^{133}Cs and ^{99}Tc, both plant part and harvest time contribute significantly to the variation in the CR for ^{237}Np for seedling and established plants. The significant differences in CR with respect to harvest day indicate that uptake may not yet

have reached equilibrium by the final harvest time while the significantly lower shoot CRs compared to root CRs indicates a reduced ability of ^{237}Np to be translocated to the shoot.

Neptunium (as NpO_2^+) has been shown to be mobile under oxic environmental conditions due to its relatively weak complexation affinity and its resistance to hydrolysis at low and neutral pH values compared to actinides with greater effective charge (Choppin, 2007). Thus, the bioavailability of neptunium is expected to be higher than other actinides (Robertson et al., 2003). However, as ^{237}Np does not have a nutrient analog, uptake is expected to be less than analytes that are chemically similar to plant nutrients. Thus, the decreased ability of ^{237}Np to translocate to the shoots, compared to ^{133}Cs and ^{99}Tc, indicates the possible activation of a sequestration or other protective response by the plant that limits translocation of non-essential or toxic metals to aerial portions of the plant resulting in lower shoot uptake and CRs.

Of the radioisotopes examined in this work, uranium exhibited the strongest association with the roots. Under these experimental conditions, uranium should persist as a dioxycation, UO_2^{+2}, characterized by comparatively strong sorption and complexation affinity (vs. Tc^{VII} or Np^{V}), and thus may be less bioavailable to plants grown in soil depending upon the presence of other complexants, plant exudates and sorbents in the system (Clark et al., 1995; Morss et al., 2010). However, under these hydroponic conditions, the CR for ^{238}U in the roots is two to three orders of magnitude greater than that of any other ion for this study (**Figure 3.3d**). This is proposed to be mainly due to sorption to the root surface (in the absence of soil as a sorbing medium), an effect previously noted (Adriano et al., 2000). Additionally, similarly strong sorption to microbial cell walls has

been previously observed (Fein and Powell, 2013). Despite the prominent concentration of ^{238}U in (or on) the roots, the translocation to the shoots was of similar magnitude to ^{133}Cs and ^{99}Tc. Analogous to ^{237}Np, ^{238}U does not have a nutrient analog and thus the limited root to shoot translocation may be an effect of a plant protective mechanism partially sequestering the ^{238}U in the root tissues or due to ^{238}U mainly sorbing to the surface of the roots with a smaller fraction being available to be taken up into the root tissue internally. Additionally, the uptake, translocation and sorption of ^{238}U into or onto the plant tissues appears to have reached equilibrium relatively quickly for the seedling specimens as harvest day is not significant and both root and shoot CRs are reasonably constant throughout the study time frame. This is also the case for established specimen root CRs, but not for shoots. Although not statistically significant, CR in established shoots may generally show the same trend, but with the current sample size, the variability in plant mass (compared to seedlings) led to less confidence in the CR trend. The rapid (probable) attainment of equilibrium conditions is likely another result of the strong and rapid sorption to the roots due to the high complexation affinity of UO_2^{+2}.

In addition to CRs typically being greater for seedlings than for established plants, the average radionuclide mass per seedling shoot (i.e. whole plant part) is also greater than in established shoots for ^{237}Np and ^{238}U, even though the seedling shoot mass is considerably less than the established shoot mass (**Table 3.2**). The increased overall translocation to the shoots further indicates that the seedling specimens are likely in a high growth rate stage with associated high nutrient uptake and high relative transpiration rate as compared to the established specimens that may not be channeling their energy toward

growth of plant biomass to as great of an extent. In addition, for the specific radionuclides that do not have nutrient analogs, a combination of the increased uptake and transpiration rates along with other factors may be interdependently contributing to this notable age related effect. For example, possible decreased relative ability of seedlings to effectively sequester or limit translocation of these radionuclides, increased passive transport due to higher relative root concentrations, and more delicate root tissue may contribute to the greater translocation to shoots.

Table 3.2: Average mass of radionuclide (μg) per whole plant part (whole root or whole shoot) at harvest day 5 and associated standard deviation of the four replicate specimens

	Roots		Shoots	
	Seedlings	Established	Seedlings	Established
^{99}Tc	0.039 ± 0.013	0.186 ± 0.047	0.148 ± 0.129	0.280 ± 0.051
^{133}Cs	0.006 ± 0.002	0.038 ± 0.016	0.017 ± 0.016	0.031 ± 0.009
^{237}Np	0.008 ± 0.002	0.038 ± 0.013	**0.009 ± 0.012**	0.006 ± 0.003
^{238}U	1.078 ± 0.299	1.378 ± 0.181	**0.007 ± 0.001**	0.003 ± 0.000

The average CRs (shoot:HP solution for fresh plant mass) on harvest day 5 for both seedlings and established plants are compared to the geometric mean CRs (whole plant:soil for fresh plant mass) of terrestrial grasses and wild grasses reported by the IAEA and ICRP respectively in **Figure 3.4** (IAEA, 2014; ICRP, 2009a).

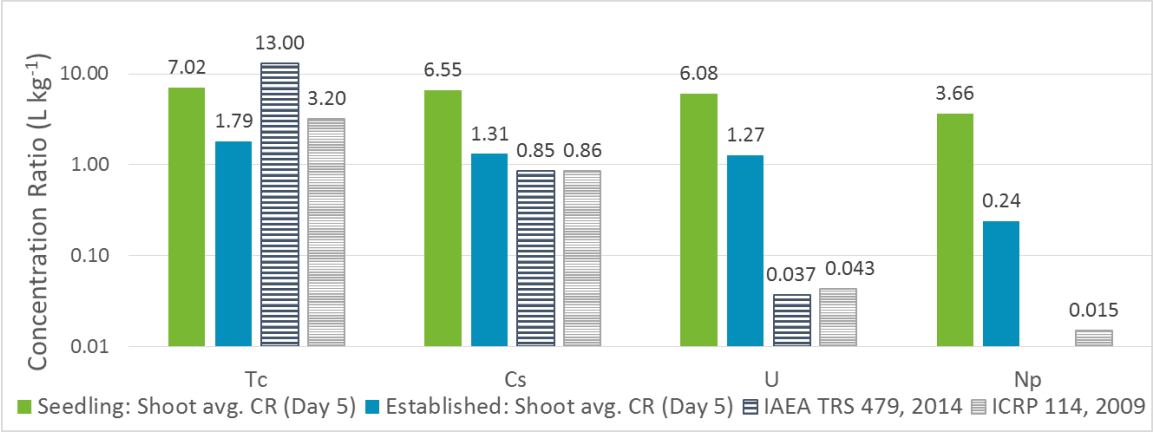

Figure 3.4: Comparison of seedling and established average shoot CRs (µg kg^{-1} fresh weight shoots per µg L^{-1} HP solution) for harvest day 5 to CRs of terrestrial grasses and wild grasses reported by the IAEA and ICRP (Bq kg^{-1} fresh whole organism per Bq kg^{-1} soil) (IAEA, 2014; ICRP, 2009a). Note that the ICRP reported CR for Np is a derived CR, not empirical.

Experimental CRs displayed in **Figure 3.4** were converted to values based on fresh plant mass for more consistent comparison to IAEA and ICRP summarized values also based on fresh plant mass. Additionally, experimental shoot CRs are utilized here due to high root CRs, particularly of ^{133}Cs and ^{238}U, under hydroponic conditions that would be lower for soil-plant systems due to competition with soil sorption of those radionuclides (Montgomery et al., 2017; Robertson et al., 2003). However, it appears that the relative high root uptake from HP solution (for radionuclides that would otherwise sorb to soil) also contributed to the relatively high translocation to shoots, thus the more insightful comparison here is related to the general trends between radionuclides.

For seedlings, the experimental CRs for ^{99}Tc were consistent with reported CRs while the experimental seedling CRs for ^{133}Cs, ^{237}Np and ^{238}U were higher, although the ^{133}Cs CR was within the overall reported range (IAEA, 2014; ICRP, 2009a). For established plants, ^{99}Tc, ^{133}Cs and ^{238}U CRs were within reported ranges with the ^{99}Tc CR

being below the reported geometric mean and the ^{238}U CR above the geometric mean (IAEA, 2014). Additionally, experimental values compiled by the IAEA and ICRP did not include any studies uptake of neptunium into terrestrial grass, thus a derived value was reported in ICRP 114 which had no associated range (ICRP, 2009a). Particularly, the deviation of seedling CRs from reported values and the relatively high uptake and uptake rate into seedling shoots further indicates that plant life stage is an important factor to consider when evaluating a system for which plant uptake is of concern (Ekvall and Greger, 2003).

The comparability of ^{99}Tc to reported values is expected as it is highly mobile and minimally sorbing, yet may also be exhibiting somewhat suppressed uptake due to competition effects with nutrients in the HP solution (Cataldo et al., 1983). The increased ^{133}Cs CRs compared to reported values is also expected since it would otherwise moderately sorb to soil and, since it is directly analogous to K^+, is expected to exhibit increased uptake behavior more similar to ^{99}Tc under these hydroponic conditions (Montgomery et al., 2017). Uranium shoot uptake is only slightly lower than that of ^{99}Tc and ^{133}Cs for the HP system instead of exhibiting much lower CRs in reported soil-plant systems. This is due to the extreme sorption to root tissues as previously discussed. Compared to the other radionuclides ^{237}Np follows the reported trend of showing the least uptake, yet it was greater than the derived value utilized in ICRP 114 (ICRP, 2009a). However, uptake studies investigating uptake of ^{237}Np into other types of plants reported CRs of similar ranges, even in soil-plant systems (Cataldo et al., 1988). The similarity of HP-plant and available soil-plant CRs is not unexpected for the ^{237}Np case, similar to ^{99}Tc,

^{237}Np exhibits minimal sorption and complexation affinity and high bioavailability (Montgomery et al., 2017; Robertson et al., 2003).

3.4. Conclusion

The controlled evaluation of uptake provides insight into the potential mechanisms and factors (e.g. radionuclide sorption/complexation affinity, potential for translocation, effects of plant age etc.) that may affect upward migration of nuclides in the vadose zone when plants are present in the system. Further, the coupling of plant uptake presented herein with previous studies investigating the impact of simulated plant exudates on the sorption of these radionuclides to SRS soil provides motivation and direction for subsequent increasingly complicated migration and plant uptake studies (Montgomery et al., 2017). This linkage may also provide parameters and trends necessary for modeling of these more complex systems that mimic natural conditions. Additionally, it should be noted that CRs are dependent upon plant species and environmental conditions in which the plant is grown, among other factors. Thus, while general or average concentration ratios may be used in an initial evaluation, site specific studies may be necessary depending upon the prevailing environmental conditions and presence of various plant life stages in order to develop appropriate maintenance and stewardship practices as well as evaluate risks associated with a particular site.

Acknowledgements

This work is supported by the United States Department of Energy Office of Science, Office of Basic Energy Sciences and Office of Biological and Environmental Research under Award number DE-SC-00012530. Partial faculty support (NEM) was provided by

the United States Nuclear Regulatory Commission Nuclear Education Grant #NRC-HQ-13-G-38-0002.

CHAPTER FOUR

COMPARATIVE UPTAKE, TRANSLOCATION, AND PLANT MEDIATED TRANSPORT OF Tc-99, Cs-133, Np-237, AND U-238 IN SAVANNAH RIVER SITE SOIL COLUMNS FOR THE GRASS SPECIES *ANDROPOGON VIRGINICUS*

[As *prepared for* publication in a scientific journal]

Abstract

This study seeks to examine the ability of the grass species *Andropogon virginicus* to alter the subsurface transport and redistribution of a suite of radionuclides (^{99}Tc, ^{133}Cs (stable analog for ^{135}Cs and ^{137}Cs), ^{237}Np, ^{238}U) with varying chemical behaviors in a Savannah River Site (SRS) soil via the use of vegetated and unvegetated soil columns. After a brief acclimation period, allowing plants to become established in vegetated columns, a small volume of solution containing all radionuclides was introduced into the columns via Rhizon© pore water sampling tubes. Plants were allowed to grow for an additional four weeks before shoots were harvested and the columns were prepared for destructive sampling. Overall, plant presence lead to decreased radionuclide release from the columns, mainly due to radionuclide specific combinations of system hydrology differences resulting from plant transpiration as well as plant uptake. For the most mobile radionuclides, ^{99}Tc followed by ^{237}Np, plant presence resulted in significantly different soil concentration profiles between vegetated and unvegetated columns, including notable upward migration for ^{237}Np in columns with plants. Soil profiles were not significantly different across treatment groups for ^{133}Cs or ^{238}U, which are also native to the SRS soil utilized in this study. Additionally, plant uptake of ^{99}Tc was the greatest of all the radionuclides, with plant tissues containing an average of 44% of the ^{99}Tc in the system,

while plant uptake only accounted for < 2% of ^{237}Np and < 0.5 % of ^{133}Cs and ^{238}U in the system. Although overall plant uptake of ^{133}Cs and ^{238}U were similar, the majority of ^{133}Cs taken up by plants was associated with ^{133}Cs already available in the aqueous phase while ^{238}U uptake was mainly associated with the solid phase, meaning that plant activity resulted in a fraction of the native ^{238}U being mobilized and thus, made available for plant uptake. Overall, this study quantified the influence of several plant-mediated physical and biogeochemical factors that have significant influence on radionuclide mobility and transport in this complex system. The extensive data set developed within this work can be further utilized to inform future system or site-specific environmental transport and risk assessment models.

4.1. Introduction

4.1.1. Motivation and objectives

The ability of plants to take up and accumulate radionuclides from various media (e.g., aqueous solutions, sand, soils, etc.) has been studied for decades and is generally well documented for a number of radionuclides and plant species or broad plant classifications (Broadley and Willey, 1997; Cataldo et al., 1988; Garland et al., 1981; Nisbet and Shaw, 1994; Robertson et al., 2003; Sheppard et al., 1983; Soudek et al., 2004; Wildung et al., 1977). Considerable attention has been paid to determining concentration ratios (CR) or transfer factors (TF), evaluating radionuclide fluxes in various systems, and investigating the potential for phytoremediation applications (Dushenkov, 2003; IAEA, 2014, 2010; ICRP, 2009a; Kashparov et al., 2012; Sheppard and Evenden, 1988; Yoschenko et al., 2017). Additionally, in efforts to elucidate dominant factors affecting plant uptake and

environmental transport of various radionuclides, some studies have considered the influence of physical and/or chemical soil parameters (e.g., pH, soil type, etc.), radionuclide speciation and/or bioavailability, potential uptake mechanisms or pathways, and other such factors; though generally, only a few of these are considered in any given instance (Duquène et al., 2006; Ebbs et al., 1998; Edayilam et al., 2020; Ehlken and Kirchner, 2002; Robertson et al., 2003; Shalhevet, 1973; Zhu and Smolders, 2000). Further, while many studies have investigated radionuclide depth distributions in soil in the presence of plants, often considering downward migration of radionuclides from surface deposition scenarios (Almgren and Isaksson, 2006; Bunzl et al., 1992; Matisoff et al., 2011; Takahashi et al., 2015), fewer studies have investigated in detail how plant uptake and presence affects the subsurface transport of radionuclides, particularly the upward migration of contaminants (Ashworth et al., 2003; Ashworth and Shaw, 2006, 2005; Demirkanli et al., 2009, 2007; Kaplan et al., 2014, 2010; Shaw et al., 2004; Wadey et al., 2001; Wheater et al., 2007). Despite the comparatively few investigations into the upward migration of radionuclides in soils, this phenomenon may have significant impact on dynamic transport modeling of soil-plant-hydrologic systems and risk assessment modeling at sites with current or potential radionuclide contamination in the vadose zone, such as the Department of Energy's (DOE) Savannah River Site (SRS; Aiken, SC) or the Hanford Reservation (Hanford, WA) (Kaplan et al., 2010). Thus, further attention investigating plant influence on subsurface transport processes and resultant radionuclide distributions are warranted and can inform these models.

The overarching objective of this work is to comparatively quantify the influence of an indigenous grass, *Andropogon virginicus* (broomsedge), on the transport of technetium-99 (^{99}Tc), cesium-133 (^{133}Cs, stable analog for ^{135}Cs and ^{137}Cs), neptunium-237 (^{237}Np), and uranium-238 (^{238}U) in a soil-plant column system utilizing a sandy clay loam soil from SRS. Laboratory-scale soil column experiments were conducted to compare a soil-plant-hydrologic system to a soil-hydrologic system, i.e., vegetated and unvegetated soil columns. Additionally, the system was designed such that the radionuclides were introduced into the soil columns within the rooting zone of the plant (for columns with plants) thereby, increasing the likelihood of interaction between the plant roots and the radionuclides. The plant species, soil, and radionuclides were utilized to be consistent with prior studies pertaining this system; specific reasoning concerning their selection as well as the physical and chemical properties of this specific SRS soil are discussed fully elsewhere (Montgomery et al., 2017, 2018).

Multiple factors, both physical and biogeochemical in nature, are considered to have influence on radionuclide transport between the vegetated and unvegetated systems and between the different radionuclides within this study. These factors include system hydrologic differences (mainly associated with plant transpiration in this case), radionuclide speciation and sorption affinity (i.e., distribution coefficient, K_d values), plant uptake of individual radionuclides, and presence of plant exudates and their ability to alter the rhizosphere soil and/or form complexes with the radionuclides (Montgomery et al., 2017; Robertson et al., 2003). While this list is not exhaustive, other factors that could affect transport and plant uptake are likely minimal with respect to the aforementioned

factors while some are not expected to be different between columns with plants and columns without (e.g., soil type). Therefore, in order to investigate several factors associated with plant presence simultaneously and in an integrated manner, effluent volumes were measured after each irrigation event and analysis for radionuclide concentration was conducted for effluent, pore water, plant tissues, and soil (1 cm segments) samples. Radionuclide concentration and total mass in the compartments (i.e., effluent, soil, plant tissues, etc.) were compared between the three column systems individually to ascertain the major influential factors for each radionuclide. Then, systems were compared in a holistic manner; in other words, systems were compared considering the relative contributions of the components to the whole system while also considering prior work on individual system components to elucidate more nuanced factors affecting radionuclide transport (Montgomery et al., 2017, 2018).

4.1.2. Radionuclide biogeochemistry and plant uptake considerations

Radionuclide biogeochemistry and plant uptake considerations have been discussed in detail previously (Montgomery et al., 2017, 2018). Thus, only a brief review is given here. Under the oxic conditions of this study, technetium is expected to persist as the highly mobile, weakly complexing pertechnetate anion ($Tc^{(VII)}O_4^-$) with the lowest K_d values of all radionuclides in this study (Icenhower et al., 2010; Montgomery et al., 2017). Neptunium also shows weak sorption to SRS soils and thus, is expected to be relatively mobile, weakly complexing, and resistant to hydrolysis due to its presence as the pentavalent neptunyl cation ($Np^{(V)}O_2^+$) (Choppin, 2007; Miller, 2010). On the other hand, cesium and uranium exhibit much stronger sorption relative to technetium and neptunium.

Cesium exists as a monovalent cation (Cs^+) in solution and has been shown to exhibit strong sorption to clays, particularly to hydroxy-interlayered vermiculite that is present in SRS soil; thus, its subsurface mobility is limited (Bostick et al., 2002; Goto et al., 2014; NCRP, 2006; Zaunbrecher et al., 2015b). Uranium is dominantly found in the hexavalent state under oxic conditions ($U^{(VI)}O_2^{2+}$), readily undergoes hydrolysis, exhibits relatively strong sorption to mineral surfaces (highest K_d values for the radionuclides in this study), and has a high complexation affinity with many ligands which can result in increased aqueous partitioning (Alliot et al., 2005; Clark et al., 1995; Montgomery et al., 2017; Morss et al., 2010). Overall, the trends in mobility are expected to be greatly influenced by the sorption affinities of the ions to the soil thus, from most to least mobile (and least to greatest K_d):

$$Tc^{(VII)}O_4^- > Np^{(V)}O_2^+ > Cs^+ > U^{(VI)}O_2^{2+}$$

Plant uptake is also expected to follow this general trend as the ion must be present in the aqueous phase, either due to low sorption affinity or due to other system conditions affecting its partitioning, such as plant physiological and nutrient scavenging mechanisms (e.g., exudate release) that may liberate sorbed ions from the solid phase (Alliot et al., 2005; Jones and Darrah, 1994). However, there are additional considerations to take into account with regards to plant uptake. For example, plant uptake of specific ions is also related to whether the ion is chemically similar or analogous to a plant nutrient, which may influence whether the ion is transported into plant tissues through active and/or passive (i.e., diffusion) processes. Depending on other prevailing system conditions (e.g., ion sorption to soil), if the ion has nutrient analogs, plant uptake and translocation may be greater than

analytes that do not (Dakora and Phillips, 2002; Robertson et al., 2003). While the actinides (Np and U) do not have nutrient analogs, Cs^+ is analogous to the nutrient K^+ and TcO_4^- uptake may be associated with multiple transport pathways as competition studies have shown TcO_4^- uptake to be reduced in the presence of several anionic plant nutrients (Bennett and Willey, 2003; Cataldo et al., 1983; Echevarria et al., 1998; Robertson et al., 2003). Additionally, plants have also developed various protective mechanisms that limit metal uptake, such as binding metal ions to cell walls, and can detoxify high levels of metals taken into plant tissues through mechanisms such as chelation and vacuolar sequestration, all of which can affect the uptake and translocation of non-essential metal ions (Briat and Lebrun, 1999; Clemens, 2001; Manara, 2012; Robertson et al., 2003; Zenk, 1996).

4.2. Materials and Methods

4.2.1. Column design and construction

The ability of *A. virginicus* to alter the transport of the radionuclides through a soil medium was studied on a macroscale by the use of laboratory scale plant-soil columns (**Figure 4.1**). The main bodies of the columns were constructed from semi-rigid clear PETG (Polyethylene Terephthalate Glycol) tubes, 2 inches (5.08 cm) in diameter and 12 inches (30.48 cm) long. Rhizon© (Rhizosphere Research Products B.V., Wageningen, The Netherlands) pore water sampling tubes (2.5 mm diameter, 5 cm length, 0.15 μm pore size) were inserted perpendicularly into the column at a depths of approximately 3 inches (7.6 cm) and 7 inches (17.8 cm) from where the top of the soil was intended to be upon packing the columns. The Rhizon© tubes were sealed to the column body with marine grade

sealant. The Rhizon© tube ports were used to introduce radionuclides into the column in the root zone after plants were established and to sample the pore water at the conclusion of the experiment. To hold the soil in the column and to allow for drainage, the bottom of the column was covered with 50 µm nylon mesh held in place with laboratory tape on the external column wall. A thin layer of Gorilla Glue was added to the bottom edge of the column to prevent vertical wicking in the mesh around the outside of the column. Additionally, a 2 inch (5.08 cm) diameter vinyl end cap with a 1.5 inch (3.81 cm) hole stamped from its center was fitted over the mesh covered end of the tube to further secure the mesh and to facilitate a snug and stable fit in a specimen cup utilized for effluent collection.

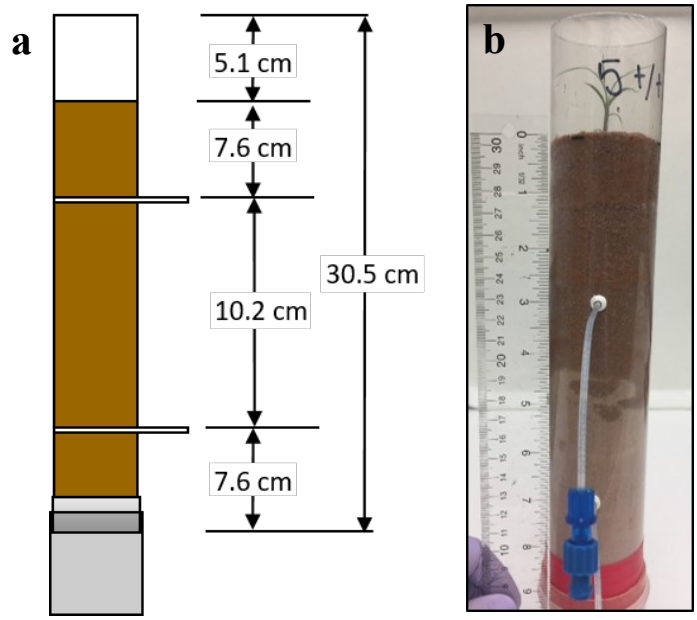

Figure 4.1: (a) Column design and (b) example column during seedling transplantation

After all of the components of the columns were assembled and the sealant was allowed to dry, the columns were dry packed with a 50:50 mixture of SRS soil:sand in lifts

of 1.5 to 2 inches to a depth of 10 inches (25.4 cm), an average of 880.12 ± 0.46 g of soil per column. Between each lift, the column was tapped several times around the top rim of the plastic tube to encourage the soil-sand mixture to settle then the surface of the soil-sand mixture was slightly disturbed with a metal laboratory spatula before the next lift was added. In all, 18 columns were constructed such that three groups of columns with six replicates each were obtained: (1) Plant columns containing plants and radionuclides, (2) No-Plant columns without plants but with radionuclides, and (3) Control columns with plants and without radionuclides (**Figure A.1**).

4.2.2. Plant specimen germination, transplantation, and acclimation

Wild type *A. virginicus* seeds, collected from Clemson, SC, were germinated and grown in a commercial germination mixture in an environmental growth chamber (CARON Products and Services, Inc., Marietta, OH, U.S.; 25 °C, 60 – 75% relative humidity (RH), 14-hr light/10-hr dark cycle, and light intensity of 200 – 300 μmol $m^{-2}s^{-1}$) until seedlings had between three and five leaves. Once an adequate number of seedlings reached an appropriate size, they were carefully removed from the germination mixture and the roots were gently rinsed with water to remove excess germination mixture. In order to transplant the seedlings into the columns without compacting the soil or damaging the seedlings, approximately 100 g of soil:sand mixture was removed from the top of each column and retained in a clean beaker. Approximately 50 mL of water was then slowly pipetted uniformly around the surface of the soil:sand mixture in each column. This was done for all three sets of columns to maintain procedural consistency. For column Groups 1 and 3 (Plant and Control columns) two seedlings were held at about the center of the

column with the root-shoot junction at the original soil surface level as the retained 100 g of soil was slowly added back to the column and leveled as necessary with a laboratory spatula. For column Group 2 (No-Plants), the retained soil was gently poured back into the column and leveled as necessary with a laboratory spatula. Finally, columns were irrigated again by slowly pipetting about 30 mL of water as uniformly as possible over the surface of the soil:sand (**Figure 4.1b**).

The plants were allowed to acclimate in the columns for approximately three weeks in the environmental growth chamber (25 °C, 50-65% RH, 14-hr light/10-hr dark cycle, and light intensity of 300 μmol $m^{-2}s^{-1}$) and were irrigated every two to three days alternating between water or Hoagland nutrient solution, 30 – 50 mL per irrigation event (Hoagland and Arnon, 1950). All column effluent was collected after each irrigation event if available and was bulked by column for further analysis. To reduce light stress to the roots, the external walls of the columns were covered with aluminum foil when the roots were visually observed in the columns (after about one week of acclimation).

4.2.3. Radionuclide introduction into plant-soil columns

A radionuclide solution containing approximately 1000 μg L^{-1} ^{99}Tc (Eckert & Ziegler Isotope Products, Valencia, CA) and 100 μg L^{-1} each of ^{133}Cs (High-Purity Standards, Charleston, SC), ^{237}Np (from Clemson Environmental Radiochemistry Laboratory stock obtained from Oak Ridge National Isotope Development Center), and ^{238}U (High-Purity Standards, Charleston, SC) was prepared and the solution was adjusted to a pH of about 5 with KOH and HNO_3. Under relatively low pH, oxic conditions of the experiments, the working solution should remain unchanged from the initial Cs^+, TcO_4^-,

NpO_2^+, and UO_2^{+2} species. On the day the radionuclide solution was to be introduced to the columns, each column was first irrigated with water and the effluent was collected. The top Rhizon© ports were used to inject approximately 1 mL of radionuclide solution into each column followed by a 1 mL flush injection of DDI water.

As was done during the acclimation period, the columns were housed in the environmental growth chamber under the same conditions and irrigation protocols listed in section *4.2.2*. Irrigation volumes were altered as the plants grew (30 – 80 mL, alternating water or Hoagland nutrient solution) due to higher demand from increased transpiration associated with increased biomass. Effluent was collected from the specimen cup at the base of the column, if present, at each irrigation event and retained for analyte concentration analysis.

4.2.4. Column processing and sample collection

Shoots were harvested four weeks after radionuclide introduction by cutting approximately 1 cm above the soil surface. The freshly cut shoots were placed in 100 mL covered beakers and fresh mass was recorded. The covered specimens were oven dried at 50 °C to a constant weight to obtain dry shoot mass and were retained for further processing.

Just after shoot harvest, the columns were covered and stored vertically at 5 °C until segmentation. Pore water samples were taken immediately prior to segmentation from the top and bottom Rhizon© ports of the columns, if possible (pore water was not able to be collected from the top ports of many columns containing plants). To segment columns, the plastic was cut lengthwise on either side of the column so that approximately half of the

column wall could be removed exposing the soil and roots (of vegetated columns), which had reached the base of the Plant and Control columns by the conclusion of the experiment (**Figure A.2a**). The soil was then cut into 1 cm segments (**Figure A.2b**) and retained in covered Petri dishes for root recovery as well as soil digestion and analysis. The wet mass of the soil segments was recorded on the day of segmentation to allow moisture content to be determined. Due to the large number of samples, the inability to effectively collect roots from the wet soil, and the time between segmentation and further sample processing, the segments were allowed to air dry in a hood before root recovery and sample processing of the roots and soil.

Harvesting the roots from the soil segments consisted of removing roots individually by hand (with tweezers) after gently mixing and breaking up larger particles of soil that were adherent on the roots with a laboratory spatula. The harvested roots and the root-shoot junctions from each column were placed in 100 mL beakers. To remove as much adherent soil as possible from the roots and to determine if there was freely releasable ^{99}Tc on the root surfaces, the roots were soaked for 24 hours in 40 mL of DDI water. The roots were then removed from the beaker containing the DDI water, placed in clean 100 mL covered beakers, and oven dried at 50 °C to a constant weight to obtain dry plant mass and were retained for further processing. The water used to soak the roots (referred to as root rinse) was retained for analyte concentration analysis.

4.2.5. Sample processing and analysis

Aqueous sample aliquots (effluent, pore water, and root rinse) were centrifuged at 8000 rpm for 20 minutes (Allegra 22R centrifuge with a R2402 rotor) and diluted as

appropriate for analysis of ^{99}Tc, ^{133}Cs, ^{237}Np and ^{238}U via inductively coupled mass spectrometry (ICP-MS, Thermo Scientific XSeries II). Limits of detection (LOD) based on the calibration curve corrected for aqueous ICP-MS sample dilution (µg of radionuclide per L of aqueous sample) were: ^{99}Tc $2.9x10^{-3}$ µg L^{-1}, ^{133}Cs $3.0x10^{-2}$ µg L^{-1}, ^{237}Np $1.5x10^{-4}$ µg L^{-1}, ^{238}U $4.8x10^{-3}$ µg L^{-1}.

The oven dried plant parts were acid digested on a hotplate using HNO_3 and H_2O_2 following EPA Method 3050B, Section 7.2 (EPA, 1996). The resulting digestate and DDI digestion beaker rinse were filtered through 0.2 µm polypropylene syringe filters and the filters were rinsed with approximately 5 mL of 2% HNO_3. The filtered digestate samples were diluted as appropriate for ICP-MS analysis of ^{99}Tc, ^{133}Cs, ^{237}Np and ^{238}U. LODs were determined based on the measured ICP-MS digestate analyte concentration corrected to the mass of plant digestate (µg of radionuclide per kg of filtered digestate): ^{99}Tc $1.5x10^{-3}$ µg kg^{-1}, ^{133}Cs $5.9x10^{-2}$ µg kg^{-1}, ^{237}Np $5.7x10^{-5}$ µg kg^{-1}, ^{238}U $1.2x10^{-2}$ µg kg^{-1}. Four method blanks were taken through the entire digestion and sample preparation process.

Soil samples were microwave digested (CEM Corporation, Matthews, NC, U.S.) following EPA method 3051a (modified to use 1 g of soil and HNO_3 only) including at least one sample blank (control soil/sand) and one method blank (acid only) per microwave digestion batch (EPA, 2007). Soil digestate samples were filtered through 0.2 µm polypropylene syringe filters and diluted as appropriate for ICP-MS analysis of ^{99}Tc, ^{133}Cs, ^{237}Np, and ^{238}U. LODs were determined based on the measured ICP-MS digestate analyte concentration corrected to the mass of digested soil (µg of radionuclide per kg of soil): ^{99}Tc $9.4x10^{-2}$ µg kg^{-1}, ^{133}Cs $9.8x10^{-1}$ µg kg^{-1}, ^{237}Np $3.9x10^{-2}$ µg kg^{-1}, ^{238}U $6.6x10^{-1}$ µg kg^{-1}.

Note that the LOD values for water, soil, and plant matter reported above from ICP-MS analysis are dependent on various factors, including the sample matrix, and may change between separate runs on the instrument; the LODs reported above are the maximum values associated with the radionuclides from all runs for the sample matrix type (i.e., aqueous, plant, or soil).

4.2.6. Statistical analysis

One-way analysis of variance (ANOVA) statistical tests were utilized for various comparisons between the three treatment groups for this study, generally comparing only two groups at a time for a given parameter (i.e., Plant vs Control, Plant vs No-Plant, and No-Plant vs Control). One-way ANOVA analyses were conducted for each radionuclide to determine if plant presence in the soil columns significantly affected the radionuclide concentration and mass present in the effluent, pore water, and soil. Additionally, one-way ANOVA analyses were used to determine if ^{133}Cs and ^{238}U concentrations and total masses in the root rinse, plant tissue, and soil samples were significantly different across the groups since these radionuclides are native to the SRS soil utilized in this study. In all cases, significance was taken as $p < 0.05$. All statistical analyses were conducted with Minitab (Minitab 18, State Collage, PA, U.S.).

4.3. Results and Discussion

In general, the presence of plants in the soil columns decreased the flux and concentration of all radionuclides through the soil columns (i.e., into the effluent) and, for ^{99}Tc and ^{237}Np (the most mobile radionuclides), significantly altered the distribution of the radionuclides within the soil column. Two primary plant related mechanisms are suggested

to account for differences in radionuclide releases and soil distribution profiles between columns with plants and columns without plants: (1) hydrologic differences due to increased evapotranspiration as plant biomass increased resulting in significantly reduced effluent volumes from columns with plants compared to the No-Plant columns and (2) plant uptake of radionuclides. However, more subtle mechanisms, such as presence of macropores in some columns, nutrient scavenging activity, and other plant physiological processes, likely influence the differences as well.

It is also important to note that ^{133}Cs and ^{238}U are native to the SRS soil at relatively high concentrations compared to the concentrations of injected radionuclides. Thus, some of the analyses on the column components from the Plant columns and the No-Plant columns are not significantly different than the Control columns for ^{133}Cs and ^{238}U. Additionally, ^{133}Cs and ^{238}U are generally less mobile with higher distribution coefficients and thus, may be less bioavailable in comparison to ^{99}Tc and ^{237}Np. For these reasons ^{99}Tc and ^{237}Np are generally grouped together and ^{133}Cs and ^{238}U are grouped together and discussed separately when appropriate.

4.3.1. Column Effluent

As plant biomass increased throughout the study, the effluent volumes from columns with plants significantly diverged from the effluent volumes from columns without plants (**Figure 4.2**). Daily effluent volumes from Plant and Control columns were significantly different than No-Plant columns after days 4 and 11, respectively and cumulative effluent volumes differed after days 2 and 16, respectively. Additionally, Plant columns and Control columns showed significant differences in cumulative effluent

volumes through day 16; however, the daily effluent volumes, while slightly higher for Control columns on average, were not statistically different from Plant columns after day 2 post-spike. The differing cumulative effluent volumes for the Control columns compared to the Plant columns are likely due to the formation of visible cracks (i.e., macropores) in at least one of the Control columns resulting in an increased percolation rate and greater cumulative effluent, on average, in the Control columns before the plant biomass and resultant increased evapotranspiration became a dominant factor in the hydrology of the system (Al Mamun et al., 2020).

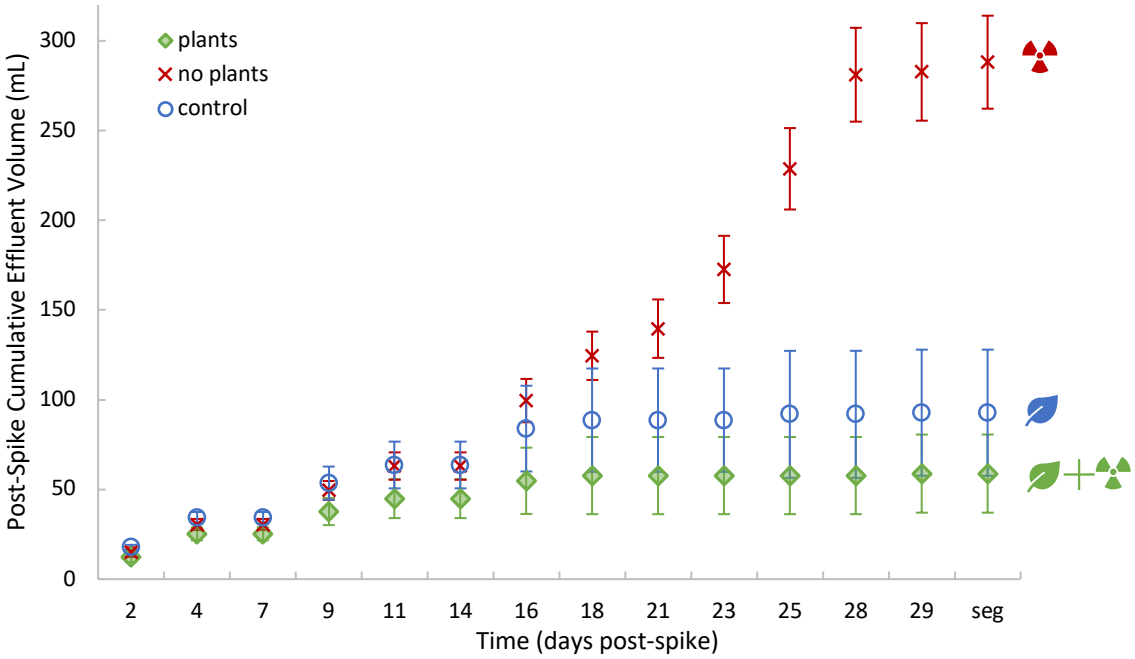

Figure 4.2: Average post-spike cumulative effluent volumes with respect to time (days post-spike) for each group. Error bars represent the standard deviation between the six replicates per group, "seg" refers to the remaining effluent collected on the day the columns were segmented.

Breakthrough curves (concentration of radionuclide in the effluent with respect to time) and cumulative radionuclide mass in the effluent with respect to post-spike cumulative effluent volume are shown in **Figure 4.3** through **Figure 4.6**. Overall, the observed trends in the effluent for ^{99}Tc and ^{237}Np are analogous and the trends for ^{133}Cs and ^{238}U are analogous. Note that "seg" on the x-axis in **Figure 4.2** through **Figure 4.6** refers to the day the columns were segmented which was different for each column.

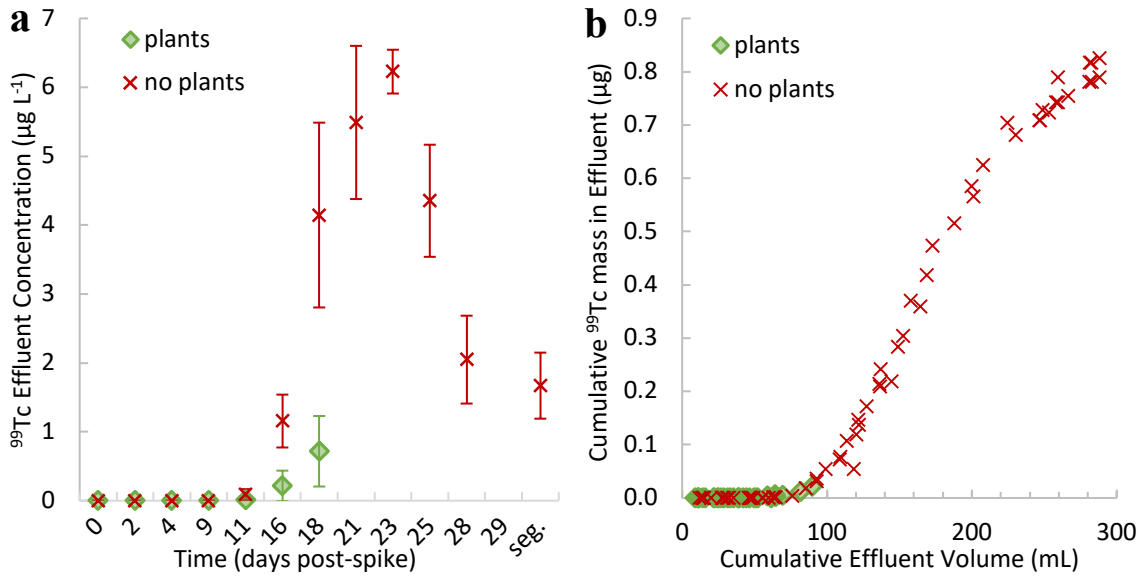

Figure 4.3: Average effluent concentration of ^{99}Tc with respect to days post-spike (a) and cumulative ^{99}Tc mass in effluent with respect to post-spike cumulative effluent volume (b) by group. Error bars represent the standard deviation between the six column replicates per group in plot a, all points are shown in plot b. Note that all control group data were zero and thus, are not shown on these plots for clarity in viewing the other data.

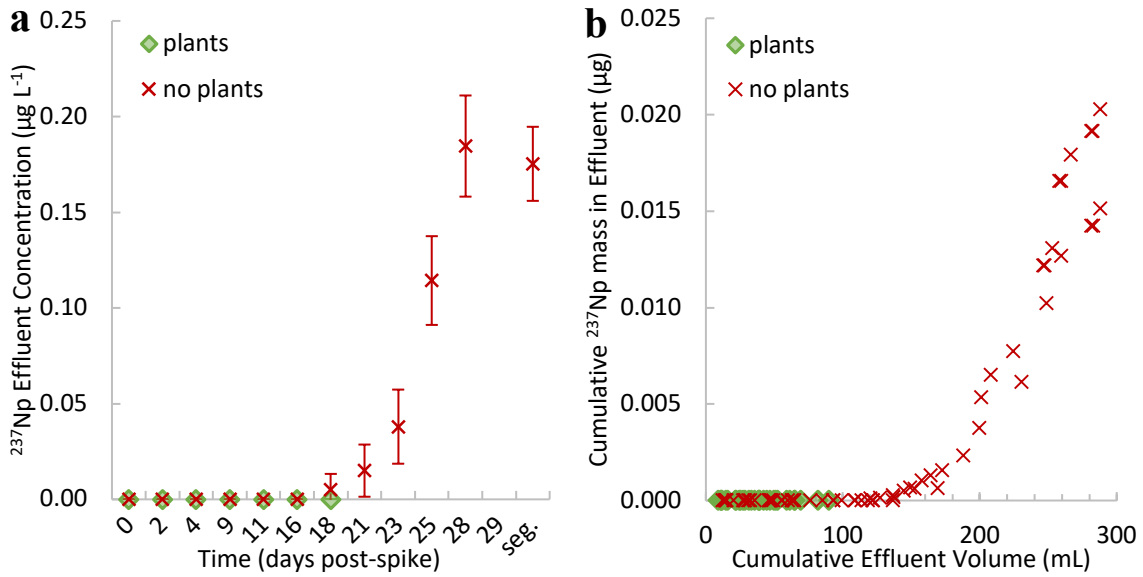

Figure 4.4: Average effluent concentration of ^{237}Np with respect to days post-spike (a) and cumulative ^{237}Np mass in effluent with respect to post-spike cumulative effluent volume (b) by group. Error bars represent the standard deviation between the six column replicates per group in plot a, all points are shown in plot b. Note that all control group data were zero and thus, are not shown on these plots for clarity in viewing the other data.

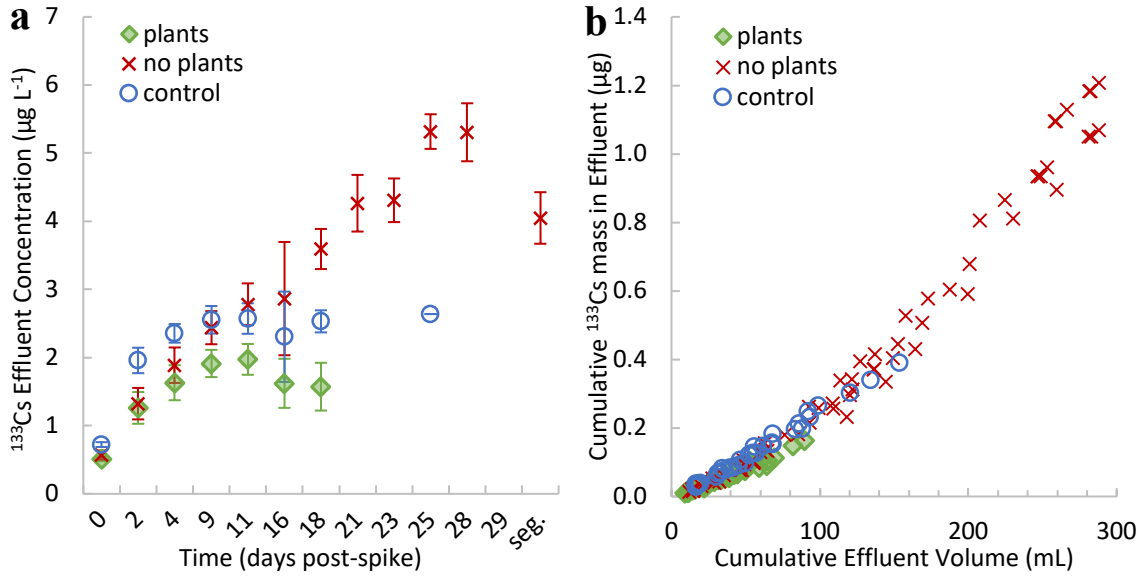

Figure 4.5: Average effluent concentration of ^{133}Cs with respect to days post-spike (a) and cumulative ^{133}Cs mass in effluent with respect to post-spike cumulative effluent volume (b) by group. Error bars represent the standard deviation between the six column replicates per group in plot a, all points are shown in plot b.

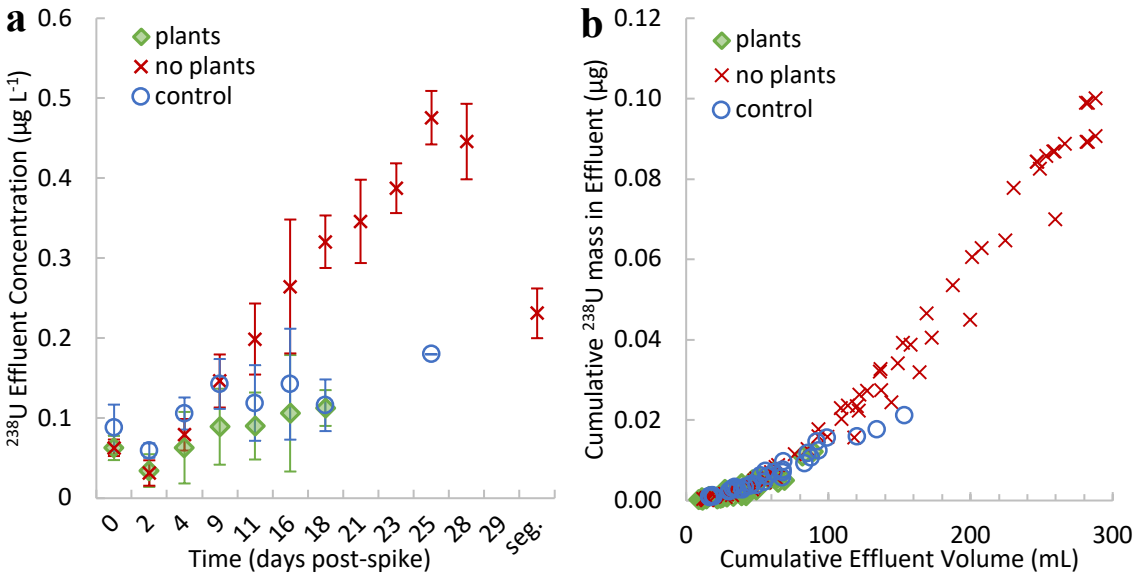

Figure 4.6: Average effluent concentration of ^{238}U with respect to days post-spike (a) and cumulative ^{238}U mass in effluent with respect to post-spike cumulative effluent volume (b) by group. Error bars represent the standard deviation between the six column replicates per group in plot a, all points are shown in plot b.

Owing to their similar environmental mobility (i.e., relatively low K_d), ^{99}Tc and ^{237}Np exhibited similar trends in the effluent (Montgomery et al., 2017). However, since $K_{d,Tc} < K_{d,Np}$, ^{99}Tc is expected to migrate faster and to a greater extent through the columns and resulted in earlier breakthrough into the effluent for ^{99}Tc (**Figure 4.3a** and **Figure 4.4a**). Additionally, ^{237}Np was not detected in the effluent of any Plant column and ^{99}Tc only reached a maximum concentration of 1.3 µg L^{-1} and maximum cumulative mass of 2.2x10^{-2} µg in the effluent of Plant columns; a clear contrast to the No-Plant columns which attained much higher maximum values (**Figure 4.3** and **Figure 4.4**). Technetium and neptunium were not detected in the effluent of any Control columns. ANOVA analysis comparing Plant to No-Plant columns indicated statistically different effluent concentrations of ^{99}Tc after day 11 post-spike and statistically different total radionuclide

mass in the effluent for both ^{99}Tc and ^{237}Np (ANOVA analysis for ^{237}Np concentration was not appropriate due to lack of ^{237}Np in Plant column effluent). The effluent concentration and cumulative radionuclide mass data coupled with the effluent volume data supports the concept that the presence of plants significantly affects (reduces and/or retards) the transport of the mobile radionuclides through the soil columns by affecting the hydrology of the system.

In contrast to ^{99}Tc and ^{237}Np, ^{133}Cs and ^{238}U were present in the effluent before the radionuclide spike introduction and were present in the Control columns since they are native to the SRS soil (**Figure 4.5a** and **Figure 4.6a**). Even still, the effluent concentrations differed significantly between the No-Plant columns and Plant or Control columns by the last several effluent collection events for columns with plants and the total radionuclide mass collected in the effluent of Plant and Control columns was significantly less than that from No-Plant columns (**Figure 4.5** and **Figure 4.6**). When considering the cumulative radionuclide mass with respect to cumulative effluent volume post-spike, ANOVA analysis was conducted by grouping the data into volume bins (0-20 mL, 20-40 mL, 40-60 mL, 60-90 mL, 90-160 mL) by group such that each bin contained at least 5 data points per group, except the last bin which was only contained data for No-Plant and Control columns. This analysis indicated that the cumulative mass was generally consistent between No-Plant columns and Plant or Control columns although, there were some exceptions below 40 mL for ^{133}Cs and ^{238}U in Control columns and in the highest volume bin for ^{133}Cs in Plant columns and ^{238}U in Control columns. Despite the cumulative radionuclide mass being generally consistent between columns with plants and columns without plants, the

lack of effluent generated after day 18 post-spike for all but one Control column leads to the same general conclusion as is applicable for ^{99}Tc and ^{237}Np; the alteration of the system hydrology due to the presence of plants results in reduced effluent overall and thus, reduced aqueous transport of the radionuclides from the soil matrix in the effluent within the timeframe examined.

4.3.2. Soil and pore water

The soil concentration profiles for ^{99}Tc and ^{237}Np further illustrate the retardation effect caused by the presence of plants in the soil columns **Figure 4.7**. For example, in the No-Plant columns, the majority of ^{99}Tc had been washed into the effluent resulting in many soil segment concentrations being below the LOD whereas, Plant columns still held a large proportion of the injected ^{99}Tc in the soil-pore water matrix (**Figure 4.3** and **Figure 4.7a**). The concentration profiles for ^{237}Np also provide additional insight into the effluent data by showing that the front of ^{237}Np pulse had not yet reached the bottom of the Plant columns while significantly higher concentrations of ^{237}Np were present at the base of No-Plant columns. In addition, the soil profiles show various degrees of upward migration, particularly evident for ^{237}Np in the Plant columns, as noted by the elevated concentrations above the injection point, 0 on the y-axis (**Figure 4.7b**). Moreover, the total radionuclide mass retained in soil columns was significantly different between Plant and No-Plant columns for both radionuclides.

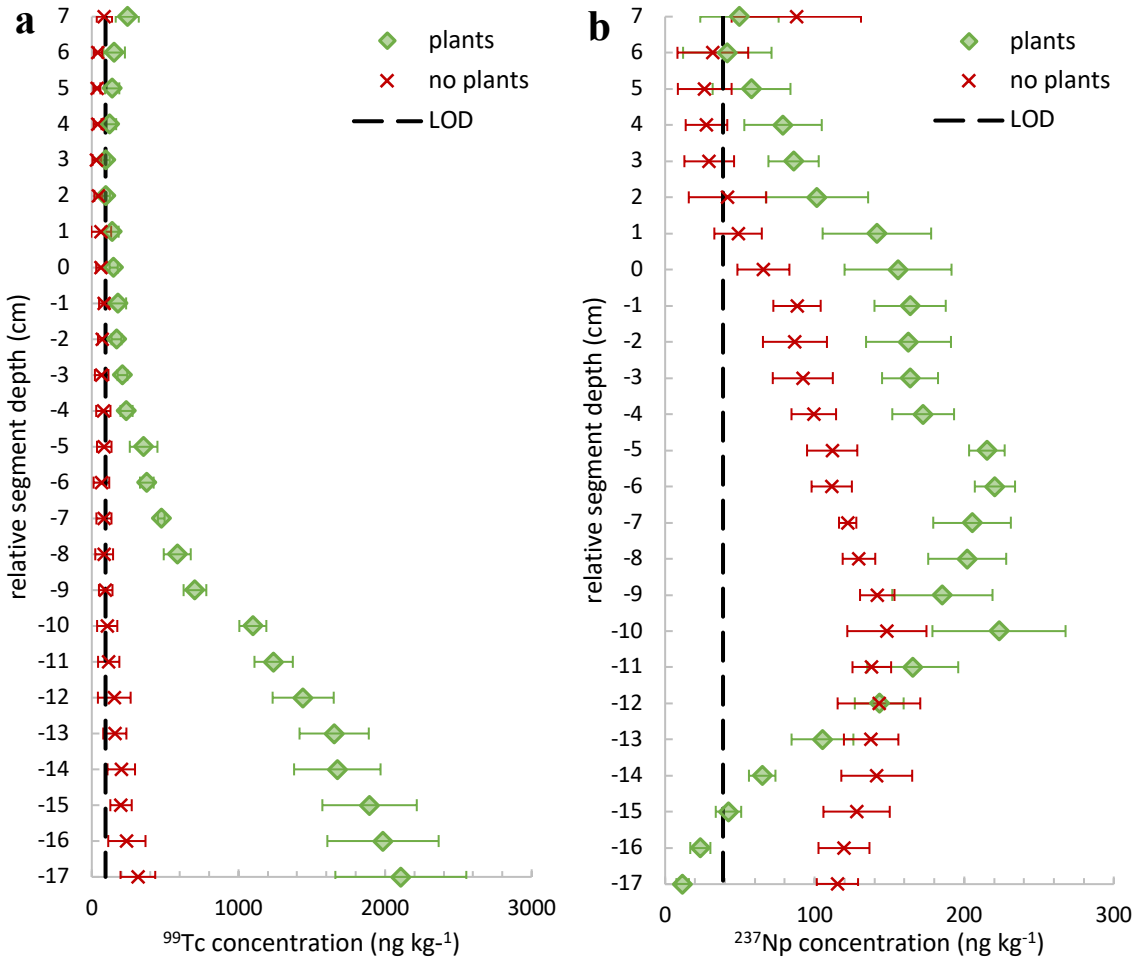

Figure 4.7: Average soil column concentration profiles by group for ^{99}Tc (a) and ^{237}Np (b) with respect to depth relative to the radionuclide injection point, i.e., the top port (the zero value on the y-axis). The error bars represent the standard deviation between the six column replicates per group. Note that all control group soil concentrations were below the LOD thus, the control soil profiles are not shown on these plots.

In contrast to ^{99}Tc and ^{237}Np, ^{133}Cs and ^{238}U soil concentration profiles were essentially indistinguishable between the three groups and did not show any distinct pattern (for ^{133}Cs) or were relatively consistent (for ^{238}U) with depth throughout the soil columns (**Figure A.3**). ANOVA analyses indicated that: (1) the mean total radionuclide mass per column was not significantly different between the three groups for both radionuclides, (2) comparing each segment by group, for all but one segment, mean segment concentrations

were not significantly different between the three groups for both radionuclides, and (3) comparing within each group by segment, for all groups, there was not a significant difference between mean segment concentrations for ^{238}U but there were significant differences in mean segment concentrations for ^{133}Cs (although there was no distinct pattern with depth). While plant presence affected the total amount of ^{133}Cs and ^{238}U released from the columns through the effluent, their native presence in the SRS soil at relatively high concentrations and their relatively high sorption affinities dominated the system. Thus, plant presence did not result in an appreciable redistribution of these radionuclides in the soil columns that was detectable with the soil sample processing and analytical methods utilized herein.

Pore water sample concentrations for top and bottom ports for all radionuclides are listed in **Table 4.1**. When comparing to the soil concentration profile depths, the top port was located at "0" cm relative segment depth and the bottom port was located at "-10" cm relative segment depth. Columns that contained plants did not always have sufficient moisture content (**Figure A.4**) to allow pore water sample collection from both ports, generally the top port was not able to liberate samples in these cases.

Table 4.1: Average pore water concentrations and standard deviations of available group replicates for top and bottom port samples. Note that not all plant columns produced pore water samples from both ports (Plant Columns: $n_{top} = 3$, $n_{bottom} = 6$; No-Plant Columns: $n_{top} = n_{bottom} = 6$; Control Columns: $n_{top} = 1$, $n_{bottom} = 5$).

		Plant Columns		No-Plant Columns		Control Columns	
		Average	S.D.	Average	S.D.	Average	S.D.
^{99}Tc ($\mu g\ L^{-1}$)	Top	0.49	0.09	0.34	0.21	< LOD	
	Bottom	3.4	0.45	0.35	0.21	< LOD	
^{237}Np ($\mu g\ L^{-1}$)	Top	0.15	0.02	0.09	0.02	< LOD	
	Bottom	0.29	0.06	0.18	0.03	< LOD	
^{133}Cs ($\mu g\ L^{-1}$)	Top	1.6	0.48	1.5	0.15	1.5[a]	
	Bottom	3.2	0.72	2.3	0.33	2.7	0.47
^{238}U ($\mu g\ L^{-1}$)	Top	0.87	0.09	0.62	0.05	0.14[a]	
	Bottom	0.36	0.05	0.24	0.05	0.34	0.04

[a]single sample

Pore water sample concentrations for ^{99}Tc and ^{237}Np aligned with the trends observed in the soil concentration profiles (**Table 4.1**, **Figure 4.3**, and **Figure 4.4**). For instance, comparing top and bottom port sample concentrations by group, for all cases except ^{99}Tc in No-Plant columns (where most of the ^{99}Tc had been washed out of the columns), the mean pore water concentrations from top ports were statistically different than bottom ports, with the bottom port sample concentrations generally being greater. Additionally, comparing groups by port, Plant column pore water samples (top or bottom port) were statistically different (except for ^{99}Tc in top ports) and generally greater than those from No-Plant columns. This agreement is expected for ^{99}Tc and ^{237}Np since these radionuclides are not native to the SRS soil thus, detection of these injected radionuclides was not overshadowed by their prior presence and since these radionuclides exhibit relatively weak, reversable sorption, they should be readily present in the pore water if they are present in the soil matrix.

Pore water samples for ^{133}Cs and ^{238}U provide a more nuanced perspective of the radionuclide's presence in freely available forms (i.e., in the aqueous phase) within the

soil-pore water matrix than could be deduced from the soil concentration profiles (**Table 4.1**, **Figure A.3**). As with ^{99}Tc and ^{237}Np, the concentrations of ^{133}Cs and ^{238}U were statistically different between top and bottom ports within groups; ^{133}Cs concentrations were greater in all bottom ports while ^{238}U concentrations were generally greater in top ports, except for the single top port sample from the Control columns. Comparing top or bottom ports between groups, ^{133}Cs concentrations were only statistically different in the bottom ports between Plant and No-Plant columns while ^{238}U concentrations are significantly different for all comparisons except bottom ports between Plant and Control columns. This indicates that plant presence may have affected the aqueous phase concentrations of ^{238}U and possibly ^{133}Cs although, this data alone is not sufficient to draw any concrete conclusions to this effect, particularly since the differences between the groups, while they may be statistically significant, are relatively small in most cases and since there was only one top port sample for Control columns.

4.3.3. Plant samples and concentration ratios

Plant tissue concentrations for each radionuclide are shown in **Figure 4.8**, percent of the total radionuclide mass (in the whole plant) for each plant part and radionuclide are listed in **Table 4.2**, and the average mass of plant tissues are listed in **Table A.1**. Additionally, concentration ratios (CR) which normalize plant concentration (C_{plant}, $\mu g_{radionuclide}\ g^{-1}$ plant) to average soil concentration (C_{soil}, $\mu g_{radionuclide}\ g^{-1}$ dry soil), were calculated so that plant uptake and trends could be more effectively compared between the radionuclides **(Equation 4.1**, **Table 4.3)** (Beresford et al., 2008; Brown et al., 2008; IAEA, 2014; ICRP, 2009a).

$$CR = \frac{C_{\text{plant}}}{C_{\text{soil}}} \tag{4.1}$$

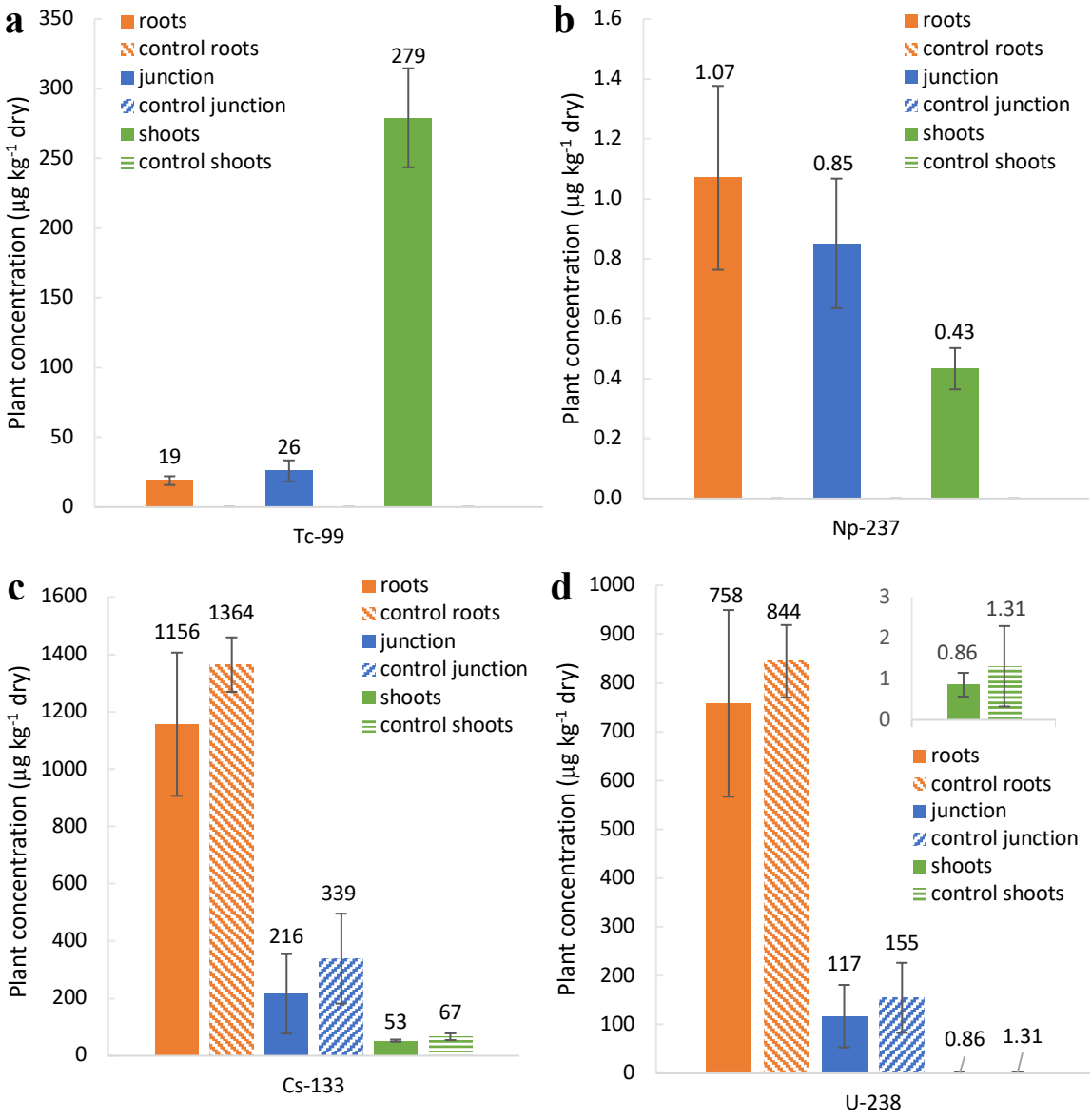

Figure 4.8: Average plant concentration by plant part (roots, root-shoot junctions shoots), radionuclide, and group. The error bars indicate the standard deviation for the six plant specimens per group. Note that all ^{99}Tc and ^{237}Np control values were less than the LOD.

Table 4.2: Average percent of total radionuclide mass in the plant by plant part and group.

		Plant Columns		Control Columns	
		Average	S.D.	Average	S.D.
^{99}Tc	Shoots	95.5%	0.6%	< LOD	
	Junction	0.5%	0.1%	< LOD	
	Roots	4.1%	0.6%	< LOD	
^{237}Np	Shoots	38.4%	7.5%	< LOD	
	Junction	4.0%	1.2%	< LOD	
	Roots	57.6%	8.4%	< LOD	
^{133}Cs	Shoots	7.2%	2.6%	7.5%	1.2%
	Junction	1.5%	1.0%	2.4%	1.0%
	Roots	91.3%	2.8%	90.2%	0.7%
^{238}U	Shoots	0.2%	0.1%	0.3%	0.3%
	Junction	1.4%	0.9%	1.9%	0.9%
	Roots	98.4%	1.0%	97.8%	1.0%

Table 4.3: Concentration ratios ($\mu g_{radionuclide}\, g^{-1}$ plant per $\mu g_{radionuclide}\, g^{-1}$ dry soil) by plant part and for the whole plant (WP). Note that the shoot CRs based off both fresh mass and dry mass are listed and other CRs are based on dry plant mass only.

		Plant Columns		Control Columns	
		Average	S.D.	Average	S.D.
^{99}Tc	Shoots[a]	280	60	< LOD	
	Shoots	400	92	< LOD	
	Junction	36	9.0	< LOD	
	Roots	27	7.1	< LOD	
	WP	250	53	< LOD	
^{237}Np	Shoots[a]	2.4	0.42	< LOD	
	Shoots	3.4	0.64	< LOD	
	Junction	6.7	1.65	< LOD	
	Roots	8.5	2.72	< LOD	
	WP	5.4	1.28	< LOD	
^{133}Cs	Shoots[a]	0.09	0.01	0.10	0.02
	Shoots	0.12	0.01	0.15	0.03
	Junction	0.49	0.27	0.78	0.38
	Roots	2.7	0.50	3.1	0.23
	WP	1.1	0.25	1.2	0.17
^{238}U	Shoots[a]	2.1×10^{-3}	5.8×10^{-4}	3.1×10^{-3}	2.6×10^{-3}
	Shoots	2.9×10^{-3}	8.2×10^{-4}	4.6×10^{-3}	3.6×10^{-3}
	Junction	0.39	0.19	0.54	0.27
	Roots	2.6	0.56	2.9	0.25
	WP	0.99	0.26	1.1	0.13

[a]based on fresh mass

Several general trends were apparent regarding plant uptake and partitioning within plant tissues:

(1) overall plant uptake followed the same pattern as radionuclide mobility (the opposite of sorption and complexation affinity)

$$^{99}Tc >> ^{237}Np > ^{133}Cs \gtrsim ^{238}U$$

(2) partitioning trends in plant tissues were similar for ^{237}Np, ^{133}Cs, and ^{238}U

$$C_{roots} > C_{junction} > C_{shoots}$$

(3) partitioning within plant tissues for ^{99}Tc was the opposite of the other radionuclides

$$C_{shoots} >> C_{junction} > C_{roots}$$

Additionally, CRs for ^{133}Cs and ^{238}U were within reported soil to plant CR ranges for grasses while ^{99}Tc and ^{237}Np CRs were greater, although ^{99}Tc CRs were within reported ranges for other plant groups (e.g., pasture) and ^{237}Np shoot CRs were similar to CRs for other plants (e.g., alfalfa, bushbean) (Cataldo et al., 1988; IAEA, 2014, 2010; ICRP, 2009a; Robertson et al., 2003). Further, in comparison to prior hydroponically (HP) determined CRs for this plant species, all ^{237}Np CRs and ^{99}Tc root and junction CRs were similar to HP CRs, ^{99}Tc shoot and whole plant CRs were greater, and ^{133}Cs and ^{238}U CRs were less than HP CRs (Montgomery et al., 2018).

Technetium behaved quite differently than any of the other radionuclides with respect to plant uptake, partitioning mainly in shoot tissues, which contained ~95% of all ^{88}Tc associated with plant tissues, whereas other radionuclides showed greater partitioning in the roots (**Figure 4.8** and **Table 4.2**). Previous hydroponic studies with *A. virginicus*

have shown that ^{99}Tc can accumulate in shoots, possibly to a greater extent in shoot tips, and shoot concentration increases with contact time while concentration in roots remains relatively constant (Montgomery et al., 2018). The high uptake of ^{99}Tc is proposed to be mainly a result of its analogous nature to multiple plant nutrients and due its dominant persistence as the mobile oxyanion (TcO_4^-) in the aqueous phase and associated low K_d under oxic conditions (Icenhower et al., 2010; Robertson et al., 2003). The continual plant uptake and translocation to shoot tissues for ^{99}Tc resulted in shoot concentrations being about an order of magnitude greater than ^{133}Cs even though the pore water concentrations of these two radionuclides were similar (**Figure 4.8**, **Table 4.1**). Additionally, ^{99}Tc exhibited the greatest relative uptake into all tissues compared to the other radionuclides resulting in ^{99}Tc CRs being one to five orders of magnitude greater than CRs of other radionuclides depending on the tissue (**Table 4.3**).

The relative uptake of ^{237}Np was intermediate in comparison to the other radionuclides (**Table 4.3**). Neptunium is the most mobile of the actinides due to its predominance in the pentavalent oxidation state (NpO_2^+) resulting in relatively high plant availability and uptake (Cataldo et al., 1988; Robertson et al., 2003). Even though ^{237}Np does not have a nutrient analog, its greater mobility (and lower K_d) compared to ^{133}Cs and ^{238}U resulted in a larger fraction of the ^{237}Np existing in pore water and thus, greater CRs over the native radionuclides. Additionally, although plant tissues did concentrate ^{237}Np more in the roots, the percent (of total ^{237}Np in the plant) translocated to the shoots, while less than ^{99}Tc, was still relatively high (~38% on average) compared to Cs (< 10 % in shoots) and U (< 1 % in shoots) (**Figure 4.8**, **Table 4.2**, **Table 4.3**); similar fractional

distributions have been observed for other plants (e.g., alfalfa, bushbean, soybean) (Cataldo et al., 1988).

Cesium and ^{238}U exhibited the lowest relative uptake of all the radionuclides (i.e., lowest CRs) in large part due to their higher K_d values. Cesium, being analogous to the nutrient K^+, is generally expected to exhibit greater uptake and translocation into shoots than radionuclides without nutrient analogs (e.g., ^{238}U). Comparing the relative uptake of ^{133}Cs and ^{238}U into plant tissues (i.e., CRs), this expected trend is observed for shoots where ^{133}Cs shoot CRs were greater than those for ^{238}U by one to two orders of magnitude. Yet, for other tissues (roots and junction) and for the whole plant, ^{133}Cs and ^{238}U exhibited similar relative uptake; ANOVA analyses did not indicate significant differences in mean CRs between these radionuclides for any tissue other than shoots (**Table 4.3**). Additionally, the lower mobility of ^{133}Cs and ^{238}U (due to higher K_d values) and, for ^{133}Cs, competition with K^+ (present in the nutrient solution used to irrigate the columns) are factors that can decrease plant uptake and result in lower CRs (Robertson et al., 2003). Thus, these factors are likely major contributors which resulted in the lower CRs for ^{133}Cs and ^{238}U in comparison to ^{99}Tc and ^{237}Np as well as lower CRs in comparison to prior HP uptake studies (**Table 4.3**) (Montgomery et al., 2018). Overall, the higher ^{133}Cs shoot CRs relative to ^{238}U are likely (in part) a result of its analogous nature to K^+ and the lack of nutrient analog for ^{238}U; however, the competition with K^+ present in the system (for ^{133}Cs) and the relatively high K_d values (compared to ^{99}Tc and ^{237}Np) contributed to the limited uptake and translocation of ^{133}Cs and ^{238}U despite the greater abundance in the soil and, in some cases, the soil solution (i.e., pore water and effluent).

In addition to the differences in plant uptake between ^{99}Tc and the other radionuclides, the fraction of ^{99}Tc contained in the root rinse was also substantial, accounting for an average of 29% (range of 11% – 54%) of what would have been attributed to the root tissues if the root rinse procedure was not performed; the root rinse fractions for ^{133}Cs and ^{238}U were much lower and no ^{237}Np was detected in root rinse samples (**Table A.2**). This indicates that a greater fraction of the ^{99}Tc associated with root tissues is easily leachable, still mobile and thus, not irreversibly incorporated into root tissues compared to other radionuclides, which were not as easily leached from roots and/or root associated soils (e.g., root adherent and rhizosphere soils) likely due to a combination of incorporation into root tissues and surface sorption to roots and associated soils by the other radionuclides.

4.3.4. System compartment percentages: a look at the system as a whole

In order to discuss the systems in an integrated, holistic manner, compartment radionuclide percentages by group are shown in **Table 4.4**; additionally, average compartment radionuclide masses are shown in **Table A.3**.

Table 4.4: Average percent of total radionuclide mass in each compartment by group. Note that pore water percentages only represent the actual percent of radionuclide mass in pore water samples, not an estimated percent of radionuclide mass in all pore water in the columns.

		Plant Columns		No-Plant Columns		Control Columns	
		Average	S.D.	Average	S.D.	Average	S.D.
^{99}Tc	Soil	53.4%	5.09%	10.5%	5.10%	< LOD	
	Plant	44.0%	5.89%	--	--	< LOD	
	Effluent	0.48%	0.75%	89.1%	5.21%	< LOD	
	Pore Water	1.26%	0.26%	0.33%	0.17%	< LOD	
	Root Rinse	0.82%	0.64%	--	--	< LOD	
^{237}Np	Soil	96.9%	0.63%	81.2%	3.76%	< LOD	
	Plant	1.78%	0.47%	--	--	< LOD	
	Effluent	< LOD		17.7%	3.86%	< LOD	
	Pore Water	1.26%	0.32%	1.08%	0.12%	< LOD	
	Root Rinse	< LOD		--	--	< LOD	
^{133}Cs	Soil	99.6%	0.10%	99.7%	0.04%	99.6%	0.05%
	Plant	0.37%	0.10%	--	--	0.31%	0.07%
	Effluent	0.04%	< 0.01%	0.33%	0.04%	0.08%	0.03%
	Pore Water	< 0.01%	< 0.01%	< 0.01%	< 0.01%	< 0.01%	< 0.01%
	Root Rinse	< 0.01%	< 0.01%	--	--	< 0.01%	< 0.01%
^{238}U	Soil	99.6%	0.10%	> 99.9%	< 0.01%	99.7%	0.06%
	Plant	0.34%	0.09%	--	--	0.26%	0.05%
	Effluent	< 0.01%	< 0.01%	0.04%	< 0.01%	< 0.01%	< 0.01%
	Pore Water	< 0.01%	< 0.01%	< 0.01%	< 0.01%	< 0.01%	< 0.01%
	Root Rinse	< 0.01%	< 0.01%	--	--	0.02%	0.01%

Overall, the effects on radionuclide migration and redistribution within the column systems due to plant presence followed the same trend as mobility and plant uptake (i.e., ^{99}Tc >> ^{237}Np > ^{133}Cs ≳ ^{238}U; discussed in section *4.3.3*). Based on the high plant uptake of ^{99}Tc (i.e. ~44% of ^{99}Tc associated with plant biomass) as well as the drastic reduction in effluent volumes and amount of ^{99}Tc in the effluent (**Figure 4.2**, **Figure 4.3**, **Table 4.4**), we can conclude that (as expected) ^{99}Tc is substantially affected by both plant uptake and plant associated hydrologic effects. Neptunium, on the other hand, was mainly affected by hydrology differences between the systems, although plant uptake did occur with relatively high CRs (**Table 4.3**, **Table 4.4**); thus, the plant uptake vector cannot be discredited when

investigating over longer time periods and for further environmental transport (e.g., food chain transport).

Although plant biomass was associated with < 0.5% of ^{133}Cs or ^{238}U in the systems, there were some notable differences in which compartment the plant "removed" these radionuclides from. For ^{133}Cs, the plant uptake seems to be directly related with what would have been in the effluent; however, for ^{238}U, the plant seemed to remove the ^{238}U mainly from the soil fraction (**Table 4.4**). This is not, however, unreasonable or unexpected since the K_d for ^{238}U is greater than ^{133}Cs for this SRS soil by about an order of magnitude thus, more ^{133}Cs would have inherently existed in the pore water and would be freely available for plant uptake (Montgomery et al., 2017). However, it is quite interesting that the CRs in roots and the root-shoot junction compartments were not statistically different for these radionuclides. While the higher shoot CR for ^{133}Cs can be attributed (at least in part) to its analogous nature to the nutrient K^+, ^{238}U has no such analog. Thus, the similar uptake into root and junction tissues despite the greater affinity for ^{238}U sorption to soil indicates that some plant metabolic or physiological process is affecting the sorption of ^{238}U to the soil and thus, resulting in some desorption from the soil and subsequent affiliation with plant tissues. Previous studies investigating the effects of plant root exudates on the sorption of these radionuclides demonstrated this phenomenon; namely that presence of relatively high concentrations of plant exudates could liberate native ^{238}U from SRS soil but had no such effect on ^{133}Cs (Montgomery et al., 2017).

4.3.5. Environmental significance

Understanding the ability of plants to accumulate, affect the overall transport, and, in some cases, affect the distribution (including upward contaminant migration) within soils is an important aspect of environmental transport and risk assessment modeling approaches. A major objective of this study was to elucidate the major factors as well as, with information gained from prior studies on components of this system, some minor factors associated with plant induced alterations in the subsurface transport of a broad suite of environmentally relevant radionuclides. The self-consistency (i.e., consistency in soil, plant species, radionuclides) between this study and prior work on the individual components of this system provides a substantial and wide-ranging data set that that can be utilized to develop more robust environmental transport and risk assessment models for these radionuclides specific to SRS soils and, potentially, other field conditions.

Acknowledgements

This work is supported by the United States Department of Energy Office of Science, Office of Basic Energy Sciences and Office of Biological and Environmental Research under Award number DE-SC-00012530. Partial faculty support (NEM) was provided by the United States Nuclear Regulatory Commission Nuclear Education Grant #NRC-HQ-13-G-38-0002.

CHAPTER FIVE

DOSIMETRIC MODELING OF Tc-99, Cs-137, Np-237, AND U-238 IN THE GRASS SPECIES *ANDROPOGON VIRGINICUS*: DEVELOPMENT AND COMPARISON OF STYLIZED, VOXEL, AND HYBRID PHANTOM GEOMETRY

[As published in the Journal of Environmental Radioactivity 211 with minor revisions]

Abstract

This paper discusses the development, comparison, and application of three anatomically representative computational phantoms for the grass species *Andropogon virginicus*, an indigenous grass species in the Southeastern United States. Specifically, the phantoms developed in this work are: (1) a stylized phantom where plant organs (roots or shoots) are represented by simple geometric shapes, (2) a voxel phantom developed from micro-CT imagery of a plant specimen, and (3) a hybrid phantom resulting from the refinement of (2) by use of non-uniform rational basis spline (NURBS) surfaces. For each computational phantom, Monte Carlo dosimetric modeling was utilized to determine whole-organism and organ specific dose coefficients (DC) associated with external and internal exposure to ^{99}Tc, ^{137}Cs, ^{237}Np, and ^{238}U for *A. virginicus*. Model DCs were compared to each other and to current values for the ICRP reference wild grass in order to determine if noteworthy differences resulted from the utilization of more anatomically realistic phantom geometry. Modeled internal DCs were comparable with ICRP values. However, modeled external DCs were more variable with respect to ICRP values; this is proposed to be primarily due to differences in organism and source geometry definitions. Overall, the three anatomical phantoms were reasonably consistent. Some noticeable differences in internal DCs were observed between the stylized model and the voxel or

hybrid models for external DCs for shoots and for cases of crossfire between plant organs. Additionally, uptake data from previous hydroponic (HP) experiments was applied in conjunction with hybrid model DCs to determine dose rates to the plant from individual radionuclides as an example of practical application. Although the models within are applied to a small-scale, hypothetical scenario as proof-of-principle, the potential, real-world utility of such complex dosimetric models for non-human biota is discussed, and a fit-for purpose approach for application of these models is proposed.

5.1. Introduction

5.1.1. Current Radiation Protection System and Dosimetric Modeling Standards for Non-human Biota

For all cases of exposure to radioactive contaminants, establishment of appropriate dose-effect relationships and protection standards requires accurate dosimetry. In order to effectively evaluate dose to an organism, quantitative measurements must be made and/or rigorous modeling must be employed to estimate dose, as is typically the case for internal dosimetry (Martinez et al., 2016). These principles apply not only to humans, but also to non-human biota, with application in radioecology and environmental radiation protection. The contemporary interpretation of environmental radiation protection has evolved from the stance of "…if man is adequately protected then other living things are also likely to be sufficiently protected" towards protecting the environment in the explicit sense, with consideration given to various worldviews (e.g., anthropocentric, ecocentric, biocentric, etc.) (ICRP, 2017, 2009a, 2008, 2007, 2003, 1977). Despite the various perspectives as to how environmental radiation protection should be implemented, the end objective of

avoiding detrimental effects within the environment is the same. With this view, then, comes the need for more refined knowledge of dose-effect relationships and potential impacts to flora and fauna in radiation exposure scenarios, which is likely to require detailed dosimetric evaluations.

Presently, the use of organism-representative ellipsoidal models with uniform distribution of radioisotopes is recommended by the ICRP and employed in RESRAD-BIOTA and the ERICA tool for evaluating whole-organism dose to non-human biota via use of Monte Carlo methods and/or analytical calculations (Brown et al., 2008; Gómez-Ros et al., 2008; ICRP, 2017, 2008; USDOE, 2002). The Monte Carlo dosimetric modeling methods involve defining appropriate organism geometry, organ and surrounding media elemental composition and densities, radiation type and energies, and source(s) and target(s) of interest thereby allowing determination of Dose Coefficients (DCs) specific to the defined variables in the model. Many whole-organism DCs have been compiled and tabulated for the representative organism geometries and select radioisotopes, for example, Reference Animals and Plants of ICRP 108 (2008). These DCs along with associated activity concentration of the organism or surrounding media allow determination of the absorbed dose rate and accumulated dose. While current non-human biota dose estimation methods are generally conservative and sufficient for a typical first-tier screening or environmental risk assessment, cases for which screening levels are exceeded generally necessitate more detailed dose assessments for at least some biota (e.g., endangered or key species) (Jackson et al., 2014; Stark et al., 2017). Consequently, the use of detailed, anatomically realistic dosimetric models, similar to those implemented for humans, is

likely more appropriate in these cases as well as in robust laboratory or organism scale dose-effect studies.

5.1.2. Evolution of Dosimetric Modeling for Non-human Biota

In recent years, interest in the development and use of more complex geometry definitions for non-human biota has increased. Development of preclinical murine models (e.g., mice and rats) was an initial focus; however, recently models for various wildlife species (generally in-line with ICRP Reference Animals and Plants, RAPs) have been and are being developed for use in radioecology, environmental radiation protection, and non-human biota dosimetry research (Martinez, 2015; Xie and Zaidi, 2016; Zaidi, 2018; Zaidi and Tsui, 2009). The three general types of these complex or refined models include complex stylized phantoms, voxel phantoms, and hybrid or boundary representation (BREP) phantoms, with the majority of non-human biota phantoms being developed for various animal species (Martinez, 2015; Xie and Zaidi, 2016; Zaidi, 2018; Zaidi and Tsui, 2009). Complex stylized models incorporate multiple geometric shapes representing (key) internal organs and surrounding media. These phantoms are more physically representative than simple, whole body, uniform distribution ellipsoidal models and the level of detail can be adjusted based on the anatomy of the specific organism (e.g., size, density, location, and elemental composition of specific organs of interest, etc.) as well as characteristics of external media (Martinez et al., 2014; Montgomery et al., 2016). As a further advance to a more realistic and representative organism geometry, voxel models utilize CT imagery (or other appropriate image acquisition modalities) and associated software to reconstruct organ geometry by defining it in terms of a voxel matrix. Several examples of non-human

voxel models (aside from the numerous murine models) include the rabbit, crab, frog, canine, and trout (Caffrey et al., 2016; Caffrey and Higley, 2013; Kinase, 2008; Kramer et al., 2012; Martinez et al., 2014a; Ruedig et al., 2014; Zaidi, 2018). The most recent and the most realistic representations are in the form of hybrid or boundary representation (BREP) phantoms that utilize Non-uniform rational B-Spline (NURBS) or surface mesh techniques. These models improve upon the geometry representation of voxel models by development of smoothed and refined surface boundaries that have the advantage of being easily manipulated. Completed hybrid phantoms have been developed for mice, rats, trout, and several canines (Martinez, 2015; Martinez et al., 2016; Padilla et al., 2008; Segars et al., 2004; Stabin et al., 2015; Zaidi, 2018; Zhang et al., 2009). Although voxel and hybrid type phantoms are more realistic and physically accurate, they also may require a significant amount of time for phantom creation and possibly increased computational time in comparison the simple ellipsoid or complex stylized models, which must be taken into account when evaluating if the level of detail and accuracy is necessary for a particular scenario (Martinez, 2015; Martinez et al., 2014a; Ruedig et al., 2015; Stark et al., 2017).

5.1.3. Study Scope and Objectives

While multiple non-human biota phantoms of varying degrees of complexity have been developed, to our knowledge, all but two are for various animal species (Biermans et al., 2014a, 2014b; Yoschenko et al., 2011). Additionally, no other voxel or hybrid plant-specific phantoms have been completed and presented in the open literature as of yet, although at least one other hybrid-type plant phantom is in development (Condon and Higley, 2018). Of particular interest in this work are the development, utilization, and

comparison of plant-specific dosimetric modeling techniques (i.e., stylized, voxel, and hybrid phantoms) for the grass species *Andropogon virginicus* (broomsedge) considering internal and external exposure to technetium-99 (^{99}Tc), cesium-137 (^{137}Cs), neptunium-237 (^{237}Np), and uranium-238 (^{238}U) based on prior laboratory hydroponic (HP) uptake experiments (Montgomery et al., 2018).

The grass species, *A. virginicus*, is a native species in the Southeastern United States and was selected as the model plant for previous uptake studies due to its widespread prevalence and high tolerance to various environmental stressors (Campbell, 1983; Ezaki et al., 2008; Montgomery et al., 2018). The basis of selection for the suite of radionuclides (i.e., ^{99}Tc, ^{137}Cs, ^{237}Np, and ^{238}U) utilized in previous experimental studies is discussed fully elsewhere (Montgomery et al., 2017, 2018). The use of this particular suite of radionuclides is not intended to be comprehensive or represent a particularly wide and encompassing range of particle types and energies, although this suite does include alpha, beta, and gamma emitters. Instead, this suite of radionuclides was utilized within the computational dosimetric evaluation process to show the direct applicability of the dosimetric models to a specific previously studied experimental system (Montgomery et al., 2018). The consistent use of the plant species between laboratory uptake experiments and the computational efforts allows the uptake data to be combined with computationally determined DCs to determine dose rate to plants in the prior uptake experiments (as an example of application). In addition, wild type grass is the ICRP small terrestrial reference plant. Therefore, utilizing a grass species as a model plant for this study allows for valuable comparison to ICRP parameters and values (ICRP, 2017, 2008).

Specific objectives for this study include:

(1) Develop increasingly realistic anatomically relevant plant-specific phantoms for use in Monte Carlo based dosimetric modeling (stylized, voxel, and hybrid phantoms) based on prior experimental conditions;

(2) Discuss the development of each type of phantom in detail and the associated benefits and/or disadvantages;

(3) Compare DCs for the selected radionuclides;

(4) Combine model DCs with prior plant experimental uptake data to evaluate dose rate as an example of application.

5.2. Materials and Methods

5.2.1. Computational Phantom Development

Monte Carlo N-Particle (MCNP) transport code[1] was used for dosimetric modeling of *A. virginicus* incorporating stylized, voxel, and hybrid phantoms to compare and evaluate differences between the three geometry definition methods (Goorley et al., 2012; Pelowitz, 2011). In general, stylized, voxel, and hybrid type phantoms were developed according to methods previously described by Martinez et al. (2016, 2014a) with details specific to this work discussed in sections *5.2.1.1* through *5.2.3* and further detail given in supplementary information (SI) as noted (**Appendix B**). Note that a conceptual model summarizing the workflow described below can be found in **SI Figure B.1**. Additionally,

[1] MCNP6 version 1.0 or MCNPX version 2.7.0; Radiation Safety Information Computational Center, Oak Ridge, TN

should other researchers desire to use the phantoms presented in this work, they are available upon request by contacting the corresponding author.

5.2.1.1. Stylized Phantom

The stylized phantom (**Figure 5.1**) was created based on measurements of a young *A. virginicus* specimen considering three shoots and three roots. The roots were submerged in HP nutrient solution (assumed to have the properties of water for computational modeling purposes) which was contained in a borosilicate glass Erlenmeyer flask to reflect the conditions of prior laboratory uptake experiments (Montgomery et al., 2018). MCNPX Visual Editor[2] was utilized to create and visually confirm the geometry of the plant organs and other key components of the stylized model ensuring that no boundary overlaps occurred; specific details of the defined geometry are described in **Table 5.1** and volumes are listed in **Table 5.2**.

[2] MCNPX 2.7E, April 2011; Radiation Safety Information Computational Center, Oak Ridge, TN

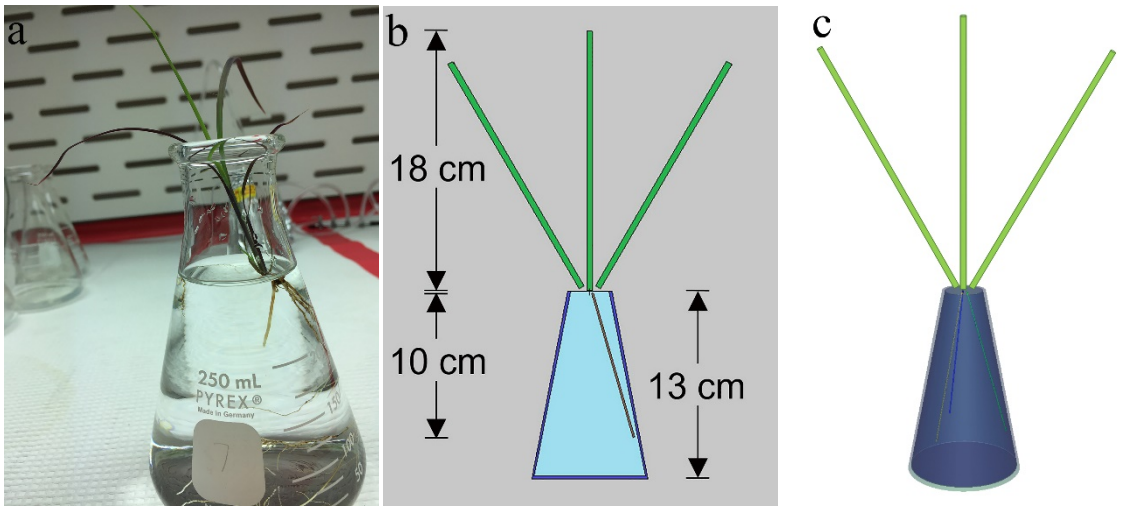

Figure 5.1: A typical *A. virginicus* specimen in a flask with HP solution (a) as well as 2D (b) and 3D (c) depictions of the stylized phantom. Three roots were modeled as right cylinders and three shoots were modeled as elliptical cylinders; note only the root intersecting the x-z transverse plane is shown in the 2D depiction (b).

Table 5.1: Geometric description of the plant organs (roots or shoots) and key components (flask and HP solution) created for the stylized model

Organ or Component	Geometric Description
Roots	3 right circular cylinders; 10.38 cm length, 0.05 cm radius; at an angle of 15.64° from vertical; rotated by 0°, 120°, and 240° with respect to the x-z plane about the z-axis
Shoots	3 right elliptical cylinders; 18 cm length, with base ellipse having a 0.2 cm major radius and 0.05 cm minor radius; in the x-z plane vertically (center shoot) or tilted 30° to the left or right of vertical (left or right shoot)
Flask	2 truncated right angle cones (nested); outer surface: 13 cm tall, 4 cm bottom radius, 1.5 cm top radius; inner surface: 12.8 cm tall, 3.8 cm bottom radius, 1.3 cm top radius
HP solution	Truncated right-angle cone filling the internal volume of the flask

Table 5.2: Plant organ and HP solution volume comparison for stylized, voxel, and hybrid phantoms (note CF indicates compression factor).

	Volume (cm^3)		
Phantom	Roots	Shoots	HP solution
Stylized	$2.45x10^{-1}$	$1.70x10^{0}$	$2.82x10^{2}$
Voxel CF4	$4.41x10^{-1}$	$3.74x10^{-1}$	$3.96x10^{2}$
Hybrid CF2	$4.14x10^{-1}$	$3.75x10^{-1}$	$4.93x10^{2}$
Hybrid CF4	$4.13x10^{-1}$	$3.75x10^{-1}$	$4.93x10^{2}$

5.2.1.2. Voxel Phantom

The *A. virginicus* specimen for which the stylized phantom length measurements were based on was also the model specimen for the voxel and hybrid phantoms **(Figure 5.2a**). A custom, vertically-oriented micro-CT[3] and associated reconstruction software was used to acquire multiple transverse CT image files of the specimen with slice thickness of 0.05 mm (3897 total slices) and pixel resolution of 0.05 mm (1280 x 1280 pixel array). A subset of the CT image files (155 slices, 1.25 mm slice thickness) were imported into 3D-Doctor software[4] where the plant organs (roots or shoots) were then manually outlined in each transverse plane to create a *.BND file, an ASCII file which defines the contours (or outlines) for the set of transverse planes. The *.BND file was then converted to a MCNP-usable lattice format via LatticeTool[5] software (version 1.0.2). LatticeTool is a multifunction code that incorporates the Voxelizer[5] code described by Kramer et al. (2010). Within LatticeTool a compression factor (CF) can be defined which reduces the pixel array in the x-y (i.e., transverse) plane resulting in a lower resolution but potentially significantly reduced file sizes, particularly for cases where a defined source is of large volume.

[3] MILabs, Utrecht, Netherlands
[4] Version 5.0, AbleSoftware Corp, Lexington, MA
[5] Human Monitoring Laboratory (HML), Health Canada, Ottawa

Specifically, a CF of 4 resulted in a pixel array of 320 x 320 pixels (0.2 mm pixel resolution) and a CF of 2 resulted in a pixel array of 640 x 640 pixels (0.1 mm pixel resolution). A CF of 4 was used to maintain reasonable input file sizes (and thus reasonable computational time) for the voxel model, particularly when the HP solution was the defined source of external exposure for MCNP calculations. A CF of 2 was initially utilized for cases where the roots or shoots were the defined source of internal exposure for MCNP calculations, but very little difference (≤1.10%) was noted when compared to the results (e.g., MeV deposited to target organ/disintegration) from a CF of 4.

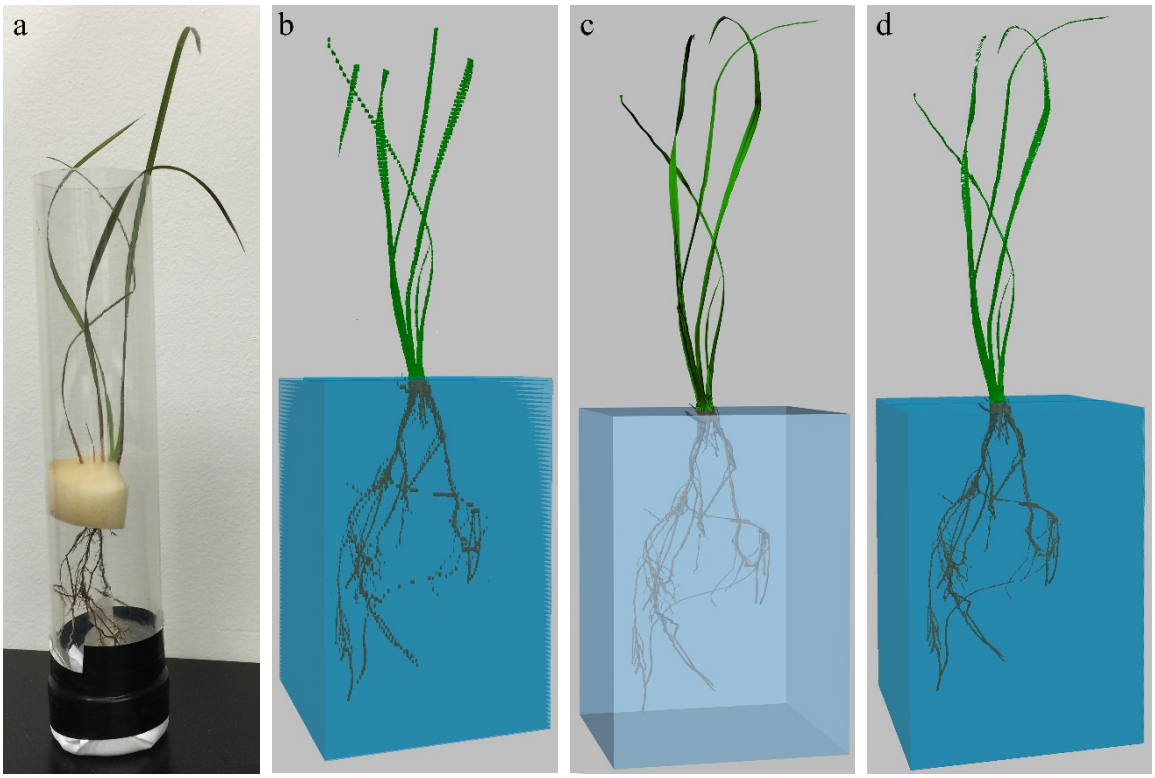

Figure 5.2: : Model A. virginicus specimen in a tube suitable for use in the micro-CT (a), 3D rendered voxel phantom (b), interim NURBS model (c), and final hybrid phantom (d).

Initially the conversion of the *.BND file to lattice geometry resulted in three defined universes: roots, shoots, and air surrounding all plant organs. In order to

incorporate the HP solution, the lattice script was altered by hand to change the air surrounding the roots to a fourth universe, water (representing HP solution). Additionally, SDEF_helper[5] (Kramer et al., 2010) was utilized to generate appropriate source definition scripts (for roots, shoots, or HP solution) corresponding to the lattice input script. The resulting 3D rendering of the voxel phantom is shown in **Figure 5.2b**. The number of voxels in each of the plant organs and HP solution as well as the total number of voxels for the model is shown in **Table 5.3** with associated volumes listed in **Table 5.2**.

Table 5.3: Number of voxels associated with the different components of the voxel and hybrid phantom models for compression factors of 2 and 4.

Phantom	Roots	Shoots	HP solution	Total
Voxel CF 2	$3.5x10^4$	$3.0x10^4$	$3.2x10^7$	$6.3x10^7$
Voxel CF 4	$8.8x10^3$	$7.5x10^3$	$7.8x10^6$	$1.6x10^7$
Hybrid CF 2	$1.7x10^5$	$1.5x10^5$	$2.0x10^8$	$4.5x10^8$
Hybrid CF 4	$4.1x10^4$	$3.8x10^4$	$4.9x10^7$	$1.1x10^8$

5.2.1.3. Hybrid Phantom

The development of the hybrid phantom builds upon the voxel phantom. In addition to a *.BND file, which defines the organ contours of each transverse cross-section, a 3D object (*.OBJ) file can also be created within 3D-Doctor; this is essentially the 3D rendering of the (voxel) phantom (**Figure 5.2b**). The *.OBJ file of the voxel phantom created in 3D-Doctor was then imported into Rhinoceros[6] where transverse contours were fit to the 3D voxel phantom. It is possible to directly import *.BND files to Rhinoceros, however, for this specific instance it was found that importing as a *.OBJ file and fitting contours at smaller intervals (than the initial number of slices of the voxel phantom) was

[6] Version 5; McNeel North America

more suitable for creating NURBS surfaces and allowed for better visualization of the 3D geometry while doing so. Within Rhinoceros, various commands, including "Loft", "BlendSrf", "MergeSrf", "Bend", and "Smooth", were utilized to fit smooth NURBS surfaces to the updated contours of the voxel phantom. Additionally, several shoot discontinuities resulting from some portions of the shoots being slightly outside the active CT area were corrected within Rhinoceros to create the interim NURBS model (**Figure 5.2c**). This geometry correction not only serves to make the hybrid phantom a more complete representation of the specimen, but also serves as an example of how hybrid phantom geometries may be easily manipulated, a key benefit of hybrid models over voxel models.

The Rhinoceros NURBS model was then exported as a *.SLC file and imported back into 3D-Doctor (**Figure 5.2d**); this process essentially re-slices the NURBS model. A slice thickness of 0.25 mm was chosen resulting in 921 transverse slices; the workspace in 3D-Doctor was resized to be 1400 x 1400 pixels and was calibrated for a pixel dimension of 0.05 mm before import of the *.SLC file to retain x-y resolution and avoid dimensional errors when importing the Rhinoceros file into 3D-Doctor. The overall size of this phantom was slightly larger (mainly taller, but also slightly larger in the x-y dimensions) than the original voxel phantom due to the alteration of the shoot geometry. Within 3D-Doctor, each cross section was inspected to correct any overlapping boundaries that may have been created while developing the NURBS surface due to the complex nature of the root and shoot structure and occasional necessity of having overlapping surfaces. In the cases where overlapping boundaries were detected the boundaries were merged such that the outer most

contour was kept and all interior contours were deleted. As was done for the voxel model (section *5.2.1.2*), the final 3D-Doctor *.BND file was imported into LatticeTool to convert the boundaries to lattice format usable by MCNP, the lattice script was updated to include HP solution (as water) as a fourth universe in the root zone, and SDEF_helper was used to generate the source definition portion of the MCNP input scripts. A CF of 2 was chosen for cases when the shoots and/or roots were the source and a CF of 4 was chosen for cases when the HP solution was the source to maintain reasonable file sizes. The numbers of voxels for each of the final input scripts are listed in **Table 5.3** with associated volumes listed in **Table 5.2**.

5.2.2. Source Definition and Model Parameters

Within MCNP, the source (i.e., the material or organ(s) that contains the radionuclide) was considered either the plant roots, shoots, roots and shoots together, or the HP solution with uniform distribution of ^{99}Tc, ^{137}Cs, ^{237}Np, or ^{238}U and where the disintegrations of the nuclide are randomly distributed throughout the defined source. The targets (i.e., the organ(s) for which the energy from decay is deposited) were considered to be plant organs only (roots and/or shoots). Separate runs were conducted for each isotope and source combination as well as for different particle types (alpha, beta, and gamma only). For beta particle runs (i.e., ^{99}Tc and ^{137}Cs), the beta energies were defined by a probability density distribution describing the beta spectrum (Stabin and da Luz, 2002). For gamma and alpha particles, discrete energy values and corresponding emission probabilities were defined from data from the National Nuclear Data Center (NNDC), Brookhaven National Laboratory (BNL) online Chart of Nuclides

(https://www.nndc.bnl.gov/nudat2/). For example, for ^{137}Cs, a gamma energy of 0.6617 MeV (associated with the isomeric transition of the daughter, ^{137m}Ba) with 85.1% yield was defined within the MCNP script. For ^{237}Np and ^{238}U, all alpha energies and probabilities listed on the BNL Chart of Nuclides were defined within the MCNP script. Progeny from ^{237}Np or ^{238}U, discrete electrons, and characteristic x-rays were excluded from calculations. Additionally, 10^8 disintegrations (particles) were chosen for all runs to maintain reasonable computational times of less than 72 hours per run. There were several cases for which 10^8 particles were not reached within the allowed compute times, specifically the stylized runs for alpha particles; however, at least 10^7 particles were obtained within the allotted times and relative errors were exceptionally small (≤ 0.0003). Plant organ elemental composition was taken to be that of southern pine and the density of the fresh plant organ was determined to be approximately 1.03 g cm^{-1} via use of a Mettler Toledo XS104 balance with density kit (McConn Jr. et al., 2011). The elemental composition and density of the HP solution and of the glass flask were taken to be that of water and borosilicate glass, respectively (McConn Jr. et al., 2011). All MCNP simulations were run on the Palmetto Cluster at Clemson University.

5.2.3. Determination of DC and Dose Rates

Within the MCNP script, the user must indicate the desired output of the MCNP calculation (e.g., current, flux, energy deposition, etc.); this is done through the use of tally cards (Pelowitz, 2011). MCNP's *f8 tally function was utilized within the MCNP input script to record and tabulate the energy deposited in each target organ (plant roots and/or shoots) per disintegration occurring in the specified source (i.e., MeV dis^{-1}). Relative error

is reported for each tally in the MCNP output which provides indication of the reliability of the tally result; generally, a relative error of < 0.1 is considered reliable (Pelowitz, 2011). Therefore, for cases where the relative error of the *f8 tally was in excess of 0.1 (10%) the tally value was excluded from further calculations; see the online supplementary information file for *f8 tally output and specific exclusions (**Appendix B, Table B.1a – 1c**). The output for each plant organ or the whole plant was used to determine the associated Dose Coefficient (DC), which is simply the ratio of the dose rate to the target organ to the activity concentration in the source. The DC is calculated by:

$$DC = K \cdot E \cdot \frac{m_{source}}{m_{target}} \quad \textbf{(5.1)}$$

where, E is the average energy deposited in the target per disintegration in the source (MeV dis^{-1}, from MCNP *f8), K is a constant (numerical value of 5.7672x10^{-4}) that converts MeV dis^{-1} (E) to μGy h^{-1} per Bq kg^{-1} (DC), and m_{source} and m_{target} are the masses of the source and target of the phantom defined in the MCNP script, respectively. The masses of the phantom components (roots, shoots, and HP solution) were calculated by multiplying the volume of the component (**Table 5.2**) by the density of the component (1.03 g cm^{-1} for plant organs or 1.00 g cm^{-1} for HP solution). The mass ratio in **Equation 5.1** reduces to one when the source organ is the same as the target organ (self-absorption) but is necessary for cases where the source is not the same as the target organ (crossfire or external source). The mass ratio is required in these cases so that the DC units correctly represent the dose rate to the target organ per activity concentration in the source due to the nature of the MCNP output, i.e., energy deposited in the target organ per disintegration in the source (Loevinger et al., 1991; Martinez et al., 2016).

The DC was used with previous experimental temporal activity concentration data to determine the dose rate to the plant (from internal and external sources) for the sampling points in the laboratory experiment (Montgomery et al., 2018). The dose rate to the target organ, $\dot{D}_{target}(t)$, at a given point in time is calculated by:

$$\dot{D}_{target}(t) = DC \cdot B_{source}(t) \quad \textbf{(5.2)}$$

where, $B_{source}\ (t)$ is the activity concentration (Bq kg^{-1}) of the source at a given time.

5.3. Results

5.3.1. Dosimetric Modeling: DC Comparisons

5.3.1.1. Whole plant DC comparisons

Modeled whole organism internal DCs (where the root and shoot together were the source and target) were notably consistent with ICRP 136 reported values (Annex B; Tables B.13, B23, B.35, B.38), but slightly lower in all cases (**Figure 5.3**) (ICRP, 2017). The maximum percent difference between internal DCs and ICRP 136 DCs were 53% for ^{137}Cs, 19% for ^{99}Tc, 3% for ^{237}Np, and 4% for ^{238}U. Note that modeled DCs are shown relative to ICRP 136 values in **Figure 5.3** and **Figure 5.4**; see online supplementary information for tabulated values and comparisons (**SI Table B.3**).

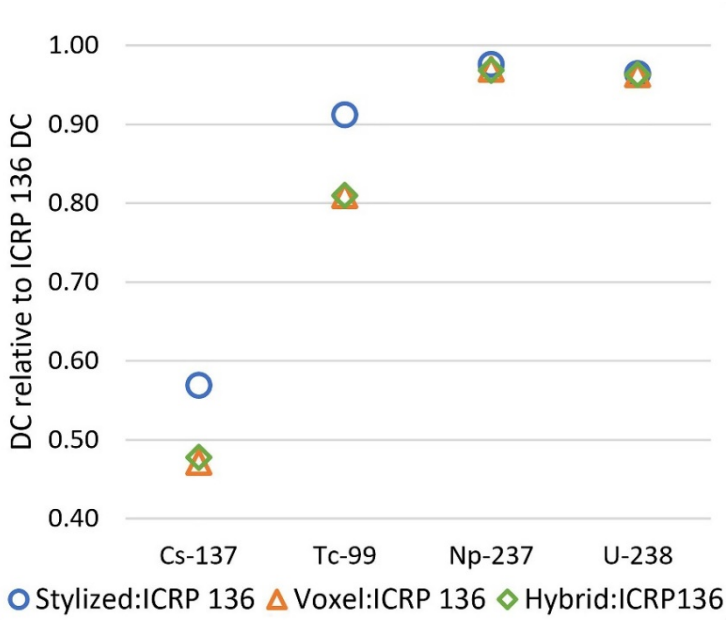

Figure 5.3: Whole plant modeled internal DCs relative to ICRP 136 reported internal DCs for wild grass (ICRP, 2017).

Modeled external DCs were more variable with respect to ICRP 136 values for wild grass on the ground (**Figure 5.4**, **SI Table B.3**) (ICRP, 2017). Modeled external DCs for ^{137}Cs (all phantoms), ^{237}Np (all phantoms), and ^{238}U (stylized phantom only) were within about one order of magnitude of ICRP values, while other modeled external DCs were greater than ICRP 136 values by up to about five orders of magnitude (greatest difference for ^{99}Tc). Additionally, modeled DCs were typically greater than ICRP values except for ^{137}Cs (all phantoms) and ^{237}Np (stylized phantom only), although these were also the DCs that were the closest to ICRP values. Given the external geometry of the models, with the roots (roughly half of the plant) being submerged in HP solution, the external DCs were also compared to one-half of the ICRP external aquatic DC for wild grass as a rough

comparison (ICRP, 2017). In this case, all of the modeled DCs, including ^{99}Tc, were within two orders of magnitude of ICRP values (**Figure 5.4**, **SI Table B.3**).

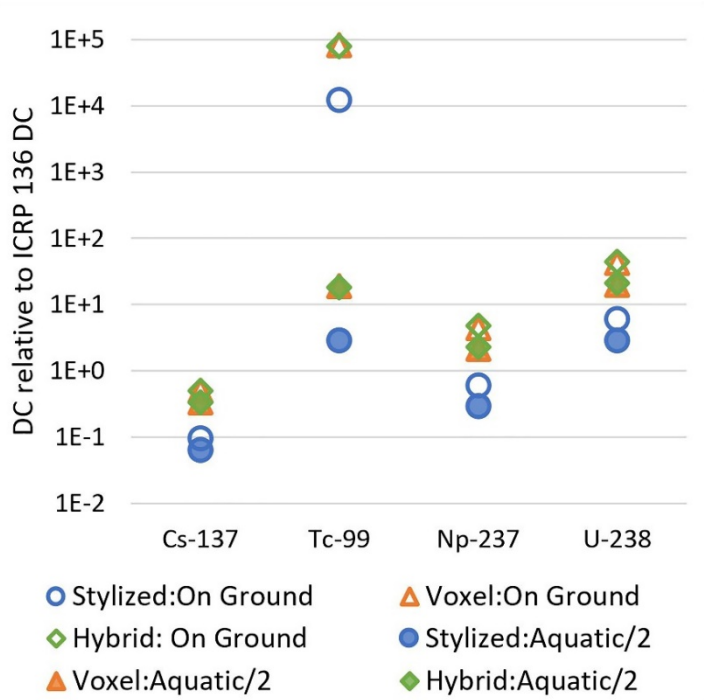

Figure 5.4: Whole plant modeled external DCs relative to ICRP 136 reported external DCs of wild grass on the ground (open points) and, as a rough comparison of experimental conditions, relative to one-half of the ICRP 136 reported external DC for aquatic exposure of wild grass (shaded points) (ICRP, 2017).

The differences between external DCs for the models developed in this work and ICRP values are likely due to a combination of several factors when comparing how the systems are defined. The most obvious disparity is between how the ICRP defines the external geometry of the system and the how the modeled system is defined (i.e., the difference in assumed geometry of the modeled plant with respect to the external source), as well as density differences (comparing the HP solution density to that of soil, for example). For this work, only the roots are submersed in the HP solution source with the shoots extending vertically above. The ICRP reference grass is modeled as a 10 cm thick

infinite homogeneous layer (mixture of biomass and air; density of 13.7 kg m^{-3}) parallel to the ground. DCs are determined assuming external exposure to this layer from an identically-sized, uniformly-distributed volume source of soil located underneath, which neglects exposure to the below ground portions of the plant (ICRP, 2017, 2008).

Another source of difference between DCs is the type of radiation accounted for. For external exposure of terrestrial organisms, the ICRP only considers external exposure to photons, neglecting contributions to dose from electrons or alpha particles, with the suggestion to apply the aquatic DC with a geometric factor of 0.5 as a conservative estimate for small organisms on or close to the ground (ICRP, 2017, 2008). Additionally, the models presented herein did not include discrete electrons (internal conversion or Auger) or characteristic x-rays, which likely contributed somewhat to differences between modeled DCs and ICRP DCs, although the geometry differences are still considered to be the dominant contributing factor.

In comparing the three models to each other, the whole plant internal DCs agreed to within 20% in all cases (**Figure 5.3**, **SI Table B.2**). The percent differences between the modeled whole plant external DCs were greatest between the voxel or hybrid and stylized models (81-87% difference, with the stylized model DCs being smaller) due to geometry differences but, voxel and hybrid models are more consistent with < 7% difference for all cases (**Figure 5.4**, **SI Table B.2**).

5.3.1.2. Plant Organ DCs: Phantom Comparisons

In addition to whole plant DCs used for comparison to literature values, individual DCs for all target←source combinations were determined. This allows for evaluation of

differences between stylized, voxel, and hybrid phantom geometry for specific plant organs as well as estimation of organ specific dose and/or dose rate. Please refer to online supplementary information (**SI Table B.2**) for tabulated data and comparisons accompanying the figures presented in this section.

The organ specific external DCs are compared in **Figure 5.5**. Please note that Shoot←HP DCs for ^{238}U are zero and thus, are not shown on the log scale in **Figure 5.5** and Shoot←HP *f8 values for ^{237}Np were previously excluded from further calculation (i.e., DCs were not calculated for these specific cases) due to high relative error (Section *5.2.3,* **SI Table B.1a– 1c**).

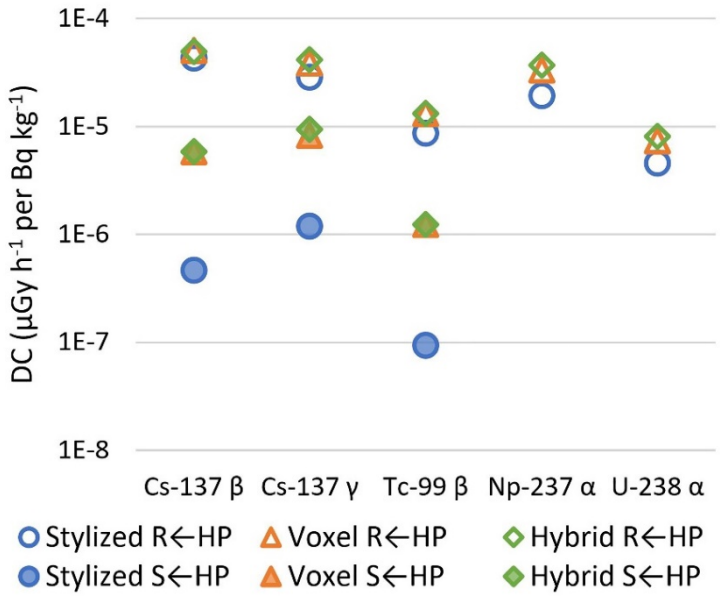

Figure 5.5: External DC (HP solution as the source) evaluated by target plant part (roots, open points, or shoots, closed points), nuclide and radiation type, and phantom type (stylized, voxel, and hybrid). Shoot←HP DCs for ^{238}U were zero thus, are not shown on the log scale and Shoot←HP ^{237}Np values were previously excluded.

Trends for the organ specific external DCs are similar to those for whole plant external DCs. For each specific nuclide/particle and target←source combination, most DCs

are comparable with a typical trend of hybrid DCs ≈ voxel DCs > stylized DCs. Additionally, the DCs for the shoots were consistently lower, than the DCs for the roots, as expected, since the roots are immersed in the HP solution and the shoots are not. Voxel and hybrid models were consistent with each other in all cases with a maximum percent difference of 12%. However, noticeable differences exist between the hybrid or voxel and stylized models, particularly for the shoots, where the DCs of the stylized model are about one order of magnitude lower than hybrid or voxel models. The stylized DCs for the roots are more comparable to the voxel and hybrid models with ≤ 48% difference between individual cases (highest differences for alpha particles). Thus, for the organ specific external DCs, similar to the comparison for the whole plant modeled external DCs, the differences in DCs are mainly associated with differences between stylized and voxel or hybrid phantom geometries. Specifically, for the case of the differences in shoot DCs, the mass of the stylized shoots (directly related to shoot volume, **Table 5.2**) and the gap between the shoots and HP solution, among other factors, contributes to the differences between models.

Individual internal DCs (root or shoot source) are shown in **Figure 5.6**. For cases where the target and the source were the same organ (i.e., root←root and shoot←shoot) all three phantoms were in good agreement with a maximum percent difference of 42% (for ^{137}Cs gamma), although differences were typically much smaller being < 1% for ^{237}Np and ^{238}U and <15% for ^{99}Tc (**Figure 5.6a** and **Figure 5.6c**).

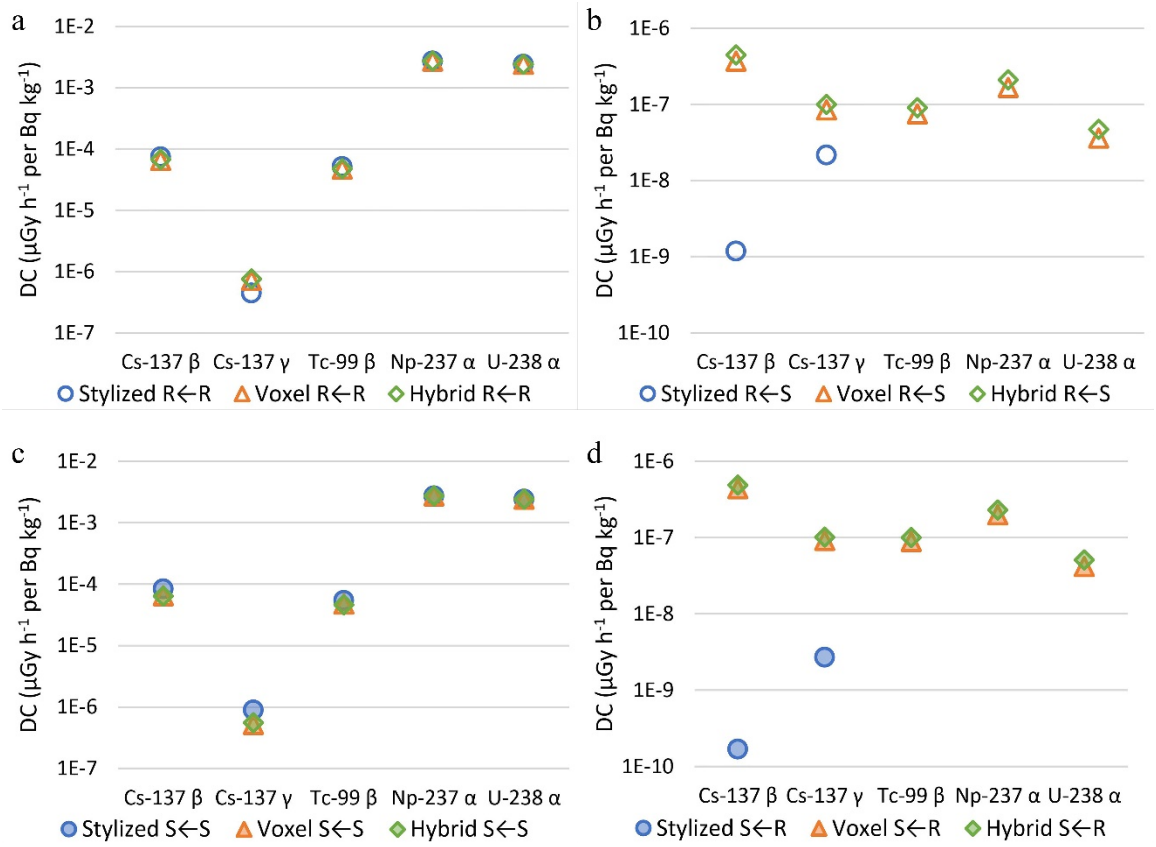

Figure 5.6: Internal DC evaluated with respect to target←source, nuclide, radiation type, and phantom type (stylized, voxel, and hybrid). Root←Root (a), Root←Shoot (b), Shoot←Shoot (c), and Shoot←Root (d). For crossfire cases (Root←Shoot and Shoot←Root), DCs associated with alphas from ^{237}Np and ^{238}U for the stylized phantom were zero thus, are not shown on the log scale and values for ^{99}Tc were previously excluded.

In the case of crossfire (where one plant part is the source and the other the target), the relative differences were greater, up to three orders of magnitude when comparing the stylized model to the hybrid or voxel models for ^{137}Cs (**Figure 5.6b** and **Figure 5.6d**). For ^{99}Tc, the *f8 values (MeV deposited per disintegration) for stylized crossfire cases were excluded from further calculations due to high relative error (> 0.1, as discussed in section *5.2.3*) and thus, are not included in **Figure 5.6b** and **Figure 5.6d**; however, these values

were exceptionally small, about five orders of magnitude lower than *f8 values for the voxel or hybrid models. Additionally, all stylized model crossfire values for the alpha emitters were zero (not shown on the log scale in **Figure 5.6b** and **Figure 5.6d**) in comparison to the voxel or hybrid models, which had DCs on the order of 10^{-8} to 10^{-7} μGy h^{-1} per Bq kg^{-1}. The voxel and hybrid models, as with other modeled DCs, were more consistent with a maximum percent difference of 23%. The disparities between the crossfire DCs of the stylized and voxel or hybrid phantoms are due to the geometry differences between the phantoms. In the stylized phantom, among other factors, there was a slight separation between the roots and the shoots due to the orientation of the geometric shapes (**Figure 5.1**). The separation between plant organs does not occur in the voxel or hybrid phantoms (**Figure 5.2**). The separation between the roots and shoots had the greatest effect on the high LET/short range particles; namely, the alpha particles of ^{237}Np and ^{238}U but also, ^{99}Tc beta particles and, to a lesser extent, ^{137}Cs beta particles. Generally, the shorter the particle range the greater the difference between the stylized and voxel or hybrid phantoms. Of additional consideration with the crossfire DCs is their relative importance with respect to the self-absorption DCs; crossfire DCs are a fraction of the self-absorption DCs, typically less than one percent, except when comparing most ^{137}Cs gamma DC values thus, their potential contribution to the internal (and total) dose or dose rate is limited (**Table 5.4**).

Table 5.4: Crossfire DCs expressed as a percent relative to self-absorption DCs by nuclide, radiation type, organ, and phantom type. Values not given for cases where crossfire DCs were zero (^{237}Np and ^{238}U for the stylized phantom) or for cases where data was previously excluded (^{99}Tc for the stylized phantom).

	Stylized		Voxel		Hybrid	
	$DC_{R\leftarrow S}$:$DC_{R\leftarrow R}$	$DC_{S\leftarrow R}$:$DC_{S\leftarrow S}$	$DC_{R\leftarrow S}$:$DC_{R\leftarrow R}$	$DC_{S\leftarrow R}$:$DC_{S\leftarrow S}$	$DC_{R\leftarrow S}$:$DC_{R\leftarrow R}$	$DC_{S\leftarrow R}$:$DC_{S\leftarrow S}$
^{137}Cs β	< 0.01%	< 0.01%	0.57%	0.67%	0.66%	0.76%
^{137}Cs γ	4.86%	0.30%	11.86%	17.54%	13.21%	18.32%
^{137}Cs total	0.03%	< 0.01%	0.69%	0.81%	0.80%	0.91%
^{99}Tc β	-	-	0.16%	0.19%	0.19%	0.22%
^{237}Np α	-	-	< 0.01%	< 0.01%	< 0.01%	< 0.01%
^{238}U α	-	-	< 0.01%	< 0.01%	< 0.01%	< 0.01%

5.3.2. Application of DCs: Determining Dose Rates

Dose rates for plants were calculated with plant organ and HP solution concentrations from previous plant uptake studies (Montgomery et al., 2018) and DCs from the hybrid model for each radionuclide as an example of utility. Note that the ^{137}Cs dose rate received by plants in the experiment is hypothetical as the previous uptake studies utilized the stable ^{133}Cs isotope; dose estimate calculations assume ^{137}Cs concentrations would be equivalent to the experimental ^{133}Cs concentrations. The dose rate to individual plant parts (roots or shoots) was calculated by **Equation 5.2** for internal and external exposure using masses of the hybrid phantom and average experimental activity concentrations (of roots, shoots, and HP solution) from Montgomery et al. (2018). Note that the internal dose rate was the sum of the self-absorbed dose rate and crossfire dose rate for the particular organ. Dose rate to the whole plant (internal or external) was calculated by:

$$\dot{D}_{plant} = \dot{D}_R \frac{m_R}{m_R + m_S} + \dot{D}_S \frac{m_S}{m_R + m_S} \quad \textbf{(5.3)}$$

where $\dot{D}_{plant}$ is the internal or external dose rate to the whole plant, $\dot{D}_R$ is the internal or external dose rate to the roots, $\dot{D}_S$ is the internal or external dose rate to the shoots, m_R is the mass of the roots for the hybrid phantom, and m_S is the mass of the shoots for the hybrid phantom. Total dose rate to the whole plant was calculated by:

$$\dot{D}_{total} = \dot{D}_{int,plant} + \dot{D}_{ext,plant} \quad \textbf{(5.4)}$$

where $\dot{D}_{int,plant}$ and $\dot{D}_{ext,plant}$ are internal and external dose rates to the whole plant respectively (calculated from **Equation 5.3**) and $\dot{D}_{total}$ is the total dose rate to the whole

plant. The resulting total, whole plant dose rates, by radionuclide, to the (hybrid model) plant for each harvest day of the experimental system is plotted in **Figure 5.7**. Additionally, dose rates were calculated based on average experimental whole plant concentrations and HP solution concentrations with ICRP 136 DCs (using one-half of the aquatic external DC for wild grass as the external DC) using **Equations 5.2** and **5.4** for comparison (**Figure 5.7**).

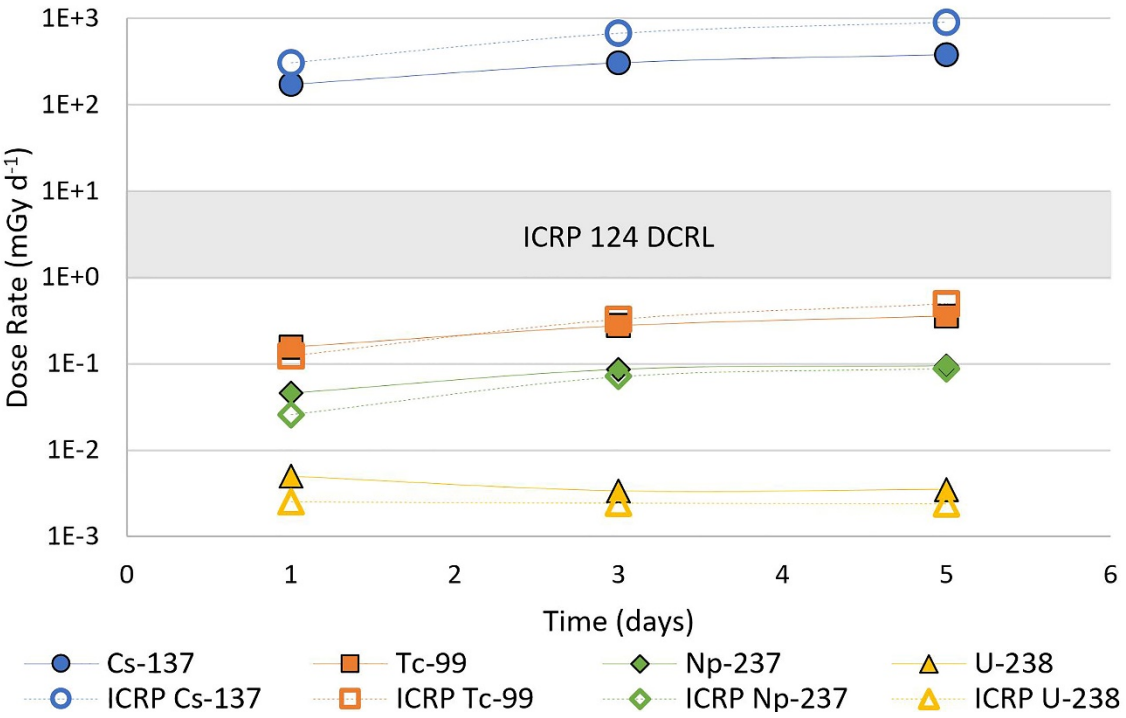

Figure 5.7: Total, whole plant dose rate by isotope determined from plant tissue and HP solution concentrations from previous experimental uptake studies for the hybrid model plant and for ICRP 136 DC values (ICRP, 2017, 2014; Montgomery et al., 2018). The ICRP 124 DCRL range is shaded in gray for reference only. Note that the ^{137}Cs dose rate is hypothetical as the previous uptake studies utilized the stable ^{133}Cs isotope; dose estimate calculations assume ^{137}Cs concentrations would be equivalent to the experimental ^{133}Cs concentrations.

Contributions from internal sources (uptake of the nuclides into the plant organs) exceeded the external dose rate from the HP source in all cases, generally by more than an order of magnitude with the exception of ^{137}Cs (**Table 5.5**, **Figure 5.8**). The trends of the internal and external contributions to total, whole plant dose rate utilizing the ICRP DCs were similar to those for the hybrid model but internal contributions were noticeably greater for ^{99}Tc (i.e., the internal dose rate accounted for a greater proportion of the total, whole plant dose rate when utilizing ICRP 136 DCs) and lower for ^{137}Cs. Please see the online supplementary information for tabulated estimated dose rates (**SI Table B.5** and **Table B.6**).

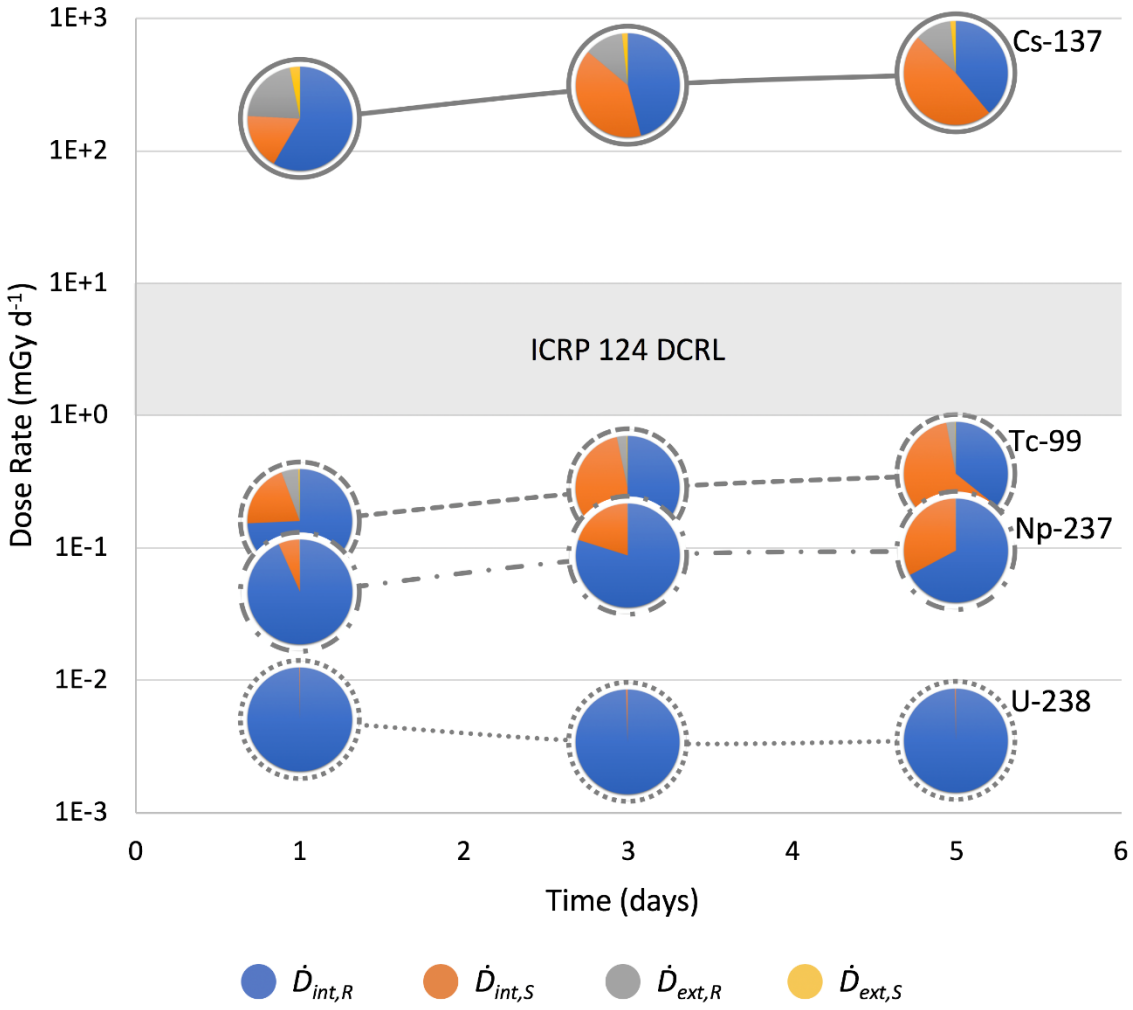

Figure 5.8: Total, whole plant dose rate by isotope with relative contributions (shown in the inset pie charts) from internal sources to roots ($\dot{D}_{int,R}$) and shoots ($\dot{D}_{int,S}$) and external sources (i.e., HP solution) to roots ($\dot{D}_{ext,R}$) and shoots ($\dot{D}_{ext,S}$) determined from plant tissue and HP solution concentrations from previous experimental uptake studies for the hybrid model plant (ICRP, 2014; Montgomery et al., 2018). The ICRP 124 DCRL range is shaded in gray for reference only. Note that the ^{137}Cs dose rate is hypothetical as the previous uptake studies utilized the stable ^{133}Cs isotope; dose estimate calculations assume ^{137}Cs concentrations would be equivalent to the experimental ^{133}Cs concentrations.

Table 5.5: Comparison of relative contributions to total, whole plant dose rate by nuclide, harvest day (1, 3, or 5), source (internal or external), and target (roots, shoots, and whole plant) determined from plant organ and HP solution concentrations from previous experimental uptake studies for the hybrid model and for ICRP 136 DCs (ICRP, 2017; Montgomery et al., 2018). Note that the ^{137}Cs dose rate is hypothetical as the previous uptake studies utilized the stable ^{133}Cs isotope; dose estimate calculations assume ^{137}Cs concentrations would be equivalent to the experimental ^{133}Cs concentrations.

		Internal				External			
	Day	^{137}Cs	^{99}Tc	^{237}Np	^{238}U	^{137}Cs	^{99}Tc	^{237}Np	^{238}U
Hybrid Roots	1	58.37%	74.28%	93.32%	99.79%	21.01%	5.23%	0.23%	< 0.01%
	3	45.92%	50.15%	79.83%	99.51%	12.05%	3.07%	0.13%	< 0.01%
	5	38.91%	35.67%	67.23%	99.70%	11.33%	2.74%	0.13%	< 0.01%
Hybrid Shoots	1	17.44%	20.05%	6.45%	0.21%	3.18%	0.44%	0%	0%
	3	40.20%	46.52%	20.04%	0.49%	1.83%	0.26%	0%	0%
	5	48.05%	61.35%	32.64%	0.30%	1.72%	0.23%	0%	0%
Hybrid Whole Plant	1	75.81%	94.33%	99.77%	100%	24.19%	5.67%	0.23%	< 0.01%
	3	86.12%	96.67%	99.87%	100%	13.88%	3.33%	0.13%	< 0.01%
	5	86.96%	97.03%	99.87%	100%	13.04%	2.97%	0.13%	< 0.01%
ICRP 136 Whole Plant	1	59.63%	99.60%	99.82%	100%	40.37%	0.40%	0.18%	< 0.01%
	3	81.05%	99.84%	99.93%	100%	18.95%	0.16%	0.07%	< 0.01%
	5	83.46%	99.88%	99.94%	100%	16.54%	0.12%	0.06%	< 0.01%

Dose and dose rate evaluations would typically be utilized for investigation of dose-effect relationships or for comparison to environmental protection standards. This type of investigation is beyond the scope for this work as we are not evaluating dose-effect relationships for our experimental system but, simply, developing and comparing several types of dosimetric models. Dose rate evaluations are presented here as an example of applicability and utility for potential future use.

5.4. Discussion

5.4.1. Model Comparisons

For this specific organism, DCs of all of the three phantoms (stylized, voxel, and hybrid) investigated were in relatively good agreement, in most cases. There were, however, a few notable exceptions to the overall agreement between the three models when comparing some DCs of the stylized model to the hybrid or voxel models. The primary disparity between three the models is evident for external whole plant DCs and external shoot DCs (**Figure 5.4** and **Figure 5.5**). In these cases, the stylized model DCs are all less than voxel or hybrid DCs by a factor of five or more, up to about an order of magnitude. This disparity is associated with the differences in the defined geometry (relative position, volume, mass, etc.) between the three models as all other factors in the MCNP scripts were otherwise the same. Although revising the volumes in the stylized phantom to be more consistent with the voxel or hybrid phantoms is something that could be easily done in retrospect, these models are typically developed without specific, *a priori* knowledge of organ volume. Our goal was not to make the models as consistent as possible but instead to compare the models as they would generally be developed. For example, it is unlikely

that an individual would create a voxel model for the specific purpose of updating a stylized model. Similarly, it would also possible to reduce the gap that is present between the shoots and roots or surface of the HP solution in the stylized phantom. However, this would require the shoot geometry to be more complex and beyond the goal of utilizing simple geometric shapes to create the stylized phantom.

The concept of crossfire between organs is similar to external exposure in that the source organ is "external" to the target organ, although this exposure is still considered internal (i.e., inside the body or organism). It follows, then, that the other exception to the overall agreement between the three models was for the case of crossfire, again due to differences in geometry (**Figure 5.6**). While this difference is interesting, the DCs for the crossfire component are a small fraction of the overall internal DC for the plant as a whole, accounting for <1% of the whole plant internal DC in all cases and is likely of low consequence in a dose evaluation (**Table 5.4**). Although the crossfire component is minimal for this specific organism and associated phantoms, it may be of greater significance for other more complex biota that have source organs with a greater region of influence on surrounding organs or tissues (e.g., animals or plants that are more complex) or when looking at this or similar organisms on a finer scale (e.g., micro-dosimetry).

Of further interest is the comparison of these more complex and anatomically realistic phantoms with those of the current ICRP RAPs (ICRP, 2017, 2008). In all cases, the internal whole organism DCs were fairly consistent to ICRP values but the modeled external whole organism DCs were typically greater and more variable with respect to ICRP DCs. Differences in external DCs approached or were in excess of an order of

magnitude in many cases, primarily due to the differences in geometry assumptions as well as some contribution due to differences in nuclear data as discussed in section *5.3.1* (**Figure 5.3** and **Figure 5.4**). However, total, whole plant dose rates (for each radionuclide) determined from the hybrid model DCs and from ICRP 136 DCs were of similar magnitude (maximum percent difference of 58% for ^{137}Cs on harvest day 5) since the internal contribution was dominant for the experimental system that was evaluated (**Figure 5.7**). This may not be the case for all systems, for example, plant uptake is lower for many nuclides in soil-plant or terrestrial systems compared to hydroponic or freshwater systems and thus, internal contributions to dose and dose rate may not be as dominant (IAEA, 2014). The extreme accumulation of uranium in and/or on roots in absence of alternate sorbing medium (i.e., soil) in previous hydroponic experiments is a good example of this, resulting in the uranium associated dose rate being dominated by contributions from internal exposure of the roots with essentially no contribution from external sources (**Table 5.5, Figure 5.8**) (Montgomery et al., 2018). Additionally, despite the similarity when comparing the total, whole plant dose rates, the absolute and relative contributions from internal and external sources differed, particularly for ^{99}Tc and ^{137}Cs, between the hybrid model and ICRP 136 estimated dose rates, in part due to the external DC differences (**Table 5.5**, **Figure 5.4**). These relative contributions to dose rate and dose rates to specific organs or tissues are likely to be of importance if evaluating dose-effect relationships, for example.

5.4.2. Model Utility

Of the phantoms investigated, voxel and hybrid phantoms are typically considered higher fidelity (for a specific specimen) over stylized phantoms or the typical simple

models utilized for the reference animals and plants (or similar) since they more accurately represent the true physical geometry of the organism. However, the time to create the voxel and hybrid phantoms is significantly greater than that required for creation of a stylized phantom or other simple models (e.g., possibly weeks to months for voxel and hybrid phantoms vs. hours to days for stylized phantoms) and they require specialty-imaging capabilities, which must be taken into consideration for practical use. Given the similarity in estimated total, whole plant dose rates for the experimental system evaluated, the use of ICRP DCs is certainly the most time efficient and is appropriate for environmental-scale radiation protection evaluations for this organism. However, this is not to say that the development and use of these complex models is unwarranted for all scenarios or applications. There may be situations that could benefit from the use of the anatomically relevant and higher fidelity models that are more reflective of the system being evaluated, perhaps within the tiered approach to environmental radiation protection for key species if environmental screening levels are exceeded. Additionally, the models that appear more anatomically accurate and system relevant may be useful for engaging with stakeholders and facilitating communication related to environmental dose and risk analysis.

Of potential practical application, the higher fidelity of the anatomically relevant models would be key in the accurate evaluation of dose to individual organisms or species in a research setting, particularly for investigating dose-effects at low dose or dose rates where highly accurate dose evaluations are required. Of course, it is worth noting here that in environmental radiation protection, we are on the whole concerned with protection of the ecosystem and maintaining biodiversity (ICRP, 2017, 2014, 2003). Although several

groups are developing progressively elegant models to predict population level effects (e.g., Alonzo et al., 2016; Kryshev and Sazykina, 2015; Sazykina, 2018; Vives I Batlle, 2012; Vives I Batlle et al., 2012), and it is generally agreed that an ecosystem approach to environmental radiation protection is needed (Bradshaw et al., 2014; Bréchignac et al., 2016; Geras'kin, 2016), we still do not have the ability to directly extrapolate molecular effects to the population and ecosystem scale due to associated complexity (Garnier-Laplace et al., 2015; Geras'kin et al., 2016). Thus, in most cases, the traditional approach is taken in radioecological risk management, which involves the use of concentration ratios, transfer factors, dose conversion factors, and reference organisms within an assessment tool (Brown et al., 2016; Yu et al., 2013), making assumptions about higher scale effects.

Within the ecotoxicology community, however, there has been more movement towards the adoption of systems-based approaches, which integrate traditional methods with computational models to perform a robust quantitative analysis across levels of biological organization (Forbes and Galic, 2016; Sturla et al., 2014). Common among systems approaches is the need for a mechanistic understanding of adverse effects at each level of organization. Adverse Outcome Pathways (AOPs), commonly used in ecotoxicology, are conceptual depictions of the contaminant or stressor initiating event (e.g. creation of reactive oxygen species) and subsequent adverse outcomes (e.g. DNA damage and reduced reproductive output) at various levels of biological organization (Ankley et al., 2010). AOPs are fluid, reflecting new knowledge and understanding as it emerges. They also have the advantage of representing various pathways potentially

leading to an effect, making it easier to develop an appropriate mathematical representation of the whole system. A refined dosimetric model is more likely to effectively contribute to an AOP than a generalized ellipsoidal model. As we start to identify mechanisms of effects, we need refined dosimetric models to truly be able to link the biological response to a dose; knowing the location of dose deposition can more appropriately inform, for example, genomic responses that are perhaps seen at the individual scale (reproductive success) and subsequently reflected in the population scale (reduction in the number of a certain species) and community scale (reduction in biodiversity if say, the reduced population is predated out of existence). As an aside, this suggested approach would necessarily also utilize population modeling approaches mentioned previously.

There are several other key benefits when considering the use of more complex and biologically relevant phantoms and geometries in computational dosimetry. In general, the use of complex and anatomically realistic models is advantageous due to the ability to evaluate dose to specific organs or tissues directly instead of only determining dose the whole organism or utilizing approximations (Gómez-Ros et al., 2008). This can be particularly important for nuclides that preferentially partition to specific organs or for tissues or organs that may be more radiosensitive, such as plant reproductive or actively growing vegetative organs (Degani and Pickholtz, 1980; USDOE, 2002). Iodine is a typical example as it partitions primarily to thyroids of animals (Martinez et al., 2014b), yet this concept can also be applied to plants. For example, uranium may be strongly correlated with root biomass for some plant types, particularly in the absence of an alternate sorbing medium, e.g., soil (Favas et al., 2014; Laurette et al., 2012; Montgomery et al., 2018).

Further, while these particular models consider root submersion in HP solution (modeled as water) representative of experimental conditions in previous HP uptake studies, the material could easily be altered to represent soil or another growth medium of interest and the geometry of the surroundings and of the plant itself is relatively easily manipulated, particularly for hybrid phantoms. For instance, the hybrid phantom geometry was manipulated in this work to correct shoot discontinuities present in the voxel model. Numerous applications of phantom manipulation can be imagined, but several possibilities include scaling or resizing phantoms to represent a smaller or larger organism, modifying the orientation of the phantom with respect to itself or its surroundings, or changing the number and spatial distribution of organisms represented by the phantom (i.e., to make a computational "field" of grass) (Xu, 2014).

5.5. Conclusion

This paper developed and compared three progressively detailed anthropomorphic phantoms for the grass species *Andropogon virginicus*, with an example of how to link the resultant dose coefficients with experimental data to determine dose to both above ground and below ground plant parts. Although other models of this style exist for non-human biota (perhaps the most similar is the detailed stylized model developed by Yoschenko *et al.,* 2011), our models include the first published voxel and hybrid phantoms of a plant.

The three phantoms developed in this work produced comparable results, which suggests that the simplest model would be the ideal choice; however, the potential need for manipulation of the phantom geometries to fit a given scenario may be a factor worth consideration in this decision. Overall, phantom selection will depend upon the application

for which the model is being used with attention given to weighting the time-cost of the model with the need for accuracy, as previous studies have similarly discussed (e.g., Martinez, 2015; Martinez et al., 2016, 2014a; Ruedig et al., 2015, 2014). For most general environmental assessments, ellipsoids or other simple stylized models are likely sufficient as they typically provide a conservative estimate of (whole organism) dose rate. However, the use of variations of more complex and/or realistic models may be worthwhile in the event that some screening levels are exceeded and a more detailed evaluation is required. Additionally, when a model is utilized to evaluate dose to an individual organism in dose-effect studies, the most physically realistic version that can be easily altered may be the ideal choice (e.g., hybrid model). This proposed fit-for-purpose approach for using different types of models of varying degrees of complexity for different applications has long been employed in human radiation protection. For example, a relatively generic human dosimetric model is typically sufficient for human population level risk assessments while, for nuclear medicine applications, use of the most accurate and individualized dosimetric model available is desired.

Within the radioecology community, the development of voxel models for non-human biota is becoming more commonplace, seemingly because once the appropriate skill set and tools/software are acquired, the process is much smoother with limited associated cost. Dosimetry groups also frequently offer existing models for use free of charge (e.g., Kramer et al., 2012). Some groups are even working on an open source process pipeline for making the development of such models more widely accessible (Neville, 2019). In human radiation protection, the ICRP has developed dose coefficients for six ages and two

sexes with 79 source regions and 43 target regions based on voxel phantoms supplemented with stylized models for structures beyond tomographic resolution (ICRP, 2016, 2009b). Additionally, the ICRP is currently developing mesh-type models, similar to the NURBS model developed herein (Kim et al., 2018). Of course, we are not recommending the development of the same for each of the reference organisms, but progressive models could be considered. For example, DCs could continue to be provided from a generic ellipsoidal model for Large Mammal. Additional DCs for select organs (e.g., thyroid, gonads) could also be available using a voxel or mesh-type phantom representing a deer, along with how one might develop specific DCs for a different Large Mammal of interest, if so desired.

Acknowledgements

This work is supported by the United States Department of Energy Office of Science, Office of Basic Energy Sciences and Office of Biological and Environmental Research under Award number DE-SC-00012530. Partial faculty support (NEM) was provided by the United States Nuclear Regulatory Commission Nuclear Education Grant #NRC-HQ-13-G-38-0002. Clemson University is acknowledged for generous allotment of compute time on the Palmetto cluster. Additionally, we would like to acknowledge the anonymous reviewers whose thorough reviews and insightful comments greatly improved the quality of this manuscript. The authors declare no competing or conflicting interests.

CHAPTER SIX

CONCLUSIONS AND FUTURE WORK

6.1. Conclusions

The body of work presented in this dissertation represents an example of the integrative and multidisciplinary nature of the radioecology and environmental radiation protection fields specific to a soil-plant-hydrologic system through the examination of plant-mediated radionuclide transport and development (and application of) computational dosimetric modeling efforts for non-human biota. This was accomplished, in part, through investigation of interactions between individual system components in the soil-plant-hydrologic system (i.e., the soil-pore water sub-system through batch sorption experiments and the plant-hydrologic sub-system through hydroponic uptake experiments) followed by experimental investigation of the integrated system (i.e., soil-plant-hydrologic system through column experiments). Concurrent with the transport experiments, three anatomically representative computational dosimetric models specific to the plant species of this work (*A. virginicus*) were developed, compared, and integrated with plant uptake data to determine organism specific dose rates as an example of application.

6.1.1. Major Findings

In addition to the overall objective of the work as a whole summarized above (see sections *6.1* and *1.1*), the individual experimental and modeling systems operated under objectives specific to each study sub-system such that early study results (i.e., batch sorption and HP uptake studies) informed the interpretation of later studies (i.e., column

experiments) or were directly integrated into dosimetric modeling calculations. Specifically, the studies within this work established the following:

(1) Plant exudate surrogates (citrate and/or oxalate) affect sorption of ^{99}Tc, ^{237}Np, and ^{238}U at higher ligand concentrations through (several proposed) radionuclide and ligand specific combinations of ligand-metal aqueous complexation, ternary (surface-ligand-metal) complex formation, and ligand promoted dissolution of soil surfaces In general, ^{99}Tc and ^{237}Np sorption increased, decreased sorption of ^{238}U and desorption of native ^{238}U occurred, and little to no effects were observed for ^{133}Cs; the desorption of native ^{238}U was likely also observed in the combined soil-plant-hydrologic system.

(2) For HP uptake, root to shoot translocation was greater for radionuclides with nutrient analogs (i.e., ^{99}Tc and ^{133}Cs) while actinides exhibited stronger association in root tissues, plant age was associated with significant differences in uptake (with seedlings generally exhibiting greater uptake), and seedling translocation to shoots increased significantly with treatment time for ^{99}Tc and ^{133}Cs. It was noted that uptake of ^{133}Cs and ^{238}U from a soil system is expected to be (and was) much lower than from the HP system due to soil sorption.

(3) In the combined soil-plant-hydrologic system, all radionuclides exhibited a significant decrease in release through the effluent stream in columns with plants. However, the most drastic effects were noted for the mobile radionuclides, ^{99}Tc and ^{237}Np, which exhibited significant soil profile distribution differences compared to columns without plants. Overall, the system was greatly affected by hydrologic differences resulting from plant transpiration as well as varying contributions due to radionuclide specific

plant uptake, both of which are dependent on relative sorption affinity of the ion, among other factors. Additionally, as observed in batch sorption experiments, desorption of native ^{238}U and subsequent affiliation with plant tissues occurred and, as observed in HP uptake studies, ^{99}Tc exhibited high plant uptake and translocation to shoots, actinides predominantly partitioned to roots, and, while the majority of the ^{133}Cs affiliated with plant tissues was associated with roots, ^{133}Cs exhibited greater translocation to shoots over ^{238}U. These phenomena are a result of the complex and coupled nature of the soil-plant-hydrologic system and the underlying processes occurring between the three main compartments of this system that were, in part, investigated in the first two phases of this experimental work.

(4) Establishing a clear link between environmental transport work (utilizing HP plant uptake data as an example of application) and environmental radiation protection is the development, comparison, and application of anatomically relevant computational dosimetric models. While most of the developed models provided similar results, there were some differences resulting from the defined geometry of the models, particularly for some external DCs and for crossfire DCs between roots and shoots. Additionally, greater disparities were noted between modeled DCs and ICRP DCs for wild grass, again, due to geometry considerations; while these differences did not affect the calculated total whole-organism dose rates (i.e., for the plant as a whole), there were some notable differences between the internal and external contributions to total dose rates. Further, modeled DCs allowed calculation of organ specific dose rates that are not directly attainable from ICRP DCs. While the more simplistic ICRP DCs are likely

sufficient for environmental-scale application (at least for this organism and system evaluated), the differences noted between the DCs of the three models developed in this work and between ICRP DCs are likely to be an important consideration for certain applications (in organism-specific dose-effect studies, for example) or for more complex organisms. Given these considerations, it was suggested that a fit-for-purpose approach be utilized when determining whether to use anatomically relevant models, such as the ones developed in this work, taking into account the organism of interest and level of detail required for the specific application.

6.1.2. Novelty and Scientific Merit

Part of the novelty in this work lies in the self-consistency throughout, not only in the soil type, plant species, and radionuclides carried through all phases of this body of work, but also that the experiments were conducted with the simultaneous inclusion of all of the radionuclides in each study system. Investigating plant-associated effects on this broad suite radionuclides simultaneously allows for a unique opportunity to intercompare the radionuclides in these systems thereby, resulting in the ability to draw more nuanced conclusions regarding notable plant-mediated affects and associated radionuclide transport differences than may be possible when investigating radionuclides on an individual basis. For example, the dissolution of native uranium observed in the citrate and/or oxalate batch sorption experiments of Chapter 2 informing similar observations for the integrated soil-plant-hydrologic column experiments of Chapter 5. Additionally, the column transport studies provide an opportunity to apply the conceptual understanding of radionuclide sorption and plant uptake gained in Chapter 2 and 3, respectively, to an integrated

experiment with all processes occurring simultaneously. Modeling the observed transport of the analytes in this complex system will help to inform upscaling of transport and environmental risk assessment models to larger spatial and temporal scales. For example, does a model based on understanding the individual components (soil-water and plant-water) accurately predict the soil-plant-water system or are there more complex interactions in the ternary system that must be considered. Furthermore, the dosimetry work not only has implications for this particular organism and serves as a demonstration of the integrative, multidisciplinary, and holistic approach to environmental radiation protection, but it is also a significant contribution to the radioecology and environmental protection communities in general as it represents the first published voxel or hybrid dosimetric models for any plant species.

6.2. Future work

Due to the extremely complex nature of the soil-plant-hydrologic system, every potential system variable affecting radionuclide transport could not be evaluated effectively. However, the substantial and integrated radionuclide transport data sets developed in this dissertation have provided valuable insight and quantification of many of the major plant-mediated processes that affect the transport and mobility of the radionuclides in SRS soil. Therefore, these data sets are likely to be useful as a basis for the development, parameterization, and validation of future environmental transport modeling efforts on this or similar systems, to include investigation of model scalability to larger spatial or temporal scales as mentioned above, or to inform larger scale or more environmentally realistic studies subject to natural conditions (e.g., lysimeter experiments).

Additionally, while the native ^{133}Cs and ^{238}U in the SRS soil revealed interesting and meaningful conclusions, future studies should incorporate non-native isotopes to probe the variability in the soil profile distributions with relation to plant presence and to elucidate other plant-mediated biogeochemical effects that were not able to be ascertained through this work due to their relatively high native soil concentrations.

With respect to the dosimetric models, as mentioned in Chapter 5, the plant surroundings could be easily updated to reflect the soil-plant-hydrologic system instead of the plant-hydrologic system (i.e., HP system) and the number of plants in the system could be increased (i.e., creating a virtual field of grass instead of a single specimen) in future work. This would be a relatively easy modification and would provide a valuable environmentally relevant comparison to the DCs for the HP system and to ICRP values. Further, a more substantial future effort could involve integrating dynamic plant growth and radionuclide transport experiments and/or modeling with the dosimetric evaluations, and, as previously mentioned, potentially incorporating these models into low-dose dose-effect studies.

APPENDICES

APPENDIX A

CHAPTER 4 SUPPLEMENTARY INFORMATION

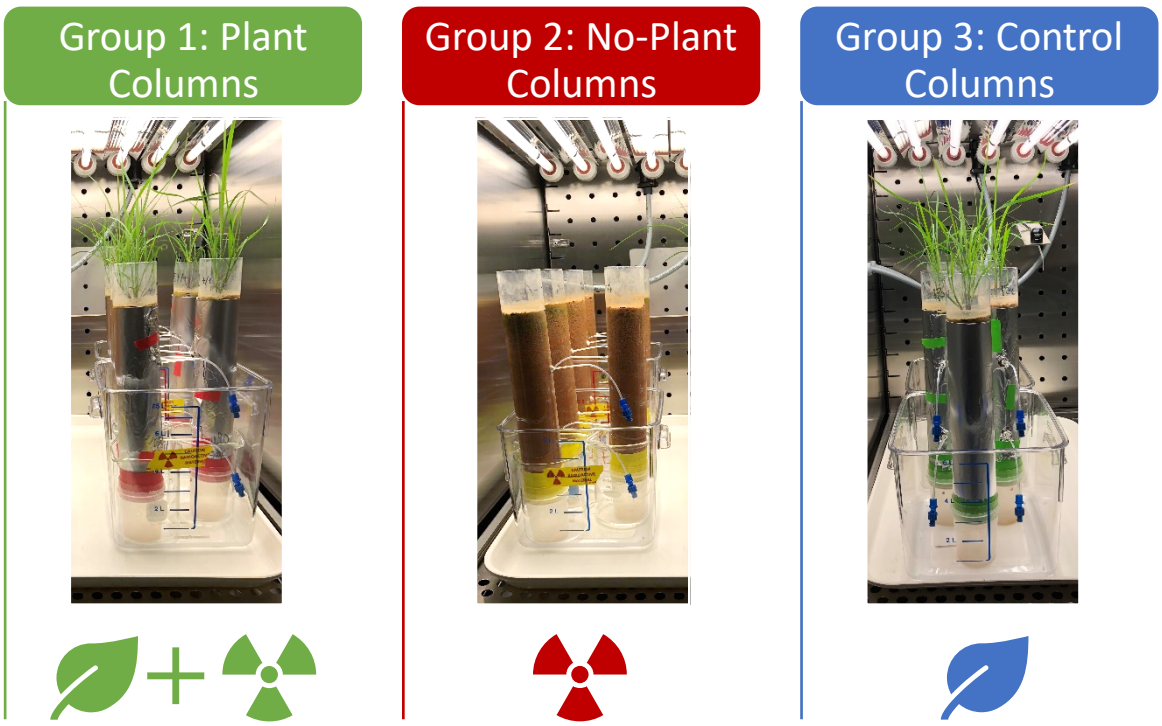

Figure A.1: Depiction of the three treatment groups. Group 1: Plant columns contains plants and was injected with radionuclides, Group 2: No-Plant columns were only injected with radionuclides, and Group 3: Control columns contained plants but were not injected with radionuclides.

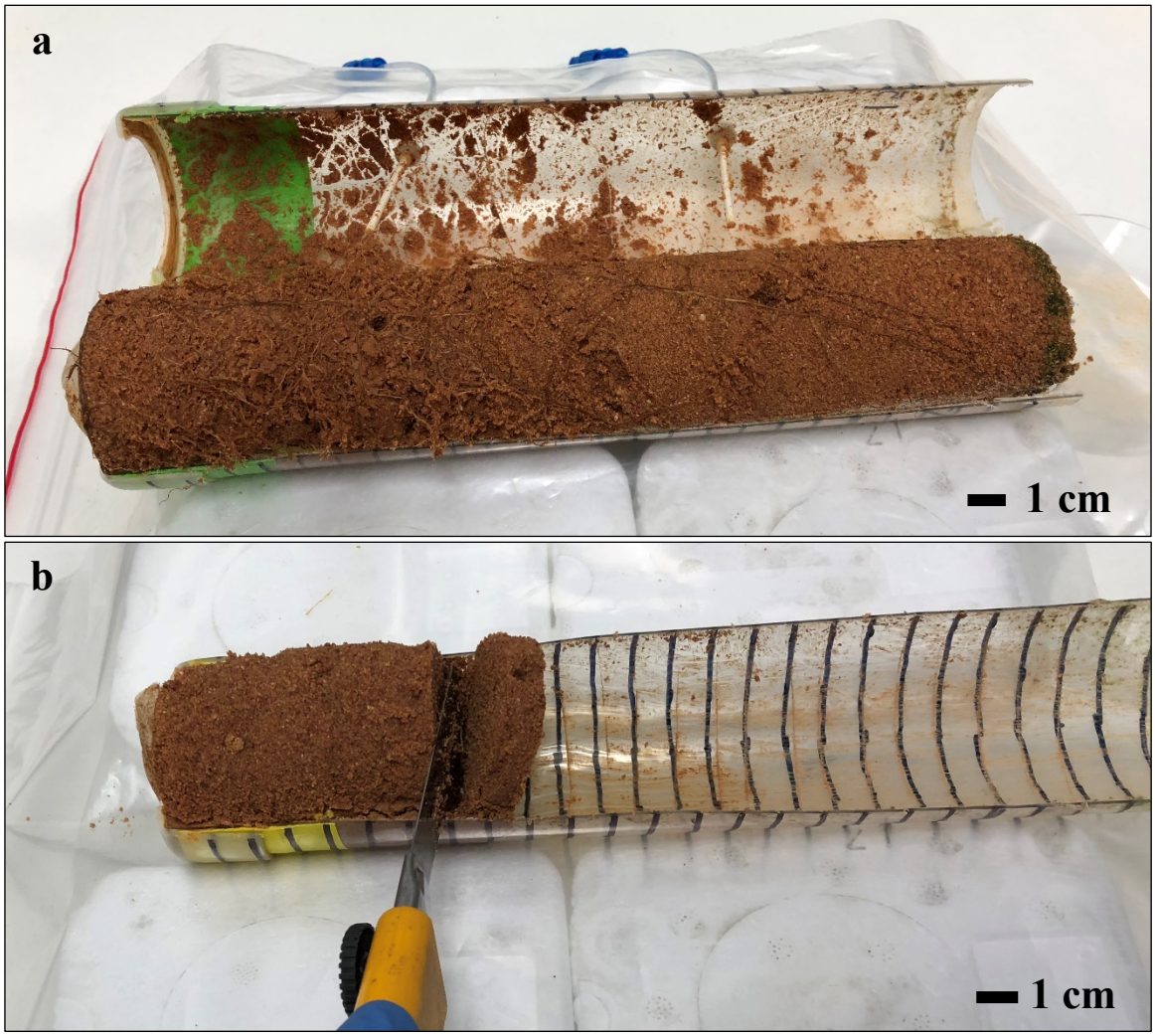

Figure A.2: Examples of a column cut open (a) and of column segmentation (b). The column in (a) was a Control column where the roots are visible throughout the column depth and the column in (b) was a No-Plant column thus, there were no roots.

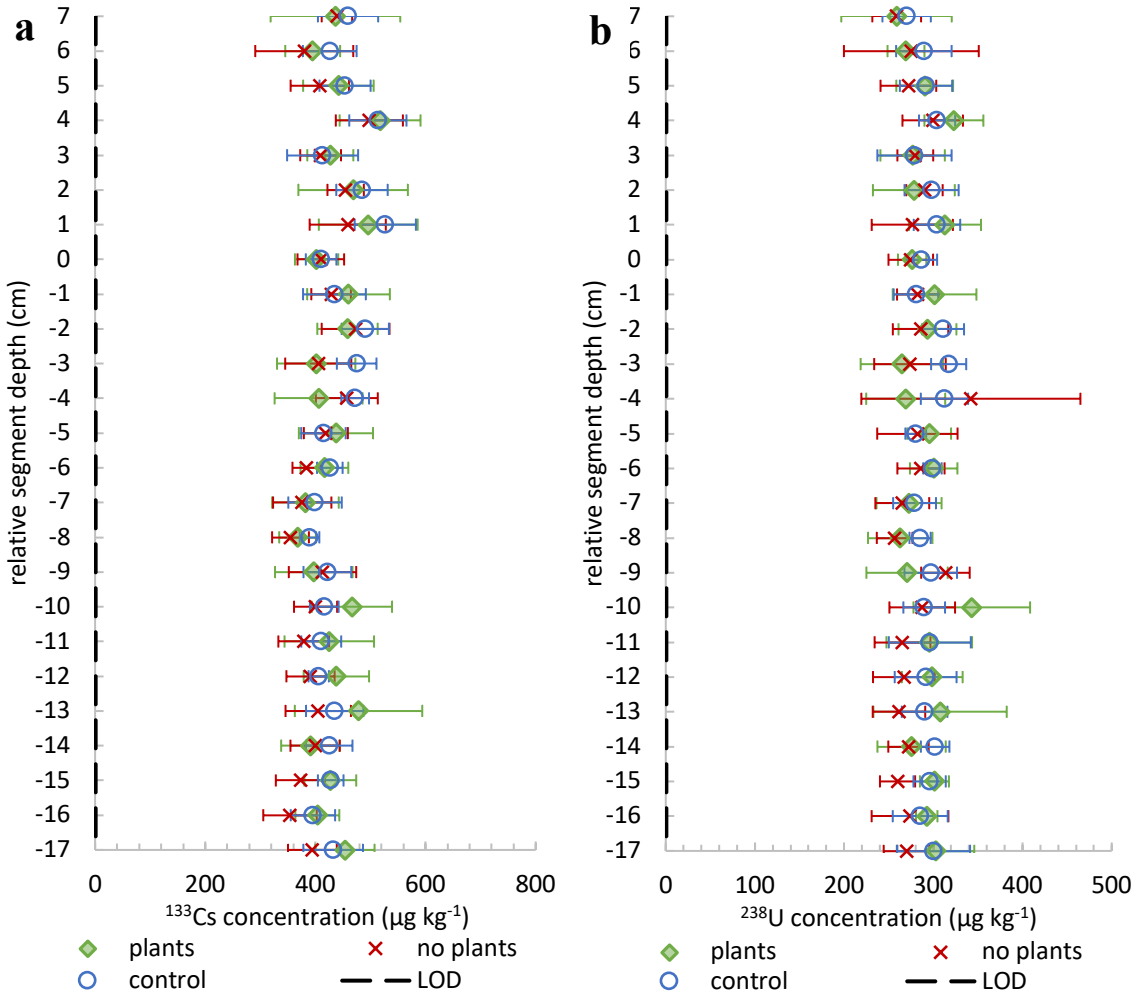

Figure A.3: Average soil column concentration profiles by group for ^{133}Cs (a) and ^{238}U (b) with respect to depth relative to the radionuclide injection point, i.e., the top port (the zero value on the y-axis). The error bars represent the standard deviation between the six column replicates per group.

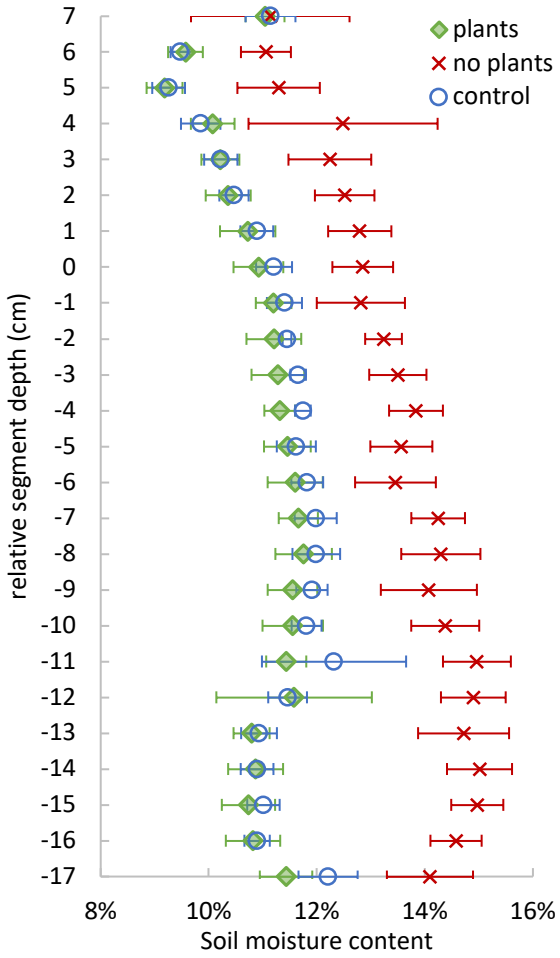

Figure A.4: Average soil moisture content profiles by group.

Table A.1: Average mass and standard deviation for each plant part and the whole plant by treatment group (Plant or Control Columns)

	Plants Columns Average mass (g)	Control Columns Average mass (g)
Shoots*	2.52 ± 0.11	1.93 ± 0.22
Shoots	1.76 ± 0.06	1.32 ± 0.15
Junction	0.09 ± 0.02	0.09 ± 0.03
Roots	1.10 ± 0.15	0.79 ± 0.18
whole plant	2.96 ± 0.16	2.19 ± 0.29

*fresh mass

Table A.2: Average root rinse total radionuclide mass and percent of total root associated radionuclide mass (i.e., total radionuclide mass in roots and root rinse) in root rinse by group with respective standard deviations between the six replicates per group.

	Plant Columns		Control Columns	
	Average (μg)	Average percent	Average(μg)	Average percent
^{99}Tc	$9.6\times10^{-3} \pm 7.5\times10^{-3}$	29 ± 19%	< LOD	< LOD
^{237}Np	< LOD	< LOD	< LOD	< LOD
^{133}Cs	$4.9\times10^{-3} \pm 1.1\times10^{-3}$	0.43 ± 0.22%	$2.4\times10^{-2} \pm 1.0\times10^{-2}$	2.10 ± 0.64%
^{238}U	$8.8\times10^{-3} \pm 7.5\times10^{-3}$	1.09 ± 0.88%	$4.4\times10^{-2} \pm 3.0\times10^{-2}$	5.79 ± 3.48%

Table A.3: Average radionuclide mass (μg) in each compartment by group with respective standard deviations between the six replicates per group.

		Plant Columns		No-Plant Columns		Control Columns	
		Average	S.D.	Average	S.D.	Average	S.D.
^{99}Tc	Soil	6.26×10^{-1}	7.05×10^{-2}	9.43×10^{-2}	4.71×10^{-2}	< LOD	
	Plant: Shoots	4.92×10^{-1}	6.48×10^{-2}	--	--	< LOD	
	Plant: Junction	2.34×10^{-3}	5.66×10^{-4}	--	--	< LOD	
	Plant: Roots	2.10×10^{-2}	4.70×10^{-3}	--	--	< LOD	
	Effluent	5.56×10^{-3}	8.62×10^{-3}	7.96×10^{-1}	5.15×10^{-2}	< LOD	
	Pore Water	1.47×10^{-2}	2.83×10^{-3}	2.97×10^{-3}	1.50×10^{-3}	< LOD	
	Root Rinse	9.59×10^{-3}	7.50×10^{-3}	--	--	< LOD	
	Total	1.17×10^{0}	4.22×10^{-2}	8.94×10^{-1}	3.08×10^{-2}	< LOD	
^{237}Np	Soil	1.12×10^{-1}	4.21×10^{-3}	8.59×10^{-2}	4.84×10^{-3}	< LOD	
	Plant: Shoots	7.64×10^{-4}	1.27×10^{-4}	--	--	< LOD	
	Plant: Junction	7.77×10^{-5}	1.76×10^{-5}	--	--	< LOD	
	Plant: Roots	1.20×10^{-3}	4.22×10^{-4}	--	--	< LOD	
	Effluent	< LOD		1.88×10^{-2}	4.32×10^{-3}	< LOD	
	Pore Water	1.45×10^{-3}	3.67×10^{-4}	1.14×10^{-3}	1.36×10^{-4}	< LOD	
	Root Rinse	< LOD		--	--	< LOD	
	Total	1.15×10^{-1}	3.75×10^{-3}	1.06×10^{-1}	4.10×10^{-3}	< LOD	
^{133}Cs	Soil	3.78×10^{2}	4.29×10^{1}	3.60×10^{2}	2.53×10^{1}	3.82×10^{2}	1.26×10^{1}
	Plant: Shoots	9.30×10^{-2}	8.04×10^{-3}	--	--	8.81×10^{-2}	2.14×10^{-2}
	Plant: Junction	2.14×10^{-2}	1.90×10^{-2}	--	--	2.86×10^{-2}	1.57×10^{-2}
	Plant: Roots	1.29×10^{0}	3.90×10^{-1}	--	--	1.07×10^{0}	2.18×10^{-1}
	Effluent	1.58×10^{-1}	4.07×10^{-2}	1.19×10^{0}	1.13×10^{-1}	3.23×10^{-1}	1.06×10^{-1}
	Pore Water	1.61×10^{-2}	6.14×10^{-3}	1.61×10^{-2}	1.91×10^{-3}	9.70×10^{-3}	2.94×10^{-3}
	Root Rinse	4.91×10^{-3}	1.08×10^{-3}	--	--	2.36×10^{-2}	1.04×10^{-2}
	Total	3.80×10^{2}	4.31×10^{1}	3.61×10^{2}	2.53×10^{1}	3.84×10^{2}	1.26×10^{1}
^{238}U	Soil	2.54×10^{2}	2.14×10^{1}	2.45×10^{2}	1.28×10^{1}	2.56×10^{2}	1.01×10^{1}
	Plant: Shoots	1.52×10^{-3}	5.29×10^{-4}	--	--	1.63×10^{-3}	1.02×10^{-3}
	Plant: Junction	1.14×10^{-2}	8.38×10^{-3}	--	--	1.31×10^{-2}	7.40×10^{-3}
	Plant: Roots	8.48×10^{-1}	2.74×10^{-1}	--	--	6.63×10^{-1}	1.30×10^{-1}
	Effluent	1.26×10^{-2}	3.30×10^{-3}	1.01×10^{-1}	9.39×10^{-3}	2.38×10^{-2}	8.99×10^{-3}
	Pore Water	3.17×10^{-3}	1.87×10^{-3}	3.62×10^{-3}	2.59×10^{-4}	1.21×10^{-3}	4.16×10^{-4}
	Root Rinse	8.81×10^{-3}	7.48×10^{-3}	--	--	4.41×10^{-2}	3.05×10^{-2}
	Total	2.55×10^{2}	2.16×10^{1}	2.45×10^{2}	1.28×10^{1}	2.57×10^{2}	1.02×10^{1}

APPENDIX B

CHAPTER 5 SUPPLEMENTARY INFORMATION

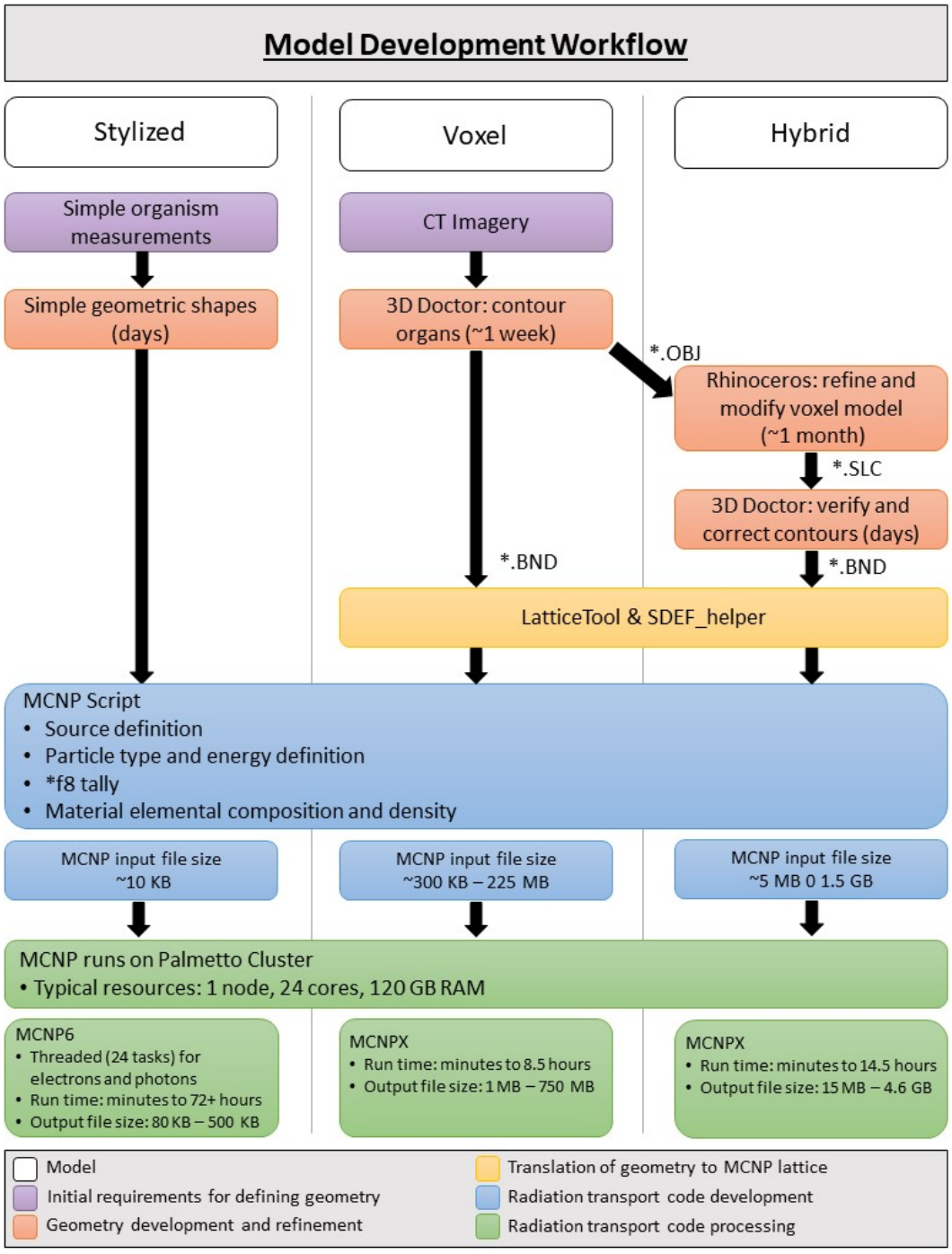

Figure B.1: Workflow showing key steps of the development of the stylized, voxel, and hybrid models with approximate times, resources, and file sizes

Table B.1a: Stylized model *f8 tally values (MeV dis^{-1}) and corresponding relative error (r.e.) listed by nuclide and associated particle(s) for each target←source combination (hydroponic solution (HP), roots (R), shoots (S), and the whole plant (WP). Cases with high relative error (r.e. > 0.1) that are excluded from further calculations are indicated with bold text and cases for which 10^8 particles were not reached within the MCNP allotted compute time are indicated with italicized text (minimum number of particles reached for these cases were 10^7).

		Target *f8 values (MeV dis^{-1})					
Nuclide & Particle	Source	Roots	r.e.	Shoots	r.e.	Whole Plant	r.e.
^{137}Cs β	HP	6.69E-5	0.0058	4.96E-6	0.0217	7.18E-5	0.0056
	R	1.28E-1	0.0001	2.04E-6	0.0386	1.28E-1	0.0001
	S	2.95E-7	0.0909	1.46E-1	0.0001	1.46E-1	0.0001
	WP	6.41E-2	0.0001	7.29E-2	0.0001	1.37E-1	0.0001
^{137}Cs γ	HP	4.43E-5	0.0071	1.28E-5	0.0142	5.71E-5	0.0063
	R	7.68E-4	0.0017	3.24E-5	0.0090	8.00E-4	0.0016
	S	5.39E-6	0.0207	1.55E-3	0.0013	1.56E-3	0.0013
	WP	3.86E-4	0.0023	7.91E-4	0.0018	1.18E-3	0.0014
^{99}Tc β	HP	1.34E-5	0.0098	1.00E-6	0.0350	1.44E-5	0.0095
	R	8.97E-2	0.0001	**9.30E-9**	**0.1437**	8.97E-2	0.0001
	S	**1.08E-9**	**0.4091**	9.38E-2	0.0001	9.38E-2	0.0001
	WP	4.49E-2	0.0001	4.69E-2	0.0001	9.18E-2	0.0001
^{237}Np α	HP	2.98E-5	0.0385	**5.91E-7**	**0.2673**	3.04E-5	0.0381
	R	*4.73E+0*	*0.0000*	*0.00E+0*	*0.0000*	*4.73E+0*	*0.0000*
	S	0.00E+0	0.0000	4.74E+0	0.0000	4.74E+0	0.0000
	WP	*2.37E+0*	*0.0003*	*2.37E+0*	*0.0003*	*4.74E+0*	*0.0000*
^{238}U α	HP	7.06E-6	0.0763	0.00E+0	0.0000	7.06E-6	0.0763
	R	4.18E+0	0.0000	0.00E+0	0.0000	4.18E+0	0.0000
	S	0.00E+0	0.0000	4.18E+0	0.0000	4.18E+0	0.0000
	WP	*2.09E+0*	*0.0003*	*2.09E+0*	*0.0003*	*4.18E+0*	*0.0000*

Table B.1b: Voxel model *f8 tally values (MeV dis^{-1}) and corresponding relative error (r.e.) listed by nuclide and associated particle(s) for each target←source combination (hydroponic solution (HP), roots (R), shoots (S), and the whole plant (WP). Cases with high relative error (r.e. > 0.1) that are excluded from further calculations are indicated with bold text.

		Target *f8 values (MeV dis^{-1})					
Nuclide & Particle	Source	Roots	r.e.	Shoots	r.e.	Whole Plant	r.e.
^{137}Cs β	HP	1.01E-4	0.0042	9.86E-6	0.0144	1.11E-4	0.0040
	R	1.13E-1	0.0001	6.39E-4	0.0020	1.13E-1	0.0001
	S	7.60E-4	0.0019	1.12E-1	0.0001	1.13E-1	0.0001
	WP	6.14E-2	0.0001	5.18E-2	0.0002	1.13E-1	0.0001
^{137}Cs γ	HP	7.69E-5	0.0049	1.39E-5	0.0130	9.07E-5	0.0046
	R	1.24E-3	0.0014	1.34E-4	0.0045	1.38E-3	0.0013
	S	1.74E-4	0.0039	9.04E-4	0.0016	1.08E-3	0.0015
	WP	7.51E-4	0.0018	4.85E-4	0.0022	1.24E-3	0.0014
^{99}Tc β	HP	2.63E-5	0.0066	2.08E-6	0.0237	2.84E-5	0.0064
	R	8.10E-2	0.0001	1.30E-4	0.0031	8.11E-2	0.0001
	S	1.54E-4	0.0029	8.16E-2	0.0001	8.18E-2	0.0001
	WP	4.39E-2	0.0001	3.75E-2	0.0002	8.14E-2	0.0001
^{237}Np α	HP	6.63E-5	0.0258	**4.20E-7**	**0.3164**	6.67E-5	0.0257
	R	4.70E+0	0.0000	2.91E-4	0.0123	4.70E+0	0.0000
	S	3.43E-4	0.0113	4.71E+0	0.0000	4.71E+0	0.0000
	WP	2.55E+0	0.0001	2.16E+0	0.0001	4.71E+0	0.0000
^{238}U α	HP	1.47E-5	0.0528	0.00E+0	0.0000	1.47E-5	0.0528
	R	4.17E+0	0.0000	6.15E-5	0.0258	4.17E+0	0.0000
	S	7.39E-5	0.0235	4.18E+0	0.0000	4.18E+0	0.0000
	WP	2.26E+0	0.0001	1.91E+0	0.0001	4.17E+0	0.0000

Table B.1c: Hybrid model *f8 tally values (MeV dis^{-1}) and corresponding relative error (r.e.) listed by nuclide and associated particle(s) for each target←source combination (hydroponic solution (HP), roots (R), shoots (S), and the whole plant (WP). Cases with high relative error (r.e. > 0.1) that are excluded from further calculations are indicated with bold text.

		Target *f8 values (MeV dis^{-1})					
Nuclide & Particle	Source	Roots	r.e.	Shoots	r.e.	Whole Plant	r.e.
^{137}Cs β	HP	7.39E-5	0.0048	7.90E-6	0.0162	8.18E-5	0.0047
	R	1.17E-1	0.0001	7.68E-4	0.0018	1.17E-1	0.0001
	S	8.51E-4	0.0018	1.11E-1	0.0001	1.12E-1	0.0001
	WP	6.15E-2	0.0001	5.32E-2	0.0002	1.15E-1	0.0001
^{137}Cs γ	HP	6.22E-5	0.0055	1.28E-5	0.0135	7.50E-5	0.0051
	R	1.31E-3	0.0014	1.60E-4	0.0041	1.47E-3	0.0013
	S	1.91E-4	0.0038	9.63E-4	0.0016	1.15E-3	0.0015
	WP	7.78E-4	0.0018	5.42E-4	0.0021	1.32E-3	0.0014
^{99}Tc β	HP	1.97E-5	0.0076	1.68E-6	0.0264	2.13E-5	0.0073
	R	8.21E-2	0.0001	1.58E-4	0.0028	8.22E-2	0.0001
	S	1.74E-4	0.0027	8.03E-2	0.0000	8.05E-2	0.0001
	WP	4.31E-2	0.0001	3.83E-2	0.0001	8.14E-2	0.0001
^{237}Np α	HP	5.55E-5	0.0281	**2.54E-7**	**0.4086**	5.58E-5	0.0281
	R	4.70E+0	0.0000	3.61E-4	0.0110	4.70E+0	0.0000
	S	3.99E-4	0.0105	4.71E+0	0.0000	4.71E+0	0.0000
	WP	2.46E+0	0.0001	2.24E+0	0.0001	4.70E+0	0.0000
^{238}U α	HP	1.21E-5	0.0582	0.00E+0	0.0000	1.21E-5	0.0582
	R	4.17E+0	0.0000	8.01E-5	0.0226	4.17E+0	0.0000
	S	8.92E-5	0.0214	4.17E+0	0.0000	4.17E+0	0.0000
	WP	2.19E+0	0.0001	1.99E+0	0.0001	4.17E+0	0.0000

Table B.2: Modeled DCs listed for each nuclide and phantom type with maximum percent and absolute differences as well as minimum percent and absolute. Cases where the percent difference is ≥ 99% corresponds to a difference of two or more orders of magnitude thus, order of magnitude difference is listed instead (indicated with an asterisk). Cases for which *f8 values were previously excluded are indicated by dashes.

		DC (μGy hr^{-1} per Bq kg^{-1})			Max. %	Min. %	Max abs.	Min. abs.
Source←Target	Nuclide	Stylized	Voxel	Hybrid	difference	difference	difference	difference
Internal: Self-Absorption								
Root←Root	^{137}Cs β	7.40E-5	6.50E-5	6.73E-5	12.14%	3.35%	8.98E-6	2.25E-6
	^{137}Cs γ	4.43E-7	7.16E-7	7.58E-7	41.59%	5.55%	3.15E-7	4.20E-8
	^{137}Cs β,γ	7.44E-5	6.57E-5	6.80E-5	11.70%	3.37%	8.71E-6	2.29E-6
	^{99}Tc	5.18E-5	4.67E-5	4.73E-5	9.77%	1.34%	5.05E-6	6.36E-7
	^{237}Np	2.73E-3	2.71E-3	2.71E-3	0.75%	0.11%	2.05E-5	3.11E-6
	^{238}U	2.41E-3	2.41E-3	2.41E-3	0.20%	0.03%	4.71E-6	7.50E-7
Shoot←Shoot	^{137}Cs β	8.41E-5	6.47E-5	6.39E-5	23.97%	1.17%	2.02E-5	7.57E-7
	^{137}Cs γ	8.95E-7	5.21E-7	5.55E-7	41.75%	6.19%	3.73E-7	3.44E-8
	^{137}Cs β,γ	8.50E-5	6.52E-5	6.45E-5	24.12%	1.11%	2.05E-5	7.22E-7
	^{99}Tc	5.41E-5	4.71E-5	4.63E-5	14.38%	1.64%	7.78E-6	7.72E-7
	^{237}Np	2.74E-3	2.72E-3	2.72E-3	0.72%	0.10%	1.97E-5	2.83E-6
	^{238}U	2.41E-3	2.41E-3	2.41E-3	0.19%	0.02%	4.69E-6	4.84E-7
WP←WP	^{137}Cs β	7.90E-5	6.53E-5	6.62E-5	17.43%	1.35%	1.38E-5	8.90E-7
	^{137}Cs γ	6.79E-7	7.13E-7	7.61E-7	10.76%	6.31%	8.19E-8	4.81E-8
	^{137}Cs β,γ	7.97E-5	6.60E-5	6.69E-5	17.24%	1.40%	1.37E-5	9.39E-7
	^{99}Tc	5.29E-5	4.70E-5	4.69E-5	11.29%	0.03%	5.97E-6	1.46E-8
	^{237}Np	2.73E-3	2.72E-3	2.71E-3	0.73%	0.10%	2.00E-5	2.77E-6
	^{238}U	2.41E-3	2.41E-3	2.41E-3	0.19%	0.02%	4.67E-6	6.00E-7

Table B.2 (continued)

Source←Target	Nuclide	DC (μGy hr^{-1} per Bq kg^{-1}) Stylized	Voxel	Hybrid	Max. % difference	Min. % difference	Max abs. difference	Min. abs. difference
Internal: Crossfire								
Root←Shoot	^{137}Cs β	1.18E-9	3.71E-7	4.46E-7	2.58*	16.78%	4.44E-7	7.48E-8
	^{137}Cs γ	2.15E-8	8.49E-8	1.00E-7	78.48%	15.19%	7.85E-8	1.52E-8
	^{137}Cs β,γ	2.27E-8	4.56E-7	5.46E-7	95.84%	16.49%	5.23E-7	9.00E-8
	^{99}Tc	---	7.54E-8	9.09E-8	---	17.04%	1.55E-8	1.55E-8
	^{237}Np	0.00E+0	1.67E-7	2.09E-7	n/a	19.87%	2.09E-7	4.15E-8
	^{238}U	0.00E+0	3.61E-8	4.67E-8	n/a	22.70%	4.67E-8	1.06E-8
Shoot←Root	^{137}Cs β	1.70E-10	4.35E-7	4.88E-7	3.46*	10.75%	4.87E-7	5.24E-8
	^{137}Cs γ	2.70E-9	9.14E-8	1.02E-7	97.35%	10.18%	9.90E-8	1.04E-8
	^{137}Cs β,γ	2.87E-9	5.27E-7	5.89E-7	2.31*	10.65%	5.86E-7	6.28E-8
	^{99}Tc	---	8.89E-8	1.00E-7	---	11.19%	1.12E-8	1.12E-8
	^{237}Np	0.00E+0	1.98E-7	2.29E-7	n/a	13.71%	2.29E-7	3.15E-8
	^{238}U	0.00E+0	4.19E-8	5.08E-8	n/a	17.60%	5.08E-8	8.95E-9

Table B.2 (continued)

Source←Target	Nuclide	DC (μGy hr^{-1} per Bq kg^{-1}) Stylized	Voxel	Hybrid	Max. % difference	Min. % difference	Max abs. difference	Min. abs. difference
External								
Root←HP	^{137}Cs β	4.32E-5	5.08E-5	4.94E-5	15.00%	2.85%	7.63E-6	1.45E-6
	^{137}Cs γ	2.86E-5	3.87E-5	4.16E-5	31.10%	6.99%	1.29E-5	2.90E-6
	^{137}Cs β,γ	7.18E-5	8.95E-5	9.09E-5	21.01%	1.60%	1.91E-5	1.46E-6
	^{99}Tc	8.65E-6	1.32E-5	1.31E-5	34.58%	0.67%	4.57E-6	8.90E-8
	^{237}Np	1.93E-5	3.33E-5	3.71E-5	48.08%	10.11%	1.78E-5	3.75E-6
	^{238}U	4.57E-6	7.39E-6	8.07E-6	43.44%	8.48%	3.51E-6	6.84E-7
Shoot←HP	^{137}Cs β	4.63E-7	5.86E-6	5.81E-6	92.10%	0.84%	5.40E-6	4.90E-8
	^{137}Cs γ	1.19E-6	8.23E-6	9.37E-6	87.31%	12.17%	8.18E-6	1.14E-6
	^{137}Cs β,γ	1.65E-6	1.41E-5	1.52E-5	89.12%	7.19%	1.35E-5	1.09E-6
	^{99}Tc	9.35E-8	1.24E-6	1.23E-6	92.43%	0.28%	1.14E-6	3.42E-9
	^{237}Np	---	---	---	---	---	---	---
	^{238}U	0.00E+0	0.00E+0	0.00E+0	n/a	n/a	0.00E+0	0.00E+0
WP←HP	^{137}Cs β	5.85E-6	3.02E-5	2.86E-5	80.64%	5.22%	2.44E-5	1.58E-6
	^{137}Cs γ	4.65E-6	2.47E-5	2.62E-5	82.28%	5.82%	2.16E-5	1.53E-6
	^{137}Cs β,γ	1.05E-5	5.49E-5	5.49E-5	80.88%	0.09%	4.44E-5	5.12E-8
	^{99}Tc	1.17E-6	7.73E-6	7.47E-6	84.83%	3.37%	6.56E-6	2.61E-7
	^{237}Np	2.48E-6	1.82E-5	1.95E-5	87.32%	6.91%	1.70E-5	1.35E-6
	^{238}U	5.76E-7	4.00E-6	4.23E-6	86.39%	5.38%	3.65E-6	2.28E-7

Table B.3: Comparison of whole plant modeled DCs and ICRP 136 DCs for wild grass (internal, external on the ground, and on half of external aquatic) listed for each nuclide and phantom type (ICRP, 2017; Montgomery et al., 2018). Maximum and minimum percent and absolute differences between the three models are listed next to model DCs. Maximum and minimum percent and absolute differences between ICRP 136 DCs and model DCs are listed next to ICRP 136 DCs. Note that comparisons in the percent columns for the ^{99}Tc external ICRP 136 DC for of wild grass on the ground are order of magnitude differences not percent differences since the ICRP values were lower by more than two orders of magnitude compared to model DCs (indicated with an asterisk). ICRP DCs were obtained from ICRP 136 Tables B.13 (^{137}Cs), B.35 (^{99}Tc), B.23 (^{237}Np), and B.38 (^{238}U) (2017).

		DC (μGy hr^{-1} per Bq kg^{-1} or μGy hr^{-1} per Bq L^{-1})			Max. %	Min. %	Max abs.	Min. abs.
Source←Target	Nuclide	Stylized	Voxel	Hybrid	difference	difference	difference	difference
Model								
Internal	^{137}Cs	7.97E-5	6.60E-5	6.69E-5	17.24%	1.40%	1.37E-5	9.39E-7
(WP←WP)	^{99}Tc	5.29E-5	4.70E-5	4.69E-5	11.29%	0.03%	5.97E-6	1.46E-8
	^{237}Np	2.73E-3	2.72E-3	2.71E-3	0.73%	0.10%	2.00E-5	2.77E-6
	^{238}U	2.41E-3	2.41E-3	2.41E-3	0.19%	0.02%	4.67E-6	6.00E-7
External	^{137}Cs	1.05E-5	5.49E-5	5.49E-5	80.88%	0.09%	4.44E-5	5.12E-8
(WP←HP)	^{99}Tc	1.17E-6	7.73E-6	7.47E-6	84.83%	3.37%	6.56E-6	2.61E-7
	^{237}Np	2.48E-6	1.82E-5	1.95E-5	87.32%	6.91%	1.70E-5	1.35E-6
	^{238}U	5.76E-7	4.00E-6	4.23E-6	86.39%	5.38%	3.65E-6	2.28E-7

Table B.3 (continued)

Source←Target	Nuclide	DC (μGy hr^{-1} per Bq kg^{-1} or μGy hr^{-1} per Bq L^{-1})	Max. % difference	Min. % difference	Max abs. difference	Min. abs. difference
ICRP 136: Wild Grass						
Internal	^{137}Cs	1.40E-4	52.87%	43.06%	7.40E-5	6.03E-5
	^{99}Tc	5.80E-5	19.06%	8.76%	1.11E-5	5.08E-6
	^{237}Np	2.80E-3	3.12%	2.41%	8.74E-5	6.74E-5
	^{238}U	2.50E-3	3.73%	3.54%	9.32E-5	8.85E-5
External (on ground)	^{137}Cs	1.10E-4	90.45%	50.07%	9.95E-5	5.51E-5
	^{99}Tc	9.40E-11	4.92*	4.10*	7.73E-6	1.17E-6
	^{237}Np	4.10E-6	79.00%	39.61%	1.54E-5	1.62E-6
	^{238}U	9.50E-8	97.75%	83.49%	4.13E-6	4.81E-7
External (Aquatic/2)	^{137}Cs	1.65E-4	93.64%	66.71%	1.55E-4	1.10E-4
	^{99}Tc	4.10E-7	94.70%	65.03%	7.32E-6	7.63E-7
	^{237}Np	8.50E-6	70.87%	53.23%	1.10E-5	6.02E-6
	^{238}U	2.00E-7	95.27%	65.25%	4.03E-6	3.76E-7

Table B.4: Average concentrations of plant tissues (roots, shoots, whole plant) and HP solution on the three harvest days from previous laboratory uptake experiments (Montgomery et al., 2018). Note that ^{133}Cs was utilized in uptake experiments but dose estimate calculations assume ^{137}Cs concentrations would be equivalent.

		Average Concentration (Bq L_{HP}^{-1} or Bq kg_{fresh}^{-1})			
Nuclide	Harvest Day	HP Solution	Roots	Shoots	Whole Plant
^{137}Cs	1	3.14E+7	1.16E+8	3.94E+7	5.47E+7
	3	3.24E+7	1.64E+8	1.66E+8	1.63E+8
	5	3.79E+7	1.72E+8	2.48E+8	2.26E+8
^{99}Tc	1	4.97E+4	1.96E+5	5.91E+4	8.83E+4
	3	5.16E+4	2.34E+5	2.44E+5	2.35E+5
	5	5.98E+4	2.15E+5	4.18E+5	3.54E+5
^{237}Np	1	2.27E+2	1.25E+3	9.52E+1	3.86E+2
	3	2.33E+2	2.02E+3	5.56E+2	1.06E+3
	5	2.72E+2	1.87E+3	9.98E+2	1.31E+3
^{238}U	1	7.25E-2	1.64E+2	3.73E-1	4.24E+1
	3	7.32E-2	1.11E+2	5.94E-1	4.04E+1
	5	6.24E-2	1.16E+2	3.82E-1	3.95E+1

Table B.5: Tissue specific dose rate by nuclide, harvest day, and target←source combination determined from plant tissue and HP solution concentrations from previous experimental uptake studies for the hybrid model (Montgomery et al., 2018). Cases for which *f8 values were previously excluded are indicated by dashes (---).

		Hybrid Model estimated $\dot{D}$(mGy d^{-1})					
Nuclide	Harvest Day	Root←Root	Shoot←Shoot	Root←Shoot	Shoot←Root	Root←HP	Shoot←HP
^{137}Cs	1	1.90E+2	6.11E+1	5.17E-1	1.65E+0	6.86E+1	1.14E+1
	3	2.67E+2	2.57E+2	2.18E+0	2.31E+0	7.07E+1	1.18E+1
	5	2.81E+2	3.85E+2	3.25E+0	2.44E+0	8.28E+1	1.38E+1
^{99}Tc	1	2.23E-1	6.57E-2	1.29E-4	4.71E-4	1.57E-2	1.47E-3
	3	2.66E-1	2.72E-1	5.33E-4	5.62E-4	1.63E-2	1.53E-3
	5	2.44E-1	4.64E-1	9.11E-4	5.17E-4	1.89E-2	1.77E-3
^{237}Np	1	8.16E-2	6.21E-3	4.77E-7	6.91E-6	2.02E-4	---
	3	1.31E-1	3.62E-2	2.79E-6	1.11E-5	2.08E-4	---
	5	1.22E-1	6.51E-2	5.01E-6	1.03E-5	2.42E-4	---
^{238}U	1	9.46E-3	2.16E-5	4.18E-10	2.00E-7	1.41E-8	0.00E+0
	3	6.41E-3	3.43E-5	6.66E-10	1.35E-7	1.42E-8	0.00E+0
	5	6.68E-3	2.21E-5	4.28E-10	1.41E-7	1.21E-8	0.00E+0

Table B.6: Comparison of whole plant internal dose rate, external dose rate, and the ratio of internal:external dose rate by nuclide and harvest day determined from plant tissue and HP solution concentrations from previous experimental uptake studies for the hybrid model and for ICRP 136 DCs (ICRP, 2017; Montgomery et al., 2018).

	Day 1 $\dot{D}$ (mGy d^{-1})			Day 3 $\dot{D}$ (mGy d^{-1})			Day 5 $\dot{D}$ (mGy d^{-1})		
	Internal	External	Ratio	Internal	External	Ratio	Internal	External	Ratio
Hybrid Model									
^{137}Cs	1.30E+2	4.14E+1	3.13	2.65E+2	4.27E+1	6.21	3.33E+2	5.00E+1	6.67
^{99}Tc	1.48E-1	8.91E-3	1.66E+1	2.69E-1	9.26E-3	2.91E+1	3.50E-1	1.07E-2	3.26E+1
^{237}Np	4.57E-2	1.06E-4	4.32E+2	8.60E-2	1.09E-4	7.89E+2	9.48E-2	1.27E-4	7.48E+2
^{238}U	4.97E-3	7.36E-9	6.75E+5	3.38E-3	7.43E-9	4.54E+5	3.51E-3	6.34E-9	5.55E+5
ICRP 136									
^{137}Cs	1.84E+2	1.24E+2	1.48	5.48E+2	1.28E+2	4.28	7.58E+2	1.50E+2	5.05
^{99}Tc	1.23E-1	4.89E-4	2.51E+2	3.27E-1	5.08E-4	6.43E+2	4.93E-1	5.88E-4	8.37E+2
^{237}Np	2.59E-2	4.63E-5	5.60E+2	7.13E-2	4.76E-5	1.50E+3	8.83E-2	5.54E-5	1.59E+3
^{238}U	2.55E-3	3.48E-10	7.32E+6	2.42E-3	3.51E-10	6.89E+6	2.37E-3	3.00E-10	7.92E+6

APPENDIX C

MCNP SCRIPTS

MCNP scripts for the computational dosimetric modeling in Chapter 5 are shown below. An example script is shown for each phantom. For the Voxel and Hybrid phantom scripts, the majority of the lattice and source definition portions of the scripts are omitted for brevity as they are in excess of 1,000 lines and 7,400 lines, respectively (up to $4x10^7$ lines in some cases). Following the example script for each phantom, script excerpts are shown for portions of the example script that were altered for a given source (HP solution, roots, shoots, and roots+shoots; indicated by **red text**) and for the specific nuclide and radiation type (indicated by **blue text**).

C.1: Stylized Model

C.1.1: ^{99}Tc beta spectrum, HP solution as source

```
c --------------------------------------------------------------------------
c
c                    __     |   __     _   _   __  __    _
c                   /       |  /__\  |/ \ / | /__ /  \ |/ |
c                   \__     \_ \__   |   |  | __/ \__/ |  |
c
c                      _   .        __     _   __   .  _|_
c                |  | |/ |  |  \  / /__\ |/ \ /__  |   |  |  |
c                \__| |  |  |   \/  \__, |    __/  |   \  \__|
c                                                        __|
c                         ~~~~~~~~~~~~~~~~~~~~~~~~~~
c                       DAWN MONTGOMERY / NICOLE MARTINEZ
c                                 Fall 2016
c                         ~~~~~~~~~~~~~~~~~~~~~~~~~~
c                      Nuclides: 99Tc beta spectrum
c
c
c                               Stylized Grass
c
c  ORGANS:
c  roots
c  shoots
c
c  OTHER:
c  flask inner
c  flask outer
c  HP solution
c
c                               SOURCE:HP solution
c
```

```
c                      TALLIES ON:Roots and Shoots
c
c                           UNION OF ALL CELLS
c
c ---------------------------------------------------------------------------
c                              CELL CARDS
c ---------------------------------------------------------------------------
c ------------------------------ CELLS ---------------------------------------
c                            for alpha: imp: a=1
50  1  -2.23  -1  2      imp:n=0 imp:p,e=1   $flask - borosilicate glass
51  10 -1.00  -2  3 4 5  imp:n=0 imp:p,e=1   $HP solution
52  2  -1.03  -3         imp:n=0 imp:p,e=1   $roots
53  2  -1.03  -4         imp:n=0 imp:p,e=1   $roots
54  2  -1.03  -5         imp:n=0 imp:p,e=1   $roots
55  2  -1.03  -6         imp:n=0 imp:p,e=1   $shoots
56  2  -1.03  -7         imp:n=0 imp:p,e=1   $shoots
57  2  -1.03  -8         imp:n=0 imp:p,e=1   $shoots
c ---------------------------- Air space ----------------------------------
99 11 -0.001205 -25 1 6 7 8  imp:n=0 imp:p,e=1
c ---------------------------- Universe (void) -----------------------------
100  0           25          imp:n,p,e=0
c ------------------------check sdef geometry-----------------------------------
c 90  1 -1.00  -30 6 7 8  imp:n=0 imp:p,e=1    $ SHOOTS
c 90  1 -1.00  -30 1  imp:n=0 imp:p,e=1        $ ROOTS or HP soln
c ===========================================================================

c ===========================================================================
c                            SURFACE CARDS
c ---------------------------------------------------------------------------
c ---------------------------------Flask-------------------------------------
c center of base/axis vector/radius 1/radius 2 (cm)
1 trc   0 0 -13     0 0 13     4     1.5  $flask outer
2 trc   0 0 -12.8   0 0 12.8   3.8   1.3  $flask inner
c -------------------------------Roots---------------------------------------
c    center of base/axis vector/radius (cm)
3     rcc 3 0 -10.1  -2.8 0 10    0.05   $base@ (3,0,-10) top @(0.2,0,0)
4  1  rcc 3 0 -10.1  -2.8 0 10    0.05   $rotated 120 degrees about z-axis
5  2  rcc 3 0 -10.1  -2.8 0 10    0.05   $rotated 240 degrees about z-axis
c -------------------------------Shoots--------------------------------------
c  center of base/axis vector/radius1/radius2
6     rec 0 0 0.1   0 0 18   0.2 0 0   0 0.05 0   $2 mm x 0.5 mm radii
7  3  rec 0 0 0.1   0 0 18   0.2 0 0   0 0.05 0   $left 30 deg, -0.5cm shift
8  4  rec 0 0 0.1   0 0 18   0.2 0 0   0 0.05 0   $right 30 deg, +0.5cm shift
c ---------------------------Universe VOID-------------------------------------
25 SO 25
c ------------------------check sdef geometry-----------------------------------
c 30  box -9.8 -0.12 0.05 0 0.24 0 19.6 0 0 0 0 18.1    $ SHOOTS
c 30  rcc 0 0 -13.05 0 0 13.1 4.1    $ ROOTS or HP soln
c ===========================================================================

c ===========================================================================
c                              DATA CARDS
c ---------------------------------------------------------------------------
c ---------------------- COORDINATE TRANSFORMS ------------------------------
c '*'  indicates that values are in degrees vice cos(theta)
c roots: rotating about the z axis 120 and 240 degrees so that the
c        3 roots are equidistantly spread in the "flask"
c shoots: rotating 30 deg L and R about the y axis
c         with origin shifted +/- 1cm in the x direction
c      Origin      xx' xy' xz'  yx' yy' yz'  zx' zy' zz'   How origin defined
c ---------------------------------------------------------------------------
*tr1   0 0 0      120  30   90  210 120 90   90 90   0 $root2
*tr2   0 0 0      240 150   90  330 240 90   90 90   0 $root3
*tr3  -0.5 0 0.2   30  90  -60   90   0 90  120 90  30 $shoot2
*tr4   0.5 0 0.2  -30  90 -120   90   0 90   60 90 -30 $shoot3
```

```
c ------------------------ SOURCE DEFININION --------------------------------
c Particles started within the sampling boundary (box) - any particle
c  that is started within the boundary but not within the specified source
c  cells are rejected.  Sampling boundary MUST include all source cells.
c
c  In source definition, "d1" is described by "si1" and "sp1" cards
c                                          where "i" info, "p" probability
c  Source information definition (si)
c  L-discrete source variable values
c  A-points where a probability density distribution is defined
c  S-distribution numbers
c  H—bin boundaries for a histogram distribution
c  Source probability (sp)
c  D-bin probabilities for an H or L distribution on SI card. Default.
c  C-cumulative bin probabilities for an H or L distribution on SI card.
c  V-for cell distributions only. Probability is proportional to cell volume.
c
c Energy spectra references:
c NNDC Interactive Chart of Nuclides
c www.nndc.bnl.gov/chart/reColor.jsp?newColor=dm
c ---------------------------------------------------------------------------
sdef cel=d5             $ Define source cells: which ones and what fraction
     axs=0 0 1          $ Define sampling boundary: cylinder along z-axis
     pos=0 0 -13.05     $ Base centered at 0 0 -13.05
     rad=d1             $ Define radius (in x and y direction)
     ext=d2             $ Define height (extend up z-axis)
     erg=d4             $ Define energy of source
     par=3              $ electron (3), gamma (2), alpha (34)
     eff=0.001          $ Sampling efficiency
c ------------------------ Sampling boundary ---------------------------------
si1  0    4.1      $ Radius of sampling cylinder that contains source
sp1 -21   1        $ -21 1 for radial sample (dependent on r)
si2  0    13.1     $ Height of sampling cylinder that contains source
sp2 -21   0        $ Weighting for axial sample (not dependent on r)
c ---------------------------------------------------------------------------
c ------------------------ Energy Definition ---------------------------------
si4 A  7.35E-03  2.20E-02  3.67E-02  5.14E-02  6.61E-02  $Tc-99 Beta spectra
       8.07E-02  9.54E-02  1.10E-01  1.25E-01  1.39E-01
       1.54E-01  1.69E-01  1.83E-01  1.98E-01  2.13E-01
       2.27E-01  2.42E-01  2.57E-01  2.71E-01  2.86E-01
sp4    8.27E-02  8.02E-02  7.89E-02  7.76E-02  7.61E-02
       7.43E-02  7.20E-02  6.90E-02  6.54E-02  6.10E-02
       5.59E-02  5.00E-02  4.34E-02  3.64E-02  2.90E-02
       2.16E-02  1.45E-02  8.20E-03  3.29E-03  5.83E-04
c ---------------------------------------------------------------------------
c ------------ Specific source cells with equal distribution ----------------
si5 L 51            $ HP solution
sp5   1
c ---------------------------------------------------------------------------
c ---------------------------- TALLY ----------------------------------------
mode p e          $ use a for alpha
nps 100000000     $ particle cutoff: 10^8
lost 10
c dbcn 12J 5444034  $ 12J skips first 12 descriptors to the 13th (stride)
rand gen=2 stride=5444034 $ more random numbers, recommended over dbcn
*f18:p,e  52 53 54 T                $ Roots
*f28:p,e  55 56 57 T                $ Shoots
*f38:p,e (52 53 54 55 56 57) T      $ Contents not bio relevant
c                                   $ Style to match above, total tally
c                                   $ for QA/QC
c                                   $ --> Parenthesis indicate union average
E0  0  1E-5 5.0      $ 0 catches "negative" energy from knock-on electrons
c                      With combined line above will not get tally fluctuation
c                      charts for each cell or individual statistical check
PRINT 110
```

```
PRDMP 1E7                 $do one order of magnitude less than # particles
c ---------------------------------------------------------------------------
c ---------------------------- MATERIALS ------------------------------------
c
c Compendium of Material Composition Data for Radiation Transport Modeling
c Revidion 1, March 4 2011; PNNL-15870 Rev.1; PIET-43741-TM-963
c
c Experimental densities in parenthesis
c
c ---------------------------------------------------------------------------
c Flask: Borosilicate Glass (Pyrex) - PNNL by mass fraction, p = 2.23 g/cm^3
m1    5000  -0.040   $ B
      8000  -0.540   $ O
     11000  -0.028   $ Na
     13000  -0.012   $ Al
     14000  -0.377   $ Si
     19000  -0.003   $ K
c Plant Tissue - PNNL (#359 Wood (Southern Pine)) by mass fraction
c     p = 0.64 g/cm^3 (PNNL, for wood) (1.03 experimental)
m2    1000  -0.060   $ H
      6000  -0.497   $ C
      7000  -0.005   $ N
      8000  -0.427   $ O
     12000  -0.002   $ Mg
     16000  -0.005   $ S
     19000  -0.002   $ K
     20000  -0.002   $ Ca
c Water
m10  1000  -0.11190  $ H
     8000  -0.88810  $ O
c Air
m11   7000  -0.755   $ N
      8000  -0.232   $ O
     18000  -0.013   $ Ar
```

C.1.2: Roots as source

```
c ------------------------ SOURCE DEFININION ---------------------------------
...
...
...
c ---------------------------------------------------------------------------
sdef cel=d5             $ Define source cells: which ones and what fraction
     axs=0 0 1          $ Define sampling boundary: cylinder along z-axis
     pos=0 0 -13.05     $ Base centered at 0 0 -13.05
     rad=d1             $ Define radius (in x and y direction)
     ext=d2             $ Define height (extend up z-axis)
     erg=d4             $ Define energy of source
     par=3              $ electron (3), gamma (2), alpha (34)
     eff=0.00000001     $ Sampling efficiency reduced for small source
c ------------------------ Sampling boundary ---------------------------------
si1  0    4.1      $ Radius of sampling cylinder that contains source
sp1 -21   1        $ -21 1 for radial sample (dependent on r)
si2  0    13.1     $ Height of sampling cylinder that contains source
sp2 -21   0        $ Weighting for axial sample (not dependent on r)
c ---------------------------------------------------------------------------
...
...
...
c ---------------------------------------------------------------------------
c ------------ Specific source cells with equal distribution ----------------
si5 L 52  53  54              $ ROOTS
sp5   1   1   1
c ---------------------------------------------------------------------------
```

C.1.3: Shoots as source

```
c ------------------------ SOURCE DEFININION --------------------------------
...
...
...
c ---------------------------------------------------------------------------
sdef cel=d5             $ Define source cells: which ones and what fraction
     x=d1               $ Define sampling boundary: box length x-dir
     y=d2               $ box width y-dir
     z=d3               $ box height z-dir
     erg=d4             $ Define energy of source
     par=3              $ electron (3), gamma (2), alpha (34)
     eff=0.000001       $ Sampling efficiency reduced for small source
c ------------------------ Sampling boundary --------------------------------
si1  -9.8     9.8       $ box x-dimensions
sp1   0       1         $ Weighting for box 1=uniform probability
si2  -0.12    0.12      $ box y-dimensions
sp2   0       1         $ Weighting for box 1=uniform probability
si3   0.05    18.1      $ box z-dimensions
sp3   0       1         $ Weighting  for box 1=uniform probability
c ---------------------------------------------------------------------------
...
...
...
c ---------------------------------------------------------------------------
c ------------ Specific source cells with equal distribution ------------------
si5 L 55  56  57              $ SHOOTS
sp5   1   1   1
c ---------------------------------------------------------------------------
```

C.1.4: Roots+Shoots as source

```
c ------------------------ SOURCE DEFININION --------------------------------
...
...
...
c ---------------------------------------------------------------------------
sdef cel=d5             $ Define source cells: which ones and what fraction
     x=d1               $ Define sampling boundary: box length x-dir
     y=d2               $ box width y-dir
     z=d3               $ box height z-dir
     erg=d4             $ Define energy of source
     par=3              $ electron (3), gamma (2), alpha (34)
     eff=0.00000001     $ Sampling efficiency reduced for small source
c ------------------------ Sampling boundary --------------------------------
si1  -9.8     9.8       $ box x-dimensions
sp1   0       1         $ Weighting for box 1=uniform probability
si2  -4.1     4.1       $ box y-dimensions
sp2   0       1         $ Weighting for box 1=uniform probability
si3  -13.05   18.1      $ box z-dimensions
sp3   0       1         $ Weighting  for box 1=uniform probability
c ---------------------------------------------------------------------------
...
...
...
c ---------------------------------------------------------------------------
c ------------ Specific source cells with equal distribution ------------------
si5 L 52  53  54  55  56  57        $ ROOTS + SHOOTS
sp5   1   1   1   1   1   1
c ---------------------------------------------------------------------------
```

C.1.5: ^{137}Cs beta spectra

```
c ------------------------ Energy Definition ---------------------------------
si4 A  2.94E-02  8.80E-02  1.47E-01  2.05E-01  2.64E-01  $Cs-137 Beta spectra
       3.23E-01  3.81E-01  4.40E-01  4.99E-01  5.57E-01
       6.16E-01  6.75E-01  7.33E-01  7.92E-01  8.51E-01
       9.09E-01  9.68E-01  1.03E+00  1.09E+00  1.14E+00
sp4    1.93E-01  1.76E-01  1.61E-01  1.43E-01  1.22E-01
       9.38E-02  6.01E-02  2.64E-02  5.70E-03  3.30E-03
       3.07E-03  2.82E-03  2.53E-03  2.20E-03  1.83E-03
       1.42E-03  9.92E-04  5.91E-04  2.45E-04  5.38E-05
c ------------------------------------------------------------------------------
```

C.1.6: ^{137}Cs gamma energy

```
c ------------------------------------------------------------------------------
sdef cel=d5             $ Define source cells: which ones and what fraction
     axs=0 0 1          $ Define sampling boundary: cylinder along z-axis
     pos=0 0 -13.05     $ Base centered at 0 0 -13.05
     rad=d1             $ Define radius (in x and y direction)
     ext=d2             $ Define height (extend up z-axis)
     erg=d4             $ Define energy of source
     par=2              $ electron (3), gamma (2), alpha (34)
     eff=0.001          $ Sampling efficiency
c ------------------------------------------------------------------------------
...
...
...
c ------------------------ Energy Definition ---------------------------------
c ***discrete photon energies for I>1%
si4 L  6.617E-01                                          $Cs-137 photons
sp4    8.510E-01
c ------------------------------------------------------------------------------
```

C.1.7: ^{237}Np alpha energies

```
c ------------------------------ CELLS ---------------------------------------
c                         for alpha: imp: a=1
50  1  -2.23  -1  2      imp:n=0 imp:p,e,a=1   $flask - borosilicate glass
51  10 -1.00  -2  3 4 5  imp:n=0 imp:p,e,a=1   $HP solution
52  2  -1.03  -3         imp:n=0 imp:p,e,a=1   $roots
53  2  -1.03  -4         imp:n=0 imp:p,e,a=1   $roots
54  2  -1.03  -5         imp:n=0 imp:p,e,a=1   $roots
55  2  -1.03  -6         imp:n=0 imp:p,e,a=1   $shoots
56  2  -1.03  -7         imp:n=0 imp:p,e,a=1   $shoots
57  2  -1.03  -8         imp:n=0 imp:p,e,a=1   $shoots
c ------------------------------ Air space -----------------------------------
99 11 -0.001205 -25 1 6 7 8  imp:n=0 imp:p,e,a=1
c ---------------------------- Universe (void) --------------------------------
100  0           25          imp:n,p,e,a=0
c ------------------------check sdef geometry---------------------------------
c 90  1 -1.00  -30 6 7 8  imp:n=0 imp:p,e,a=1    $ SHOOTS
c 90  1 -1.00  -30 1  imp:n=0 imp:p,e,a=1        $ ROOTS or HP soln
c ==============================================================================
...
...
...
c ------------------------ SOURCE DEFININION ---------------------------------
...
...
...
     par=34             $ electron (3), gamma (2), alpha (34)
...
```

```
...
...
c -------------------------------------------------------------------------
c ------------------------ Energy Definition ---------------------------------
c ***discrete alpha energies
si4 L  4.5151    4.5730    4.5786    4.5949    4.5991     $Np-237 alphas
       4.6197    4.6400    4.6591    4.6650    4.6982
       4.7083    4.7123    4.7413    4.7665    4.7714
       4.7880    4.8035    4.8168    4.8664    4.8727
sp4    3.50E-04  4.80E-04  3.69E-03  8.50E-04  3.71E-03
       3.20E-04  6.43E-02  3.00E-03  3.48E-02  5.35E-03
       6.00E-03  6.00E-03  1.90E-04  9.30E-02  2.32E-01
       4.76E-01  2.01E-02  2.43E-02  5.30E-03  2.39E-02
c -------------------------------------------------------------------------
...
...
...
c ---------------------------- TALLY ----------------------------------------
mode p e a        $ use a for alpha
nps 100000000     $ particle cutoff: 10^8
lost 10
c dbcn 12J 5444034  $ 12J skips first 12 descriptors to the 13th (stride)
rand gen=2 stride=5444034 $ more random numbers, recommended over dbcn
*f18:p,e,a  52 53 54 T                 $ Roots
*f28:p,e,a  55 56 57 T                 $ Shoots
*f38:p,e,a (52 53 54 55 56 57) T       $ Contents not bio relevant
```

C.1.8: ^{238}U alpha energies

```
c ------------------------------ CELLS ----------------------------------------
c                         for alpha: imp: a=1
50  1  -2.23  -1  2      imp:n=0 imp:p,e,a=1   $flask - borosilicate glass
51  10 -1.00  -2  3 4 5  imp:n=0 imp:p,e,a=1   $HP solution
52  2  -1.03  -3         imp:n=0 imp:p,e,a=1   $roots
53  2  -1.03  -4         imp:n=0 imp:p,e,a=1   $roots
54  2  -1.03  -5         imp:n=0 imp:p,e,a=1   $roots
55  2  -1.03  -6         imp:n=0 imp:p,e,a=1   $shoots
56  2  -1.03  -7         imp:n=0 imp:p,e,a=1   $shoots
57  2  -1.03  -8         imp:n=0 imp:p,e,a=1   $shoots
c ------------------------------ Air space ------------------------------------
99 11 -0.001205 -25 1 6 7 8  imp:n=0 imp:p,e,a=1
c ---------------------------- Universe (void) --------------------------------
100  0           25          imp:n,p,e,a=0
c ------------------------check sdef geometry---------------------------------
c 90  1 -1.00  -30 6 7 8  imp:n=0 imp:p,e,a=1    $ SHOOTS
c 90  1 -1.00  -30 1  imp:n=0 imp:p,e,a=1        $ ROOTS or HP soln
c =========================================================================
...
...
...
c ------------------------ SOURCE DEFININION ---------------------------------
...
...
...
     par=34             $ electron (3), gamma (2), alpha (34)
...
...
...
c -------------------------------------------------------------------------
c ------------------------ Energy Definition ---------------------------------
c ***discrete alpha energies
si4 L  4.038     4.151     4.198                          $U-238 alphas
sp4    7.80E-04  2.10E-01  7.90E-01
c -------------------------------------------------------------------------
```

```
...
...
...
c ------------------------------------------------------------------------------
c ---------------------------- TALLY -------------------------------------------
mode p e a        $ use a for alpha
nps 100000000     $ particle cutoff: 10^8
lost 10
c dbcn 12J 5444034  $ 12J skips first 12 descriptors to the 13th (stride)
rand gen=2 stride=5444034 $ more random numbers, recommended over dbcn
*f18:p,e,a  52 53 54 T                 $ Roots
*f28:p,e,a  55 56 57 T                 $ Shoots
*f38:p,e,a (52 53 54 55 56 57) T       $ Contents not bio relevant
```

C.2: Voxel Models (CF 4)

C.2.1: ^{99}Tc Beta spectra, HP solution as source

```
c ------------------------------------------------------------------------------
c
c                __   |   __      _   _   __  __   _
c               /     |  /__\  |/ \ / | /__ /  \ |/ |
c               \__   \_ \__   |   |  | __/ \__/ |  |
c
c                     _   .        __    _   __  .  _|_
c            |  | |/ |  |  \  / /__\ |/ \ /__  |   |  |  |
c            \__| |  |  |   \/  \__, |    __/  |   \  \__|
c                                                    __|
c                     ~~~~~~~~~~~~~~~~~~~~~~~~~~
c                  DAWN MONTGOMERY / NICOLE MARTINEZ
c                            Fall 2016
c                     ~~~~~~~~~~~~~~~~~~~~~~~~~~
c                   VOXILIZED ANDROPOGON VIRGINICUS
C
c                   Nuclides: 99Tc beta spectrum
c
c                        SOURCE:HP solution
c
c                     TALLIES ON:Roots and Shoots
c ------------------------------------------------------------------------------
c
c This input file was made with the MCNP Lattice Tool
c originally created by Erick Daniel Cardenas-Mendez (a.k.a. Ace Wave)
c for the Human Monitoring Laboratory of Health Canada
c
c Input file originally created on:
c Tue Oct 18 2016
c
c Empty space universe: 3
c compression factor: 4
c
c
c
c +++++++++++++++++++++++++++++++++++++++++++++++++++++++++
c
c     Cells
c
c +++++++++++++++++++++++++++++++++++++++++++++++++++++++++
c
c _____________________________________________________
c  ID#  | Material# |Density|Definition:   |Importance
c       |(0 if void)| N/A if| Surface      |
c       |           |  void | relationships|
c -----------------------------------------------------
   999    0                     999          imp:n,p,e=0        $ outside
   998    3        -0.001205   -999  1 #997   imp:n=0 imp:p,e=1  $ air
c
c ------------------Filling Universes--------------------
c _____________________________________________________
c Cell#|Mat#|Density|Defn:    | Define |Importance
c      |    |       |in void  |Universe|
c      |    |       |"mortar"|        |
c -----------------------------------------------------
    1     1  -1.03       -2    u = 1     imp:n=0 imp:p,e=1    $Root
    2     2  -1.03       -2    u = 2     imp:n=0 imp:p,e=1    $Shoot
    3     3  -0.001205   -2    u = 3     imp:n=0 imp:p,e=1    $Default Air
    4     4  -1.00       -2    u = 4     imp:n=0 imp:p,e=1    $HP soln @roots
```

```
c
c -------------------Lattice Unit Cell-------------------
c ____________________________________________________________________________
c ID#|Mat#|Density |Defn:  |Lattice|Define  |Imp|Fill: long list of
c    |    |  n/a   | in    | Type  |Universe|   | universes in specified
c    |    |if 0 mat|"house"|       |        |   | x,y,z grid
c ----------------------------------------------------------------------------
c
    996    0   -2    lat = 1   u = 996   imp:n=0 imp:p,e=1
                     fill = 0:319  0:319 0:154
     4 161520r 1 4 317r 1 2r 4 316r 1 2r 4 101435r 1 2r 4 316r 1
     3r 4 314r 1 4r 4 315r 1 2r 4 100475r 1 3r 4 315r 1 3r 4 316r 1
     2r 4 26422r 1 3r 4 317r 1 4 74049r 1 2r 4 316r 1 2r 4 317r 1
...
...
...
     1r 3 318r 2 3r 3 318r 2 3 318r 2 1r 3 318r 2 1r 3 591r 2 3 318r 2
     3 317r 2 3 317r 2 3 317r 2 1r 3 314r 2 2r 3 316r 2 3 317r 2
     1r 3 316r 2 1r 3 316r 2 1r 3 315r 2 2r 3 315r 2 1r 3
     18401r
c
c ------------- Cell Containing Lattice -----------------
c ____________________________________________________
c ID#|Mat#|Density|Defn:  |Fill with|Importance
c    |    |       | in    | lattice |
c    |    |       |"house"|i.e. 996 |
c ----------------------------------------------------
    997    0     -1   fill = 996   imp:n=0 imp:p,e=1
c
c ============================================================================

c ++++++++++++++++++++++++++++++++++++++++++++++++++++++++++++
c
c     Surfaces
c
c ++++++++++++++++++++++++++++++++++++++++++++++++++++++++++++
c
  999 so  500     $(MAKE SURE UNIVERSE SPHERE IS BIG ENOUGH FOR LATTICE STRUCTURE)
c
c ----------------Box for Filling Universes-----------------------------------
c This information comes from Image-->Image Information in 3D doctor
c   namely: # columns, # rows, # planes, pixel width, and slice thickness
c   Note that pixel width and slice thickness are given in mm in 3D doctor
c     but need to be in cm for Voxelizer and MCNP
c
c  In our case, # columns = 1280, # rows = 1280, planes (slices) = 155
c   Pixel width = 0.005 cm, slice thickness = 0.125 cm
c   For compression factor = 4, then # columns = 1280 / 4 = 320
c                                    # rows = 1280 / 4 = 320
c    0.005(4)=0.02; 320(0.005)(4)=6.4;  155(0.125)=19.375
c
c
c  RPP 1: Dimensions of "house" in which to build the lattice
c  RPP 2: Dimensions for "brick" in which each voxel is placed
c
  1  rpp        0.000     6.400     0.000     6.400     0.000     19.375
  2  rpp        0.000     0.020     0.000     0.020     0.000     0.125
c
c ============================================================================

c ----------------------------------------------------------------------------
c                             DATA CARDS
c ----------------------------------------------------------------------------
c ------------------------ SOURCE DEFININION -------------------------------
c Particles started within the sampling boundary (cylinder) - any particle
```

```
c that is started within the boundary but not within the specified source cells
c is rejected.  Sampling boundary MUST include all source cells.
c
c  In source definition, "d1" is described by "si1" and "sp1" cards
c                                          where "i" info, "p" probability
c Source information definition
c  L-discrete source variable values
c  A-points where a probability density distribution is defined
c  S-distribution numbers
c  H-bin boundaries for a histogram distribution
c Source probability
c  D-bin probabilities for an H or L distribution on SI card. Default.
c  C-cumulative bin probabilities for an H or L distribution on SI card.
c  V-for cell distributions only. Probability is proportional to cell volume.
c
c Energy spectra references:
c  Stabin MG, and CQP da Luz, L. “Decay data for internal and external dose
c   assessment.” Health Phys. 83:471-475; 2002. http://www.doseinfo-radar.com/
c  K. F. Eckerman, R. J. Westfall, J. C. Ryman, and M. Christy.
c   "Availability of Nuclear Decay Data in Electronic Form, Including Beta
c   Spectra not Previously Published," Health Phys. 67(4):338-345 (1994).
c
c NNDC Interactive Chart of Nuclides
c www.nndc.bnl.gov/chart/reColor.jsp?newColor=dm
c
c ---------------------------------------------------------------------------
sdef cel=d5            $ Define source cells: which ones and what fraction
     X=d1              $ Sampling boundary by X, Y, Z
     Y=d2
     Z=d3
     erg=d4            $ Define energy of source (beta)
     par=3             $ electron (3), gamma (2), alpha (34)
     eff=0.001         $ Sampling efficiency (reduce because source is small)
c ----------------- Sampling boundary from 2 RPP above ----------------------
si1 h 0.0    0.02       $ range of X
sp1 d 0      1
si2 h 0.0    0.02       $ range of Y
sp2 d 0      1
si3 h 0.0    0.125      $ range of Z
sp3 d 0      1
c ----------------- Energy definition ----------------------
si4 A  7.35E-03  2.20E-02  3.67E-02  5.14E-02  6.61E-02  $Tc-99 Beta spectra
       8.07E-02  9.54E-02  1.10E-01  1.25E-01  1.39E-01
       1.54E-01  1.69E-01  1.83E-01  1.98E-01  2.13E-01
       2.27E-01  2.42E-01  2.57E-01  2.71E-01  2.86E-01
sp4    8.27E-02  8.02E-02  7.89E-02  7.76E-02  7.61E-02
       7.43E-02  7.20E-02  6.90E-02  6.54E-02  6.10E-02
       5.59E-02  5.00E-02  4.34E-02  3.64E-02  2.90E-02
       2.16E-02  1.45E-02  8.20E-03  3.29E-03  5.83E-04
c ------ Specific source cells with equal distribution -------
c  L = List, equal probability (1) each cell (organ) listed
c  source cell < lattice universe < universe box that contains lattice
c   using SDEF HELPER
si5 l  (4<996[0 0 0]<997)
     (4<996[1 0 0]<997)
     (4<996[2 0 0]<997)
...
...
...
     (4<996[168 129 78]<997)
     (4<996[169 129 78]<997)
     (4<996[170 129 78]<997)
sp5 1 8019824r
c ---------------------------------------------------------------------------
c ---------------------------- TALLY ----------------------------------------
```

```
mode p e                            $ use a for alpha
nps 100000000                       $ **Particle cutoff: 10^8
lost 10
c dbcn 12J 5444034                  $ more random #'s
 *f8:p,e u=(1 2 3 4) $ all universes
 *f18:p,e u=(1)      $ roots
 *f28:p,e u=(2)      $ shoots
 *f38:p,e u=(3)      $ surrounding air
 *f48:p,e u=(4)      $ HP solution
 *f58:p,e u=(1 2)    $ WHOLE PLANT
E0 0 1E-5 5.0        $ Energy bins
c
PRINT 110
PRDMP 1E7
c
c +++++++++++++++++++++++++++++++++++++++++++++++++++++++++
c
c     Materials
c
c +++++++++++++++++++++++++++++++++++++++++++++++++++++++++
c
c Root
c Plant Tissue - PNNL (#359 Wood (Southern Pine)) by mass fraction
c     p = 0.64 g/cm^3 (PNNL, for wood) (1.03 experimental)
m1    1000  -0.060   $ H
      6000  -0.497   $ C
      7000  -0.005   $ N
      8000  -0.427   $ O
     12000  -0.002   $ Mg
     16000  -0.005   $ S
     19000  -0.002   $ K
     20000  -0.002   $ Ca
c
c Shoot
c Plant Tissue - PNNL (#359 Wood (Southern Pine)) by mass fraction
c     p = 0.64 g/cm^3 (PNNL, for wood) (1.03 experimental)
m2    1000  -0.060   $ H
      6000  -0.497   $ C
      7000  -0.005   $ N
      8000  -0.427   $ O
     12000  -0.002   $ Mg
     16000  -0.005   $ S
     19000  -0.002   $ K
     20000  -0.002   $ Ca
c
c Default Surrounding Air
m3    7000  -0.755   $ N
      8000  -0.232   $ O
     18000  -0.013   $ Ar
c
c Water
m4  1000  -0.11190  $ H
     8000  -0.88810  $ O
c
c Flask: Borosilicate Glass (Pyrex) - PNNL by mass fraction, p = 2.23 g/cm^3
m9    5000  -0.040   $ B
      8000  -0.540   $ O
     11000  -0.028   $ Na
     13000  -0.012   $ Al
     14000  -0.377   $ Si
     19000  -0.003   $ K
C
```

C.2.2: Roots as source

```
c ------ Specific source cells with equal distribution -------
c  L = List, equal probability (1) each cell (organ) listed
c  source cell < lattice universe < universe box that contains lattice
c   using SDEF HELPER
si5 l  (1<996[241 184 1]<997)
     (1<996[240 185 1]<997)
     (1<996[241 185 1]<997)
...
...
...
     (1<996[136 159 77]<997)
     (1<996[137 159 77]<997)
     (1<996[143 159 77]<997)
sp5 1 8825r
c ---------------------------------------------------------------------------
```

C.2.3: Shoots as source

```
c ------ Specific source cells with equal distribution -------
c  L = List, equal probability (1) each cell (organ) listed
c  source cell < lattice universe < universe box that contains lattice
c   using SDEF HELPER
si5 l  (2<996[171 129 78]<997)
     (2<996[172 129 78]<997)
     (2<996[170 130 78]<997)
...
...
...
     (2<996[159 261 154]<997)
     (2<996[156 262 154]<997)
     (2<996[157 262 154]<997)
sp5 1 7470r
c ---------------------------------------------------------------------------
```

C.2.4: Roots+Shoots as source

```
c ------ Specific source cells with equal distribution -------
c  L = List, equal probability (1) each cell (organ) listed
c  source cell < lattice universe < universe box that contains lattice
c   using SDEF HELPER
si5 l  (1<996[241 184 1]<997)
     (1<996[240 185 1]<997)
     (1<996[241 185 1]<997)
...
...
...
     (2<996[159 261 154]<997)
     (2<996[156 262 154]<997)
     (2<996[157 262 154]<997)
sp5 1 8825r
    1 7470r
c ---------------------------------------------------------------------------
```

C.2.5: ^{137}Cs Beta spectra

```
c ------------------ Energy definition ----------------------
si4 A  2.94E-02  8.80E-02  1.47E-01  2.05E-01  2.64E-01  $Cs-137 Beta spectra
       3.23E-01  3.81E-01  4.40E-01  4.99E-01  5.57E-01
       6.16E-01  6.75E-01  7.33E-01  7.92E-01  8.51E-01
       9.09E-01  9.68E-01  1.03E+00  1.09E+00  1.14E+00
sp4    1.93E-01  1.76E-01  1.61E-01  1.43E-01  1.22E-01
       9.38E-02  6.01E-02  2.64E-02  5.70E-03  3.30E-03
       3.07E-03  2.82E-03  2.53E-03  2.20E-03  1.83E-03
       1.42E-03  9.92E-04  5.91E-04  2.45E-04  5.38E-05
```

C.2.6: ^{137}Cs Gamma energy

```
c ------------------------- SOURCE DEFININION --------------------------------
...
...
...
     par=2             $ electron (3), gamma (2), alpha (34)
...
...
...
c ------------------ Energy definition ----------------------
c ***discrete photon energies for I>1%
si4 L  6.617E-01                                          $Cs-137 photons
sp4    8.510E-01
c ------------------------------------------------------------------------------
```

C.2.7: ^{237}Np Alpha energies

```
c ++++++++++++++++++++++++++++++++++++++++++++++++++++++++++++
c
c     Cells
c
c ++++++++++++++++++++++++++++++++++++++++++++++++++++++++++++
...
...
...
   999    0                     999           imp:n,p,e,a=0        $ outside
   998    3        -0.001205   -999  1 #997   imp:n=0 imp:p,e,a=1  $ air
c
c ------------------Filling Universes--------------------
c _____________________________________________________
c Cell#|Mat#|Density|Defn:   | Define |Importance
c      |    |       |in void |Universe|
c      |    |       |"mortar"|        |
c -----------------------------------------------------
    1     1  -1.03       -2    u = 1     imp:n=0 imp:p,e,a=1   $Root
    2     2  -1.03       -2    u = 2     imp:n=0 imp:p,e,a=1   $Shoot
    3     3  -0.001205   -2    u = 3     imp:n=0 imp:p,e,a=1   $Default Air
    4     4  -1.00       -2    u = 4     imp:n=0 imp:p,e,a=1   $HP soln @roots
c
c ------------------Lattice Unit Cell-------------------
c ____________________________________________________________________________
c ID#|Mat#|Density |Defn:  |Lattice|Define  |Imp|Fill: long list of
c    |    |  n/a   | in    | Type  |Universe|   | universes in specified
c    |    |if 0 mat|"house"|       |        |   | x,y,z grid
c ----------------------------------------------------------------------------
c
    996   0   -2   lat = 1   u = 996   imp:n=0 imp:p,e,a=1
...
...
...
c ------------- Cell Containing Lattice -----------------
```

```
c _____________________________________________________
c ID#|Mat#|Density|Defn:  |Fill with|Importance
c    |    |       | in    | lattice |
c    |    |       |"house"|i.e. 996 |
c -------------------------------------------------------
    997    0     -1   fill = 996  imp:n=0 imp:p,e,a=1
c
c ===============================================================================
...
...
...
c ------------------------ SOURCE DEFININION --------------------------------
...
...
...
     par=34            $ electron (3), gamma (2), alpha (34)
...
...
...
c ------------------ Energy definition ----------------------
c ***discrete alpha energies
si4 L  4.5151    4.5730    4.5786    4.5949    4.5991     $Np-237 alphas
       4.6197    4.6400    4.6591    4.6650    4.6982
       4.7083    4.7123    4.7413    4.7665    4.7714
       4.7880    4.8035    4.8168    4.8664    4.8727
sp4    3.50E-04  4.80E-04  3.69E-03  8.50E-04  3.71E-03
       3.20E-04  6.43E-02  3.00E-03  3.48E-02  5.35E-03
       6.00E-03  6.00E-03  1.90E-04  9.30E-02  2.32E-01
       4.76E-01  2.01E-02  2.43E-02  5.30E-03  2.39E-02
...
...
...
c ----------------------------- TALLY ----------------------------------------
mode p e a                          $ use a for alpha
nps 100000000                       $ **Particle cutoff: 10^8
lost 10
c dbcn 12J 5444034                  $ more random #'s
 *f8:p,e,a u=(1 2 3 4) $ all universes
 *f18:p,e,a u=(1)      $ roots
 *f28:p,e,a u=(2)      $ shoots
 *f38:p,e,a u=(3)      $ surrounding air
 *f48:p,e,a u=(4)      $ HP solution
 *f58:p,e,a u=(1 2)    $ WHOLE PLANT
```

C.2.8: ^{238}U Alpha energies

```
c ++++++++++++++++++++++++++++++++++++++++++++++++++++++++++
c
c     Cells
c
c ++++++++++++++++++++++++++++++++++++++++++++++++++++++++++
...
...
...
c -------------------------------------------------------
   999    0                     999          imp:n,p,e,a=0        $ outside
   998    3        -0.001205   -999  1 #997   imp:n=0 imp:p,e,a=1  $ air
c
c ------------------Filling Universes--------------------
c _____________________________________________________
c Cell#|Mat#|Density|Defn:   | Define |Importance
c      |    |       |in void |Universe|
c      |    |       |"mortar"|        |
c -------------------------------------------------------
```

```
    1     1  -1.03       -2    u = 1     imp:n=0 imp:p,e,a=1    $Root
    2     2  -1.03       -2    u = 2     imp:n=0 imp:p,e,a=1    $Shoot
    3     3  -0.001205   -2    u = 3     imp:n=0 imp:p,e,a=1    $Default Air
    4     4  -1.00       -2    u = 4     imp:n=0 imp:p,e,a=1    $HP soln @root
c
c -------------------Lattice Unit Cell-------------------
c _____________________________________________________________________________
c ID#|Mat#|Density |Defn:  |Lattice|Define  |Imp|Fill: long list of
c    |    |  n/a   | in    | Type  |Universe|   | universes in specified
c    |    |if 0 mat|"house"|       |        |   | x,y,z grid
c -----------------------------------------------------------------------------
c
    996    0   -2    lat = 1   u = 996   imp:n=0 imp:p,e,a=1
...
...
...
c ------------- Cell Containing Lattice -----------------
c _____________________________________________________
c ID#|Mat#|Density|Defn:  |Fill with|Importance
c    |    |       | in    | lattice |
c    |    |       |"house"|i.e. 996 |
c -----------------------------------------------------
    997    0     -1   fill = 996   imp:n=0 imp:p,e,a=1
c
c ==============================================================================
...
...
...
c ------------------------ SOURCE DEFININION --------------------------------
...
...
     par=34            $ electron (3), gamma (2), alpha (34)
...
...
...
c ------------------ Energy definition ----------------------
c ***discrete alpha energies
si4 L  4.038     4.151     4.198                        $U-238 alphas
sp4    7.80E-04  2.10E-01  7.90E-01
...
...
...
c -----------------------------------------------------------------------------
c ---------------------------- TALLY ------------------------------------------
mode p e a                          $ use a for alpha
nps 100000000                       $ **Particle cutoff: 10^8
lost 10
c dbcn 12J 5444034                  $ more random #'s
 *f8:p,e,a u=(1 2 3 4) $ all universes
 *f18:p,e,a u=(1)      $ roots
 *f28:p,e,a u=(2)      $ shoots
 *f38:p,e,a u=(3)      $ surrounding air
 *f48:p,e,a u=(4)      $ HP solution
 *f58:p,e,a u=(1 2)    $ WHOLE PLANT
```

C.3: Hybrid Models

C.3.1: ^{99}Tc beta spectra, HP solution as source (CF4)

```
c -------------------------------------------------------------------------
c
c                 __    |   __      _   _   __  __   _
c                /     |  /__\  |/ \ / | /__ /  \ |/ |
c                \__   \_ \__   |   |  | __/ \__/ |  |
c
c                      _   .        __    _   __  .  _|_
c              |  | |/ |  |  \  / /__\ |/ \ /__  |   |  |  |
c              \__| |  |  |   \/  \__, |    __/  |   \  \__|
c                                                     __|
c                       ~~~~~~~~~~~~~~~~~~~~~~~~~~
c                   DAWN MONTGOMERY / NICOLE MARTINEZ
c                             Fall 2018
c                       ~~~~~~~~~~~~~~~~~~~~~~~~~~
c                    HYBRID ANDROPOGON VIRGINICUS
C                    slice thickness = 0.25 mm (0.025 cm)
c                    voxel width & length = 0.05 mm (0.005 cm)
C
c                    Nuclides:99Tc beta spectrum
c
c                    SOURCE:HP solution
c
c                    TALLIES ON:Roots and Shoots
c -------------------------------------------------------------------------
c This input file was made with the MCNP Lattice Tool
c originally created by Erick Daniel Cardenas-Mendez (a.k.a. Ace Wave)
c for the Human Monitoring Laboratory of Health Canada
c
c Input file originally created on:
c Mon Nov 26 2018
c
c Empty space universe: 3
c compression factor: 4
c
c +++++++++++++++++++++++++++++++++++++++++++++++++++++++++++++
c
c     Cells
c
c +++++++++++++++++++++++++++++++++++++++++++++++++++++++++++++
c ____________________________________________________________
c  ID#  | Material# |Density|Definition:   |Importance
c       |(0 if void)| N/A if| Surface      |
c       |           |  void | relationships|
c ------------------------------------------------------------
   999    0                     999          imp:n,p,e=0        $ outside
   998    3        -0.001205   -999  1 #997   imp:n=0 imp:p,e=1  $ air
c
c ------------------Filling Universes--------------------
c ____________________________________________________________
c Cell#|Mat#|Density|Defn:    | Define |Importance
c      |    |       |in void  |Universe|
c      |    |       |"mortar"|        |
c ------------------------------------------------------------
    1     1  -1.03       -2    u = 1     imp:n=0 imp:p,e=1    $Root
    2     2  -1.03       -2    u = 2     imp:n=0 imp:p,e=1    $Shoot
    3     3  -0.001205   -2    u = 3     imp:n=0 imp:p,e=1    $Default Air
    4     4  -1.00       -2    u = 4     imp:n=0 imp:p,e=1    $HP soln @roots
c
c ------------------Lattice Unit Cell-------------------
```

```
c _____________________________________________________________________
c ID#|Mat#|Density |Defn:  |Lattice|Define  |Imp|Fill: long list of
c    |    |  n/a   | in    | Type  |Universe|   | universes in specified
c    |    |if 0 mat|"house"|       |        |   | x,y,z grid
c ---------------------------------------------------------------------
  996  0            -2      lat = 1 u = 996  imp:n=0 imp:p,e=1
                   fill = 0:349  0:349 0:920
     4 2529017r 1 4 347r 1 3r 4 345r 1 3r 4 121796r 1 4 347r 1 3r 4
     345r 1 2r 4 121796r 1 2r 4 346r 1 3r 4 345r 1 2r 4 121446r 1
     4 348r 1 2r 4 345r 1 3r 4 346r 1 2r 4 121446r 1 1r 4 346r 1
...
...
...
     3 348r 2 3 348r 2 3 348r 2 1r 3 348r 2 3 348r 2 3 348r 2 1r 3
     348r 2 3 348r 2 3 348r 2 1r 3 348r 2 3 348r 2 3 349r 2 3 348r 2
     3 348r 2 3 349r 2 3 348r 2 3 348r 2 3
     1482475r
c
c ------------- Cell Containing Lattice -----------------
c _____________________________________________________
c ID#|Mat#|Density|Defn:  |Fill with|Importance
c    |    |       | in    | lattice |
c    |    |       |"house"|i.e. 996 |
c -----------------------------------------------------
    997    0     -1   fill = 996  imp:n=0 imp:p,e=1
c
c =====================================================================

c =====================================================================
c +++++++++++++++++++++++++++++++++++++++++++++++++++++++
c
c     Surfaces
c
c +++++++++++++++++++++++++++++++++++++++++++++++++++++++
c
  999 so  500  $(MAKE SURE UNIVERSE SPHERE IS BIG ENOUGH FOR LATTICE STRUCTURE)
c
c ---------------Box for Filling Universes-----------------------------------
c This information comes from Image-->Image Information in 3D doctor
c   or from "File->Modify Window" and "calibration" for pixel sizes
c   namely: # columns, # rows, # planes, pixel width, and slice thickness
c Note that pixel width and slice thickness are given in mm in 3D doctor
c     but need to be in cm for Voxelizer and MCNP
c
c In our case, # columns = 1400, # rows = 1400, planes (slices) = 921
c   Pixel width = 0.005 cm, slice thickness = 0.025 cm
c   For compression factor = 4, then # columns = 1400 / 4 = 350
c                                    # rows = 1400 / 4 = 350
c   0.005(4)=0.020; 350(0.005)(4)=7.00; 921(0.025)=23.025
c
c
c  RPP 1: Dimensions of "house" in which to build the lattice
c  RPP 2: Dimensions for "brick" in which each voxel is placed
c
  1  rpp        0.000     7.000     0.000     7.000     0.000     23.025
  2  rpp        0.000     0.020     0.000     0.020     0.000     0.025
c =====================================================================

c =====================================================================
c ---------------------------------------------------------------------
c                             DATA CARDS
c ---------------------------------------------------------------------
c ------------------------ SOURCE DEFININION ----------------------------
c Particles started within the sampling boundary (cylinder) - any particle
c that is started within the boundary but not within the specified source cells
```

```
c is rejected.  Sampling boundary MUST include all source cells.
c
c  In source definition, "d1" is described by "si1" and "sp1" cards
c                                              where "i" info, "p" probability
c Source information definition
c  L-discrete source variable values
c  A-points where a probability density distribution is defined
c  S-distribution numbers
c  H-bin boundaries for a histogram distribution
c Source probability
c  D-bin probabilities for an H or L distribution on SI card. Default.
c  C-cumulative bin probabilities for an H or L distribution on SI card.
c  V-for cell distributions only. Probability is proportional to cell volume.
c
c Energy spectra references:
c  Stabin MG, and CQP da Luz, L. "Decay data for internal and external dose
c   assessment." Health Phys. 83:471-475; 2002. http://www.doseinfo-radar.com/
c  K. F. Eckerman, R. J. Westfall, J. C. Ryman, and M. Christy.
c   "Availability of Nuclear Decay Data in Electronic Form, Including Beta
c   Spectra not Previously Published," Health Phys. 67(4):338-345 (1994).
c
c NNDC Interactive Chart of Nuclides
c www.nndc.bnl.gov/chart/reColor.jsp?newColor=dm
c
c --------------------------------------------------------------------------
sdef cel=d5            $ Define source cells: which ones and what fraction
     X=d1              $ Sampling boundary by X, Y, Z
     Y=d2
     Z=d3
     erg=d4            $ Define energy of source (beta)
     par=3             $ electron (3), gamma (2), alpha (34)
     eff=0.001         $ Sampling efficiency (reduce because source is small)
c ------------------ Sampling boundary from 2 RPP above ----------------------
si1 h 0.0    0.020       $ range of X
sp1 d 0      1
si2 h 0.0    0.020       $ range of Y
sp2 d 0      1
si3 h 0.0    0.025       $ range of Z
sp3 d 0      1
c ------------------ Energy definition ----------------------
si4 A  7.35E-03  2.20E-02  3.67E-02  5.14E-02  6.61E-02  $Tc-99 Beta spectra
       8.07E-02  9.54E-02  1.10E-01  1.25E-01  1.39E-01
       1.54E-01  1.69E-01  1.83E-01  1.98E-01  2.13E-01
       2.27E-01  2.42E-01  2.57E-01  2.71E-01  2.86E-01
sp4    8.27E-02  8.02E-02  7.89E-02  7.76E-02  7.61E-02
       7.43E-02  7.20E-02  6.90E-02  6.54E-02  6.10E-02
       5.59E-02  5.00E-02  4.34E-02  3.64E-02  2.90E-02
       2.16E-02  1.45E-02  8.20E-03  3.29E-03  5.83E-04
c ------ Specific source cells with equal distribution -------
c  L = List, equal probability (1) each cell (organ) listed
c  source cell < lattice universe < universe box that contains lattice
c   using SDEF HELPER
c *************************SDEF Helper output here**************************
si5 l  (4<996[0 0 0]<997)
     (4<996[1 0 0]<997)
     (4<996[2 0 0]<997)
...
...
...
     (4<996[187 173 402]<997)
     (4<996[188 173 402]<997)
     (4<996[189 173 402]<997)
sp5 1 49264450r
c --------------------------------------------------------------------------
c ---------------------------- TALLY -----------------------------------------
```

```
mode p e                            $ use a for alpha
nps 100000000                       $ **Particle cutoff: 10^8
lost 10
c dbcn 12J 5444034                  $ more random #'s
 *f8:p,e u=(1 2 3 4) $ all universes
 *f18:p,e u=(1)      $ roots
 *f28:p,e u=(2)      $ shoots
 *f38:p,e u=(3)      $ surrounding air
 *f48:p,e u=(4)      $ HP solution
 *f58:p,e u=(1 2)    $ WHOLE PLANT
E0 0 1E-5 5.0        $ Energy bins
c
PRINT 110
PRDMP 1E7
c
c +++++++++++++++++++++++++++++++++++++++++++++++++++++++++
c
c     Materials
c
c +++++++++++++++++++++++++++++++++++++++++++++++++++++++++
c
c Root
c Plant Tissue - PNNL (#359 Wood (Southern Pine)) by mass fraction
c     p = 0.64 g/cm^3 (PNNL, for wood) (1.03 experimental)
m1    1000  -0.060   $ H
      6000  -0.497   $ C
      7000  -0.005   $ N
      8000  -0.427   $ O
     12000  -0.002   $ Mg
     16000  -0.005   $ S
     19000  -0.002   $ K
     20000  -0.002   $ Ca
c
c Shoot
c Plant Tissue - PNNL (#359 Wood (Southern Pine)) by mass fraction
c     p = 0.64 g/cm^3 (PNNL, for wood) (1.03 experimental)
m2    1000  -0.060   $ H
      6000  -0.497   $ C
      7000  -0.005   $ N
      8000  -0.427   $ O
     12000  -0.002   $ Mg
     16000  -0.005   $ S
     19000  -0.002   $ K
     20000  -0.002   $ Ca
c
c Default Surrounding Air
m3    7000  -0.755   $ N
      8000  -0.232   $ O
     18000  -0.013   $ Ar
c
c Water
m4   1000  -0.11190  $ H
     8000  -0.88810  $ O
c
c Flask: Borosilicate Glass (Pyrex) - PNNL by mass fraction, p = 2.23 g/cm^3
c m9    5000  -0.040   $ B
c       8000  -0.540   $ O
c      11000  -0.028   $ Na
c      13000  -0.012   $ Al
c      14000  -0.377   $ Si
c      19000  -0.003   $ K
c
```

C.3.2: CF 2 (for Roots, Shoots, or Roots+Shoots as source)

```
...
...
...
c compression factor: 2
...
...
...
c -------------------Lattice Unit Cell-------------------
c ____________________________________________________________________________
c ID#|Mat#|Density |Defn:  |Lattice|Define  |Imp|Fill: long list of
c    |    |  n/a   | in    | Type  |Universe|   | universes in specified
c    |    |if 0 mat|"house"|       |        |   | x,y,z grid
c ----------------------------------------------------------------------------
  996  0            -2      lat = 1 u = 996  imp:n=0 imp:p,e=1
                   fill = 0:699  0:699 0:920
     4 10115534r 1 2r 4 696r 1 4r 4 693r 1 6r 4 692r 1 6r 4 692r 1
     6r 4 693r 1 4r 4 486494r 1 2r 4 695r 1 5r 4 693r 1 6r 4 692r 1
     6r 4 692r 1 5r 4 694r 1 3r 4 485795r 1 1r 4 696r 1 4r 4 693r 1
...
...
...
     698r 2 1r 3 697r 2 1r 3 697r 2 2r 3 697r 2 1r 3 697r 2 1r 3
     697r 2 2r 3 697r 2 1r 3 697r 2 1r 3 697r 2 1r 3 697r 2 1r 3
     698r 2 1r 3 697r 2 1r 3 698r 2 3
     5928751r
c
...
...
...
c ----------------Box for Filling Universes-------------------------------------
c This information comes from Image-->Image Information in 3D doctor
c   or from "File->Modify Window" and "calibration" for pixel sizes
c   namely: # columns, # rows, # planes, pixel width, and slice thickness
c Note that pixel width and slice thickness are given in mm in 3D doctor
c     but need to be in cm for Voxelizer and MCNP
c
c In our case, # columns = 1400, # rows = 1400, planes (slices) = 921
c   Pixel width = 0.005 cm, slice thickness = 0.025 cm
c   For compression factor = 2, then # columns = 1400 / 2 = 700
c                                    # rows = 1400 / 2 = 700
c   0.005(2)=0.010; 700(0.005)(2)=7.000; 921(0.025)=23.025
c
c
c  RPP 1: Dimensions of "house" in which to build the lattice
c  RPP 2: Dimensions for "brick" in which each voxel is placed
c
  1  rpp        0.000     7.000     0.000     7.000     0.000     23.025
  2  rpp        0.000     0.010     0.000     0.010     0.000     0.025
c ============================================================================
...
...
...
c ------------------ Sampling boundary from 2 RPP above ----------------------
si1 h 0.0    0.010       $ range of X
sp1 d 0      1
si2 h 0.0    0.010       $ range of Y
sp2 d 0      1
si3 h 0.0    0.025      $ range of Z
sp3 d 0      1
```

C.3.3: Roots as source

```
c ------ Specific source cells with equal distribution -------
c  L = List, equal probability (1) each cell (organ) listed
c  source cell < lattice universe < universe box that contains lattice
c   using SDEF HELPER
c *************************SDEF Helper output here**************************
si5 l  (1<996[535 450 20]<997)
     (1<996[536 450 20]<997)
     (1<996[537 450 20]<997)
...
...
...
     (1<996[341 400 401]<997)
     (1<996[342 400 401]<997)
     (1<996[343 400 401]<997)
sp5 1 165404r
c ------------------------------------------------------------------------------
```

C.3.4: Shoots as source

```
c ------ Specific source cells with equal distribution -------
c  L = List, equal probability (1) each cell (organ) listed
c  source cell < lattice universe < universe box that contains lattice
c   using SDEF HELPER
c *************************SDEF Helper output here**************************
si5 l  (2<996[382 345 402]<997)
     (2<996[383 345 402]<997)
     (2<996[384 345 402]<997)
...
...
...
     (2<996[246 629 908]<997)
     (2<996[247 629 908]<997)
     (2<996[247 630 908]<997)
sp5 1 150181r
c ------------------------------------------------------------------------------
```

C.3.5: Roots+Shoots as source

```
c ------ Specific source cells with equal distribution -------
c  L = List, equal probability (1) each cell (organ) listed
c  source cell < lattice universe < universe box that contains lattice
c   using SDEF HELPER
c *************************SDEF Helper output here**************************
si5 l  (1<996[535 450 20]<997)
     (1<996[536 450 20]<997)
     (1<996[537 450 20]<997)
...
...
...
     (2<996[246 629 908]<997)
     (2<996[247 629 908]<997)
     (2<996[247 630 908]<997)
sp5 1 165404r
    1 150181r
c ------------------------------------------------------------------------------
```

C.3.6: ^{137}Cs Beta spectra

```
c ------------------ Energy definition ----------------------
si4 A  2.94E-02  8.80E-02  1.47E-01  2.05E-01  2.64E-01  $Cs-137 Beta spectra
       3.23E-01  3.81E-01  4.40E-01  4.99E-01  5.57E-01
       6.16E-01  6.75E-01  7.33E-01  7.92E-01  8.51E-01
       9.09E-01  9.68E-01  1.03E+00  1.09E+00  1.14E+00
sp4    1.93E-01  1.76E-01  1.61E-01  1.43E-01  1.22E-01
       9.38E-02  6.01E-02  2.64E-02  5.70E-03  3.30E-03
       3.07E-03  2.82E-03  2.53E-03  2.20E-03  1.83E-03
       1.42E-03  9.92E-04  5.91E-04  2.45E-04  5.38E-05
c ---------------------------------------------------------------------------
```

C.3.7: ^{137}Cs Gamma energy

```
c ------------------------ SOURCE DEFININION --------------------------------
...
...
...
     par=2             $ electron (3), gamma (2), alpha (34)
...
...
...
c ------------------ Energy definition ----------------------
c ***discrete photon energies for I>1%
si4 L  6.617E-01                                          $Cs-137 photons
sp4    8.510E-01
c ---------------------------------------------------------------------------
```

C.3.8: ^{237}Np Alpha energies

```
c +++++++++++++++++++++++++++++++++++++++++++++++++++++++++++++
c
c     Cells
c
c +++++++++++++++++++++++++++++++++++++++++++++++++++++++++++++
...
...
...
   999    0                     999           imp:n,p,e,a=0        $ outside
   998    3        -0.001205   -999  1 #997   imp:n=0 imp:p,e,a=1  $ air
c
c ------------------Filling Universes--------------------
c _____________________________________________________
c Cell#|Mat#|Density|Defn:   | Define |Importance
c      |    |       |in void |Universe|
c      |    |       |"mortar"|        |
c -----------------------------------------------------
    1     1  -1.03       -2    u = 1     imp:n=0 imp:p,e,a=1   $Root
    2     2  -1.03       -2    u = 2     imp:n=0 imp:p,e,a=1   $Shoot
    3     3  -0.001205   -2    u = 3     imp:n=0 imp:p,e,a=1   $Default Air
    4     4  -1.00       -2    u = 4     imp:n=0 imp:p,e,a=1   $HP soln @roots
c
c ------------------Lattice Unit Cell-------------------
c ____________________________________________________________________________
c ID#|Mat#|Density |Defn:  |Lattice|Define  |Imp|Fill: long list of
c    |    |  n/a   | in    | Type  |Universe|   | universes in specified
c    |    |if 0 mat|"house"|       |        |   | x,y,z grid
c ----------------------------------------------------------------------------
c
    996   0   -2   lat = 1   u = 996   imp:n=0 imp:p,e,a=1
...
```

```
...
...
c ------------- Cell Containing Lattice -----------------
c _____________________________________________________
c ID#|Mat#|Density|Defn:  |Fill with|Importance
c    |    |       | in    | lattice |
c    |    |       |"house"|i.e. 996 |
c -------------------------------------------------------
    997    0     -1   fill = 996  imp:n=0 imp:p,e,a=1
c
c ===========================================================================
...
...
...
c ------------------------ SOURCE DEFININION -------------------------------
...
...
...
     par=34            $ electron (3), gamma (2), alpha (34)
...
...
...
c ------------------ Energy definition ----------------------
c ***discrete alpha energies
si4 L  4.5151    4.5730    4.5786    4.5949    4.5991     $Np-237 alphas
       4.6197    4.6400    4.6591    4.6650    4.6982
       4.7083    4.7123    4.7413    4.7665    4.7714
       4.7880    4.8035    4.8168    4.8664    4.8727
sp4    3.50E-04  4.80E-04  3.69E-03  8.50E-04  3.71E-03
       3.20E-04  6.43E-02  3.00E-03  3.48E-02  5.35E-03
       6.00E-03  6.00E-03  1.90E-04  9.30E-02  2.32E-01
       4.76E-01  2.01E-02  2.43E-02  5.30E-03  2.39E-02
...
...
...
c ---------------------------- TALLY ------------------------------------------
mode p e a                          $ use a for alpha
nps 100000000                       $ **Particle cutoff: 10^8
lost 10
c dbcn 12J 5444034                  $ more random #'s
 *f8:p,e,a u=(1 2 3 4) $ all universes
 *f18:p,e,a u=(1)      $ roots
 *f28:p,e,a u=(2)      $ shoots
 *f38:p,e,a u=(3)      $ surrounding air
 *f48:p,e,a u=(4)      $ HP solution
 *f58:p,e,a u=(1 2)    $ WHOLE PLANT
```

C.3.9: ^{238}U Alpha energies

```
c +++++++++++++++++++++++++++++++++++++++++++++++++++++++++++++++
c
c     Cells
c
c +++++++++++++++++++++++++++++++++++++++++++++++++++++++++++++++
...
...
...
c -------------------------------------------------------
   999    0                     999           imp:n,p,e,a=0        $ outside
   998    3        -0.001205   -999  1 #997   imp:n=0 imp:p,e,a=1  $ air
c
c ------------------Filling Universes--------------------
c _____________________________________________________
c Cell#|Mat#|Density|Defn:    | Define |Importance
```

```
c      |    |       |in void |Universe|
c      |    |       |"mortar"|        |
c ------------------------------------------------------
    1     1  -1.03       -2    u = 1     imp:n=0 imp:p,e,a=1    $Root
    2     2  -1.03       -2    u = 2     imp:n=0 imp:p,e,a=1    $Shoot
    3     3  -0.001205   -2    u = 3     imp:n=0 imp:p,e,a=1    $Default Air
    4     4  -1.00       -2    u = 4     imp:n=0 imp:p,e,a=1    $HP soln @root
c
c -------------------Lattice Unit Cell-------------------
c ____________________________________________________________________________
c ID#|Mat#|Density |Defn:  |Lattice|Define  |Imp|Fill: long list of
c    |    |  n/a   | in    | Type  |Universe|   | universes in specified
c    |    |if 0 mat|"house"|       |        |   | x,y,z grid
c ----------------------------------------------------------------------------
c
    996    0   -2    lat = 1   u = 996   imp:n=0 imp:p,e,a=1
...
...
...
c ------------- Cell Containing Lattice -----------------
c ____________________________________________________
c ID#|Mat#|Density|Defn:  |Fill with|Importance
c    |    |       | in    | lattice |
c    |    |       |"house"|i.e. 996 |
c ----------------------------------------------------
    997    0     -1   fill = 996   imp:n=0 imp:p,e,a=1
c
c ============================================================================
...
...
...
c ------------------------ SOURCE DEFININION --------------------------------
...
...
     par=34            $ electron (3), gamma (2), alpha (34)
...
...
...
c ------------------ Energy definition ----------------------
c ***discrete alpha energies
si4 L  4.038     4.151     4.198                          $U-238 alphas
sp4    7.80E-04  2.10E-01  7.90E-01
...
...
...
c ----------------------------------------------------------------------------
c ---------------------------- TALLY -----------------------------------------
mode p e a                          $ use a for alpha
nps 100000000                       $ **Particle cutoff: 10^8
lost 10
c dbcn 12J 5444034                  $ more random #'s
 *f8:p,e,a u=(1 2 3 4) $ all universes
 *f18:p,e,a u=(1)      $ roots
 *f28:p,e,a u=(2)      $ shoots
 *f38:p,e,a u=(3)      $ surrounding air
 *f48:p,e,a u=(4)      $ HP solution
 *f58:p,e,a u=(1 2)    $ WHOLE PLANT
```

REFERENCES

Adriano, D.C., Doswell, A.C., Ciravolo, T.G., Pinder, J.E., McLeod, K.W., 2000. Radionuclide content of selected root vegetables as influenced by culinary preparation. J. Environ. Radioact. 49, 307–317. https://doi.org/10.1016/S0265-931X(99)00116-2

Al Mamun, A., Dogan, M., Powell, B.A., DeVol, T.A., Moysey, S., 2020. In-situ visualization of flow mechanisms in microporous soils using 4D X-ray computed tomography. Water Resour. Res. In Review.

Alliot, C., Pierre, V., Bion, L., Mercier, F., 2005. Effect of aqueous acetic, oxalic, and carbonic acids on the adsorption of uranium(VI) onto alpha-alumina. New J. Chem. 29, 1409–1415.

Almgren, S., Isaksson, M., 2006. Vertical migration studies of 137Cs from nuclear weapons fallout and the Chernobyl accident. J. Environ. Radioact. 91, 90–102. https://doi.org/10.1016/j.jenvrad.2006.08.008

Alonzo, F., Hertel-Aas, T., Real, A., Lance, E., Garcia-Sanchez, L., Bradshaw, C., Vives i Batlle, J., Oughton, D.H., Garnier-Laplace, J., 2016. Population modelling to compare chronic external radiotoxicity between individual and population endpoints in four taxonomic groups. J. Environ. Radioact. 152, 46–59. https://doi.org/10.1016/j.jenvrad.2015.11.001

Ambe, S., Ozaki, T., Enomoto, S., Shinonaga, T., 1999. Multitracer Study on the Soil-to-Plant Transfer of Radionuclides in Komatsuna at Different Growth Stages. Environ. Technol. 20, 111–116. https://doi.org/10.1080/09593332008616800

Ankley, G.T., Bennett, R.S., Erickson, R.J., Hoff, D.J., Hornung, M.W., Johnson, R.D., Mount, D.R., Nichols, J.W., Russom, C.L., Schmieder, P.K., Serrrano, J.A., Tietge, J.E., Villeneuve, D.L., 2010. Adverse outcome pathways: A conceptual framework to support ecotoxicology research and risk assessment. Environ. Toxicol. Chem. 29, 730–741. https://doi.org/10.1002/etc.34

Arai, Y., Moran, P.B., Honeyman, B.D., Davis, J.A., 2007. In Situ Spectroscopic Evidence for Neptunium (V)-Carbonate Inner-Sphere and Outer-Sphere Ternary Surface Complexes on Hematite Surfaces. Environ. Sci. Technol. 41, 3940–3944.

Ashworth, D.J., Shaw, G., 2006. A comparison of the soil migration and plant uptake of radioactive chlorine and iodine from contaminated groundwater. J. Environ. Radioact. 89, 61–80. https://doi.org/10.1016/j.jenvrad.2006.03.006

Ashworth, D.J., Shaw, G., 2005. Soil migration and plant uptake of technetium from a fluctuating water table. J. Environ. Radioact. 81, 155–171.

https://doi.org/10.1016/j.jenvrad.2004.01.033

Ashworth, D.J., Shaw, G., Butler, A.P., Ciciani, L., 2003. Soil transport and plant uptake of radio-iodine from near-surface groundwater. J. Environ. Radioact. 70, 99–114. https://doi.org/10.1016/S0265-931X(03)00121-8

ASTM, 2003. D4646-03. Standard Test Method for 24-h Batch-Type Measurement of Contaminant Sorption by Soils and Sediments. West Conshohocken, PA.

Bais, H.P., Vepachedu, R., Gilroy, S., Callaway, R.M., Vivanco, J.M., 2003. Allelopathy and Exotic Plant Invasion: From Molecules and Genes to Species Interactions. Science. 301, 1377–1380. https://doi.org/10.1126/science.1083245

Bargar, J.R., Reitmeyer, R., Lenhart, J.J., Davis, J.A., 2000. Characterization of U(VI)-carbonato ternary complexes on hematite: EXAFS and electrophoretic mobility measurements. Geochim. Cosmochim. Acta 64, 2737–2749. https://doi.org/10.1016/S0016-7037(00)00398-7

Bell, J.N.B., Minski, M.J., Grogan, H.A., 1988. Plant uptake of radionuclides. Soil Use Manag. 4, 76–84.

Bennett, R., Willey, N., 2003. Soil availability, plant uptake and soil to plant transfer of 99Tc - A review. J. Environ. Radioact. 65, 215–231. https://doi.org/10.1016/S0265-931X(02)00098-X

Beresford, N.A., Barnett, C.L., Howard, B.J., Scott, W.A., Brown, J.E., Copplestone, D., 2008. Derivation of transfer parameters for use within the ERICA Tool and the default concentration ratios for terrestrial biota. J. Environ. Radioact. 99, 1393–1407. https://doi.org/10.1016/j.jenvrad.2008.01.020

Biermans, G., Horemans, N., Hens, N., Vives i Batlle, J., Vandenhove, H., Cuypers, A., 2014a. A dynamic dosimetry model for radioactive exposure scenarios in Arabidopsis thaliana. J. Theor. Biol. 347, 54–62. https://doi.org/10.1016/j.jtbi.2014.01.012

Biermans, G., Horemans, N., Vanhoudt, N., Vandenhove, H., Saenen, E., Van Hees, M., Wannijn, J., Vives i Batlle, J., Cuypers, A., 2014b. An organ-based approach to dose calculation in the assessment of dose-dependent biological effects of ionising radiation in Arabidopsis thaliana. J. Environ. Radioact. 133, 24–30. https://doi.org/10.1016/j.jenvrad.2013.03.011

Bostick, B.C., Vairavamurthy, M. a., Karthikeyan, K.G., Chorover, J., 2002. Cesium adsorption on clay minerals: An EXAFS spectroscopic investigation. Environ. Sci. Technol. 36, 2670–2676. https://doi.org/10.1021/es0156892

Bradbury, M.H., Baeyens, B., 2000. A generalised sorption model for the concentration dependent uptake of caesium by argillaceous rocks. J. Contam. Hydrol. 42, 141–163.

Bradshaw, C., Kapustka, L., Barnthouse, L., Brown, J., Ciffroy, P., Forbes, V., Geras'kin, S., Kautsky, U., Bréchignac, F., 2014. Using an Ecosystem Approach to complement protection schemes based on organism-level endpoints. J. Environ. Radioact. 136, 98–104. https://doi.org/10.1016/j.jenvrad.2014.05.017

Bréchignac, F., Oughton, D., Mays, C., Barnthouse, L., Beasley, J.C., Bonisoli-Alquati, A., Bradshaw, C., Brown, J., Dray, S., Geras'kin, S., Glenn, T., Higley, K., Ishida, K., Kapustka, L., Kautsky, U., Kuhne, W., Lynch, M., Mappes, T., Mihok, S., Møller, A.P., Mothersill, C., Mousseau, T.A., Otaki, J., Pryakhin, E., Rhodes, O.E., Salbu, B., Strand, P., Tsukada, H., 2016. Addressing ecological effects of radiation on populations and ecosystems to improve protection of the environment against radiation: Agreed statements from a Consensus Symposium. J. Environ. Radioact. 158–159, 21–29. https://doi.org/10.1016/j.jenvrad.2016.03.021

Briat, J.-F., Lebrun, M., 1999. Plant responses to metal toxicity. Comptes Rendus l'Académie des Sci. - Ser. III - Sci. la Vie 322, 43–54. https://doi.org/10.1016/S0764-4469(99)80016-X

Broadley, M.R., Willey, N.J., 1997. Differences in root uptake of radiocaesium by 30 plant taxa. Environ. Pollut. 97, 11–15. https://doi.org/10.1016/S0269-7491(97)00090-0

Brouwer, E., Baeyens, B., Maes, A., Cremers, A., 1983. Cesium and rubidium ion equilibriums in illite clay. Jounal Phys. Chem. 87, 1213–1219. https://doi.org/10.1021/j100230a024

Brown, J.C., Jolley, V.D., Lytle, C.M., 1991. Comparative evaluation of iron solubilizing substances (phytosiderophores) released by oats and corn : Iron-efficient and iron-inefficient plants. Plant ans Soil 130, 157–163.

Brown, J.E., Alfonso, B., Avila, R., Beresford, N.A., Copplestone, D., Hosseini, A., 2016. A new version of the ERICA tool to facilitate impact assessments of radioactivity on wild plants and animals. J. Environ. Radioact. 153, 141–148. https://doi.org/10.1016/j.jenvrad.2015.12.011

Brown, J.E., Alfonso, B., Avila, R., Beresford, N.A., Copplestone, D., Pröhl, G., Ulanovsky, A., 2008. The ERICA Tool. J. Environ. Radioact. 99, 1371–1383. https://doi.org/10.1016/j.jenvrad.2008.01.008

Bunzl, K., Kracke, W., Schimmack, W., 1992. Vertical migration of plutonium-239 + -240, americium-241 and caesium-137 fallout in a forest soil under spruce. Analyst

117, 469–474. https://doi.org/10.1039/an9921700469

Burger, J., 2000. Integrating environmental restoration and ecological restoration: Long-term stewardship at the Department of Energy. Environ. Manage. 26, 469–478. https://doi.org/10.1007/s002670010105

Caffrey, E.A., Higley, K.A., 2013. Creation of a voxel phantom of the ICRP reference crab. J. Environ. Radioact. 120, 14–18. https://doi.org/10.1016/j.jenvrad.2013.01.006

Caffrey, E.A., Johansen, M.P., Higley, K.A., 2016. Voxel modeling of rabbits for use in radiological dose rate calculations. J. Environ. Radioact. 151, 480–486. https://doi.org/10.1016/j.jenvrad.2015.04.008

Campbell, C.S., 1983. Systematics of the Andropogon Virginicus Comples (Gramineae). J. Arnold Arbor. 64, 171–254.

Carlton, W.H., 1997. Assessment of Neptunium, Americium, and Curium in the Savannah River Site Environment. Aiken, SC: Westinghouse Savannah River Company ;WSRC-TR-97-00266.

Carlton, W.H., Bauer, L.R., Evans, A.G., Geary, L.A., Murphy, Jr, C.E., Pinder, J.E., Strom, R.N., 1992. Cesium in the Savannah River Site Environment. Aiken, SC: Westinghouse Savannah River Company; WSRC-RP-92-250.

Carlton, W.H., Denham, M.E., Evans, A.G., 1993. Assessment of Technetium in the Savannah River Site Environment. Aiken, SC: Westinghouse Savannah River Company; WSRC-TR-93-217.

Cataldo, D. a, Wildung, R.E., Garland, T.R., 1983. Root absorption and transport behavior of technetium in soybean. Plant Physiol. 73, 849–852. https://doi.org/10.1104/pp.73.3.849

Cataldo, D.A., Garland, T.R., Wildung, R.E., 1988. Absorption, distribution, and fate of neptunium in plants. J. Agric. Food Chem. 36, 657–662. https://doi.org/10.1021/jf00081a063

Choi, Y.H., Lee, C.W., Kim, S.R., Lee, J.H., Jo, J.S., 1998. Effect of application time of radionuclides on their root uptake by Chinese cabbage and radish. J. Environ. Radioact. 39, 183–198. https://doi.org/10.1016/S0265-931X(97)00052-0

Choppin, G.R., 2007. Actinide speciation in the environment. J. Radioanal. Nucl. Chem. 273, 695–703. https://doi.org/10.1007/s10967-007-0933-3

Clark, D.L., Hobart, D.E., Neu, M.P., 1995. Actinide Carbonate Complexes and Their

Importance in Actinide Environmental Chemistry. Chem. Rev. 95, 25–48. https://doi.org/10.1021/cr00033a002

Clemens, S., 2001. Molecular mechanisms of plant metal tolerance and homeostasis. Planta 212, 475–486. https://doi.org/10.1007/s004250000458

Comans, R.N.J., Hockley, D.E., 1992. Kinetics of Cesium Sorption on Illite. Geochim. Cosmochim. Acta 56, 1157–1164.

Condon, C.A., Higley, K.A., 2018. Sectional 3D Model Development for the reference tree in Sixty-Third Annual Meeting of The Health Physics Society. Health Phys. 115, S54.

Curie, C., Briat, J.-F., 2003. Iron Transport and Signaling in Plants. Annu. Rev. Plant Biol. 54, 183–206. https://doi.org/10.1146/annurev.arplant.54.031902.135018

Dakora, F.D., Phillips, D.A., 2002. Root exudates as mediators of mineral acquisition in low-nutrient environments. Plant Soil 245, 201–213.

DalCorso, G., 2012. Heavy Metal Toxicity in Plants, in: Furini, A. (Ed.), Plants and Heavy Metals, SpringerBriefs in Molecular Science. Springer, Dordrecht, pp. 1–25.

Degani, N., Pickholtz, D., 1980. Radiosensitivity of Different Tissues from Carrot Root at Different Phases of Growth in Culture. Radiat. Res. 83, 559–565.

Delany, J.M., Lundeeen, S.R., 1990. The LLNL thermochemical database; UCRL-21658. Livermore, CA.

Demirkanli, D.I., Molz, F.J., Kaplan, D.I., Fjeld, R.A., 2009. Soil–Root Interactions Controlling Upward Plutonium Transport in Variably Saturated Soils. Vadose Zo. J. 8, 574. https://doi.org/10.2136/vzj2008.0159

Demirkanli, D.I., Molz, F.J., Kaplan, D.I., Fjeld, R.A., Serkiz, S.M., 2007. Modeling Long-Term Plutonium Transport in the Savannah River Site Vadose Zone. Vadose Zo. J. 6, 344. https://doi.org/10.2136/vzj2006.0042

Dinelli, E., Lombini, A., 1996. Metal distributions in plants growing on copper mine spoils in Northern Apennines, Italy: The evaluation of seasonal variations. Appl. Geochemistry 11, 375–385. https://doi.org/10.1016/0883-2927(95)00071-2

Dixon, W.J., 1953. Processing Data for Outliers. Biometrics 9, 74–89.

Dogan, M., Moysey, S.M.J., Ramakers, R.M., DeVol, T.A., Beekman, F.J., Groen, H.C., Powell, B.A., 2017. High-resolution 4D pre-clinical SPECT/CT imaging of technetium transport within a heterogeneous porous media. Environ. Sci. Technol. 51, 2864–2870. https://doi.org/10.1021/acs.est.6b04172

Dong, W., Wan, J., 2014. Additive surface complexation modeling of uranium(VI) adsorption onto quartz-sand dominated sediments. Environ. Sci. Technol. 48, 6569–6577. https://doi.org/10.1021/es501782g

Duquène, L., Vandenhove, H., Tack, F., Van der Avoort, E., Van Hees, M., Wannijn, J., 2006. Plant-induced changes in soil chemistry do not explain differences in uranium transfer. J. Environ. Radioact. 90, 1–14. https://doi.org/10.1016/j.jenvrad.2006.06.001

Dushenkov, S., 2003. Trends in phytoremediation of radionuclides. Plant Soil 249, 167–175. https://doi.org/10.1023/A:1022527207359

Ebbs, S.D., Brady, D.J., Kochian, L. V, 1998. Role of uranium speciation in the uptake and translocation of uranium by plants. J. Exp. Bot. 49, 1183–1190. https://doi.org/10.1093/jxb/49.324.1183

Echevarria, G., Vong, P.C., Morel, J.L., 1998. Effect of NO3- on the fate of 99TcO4- in the soil-plant system. J. Environ. Radioact. 38, 163–171. https://doi.org/10.1016/S0265-931X(97)00032-5

Edayilam, N., Ferguson, B., Montgomery, D., Al Mamun, A., Martinez, N., Powell, B.A., Tharayil, N., 2020. Dissolution and Vertical Transport of Uranium from Stable Mineral Forms by Plants as Influenced by the Co-occurrence of Uranium with Phosphorus. Environ. Sci. Technol. 54, 6602–6609. https://doi.org/10.1021/acs.est.9b06559

Ehlken, S., Kirchner, G., 2002. Environmental processes affecting plant root uptake of radioactive trace elements and variability of transfer factor data: A review. J. Environ. Radioact. 58, 97–112. https://doi.org/10.1016/S0265-931X(01)00060-1

Ekvall, L., Greger, M., 2003. Effects of environmental biomass-producing factors on Cd uptake in two Sweedish ecotypes of Pinus sylvestris. Environ. Pollut. 121, 401–411.

EPA, 2007. Method 3051A: Microwave assisted acid digestion of sediments, sludges, soils, and oils.

EPA, 1996. Method 3050B: Acid Digestion of Sediments, Sludges, and Soils.

Evans, A.G., Bauer, L.R., Haselow, J.S., Hayes, D.W., Martin, H.L., McDowell, W.L., Pickett, J.B., 1992. Uranium in the Savannah River Site Environment. Aiken, SC: Westinghouse Savannah River Company; WSRC-RP--92-315.

Ezaki, B., Nagao, E., Yamamoto, Y., 2008. Wild plants , Andropogon virginicus L . and Miscanthus sinensis Anders , are tolerant to multiple stresses including aluminum , heavy metals and oxidative stresses. Plant Cell Rep 27, 951–961.

https://doi.org/10.1007/s00299-007-0503-8

Falta, R.W., Wang, W., 2017. A semi-analytical method for simulating matrix diffusion in numerical transport models. J. Contam. Hydrol. 197, 39–49. https://doi.org/10.1016/j.jconhyd.2016.12.007

Farrar, J., Hawes, M., Jones, D., Lindow, S., 2003. How Roots Control the Flux of Carbon to the Rhizosphere. Ecology 84, 827–837.

Favas, P.J.C., Pratas, J., Varun, M., D'Souza, R., Paul, M.S., 2014. Accumulation of uranium by aquatic plants in field conditions: Prospects for phytoremediation. Sci. Total Environ. 470–471, 993–1002. https://doi.org/10.1016/j.scitotenv.2013.10.067

Fein, J.B., B.A. Powell, 2013. Uranium adsorption: Speciation at mineral-water and bacterial cell-water interfaces, in: Burns, P.C., Sigmon, G.E. (Eds.), Uranium: Cradle to Grave. Mineralogical Association of Canada, Winniped, Manitoba.

Forbes, V.E., Galic, N., 2016. Next-generation ecological risk assessment: Predicting risk from molecular initiation to ecosystem service delivery. Environ. Int. 91, 215–219. https://doi.org/10.1016/j.envint.2016.03.002

Garland, T.R., Cataldo, D.A., Wildung, R.E., 1981. Absorption, transport, and chemical fate of plutonium in soybean plants. J. Agric. Food Chem. 29, 915–920.

Garnier-Laplace, J., Alonzo, F., Adam-Guillermin, C., 2015. Establishing relationships between environmental exposures to radionuclides and the consequences for wildlife: inferences and weight of evidence. Ann. ICRP 44, 295–303. https://doi.org/10.1177/0146645315572311

Garten, Jr, C.T., Tucker, C.S., Scott, T.G., 1986. Plant Uptake of Neptunium-237 and Technetium-99 Under Field Conditions. J. Environ. Radioact. 4, 91–99.

Gee, G.W., Bauder, J.W., 1996. Particle Size Analysis, in: Klute, A. (Ed.), Methods of Soil Analysis: Part 1 Physical Methods. Soil Science Society of America, Inc., Madison, WI, pp. 383–411.

Geras'kin, S.A., 2016. Ecological effects of exposure to enhanced levels of ionizing radiation. J. Environ. Radioact. 162–163, 347–357. https://doi.org/10.1016/j.jenvrad.2016.06.012

Geras'kin, S.A., Alexakhin, R.M., Oudalova, A.A., 2016. Effects of Ionizing Radiation on Populations and Ecosystems, in: Korogodina, V.L., Mothersill, C.E., Inge-Vechtomov, S.G., Seymour, C.B. (Eds.), Genetics, Evolution and Radiation: Crossing Borders, The Interdisciplinary Legacy of Nikolay W. Timofeeff-Ressovsky. Springer International Publishing, Cham, pp. 237–250.

https://doi.org/10.1007/978-3-319-48838-7_20

Giammar, D.E., Hering, J.G., 2001. Time scales for sorption - Desorption and surface precipitation of uranyl on goethite. Environ. Sci. Technol. 35, 3332–3337. https://doi.org/10.1021/es0019981

Girvin, D.C., Ames, L.L., Schwab, A.P., McGarrah, J.E., 1991. Neptunium Adsorption on Synthetic Amorphous Iron Oxyhydroxide. J. Colloid Interface Sci. 141, 67–78.

Gómez-Ros, J.M., Pröhl, G., Ulanovsky, A., Lis, M., 2008. Uncertainties of internal dose assessment for animals and plants due to non-homogeneously distributed radionuclides. J. Environ. Radioact. 99, 1449–1455. https://doi.org/10.1016/j.jenvrad.2008.01.005

Goorley, T., James, M., Booth, T., Brown, F., Bull, J., Cox, L.J., Durkee, J., Elson, J., Fensin, M., Forster, R.A., Hendricks, J., Hughes, H.G., Johns, R., Kiedrowski, B., Martz, R., Mashnik, S., McKinney, G., Pelowitz, D., Prael, R., Sweezy, J., Waters, L., Wilcox, T., Zukaitis, T., 2012. Initial MCNP6 Release Overview. Nucl. Technol. 180, 298–315. https://doi.org/10.13182/nt11-135

Goto, M., Rosson, R., Elliott, W.C., Wampler, J.M., Serkiz, S., Kahn, B., 2014. Interactions of radioactive and stable cesium with hydroxy-interlayered vermiculite grains in soils of the Savannah River site, South Carolina, USA. Clays Clay Miner. 62, 161–173. https://doi.org/10.1346/CCMN.2014.0620301

Goto, M., Rosson, R., Wampler, J.M., Elliot, W.C., Serkiz, S., Kahn, B., 2008. Freundlich and Dual Langmuir Isotherm Models for Predicting 137Cs Binding on Savannah River Site Soils. Health Phys. 94, 18–32.

Greger, M., 2004. Uptake of nuclides by plants. Stockholm, Sweden: SKB, Swedish Nuclear Fuel and Waste Management Co; Technical Report TR-04-14.

Hattink, J., De Goeij, J.J.M., Wolterbeek, H.T., 2000. Uptake kinetics of 99Tc in common duckweed. Environ. Exp. Bot. 44, 9–22. https://doi.org/10.1016/S0098-8472(00)00045-9

Hinton, T.G., Garnier-laplace, J., Vandenhove, H., Dowdall, M., Adam-Guillermin, C., Alonzo, F., Barnett, C., Beaugelin-Seiller, K., Beresford, N.A., Bradshaw, C., Brown, J., Eyrolle, F., Fevrier, L., Gariel, J.-C., Gilbin, R., Hertel-Aas, T., Horemans, N., Howard, B.J., Ikäheimonen, T., Mora, J.C., Oughton, D., Real, A., Salbu, B., Simon-Cornu, M., Steiner, M., Sweeck, L., Vives i Batlle, J., 2013. An invitation to contribute to a strategic research agenda in radioecology. J. Environ. Radioact. 115, 73–82. https://doi.org/10.1016/j.jenvrad.2012.07.011

Hoagland, D.R., Arnon, D.I., 1950. The Water-Culture Method for Growing Plants

without Soil. Calif. Agric. Exp. Station. Circ. 347.

Huang, J.W., Blaylock, M.J., Kapulnik, Y., Ensley, B.D., 1998. Phytoremediation of uranium-contaminated soils: Role of organic acids in triggering uranium hyperaccumulation in plants. Environ. Sci. Technol. 32, 2004–2008. https://doi.org/10.1021/es971027u

IAEA, 2014. Handbook of Parameter Values for the Prediction of Radionuclide Transfer to Wildlife. IAEA TRS 479. Vienna.

IAEA, 2010. Handbook of Parameter Values for the Prediction of Radionuclide Transfer in Terrestrial and Freshwater Environments. IAEA TRS 472. Vienna.

Icenhower, J.P., Qafoku, N.P., Zachara, J.M., Martin, W.J., 2010. The biogeochemistry of technetium: A review of the behavior of an artificial element in the natural environment. Am. J. Sci. 310, 721–752. https://doi.org/10.2475/08.2010.02

ICRP, 2017. Dose Coefficients for Non-human Biota Environmentally Exposed to Radiation. ICRP Publication 136. Ann. ICRP 46(2).

ICRP, 2016. The ICRP computational framework for internal dose assessment for reference adults: specific absorbed fractions. ICRP Publication 133. Ann. ICRP 45(2), 1–74.

ICRP, 2014. Protection of the environment under different exposure situations. ICRP Publication 124. Ann. ICRP 43(1), 1–58. https://doi.org/10.1177/0146645313497456

ICRP, 2009a. Environmental Protection: Transfer Parameters for Reference Animals and Plants. ICRP Publication 114. Ann. ICRP 39(6).

ICRP, 2009b. Adult Reference Computational Phantoms. ICRP Publication 110. Ann. ICRP 39(2).

ICRP, 2008. Environmental Protection: the Concept and Use of Reference Animals and Plants. ICRP Publication 108. Ann. ICRP 38(4–6). https://doi.org/10.1016/j.icrp.2009.04.001

ICRP, 2007. The 2007 Recommendations of the International Commission on Radiological Protection. ICRP Publication 103. Ann. ICRP 37(2–4). https://doi.org/10.1016/j.icrp.2006.06.001

ICRP, 2003. A Framework for Assessing the Impact of Ionising Radiation on Non-human Species. ICRP Publication 91. Ann. ICRP 33(3). https://doi.org/10.1016/j.icrp.2004.12.002

ICRP, 1977. Recommendations of the International Commission on Radiological Protection. ICRP Publication 26. Ann. ICRP 1(3), 1–53.

Jackson, D., Smith, K., Wood, M.D., 2014. Demonstrating compliance with protection objectives for non-human biota within post-closure safety cases for radioactive waste repositories. J. Environ. Radioact. 133, 60–68. https://doi.org/10.1016/j.jenvrad.2013.07.005

Jantzen, C.M., Kaplan, D.I., Bibler, N.E., Peeler, D.K., John Plodinec, M., 2008. Performance of a buried radioactive high level waste (HLW) glass after 24 years. J. Nucl. Mater. 378, 244–256. https://doi.org/10.1016/j.jnucmat.2008.06.040

Jones, D.L., Darrah, P.R., 1994. Role of root derived organic acids in the mobilization of nutrients from the rhizosphere. Plant Soil 166, 247–257.

Jones, D.L., Darrah, P.R., Kochian, L. V., 1996. Critical evaluation of organic acid mediated iron dissolution in the rhizosphere and its potential role in root iron uptake. Plant Soil 180, 57–66.

Kantar, C., Honeyman, B.D., 2006. Citric acid enhanced remediation of soils contaminated with uranium by soil flushing and soil washing. J. Environ. Eng. 132, 247–255. https://doi.org/Doi 10.1061/(Asce)0733-9372(2006)132:2(247)

Kaplan, D.I., 2009. Geochemical Data Package for Performance Assessment Calculations Related to the Savannah River Site, SRNL-STI-2009-00473. Energy.

Kaplan, D.I., Demirkanli, D.I., Molz, F.J., Beals, D.M., Cadieux, J.R., Halverson, J.E., 2010. Upward movement of plutonium to surface sediments during an 11-year field study. J. Environ. Radioact. 101, 338–344. https://doi.org/10.1016/j.jenvrad.2010.01.007

Kaplan, D.I., Miller, T.J., Diprete, D., Powell, B.A., 2014. Long-term radiostrontium interactions and transport through sediment. Environ. Sci. Technol. 48, 8919–8925. https://doi.org/10.1021/es5021108

Kaplan, D.I., Roberts, K., Shine, G., Grogan, K., Fjeld, R., Seman, J., 2008. The Range and Distribution of Technetium Kd Values in the SRS Subsurface Environment, SRNA-STI-2008-00286, Rev. 1. Aiken, SC.

Kashparov, V., Yoschenko, V., Levchuk, S., Bugai, D., Van Meir, N., Simonucci, C., Martin-Garin, A., 2012. Radionuclide migration in the experimental polygon of the Red Forest waste site in the Chernobyl zone - Part 1: Characterization of the waste trench, fuel particle transformation processes in soils, biogenic fluxes and effects on biota. Appl. Geochemistry 27, 1348–1358. https://doi.org/10.1016/j.apgeochem.2011.11.004

Kaszuba, J.P., Runde, W.H., 1999. The aqueous geochemistry of neptunium: Dynamic control of soluble concentrations with applications to nuclear waste disposal. Environ. Sci. Technol. 33, 4427–4433. https://doi.org/10.1021/es990470x

Kim, C.H., Yeom, Y.S., Nguyen, T.T., Choi, M.C., C., H., Lee, H., Han, H., Shin, B., Lee, J.-K., Kim, H.S., Zankl, M., Petoussi-Henss, N., Bolch, W.E., Lee, C., Chung, B.S., Qiu, R., Eckerman, K., 2018. New mesh-type phantoms and their dosimetric applications, including emergencies, in: Proceedings of the Fourth International Symposium on the System of Radiological Protection. Ann. ICRP 47(3/4). pp. 45–62.

Kinase, S., 2008. Voxel-based frog phantom for internal dose evaluation. J. Nucl. Sci. Technol. 45, 1049–1052. https://doi.org/10.1080/18811248.2008.9711891

Kohler, M., Curtis, G.P., Meece, D.E., Davis, J.A., 2004. Methods for estimating adsorbed uranium (VI) and distribution coefficients of contaminated sediments. Environ. Sci. Technol. 38, 240–247.

Kohler, M., Honeyman, B.D., Leckie, J.O., 1999. Npetunium(V) Sorption on Hematite (alpha-Fe2O3) in Aqueous Suspension : The Effect of CO2. Radiochim. Acta 85, 33–48.

Kramer, G.H., Capello, K., Chiang, A., Cardenas-Mendez, E., Sabourin, T., 2010. Tools for creating and manipulating voxel phantoms. Health Phys. 98, 542–548. https://doi.org/10.1097/HP.0b013e3181c34ced

Kramer, G.H., Capello, K., Strocchi, S., Bearrs, B., Leung, K., Martinez, N., 2012. The HML's New Voxel Phantoms. Health Phys. 103, 802–807. https://doi.org/10.1109/KIMAS.2007.369836

Kryshev, A.I., Sazykina, T.G., 2015. Modelling the effects of ionizing radiation on survival of animal population: acute versus chronic exposure. Radiat. Environ. Biophys. 54, 103–109. https://doi.org/10.1007/s00411-014-0578-x

Laurette, J., Larue, C., Mariet, C., Brisset, F., Khodja, H., Bourguignon, J., Carriere, M., 2012. Influence of uranium speciation on its accumulation and translocation in three plant species: Oilseed rape, sunflower and wheat. Environ. Exp. Bot. 77, 96–107. https://doi.org/10.1016/j.envexpbot.2011.11.007

Law, G.T.W., Geissler, A., Lloyd, J.R., Livens, F.R., Boothman, C., Begg, J.D.C., Denecke, M.A., Rothe, J., Dardenne, K., Burke, I.T., Charnock, J.M., Morris, K., 2010. Geomicrobiological redox cycling of the transuranic element neptunium. Environ. Sci. Technol. 44, 8924–8929. https://doi.org/10.1021/es101911v

Lenhart, J.J., Honeyman, B.D., 1999. Uranium(VI) sorption to hematite in the presence

of humic acid. Geochim. Cosmochim. Acta 63, 2891–2901. https://doi.org/10.1016/S0016-7037(99)00269-0

Li, W., Tao, Z., 2003. Comparative study on Np (V) sorption on oxides of aluminum and silicon: effects of humic substance and carbonate in solution. J. Colloid Interface Sci. 267, 25–31. https://doi.org/10.1016/S0021-9797(03)00735-5

Lindsay, W.L., Schwab, A.P., 1982. The chemistry of iron in soils and its availability to plants. J. Plant Nutr. 5, 821–840. https://doi.org/10.1080/01904168209363012

Liu, J., Pearce, C.I., Qafoku, O., Arenholz, E., Heald, S.M., Rosso, K.M., 2012. Tc (VII) reduction kinetics by titanomagnetite (Fe3-xTixO4) nanoparticles. Geochim. Cosmochim. Acta 92, 67–81. https://doi.org/10.1016/j.gca.2012.06.004

Loeppert, R.L., Inskeep, W.P., 1996. Iron, in: Sparks, D.L. (Ed.), Methods of Soil Analysis: Part 3 Chemical Methods. Soil Science Society of America, Inc., Madison, WI, pp. 639–664.

Loevinger, R., Budinger, T.F., Watson, E.E., 1991. MIRD Primer for Absorbed Dose Calculations: Revised Edition.

Lozano, J.C., Blanco Rodriguez, P., Vera Tome, F., Prieto Calvo, C., 2011. Enhancing uranium solubilization in soils by citrate, EDTA, and EDDS chelating amendments. J. Hazard. Mater. 198, 224–231. https://doi.org/10.1016/j.jhazmat.2011.10.026

Maher, K., Bargar, J.R., Brown, G.E., 2012. Environmental Speciation of Actinides. Inorg. Chem. 52, 3510–3532.

Manara, A., 2012. Plant Responses to Heavy Metal Toxicity, in: Furini, A. (Ed.), Plants and Heavy Metals. SpringerBriefs in Molecular Science. Springer, Dordrecht, pp. 27–53.

Martinez, N.E., 2015. Review of current methods in internal dosimetry of non-human biota, in: 15th International High-Level Radioactive Waste Management Conference. Charleston, SC, pp. 848–854.

Martinez, N.E., Johnson, T.E., Capello, K., Pinder, J.E., 2014a. Development and comparison of computational models for estimation of absorbed organ radiation dose in rainbow trout (Oncorhynchus mykiss) from uptake of iodine-131. J. Environ. Radioact. 138, 50–59. https://doi.org/10.1016/j.jenvrad.2014.08.001

Martinez, N.E., Johnson, T.E., Pinder, J.E., 2016. Application of computational models to estimate organ radiation dose in rainbow trout from uptake of molybdenum-99 with comparison to iodine-131. J. Environ. Radioact. 151, 468–479. https://doi.org/10.1016/j.jenvrad.2015.05.021

Martinez, N.E., Johnson, T.E., Pinder, J.E., 2014b. Influence of Lake Trophic Structure on Iodine-131 Accumulation and Subsequent Cumulative Radiation Dose to Trout Thyroids. J. Environ. Radioact. 131, 62–71. https://doi.org/10.1016/j.jenvrad.2013.10.015

Matisoff, G., Ketterer, M.E., Rosén, K., Mietelski, J.W., Vitko, L.F., Persson, H., Lokas, E., 2011. Downward migration of Chernobyl-derived radionuclides in soils in Poland and Sweden. Appl. Geochemistry 26, 105–115. https://doi.org/10.1016/j.apgeochem.2010.11.007

McConn Jr., R.J., Gesh, C.J., Pagh, R.T., Rucker, R.A., Williams III, R.G., 2011. Compendium of material composition data for radiation transport modeling, PNNL-15870 Rev.1. https://doi.org/10.2172/1023125

Miller, T.J., 2010. Thesis: Conceptual Model Testing and Development for Neptunium and Radium Sorption. Clemson University, Clemson, SC.

Montgomery, D., Barber, K., Edayilam, N., Oqujiuba, K., Young, S., Biotidara, T., Gathers, A., Danjaji, M., Tharayil, N., Martinez, N., Powell, B., 2017. The influence of citrate and oxalate on 99Tc(VII), Cs, Np(V) and U(VI) sorption to a Savannah River Site soil. J. Environ. Radioact. 172, 130–142. https://doi.org/10.1016/j.jenvrad.2017.03.017

Montgomery, D.A., Edayilam, N., Tharayil, N., Powell, B.A., Martinez, N.E., 2018. The Uptake and Translocation of 99Tc, 133Cs, 237Np, and 238U into Andropogon Virginicus with Consideration of Plant Life Stage. Health Phys. 115, 550–560. https://doi.org/10.1097/HP.0000000000000848

Montgomery, D.A., Paloni, J., Martinez, N.E., 2016. Waterfowl-specific Computational Models for use in Internal Dosimetry, in: Proceedings of the 14th International Congress of the International Radiation Protection Association. pp. 1174–1181.

Morss, L.R., Edelstein, N.M., Fuger, J. (Eds.), 2010. The Chemistry of the Actinide and Transactinide Elements, 4th ed. Springer.

Mothersill, C., Abend, M., Bréchignac, F., Iliakis, G., Impens, N., Kadhim, M., Møller, A.P., Oughton, D., Powathil, G., Saenen, E., Seymour, C., Sutcliffe, J., Tang, F.R., Schofield, P.N., 2018. When a duck is not a duck; a new interdisciplinary synthesis for environmental radiation protection. Environ. Res. 162, 318–324. https://doi.org/10.1016/j.envres.2018.01.022

Murphy, R.J., Lenhart, J.J., Honeyman, B.D., 1999. The sorption of thorium (IV) and uranium (VI) to hematite in the presence of natural organic matter. Colloids Surfaces A Physicochem. Eng. Asp. 157, 47–62. https://doi.org/10.1016/S0927-7757(99)00115-6

Napier, B.A., Fellows, R.J., Krupka, K.M., 2007. Soil-to-Plant Concentration Ratios for Assessing Food-Chain Pathways in Biosphere Models. PNNL-16741. Richland, WA.

Nascimento, C.W.A. do, Xing, B., 2006. Phytoextraction: a review on enhanced metal availability and plant accumulation. Sci. Agric. 63, 299–311. https://doi.org/10.1590/S0103-90162006000300014

NCRP, (National Council on Radaion Protection and Measurements), 2006. Cesium-137 in the environment: radioecology and approaches to assessment and management. NCRP Report No. 154. Bethesda, MD.

Nelson, D.W., Sommers, L.E., 1996. Total carbon, organic carbon, and organic matter, in: Sparks, D.L. (Ed.), Methods of Soil Analysis: Part 3 Chemical Methods1. Soil Science Society of America, Inc., Madison, WI, pp. 961–1010.

Neville, D., 2019. Faster, Sharper and Open: A New Pipeline for Biota Phantom Creation. Oregon State University.

Nisbet, A.F., Shaw, S., 1994. Summary of a 5-Year Lysimeter Study on the Time-Dependent Transfer of Cs-137, Sr-90, Pu-239, Pu-240 and Am-241 to Crops from 3 Contrasting Soil Types .2. Distribution between Different Plant-Parts. J. Environ. Radioact. 23, 171–187. https://doi.org/Doi 10.1016/0265-931x(94)90059-0

Osawa, H., Kojima, K., 2006. Citrate-release-mediated aluminum resistance is coupled to the inducible expression of mitochondrial citrate synthase gene in Paraserianthes falcataria. Tree Physiol. 26, 565–574.

Padilla, L., Lee, C., Milner, R., Shahlaee, A., Bolch, W.E., 2008. Canine Anatomic Phantom for Preclinical Dosimetry in Internal Emitter Therapy. J. Nucl. Med. 49, 446–452. https://doi.org/10.2967/jnumed.107.046722

Parks, G.A., 1990. Surface Energy and Adsorption at Mineral/Water Interfaces: an Introduction, in: Hochella Jr, M.F., White, A.F. (Eds.), Reviews in Mineralogy, Volume 23, Mineral-Water Interface Geochemistry. Mineralogical Society of America, pp. 133–175. https://doi.org/0-939950-28-6

Payne, T.E., Lumpkin, G.R., Waite, T.D., 1998. Uranium VI adsorption on model minerals: Controlling factors and Surface complexation modeling, in: Jenne, E.A. (Ed.), Adsorption of Metals by Geomedia. Academic Press, pp. 94–95.

Pelowitz, D.B. (Ed.), 2011. MCNPX User's Manual Version 2.7.0. LA-CP-11-0.

Pentreath, R.J., 2009. Radioecology, radiobiology, and radiological protection: frameworks and fractures. J. Environ. Radioact. 100, 1019–1026.

https://doi.org/10.1016/j.jenvrad.2009.06.004

Pentreath, R.J., 2002. Radiation protection of people and the environment: developing a common approach. J. Radiol. Prot. 22, 45–56. https://doi.org/10.1088/0952-4746/22/1/304

Powell, B.A., Miller, T., Kaplan, D.I., 2015. On the Influence of Ionic Strength on Radium and Strontium Sorption to Sandy Loam Soils. J. South Carolina Acad. Sci. 13, 13–18.

Rascio, N., Navari-Izzo, F., 2011. Heavy metal hyperaccumulating plants: How and why do they do it? And what makes them so interesting? Plant Sci. 180, 169–181. https://doi.org/10.1016/j.plantsci.2010.08.016

Rauret, G., Lopez-Sanchez, J.F., Sahuquillo, A., Rubio, R., Davidson, C., Ure, A., Quevauviller, P., 1999. Improvement of the BCR three step sequential extraction procedure prior to the certification of new sediment and soil reference materials. J. Environ. Monit. 1, 57–61.

Read, D., Ross, D., Sims, R.J., 1998. The migration of uranium through Clashach Sandstone: the role of low molecular weight organics in enhancing radionuclide transport. J. Contam. Hydrol. 35, 235–248.

Reichman, S.M., 2002. The Responses of Plants to Metal Toxicity: A review focusing on Copper, Manganese and Zinc. Australian Minerals & Energy Environment Foundation, Melbourne.

Robertson, D.E., Cataldo, D.A., Napier, B.A., Krupka, K.M., Sasser, L.B., Reed, P.R., 2003. Literature Review and Assessment of Plant and Animal Transfer Factors Used in Performance Assessment Modeling. PNNL-14321. Richland, WA.

Romheld, V., Marschner, H., 1991. Function of micronutrients in Plants. In: Mordvedg, J.J., editor, Micronutrients in Agriculture, 2nd ed. SSSA Book Ser. 4. SSSA. Madison, WI.

Ruedig, E., Beresford, N.A., Gomez Fernandez, M.E., Higley, K., 2015. A comparison of the ellipsoidal and voxelized dosimetric methodologies for internal, heterogeneous radionuclide sources. J. Environ. Radioact. 140, 70–77. https://doi.org/10.1016/j.jenvrad.2014.11.004

Ruedig, E., Caffrey, E., Hess, C., Higley, K., 2014. Monte Carlo derived absorbed fractions for a voxelized model of Oncorhynchus mykiss, a rainbow trout. Radiat. Environ. Biophys. 53, 581–587. https://doi.org/10.1007/s00411-014-0546-5

Salt, C.A., Kay, J.W., Donaldson, L., Woolsey, J.M., 1997. The Influence of Defoliation

Intensity, Season and Leaf Age on Radiocaesium Concentrations in Agrostis capillaris. Br. Ecol. Soc. 35, 1177–1189. https://doi.org/10.1130/2009.1204(09).

Salt, C.A., Kay, J.W., Jarvis, K.E., 2004. The influence of season and leaf age on concentrations of radiocaesium (137Cs), stable caesium (133Cs) and potassium in Agrostis capillaris. Environ. Pollut. 130, 359–369. https://doi.org/10.1016/j.envpol.2004.01.001

Salt, D.E., Smith, R.D., Raskin, I., 1998. Phytoremediation. Annu. Rev. Plant Physiol. Plant Mol. Biol. 49, 643–648.

Savannah River Nuclear Solutions, L.L.C., 2016. Savannah River Site Environmental Report for 2015. Aiken, SC: Savannah River Site; SRNS-RP-201-00089.

Sawhney, B.L., 1972. Selective sorption and fixation of cations by clay minerals. A review. Clays Clay Miner. 20, 93–100. https://doi.org/10.1346/CCMN.1972.0200208

Sazykina, T.G., 2018. Population sensitivities of animals to chronic ionizing radiation-model predictions from mice to elephant. J. Environ. Radioact. 182, 177–182. https://doi.org/10.1016/j.jenvrad.2017.11.013

Schindler, P.W., 1990. Co-adsorption of Metal Ions and Organic Ligands: Formation of Ternary Surface Complexes, in: Hochella Jr., M.F., White, A.F. (Eds.), Reviews in Mineralogy, Volume 23, Mineral-Water Interface Geochemistry. Mineralogical Society of America, pp. 281–307.

Schmeide, K., Bernhard, G., 2010. Sorption of Np(V) and Np(IV) onto kaolinite: Effects of pH, ionic strength, carbonate and humic acid. Appl. Geochemistry 25, 1238–1247. https://doi.org/10.1016/j.apgeochem.2010.05.008

Schmidt, W., 1999. Mechanisms and regulation of reduction-based iron uptake in plants. New Phytol. 141, 1–26. https://doi.org/10.1046/j.1469-8137.1999.00331.x

Schulte, E.H., Scoppa, P., 1987. Sources and behavior of technetium in the environment. Sci. Total Environ. 64, 163–179. https://doi.org/10.1016/0198-0254(87)90691-1

Segars, W.P., Tsui, B.M.W., Frey, E.C., Johnson, G.A., Berr, S.S., 2004. Development of a 4-digital mouse phantom for molecular imaging research. Mol. Imaging Biol. 6, 149–159. https://doi.org/10.1016/j.mibio.2004.03.002

Serkiz, S.M., Johnson, W.H., 1994. Uranium Geochemistry in Soil and Goundwater at the F and H Seepage Basins (U). EPD-SGS-94-307. Aiken, SC.

Shalhevet, J., 1973. Effect of mineral type and soil moisture content on plant uptake of

137Cs. Radiat. Bot. 13, 165–171. https://doi.org/10.1016/S0033-7560(73)80003-1

Shaw, G., Wadey, P., Bell, J.N.B., 2004. Crop Uptake of Chlorine-36 and Technetium-99 , 1990 to 1993 2280, 2272–2280.

Sheppard, M.I., Vandergraaf, T.T., Thibault, D.H., Keith Reid, J.A., 1983. Technetium and uranium: Sorption by and plant uptake from peat and sand. Health Phys. 44, 635–643. https://doi.org/10.1097/00004032-198306000-00004

Sheppard, S.C., 2003. An index of radioecology, what has been important? J. Environ. Radioact. 68, 1–10. https://doi.org/10.1016/S0265-931X(03)00067-5

Sheppard, S.C., Evenden, W.G., 1988. Critical compilation and review of plant/soil concentration ratios for uranium, thorium and lead. J. Environ. Radioact. 8, 255–285. https://doi.org/10.1016/0265-931X(88)90051-3

Sheppard, S.C., Evenden, W.G., 1987. Review of effect of soil on radionuclide uptake by plants. Ottawa, Canada: Atomic Energy Control Board; INFO-0230.

Shinonaga, T., Ambe, S., Yamaguchi, I., 1999. Uptake and distribution of trace elements in maturing soybean. Biol. Trace Elem. Res. 68, 235–48. https://doi.org/10.1007/BF02783906

Soudek, P., Petrova, T., Benesova, D., Dvorakova, M., Vanek, T., 2011. Uranium uptake by hydroponically cultivated crop plants. J. Environ. Radioact. 102, 598–604. https://doi.org/10.1016/j.jenvrad.2011.03.008

Soudek, P., Tykva, R., Vaněk, T., 2004. Laboratory analyses of137Cs uptake by sunflower, reed and poplar. Chemosphere 55, 1081–1087. https://doi.org/10.1016/j.chemosphere.2003.12.011

Stabin, M.G., Da Luz, L.C.Q.P., 2002. Decay data for internal and external dose assessment. Health Phys. 83, 471–475. https://doi.org/10.1097/00004032-200210000-00004

Stabin, M.G., Kost, S.D., Segars, W.P., Guilmette, R.A., 2015. Two Realistic Beagle Models for Dose Assessment. Health Phys. 109, 198–204. https://doi.org/10.1097/HP.0000000000000324

Stark, K., Goméz-Ros, J.M., Vives i Batlle, J., Lindbo Hansen, E., Beaugelin-Seiller, K., Kapustka, L.A., Wood, M.D., Bradshaw, C., Real, A., McGuire, C., Hinton, T.G., 2017. Dose assessment in environmental radiological protection: State of the art and perspectives. J. Environ. Radioact. 175–176, 105–114. https://doi.org/10.1016/j.jenvrad.2017.05.001

Stumm, W., 1992. Chemistry of the Solid-Water Intreface: Processes at the Mineral-Water and Particle-Water Interface in Natural Systems, 1st ed. John Wiley & Sons, Inc.

Stumm, W., Morgan, J.J., 1996. Aquatic Chemistry: Chemical Equilibria and Rates in Natural Waters, 3rd ed. John Wiley & Sons.

Sturla, S.J., Boobis, A.R., Fitzgerald, R.E., Hoeng, J., Kavlock, R.J., Schirmer, K., Whelan, M., Wilks, M.F., Peitsch, M.C., 2014. Systems toxicology: From basic research to risk assessment. Chem. Res. Toxicol. 27, 314–329. https://doi.org/10.1021/tx400410s

Tagami, K., Uchida, S., 2005. A comparison of concentration ratios for technetium and nutrient uptake by three plant species. Chemosphere 60, 714–717. https://doi.org/10.1016/j.chemosphere.2005.03.087

Takahashi, J., Tamura, K., Suda, T., Matsumura, R., Onda, Y., 2015. Vertical distribution and temporal changes of 137Cs in soil profiles under various land uses after the Fukushima Dai-ichi Nuclear Power Plant accident. J. Environ. Radioact. 139, 351–361. https://doi.org/10.1016/j.jenvrad.2014.07.004

Tessier, A., Campbell, P.G.C., Bisson, M., 1979. Sequential Extraction Procedure for the Speciation of Particulate Trace Metals. Anal. Chem. 51, 844–850.

Thorne, M.C., 2018. Radioecology in Europe. J. Radiol. Prot. 38, E5–E9. https://doi.org/10.1088/1361-6498/aa9c0f

USDOE, 2002. A graded approach for evaluating radiation doses to aquatic and terrestrial biota, DOE-STD-1152-2002. Washington, DC.

Viehweger, K., Geipel, G., 2010. Uranium accumulation and tolerance in Arabidopsis halleri under native versus hydroponic conditions. Environ. Exp. Bot. 69, 39–46. https://doi.org/10.1016/j.envexpbot.2010.03.001

Vives I Batlle, J., 2012. Dual-age-class population model to assess radiation dose effects on non-human biota populations. Radiat. Environ. Biophys. 51, 225–243. https://doi.org/10.1007/s00411-012-0420-2

Vives I Batlle, J., Sazykina, T.G., Kryshev, A., Monte, L., Kawaguchi, I., 2012. Inter-comparison of population models for the calculation of radiation dose effects on wildlife. Radiat. Environ. Biophys. 51, 399–410. https://doi.org/10.1007/s00411-012-0430-0

Wadey, P., Shaw, G., Bell, J.N.B., 2001. Vadose Zone Processes and Chemical Transport and Crop Uptake of Three Gamma-Emitting Radionuclides , 1990 to 1993. J.

Environ. Qual 30, 1341–1353.

Waite, T.D., Davis, J.A., Payne, T.E., Waychunas, G.A., Xi, N., 1994. Uranium (VI) adsorption to ferrihydrite: Application of a surface complexation. Geochim. Cosmochim. Acta 58, 5465–5478.

Wang, D., Zhou, S., Liu, L., Du, L., Wang, J., Huang, Z., Ma, L., Ding, S., Zhang, D., Wang, R., Jin, Y., Xia, C., 2015. The influence of different hydroponic conditions on thorium uptake by Brassica juncea var. foliosa. Environ. Sci. Pollut. Res. 22, 6941–6949. https://doi.org/10.1007/s11356-014-3914-4

Wheater, H.S., Bell, J.N.B., Butler, A.P., Jackson, B.M., Ciciani, L., Ashworth, D.J., Shaw, G.G., 2007. Series on Environmental Science and Management - Vol. 5 BIOSPHERE IMPLICATIONS OF DEEP DISPOSAL OF NUCLEAR WASTE The Upwards Migration of Radionuclides in Vegetated Soils. Imperial College Press, London, UK.

Wildung, R.E., Garland, T.R., Cataldo, D.A., 1977. Accumulation of Technetium by Plants. Health Phys. 32, 314–317.

Xie, T., Zaidi, H., 2016. Development of computational small animal models and their applications in preclinical imaging and therapy research. Med. Phys. 43, 111–131. https://doi.org/10.1118/1.4937598

Xu, X.G., 2014. An exponential growth of computational phantom research in radiation protection, imaging, and radiotherapy: A review of the fifty-year history. Phys. Med. Biol. 59. https://doi.org/10.1088/0031-9155/59/18/R233

Yoschenko, V., Takase, T., Konoplev, A., Nanba, K., Onda, Y., Kivva, S., Zheleznyak, M., Sato, N., Keitoku, K., 2017. Radiocesium distribution and fluxes in the typical Cryptomeria japonica forest at the late stage after the accident at Fukushima Dai-Ichi Nuclear Power Plant. J. Environ. Radioact. 166, 45–55. https://doi.org/10.1016/j.jenvrad.2016.02.017

Yoschenko, V.I., Kashparov, V.A., Melnychuk, M.D., Levchuk, S.E., Bondar, Y.O., Lazarev, M., Yoschenko, M.I., Farfán, E.B., Jannik, G.T., 2011. Chronic irradiation of Scots pine trees (Pinus Sylvestris) in the chernobyl exclusion zone: Dosimetry and radiobiological effects. Health Phys. 101, 393–408. https://doi.org/10.1097/HP.0b013e3182118094

Yu, C., Cheng, J.J., Kamboj, S., 2013. Effects of the new wildlife transfer factors on RESRAD-BIOTA's screening Biota Concentration Guides and previous model comparison studies. J. Environ. Radioact. 126, 338–351. https://doi.org/10.1016/j.jenvrad.2013.01.004

Zachara, J.M., Smith, S.C., Liu, C., McKinley, J.P., Serne, R.J., Gassman, P.L., 2002. Sorption of Cs+ to micaceous subsurface sediments from the Hanford site, USA. Geochim. Cosmochim. Acta 66, 193–211. https://doi.org/10.1016/S0016-7037(01)00759-1

Zaidi, H. (Ed.), 2018. Computational Anatomical Animal Models, 2053-2563. IOP Publishing, Bristol, UK. https://doi.org/10.1088/2053-2563/aae1b4

Zaidi, H., Tsui, B.M.W., 2009. Review of computational anthropomorphic anatomical and physiological models. Proc. IEEE 97, 1938–1953. https://doi.org/10.1109/JPROC.2009.2032852

Zaunbrecher, L.K., Cygan, R.T., Elliott, W.C., 2015a. Molecular models of cesium and rubidium adsorption on weathered micaceous minerals. J. Phys. Chem. A 119, 5691–5700. https://doi.org/10.1021/jp512824k

Zaunbrecher, L.K., Elliott, W.C., Wampler, J.M., Perdrial, N., Kaplan, D.I., 2015b. Enrichment of Cesium and Rubidium in Weathered Micaceous Materials at the Savannah River Site, South Carolina. Environ. Sci. Technol. 49, 4226–4234. https://doi.org/10.1021/es5054682

Zenk, M., 1996. Heavy metal detoxification in higher plants - a review. Gene 179, 21–30. https://doi.org/10.1016/S0378-1119(96)00422-2

Zhang, G., Xie, T., Bosmans, H., Liu, Q., 2009. Development of a rat computational phantom using boundary representation method for monte carlo simulation in radiological imaging. Proc. IEEE 97, 2006–2014. https://doi.org/10.1109/JPROC.2009.2028446

Zhu, Y.G., Smolders, E., 2000. Plant uptake of radiocaesium: a review of mechanisms, regulation and application. J. Exp. Bot. 51, 1635–45. https://doi.org/10.1093/jexbot/51.351.1635